Modellering van het optische gedrag
in organische LEDs voor verlichting

Modeling of the Optical Behavior
of Organic LEDs for Illumination

Peter Vandersteegen

Promotoren: prof. dr. ir. P. Bienstman, prof. dr. ir. R. Baets
Proefschrift ingediend tot het behalen van de graad van
Doctor in de Ingenieurswetenschappen: Fotonica

Vakgroep Informatietechnologie
Voorzitter: prof. dr. ir. D. De Zutter
Faculteit Ingenieurswetenschappen
Academiejaar 2008 - 2009

UNIVERSITEIT
GENT

ISBN 978-90-8578-233-9
NUR 959
Wettelijk depot: D/2008/10.500/53

Promotor:

Prof dr. ir. Peter Bienstman	Universiteit Gent, INTEC
Prof dr. ir. Roel Baets	Universiteit Gent, INTEC

Overige leden van de examencommissie:

Prof. dr. ir. Ronny Verhoeven, voorzitter	Universiteit Gent, Civiele Techniek
Dr. ir. Björn Maes, secretaris	Universiteit Gent, INTEC
Prof. dr. Olivier Martin	EPFL, NAM
Prof. dr. ir. Kristiaan Neyts	Universiteit Gent, ELIS

Universiteit Gent
Faculteit Ingenieurswetenschappen

Vakgroep Informatietechnologie
Sint-Pietersnieuwstraat 41
B-9000 Gent, België

Tel.: +32-9-264.33.39
Fax.: +32-9-331.35.93
http://www.intec.ugent.be
http://www.photonics.intec.ugent.be

The more you try the more you fly and thats what really counts.

Tigger

Dankwoord

Een dankwoord schrijven begint met de moeilijke vraag: 'wie dank je en waarvoor?' Opgepast, dit is niet omdat ik niemand weet, eerder het tegenovergestelde. Ook worstel ik nog altijd met de vraag: 'Wat wil ik dat jullie onthouden van dit werk?'

Laat me beginnen met die laatste vraag. Ik heb het geluk gehad te kunnen meewerken aan onderzoek van energie-efficiente verlichting met vernieuwende mogelijkheden qua kleur, vorm en levensduur: de OLED. Kortom, ik had een onderwerp dat ik extreem relevant vind. Overigens, weg met beleidsmakers die een economisch onzekere situatie misbruiken om lovenswaardige klimaatplannen te willen kelderen. Nu investeren in ecologie betaalt zich later absoluut terug.

Naast het onderwerp an sich moet de manier van werken je ook aanstaan. Als doctoraatsstudent kun je alvast je manier van werken af en toe zelf bepalen. Dus, je leert wat je leuk vindt. Uiteraard leer je ook waar je echt een bloedhekel aan hebt. Bijvoorbeeld, persoonlijk weet ik nu dat ik het leuker vind vragen te verzinnen dan de antwoorden in details uit te werken. Daarnaast heb ik tijdens deze vier/vijf jaren ontdekt dat reizen me ligt. Eigenlijk heeft doctoreren me heel wat bijgeleerd op heel wat vlakken. Daarvoor ben ik dus dankbaar.

Uiteraard ben ik dan ook dank verschuldigd aan heel wat mensen.

Bedankt professor Roel Baets. Ik vind uw photonics groep zowel qua interessante projecten als qua aangename werkomgeving indrukwekkend. Professor Peter Bienstman, ik heb het gevoel dat ik tijdens dit werk enorm veel op uw inzet heb gesteund. Bovendien ben ik nog zelden iemand tegengekomen die zijn ideeen zo beknopt zo helder kan formuleren.

Andere mensen in de photonics groep waarop dit werk steunt zijn Steven en mijn vroegere thesisstudent Carl. Zonder hun werk zou alvast een groot deel van de fabricage nooit zijn uitgevoerd.

Of course, this work would not have been possible without the OLLA-project. Therefore, dear people of Work Package 4.1, thank you for our fruitful discussions. Dear Horst, Karsten, Martin, Markus, Saso and Alexandre & other people of OLLA: thanks for the not always work related talks afterwards.

Minstens even belangrijk zijn de collega's die geen directe bijdrage hebben geleverd tot dit onderzoek. Laat me beginnen bij mijn eerste bureaugenootjes: Bert, Rein en Bjorn. Volgende bureau: Stijn, Joost en Hans. De laatste collega's en veruit de meest knusse bureau: Wouter, Katrien en diezelfde Stijn. Bedankt voor jullie gezelschap.

Het duo: Lieven en Dave, bedankt voor jullie boeiende interactie. Ook dank aan het trio: Koen, Kristof en Wout. Alle mensen van de photonics groep uit de koffiepauze, bedankt voor de leuke tijd.

Dat brengt me uiteindelijk tot de andere mensen die zeer indirect een bijdrage hebben geleverd. Als eerste, mijn vroegere flatgenoten: Bart, Bert en Ingeborg, het was aangenaam toeven aan de Eedverbondkaai. Beste Barten, Berten, Fre, Rein, Pieter, ...: bedankt om 's avonds mee weg te gaan.

Als laatste kom ik nu aan mijn ouders. Jullie hebben me heel veel kansen gegeven om mijzelf te ontplooien: bedankt.

Gent, 1ste versie: januari 2008, laatste revisie: november 2008
Peter Vandersteegen

Overview

List of Symbols and Acronyms

Ag	Silver
Al	Aluminium
c	Speed of light in vacuum, c = 299 792 458 m/s
cd	Candela
cm	centimer, 10^{-2}m
EJ	exajoule, $10^{18}J$
$\eta_{external}$	External Quantum Efficiency, the ratio of radiant energy to electrical power
ϵ	Permettivity, the ratio $\mathbf{D}/\mathbf{E}$
ϵ_0	Permittivity of the vacuum, $\epsilon_0 = 1/c^2\mu_0 = 8.854187817610^{-12}F/m$
eV	electron Volt
h	Planck's Constant, h = 6.626068 $10^{-34}m^2kg/s$
fs	femtosecond, 10^{-15}s
k	Boltzmann constant, k = 1.3806503 $10^{-23}m^2kgs^{-2}K^{-1}$
lm	lumen
λ	wavelength
mm	millimeter, 10^{-3} m

μ_0	Permeability in vacuum, $4\pi 10^{-7} H/m$
μm	micrometer, 10^{-6} m
n	Refractive index
nm	nanometer, 10^{-9}m
ps	picosecond, 10^{-12}s
V	volt
W	Watt
BPM	Beam Propagation Method
CCT	Correlated Color Temperature
CIE	Commission Internationale de l'Eclairage
CJ	Complex Jacobi Method
CMOS	Complementary Metal Oxide Structure
CRI	Color Rendering Index
EME	Eigenmode Expansion
ETL	Electron Transport Layer
FDTD	Finite Differences in Time Domain
HOMO	Highest Occupied Molecular Orbit
HTL	Hole Transport Layer
IC	Integrated Circuit
ITO	Indium Tin Oxide
IQE	Internal Quantum Efficiency
OLED	Organic Light Emitting Diode
LED	Light Emitting Diode
LUMO	Lowest Unoccupied Molecular Orbit
PML	Perfectly Matched Layer
RCLED	Resonant Cavity LED
RC^{2}LED	Resonant Cavity^2 LED

RCWA Rigorous Coupled Wave Analysis

sm-OLED small molecule OLED

TFSF Total Field/Scattered Field

SSL Solid State Lighting

TE Transverse Electric

TM Transverse Magnetic

TIR Total Internal Reflection

WOLED White OLED

WVD Wave Vector Diagram

Nederlandse samenvatting

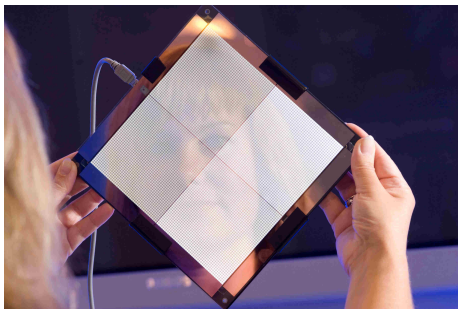

Figuur 1: Een lamp gebaseerd op Organische LEDs bestaat uit oppervlaktes die licht geven. (bron: OLLA project, [1])

Centraal in dit werk staat een beloftevolle technologie voor verlichting: de witte organische licht emitterende diode. (WOLED)

We gebruiken heel veel energie. Met enkele cijfers kun je reeds goed aangeven hoeveel je kunt besparen, zowel op gebied van grondstoffen als op gebied van economie.

Volgens rapporten uit zowel de EU als de USA, [2] en [3], verbruiken we ongeveer 20% van alle elektrische energie voor verlichting. Omdat de totale hoeveelheid energie consumptie ook afhangt van transport, verwarming en producie is onze totale energie consumptie nog een grootte-orde meer. Desalniettemin verbruiken we veel om onze huizen te verlichten. In Europa gaat 7 EJ naar verlichting. Dit is ruwweg het equivalent van het verbranden van één olympisch zwembad gevuld met olie, elke seconde! Daarenboven blijkt dat nu (2007) 40% van de verlichting gebaseerd is op gloeilampen. [4] Gloeilampen zetten slechts 5 % van de energie om in licht, de rest is warmte.

Een nieuwe klasse van verlichting zijn de vastestoflichtbronnen. Een

type van vastestoflichtbron is de organische LED. Deze bron bestaat uit een groot oppervlakte dat diffuus licht geven. Een ander type vastestoflichtbron is de LED, welke een puntbron is die zeer fel licht geeft. Beide technologien vullen elkaar goed aan naargelang de toepassing. Een lamp, bestaande uit vier OLED oppervlakten is te zien op figuur 1.

De structuur van een OLED is op het eerste zicht vrij simpel. Figuur 2 geeft een schets weer van een OLED met typische afmetingen. Bij de fabricage wordt vertrokken van een glasplaat van een tiental centimeters op een tiental centimeters. Op dit substraat worden achtereenvolgens lagen gedeponeerd die hooguit enkele tientallen nanometers zijn[1] : een **transparante** anode, meestal ITO; geleidende organische lagen en een metalen cathode, meestal Aluminium.

Een spanningsverschil over de anode en de cathode zorgt voor een elektrische stroom door de geleidende organische lagen, waardoor licht wordt gegenereerd. In 1987 is aangetoond dat zelfs bij lage spanning (toen: <10V, nu zelfs: < 3.5V) voldoende intens licht kan gegenereerd worden. [5] [6] In 1994 verscheen de eerste witte OLED, die 3 emitters combineerde met verschillende kleuren. [7] Sinds 1998 zijn er zelfs emitters, die 100% van de elektrische stroom omzetten in licht. [8] Desalniettemin vergt deze OLED technologie en de (potentieel) efficiente omzetting van elektrische energie in licht nog verder onderzoek.

De focus van dit werk zijn twee aspecten van het optische gedrag van de OLED. Het eerste aspect is de **uitkoppelefficientie** van licht uit de OLED. Deze uitkoppelefficientie geeft de verhouding tussen stralingsvermogen in lucht tegen het stralingsvermogen opgewekt in de organische laag. Figuur 2 toont dat slechts 20% van het vermogen wordt uitgestraald. Dus, hoe krijg je meer straling uit de OLED? In dit werk hebben we drie ontwerpen bekeken om de uitkoppelefficientie te verbeteren. Het tweede aspect is de **effectiviteit** van een OLED. Dit hangt samen met de fysiologie van het menselijk oog. Het oog reageert immers gevoeliger op groen licht dan op blauw of rood licht. Dus, we hebben minder stralingsvermogen voor groen licht nodig om toch dezelfde intensiteit te ervaren. Voor wit licht heb je echter alle kleuren nodig. Het tweede aspect draait rond de meest effectieve combinatie van welbepaald 'blauw', welbepaald 'groen' en welbepaald 'rood'. We zoeken het optimale spectrum van de OLED om een zo hoog mogelijke lichtstroom per stralingsvermogen te krijgen.

Verhogen van de uitkoppelefficientie

Verhogen van de uitkoppelefficientie van een OLED zorgt ervoor dat zoveel mogelijk van het opgewekte stralingsvermogen wordt uitgekoppeld. In dit

[1] Een menselijk haar heeft een dikte tussen 20000 nm tot 180000 nm. Merk ook op dat de afwijking over het gehele oppervlakte slechts enkele percenten mag zijn.

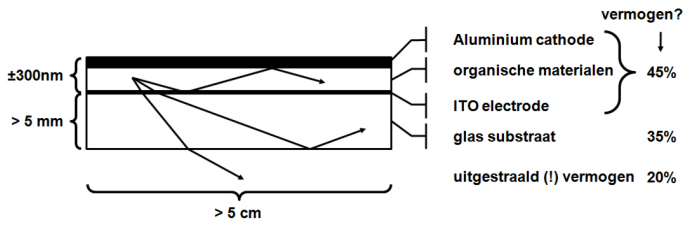

(a)

Figuur 2: De OLED bestaat uit verschillende dunne lagen op een glas substraat. Echter, licht dat gaat van de organische lagen naar glas ondervindt voor schuine hoeken volledige reflectie! Hetzelfde geldt bij de overgang van glas naar lucht. Hierdoor kan slechts 20% van het optische vermogen uitgestraald worden.

werk hebben we gekeken naar drie OLED ontwerpen om meer licht uit te koppelen.

Figuur 2 geeft de reden voor de lage uitkoppelefficientie. Schuin invallend licht aan de overgang van anode naar glas en aan de overgang van glas naar lucht ondervindt **totale interne reflectie**. Dit ligt aan de snelheid van licht in de verschillende lagen. Straling in de organische lagen en glas is respectievelijk 1.7 en 1.5 trager is dan de snelheid van straling in lucht. Uit de wet van Snellius volgt dan de kritische hoek waarvoor licht dat invalt vanuit een materiaal met lage voorplantingsnelheid op een materiaal met grotere voortplantingsnelheid **volledig gereflecteerd** wordt.

Om optimale ontwerpen voor deze drie types te berekenen, hebben we een numerieke methode ontwikkeld op basis van eigenmode expansie en rigoreuze gekoppelde golftheorie. [9] [10] Het vernieuwende aan deze methode is dat zowel coherent licht als incoherent licht in rekening worden gebracht. Omdat de dikte van deze lagen en van de organische lagen dezelfde grootteorde hebben als de golflengte van licht (450-700nm), moeten we immers licht modelleren als coherent. Omdat de dikte van de glasplaat vele grootte ordes groter is, dienen we hier licht te beschouwen als incoherent.

Het eerste ontwerp heeft betere lichtuitkoppeling door drie extra lagen tussen de electrode en het glas substraat. Deze extra lagen zijn ook aangegeven op figuur 3(a). Omdat zowel de organische lagen als de drie extra lagen kunnen beschouwd worden als optische caviteiten noemen we dit ontwerp een RC^{2}LED. [11] Figuur 4(a) geeft de relatieve verbetering van de uitkoppelefficientie van een OLED met geoptimaliseerde extra lagen tegenover diezelfde OLED zonder extra lagen. Experimentele verificatie is gebeurd door het vergelijken van spectrale vermogen van deze twee OLEDs. Onze experimenten geven goede overeenkomst met de simulatie. Zowel experiment als simulaties tonen aan dat de uitkoppelefficientie van

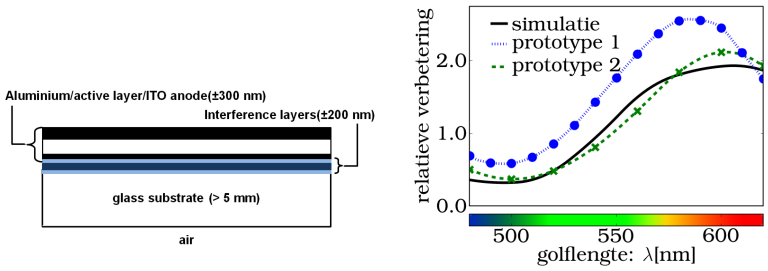

(a) (b)

Figuur 3: (a) Extra interfentie-lagen geplaatst tussen anode en glas zorgen voor golflengte afhankelijke interferentie effecten. (b) Relatieve verbetering van de extractie efficïentie door interferentie-lagen tussen ITO en glas, zowel simulatie als metingen van 2 prototypes.

een RC^{2}LED verbetert met een factor 2 over een golflengtegebied van 75 nm.

Het tweede ontwerp gebruikt een rooster dat werd geplaatst aan de overgang tussen glas en lucht. Omdat de totale interne reflectie wordt veroorzaakt door de 'vlakheid' van deze overgang, kan een verruwing de totale interne reflectie verhelpen. Een foto genomen met een elektronen microscoop van een dergelijk rooster is te zien op figuur 3. Indien licht wordt gereflecteerd, wordt het terug gereflecteerd aan de cathode kant. Dit licht kan dan evenwel bij terugkomst aan de glas lucht kant weer verstrooid worden na de tweede,derde,... rond trip. Simulaties geven een relatieve verbetering van 50%. Dit en experimenten geven evenwel aan dat deze techniek geen betere uitkoppelefficientie geeft ten opzichte van andere verruwing van het OLED oppervlak. [12]

Het derde ontwerp gebruikt een rooster aan de overgang tussen electrode en glas. Ook hier is het doel is het uitkoppelen van het licht. Hier is het belangrijk te kijken naar de invloed van meerdere rond trips in de glaslaag, figuur 4(b). De meeste artikels (bijvoorbeeld [13]) verwaarlozen deze meerdere rond trips. Bij de eerste rond trip gebeurt het volgende: de eerste keer kan licht niet ontsnappen uit de OLED. Echter, het wordt terug gestuurd naar het rooster. Na verstrooiing krijgt het een tweede kans om te ontsnappen, en een derde... Figuur 4(a) geeft nu de extractie efficïentie in de glas laag voor twee situaties. Enkel 'directe transmissie' berekent de extractie efficiëntie zonder de rond trips. 'Inclusief reflecties' geeft de extractie efficiëntie met de rond trips. Uit deze figuur kunnen we concluderen dat de verhoging van de uitkoppeling efficiëntie komt door de rond trips. In ieder geval geeft een rooster ook hier een relatieve verbetering van de

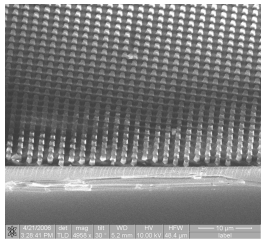

(a) Het rooster aan de glas lucht interface bestaat uit een periodieke herhaling van zuilen. (Periode = 2000nm, hoogte = 300nm)

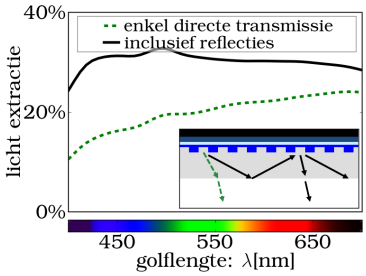

(b) Fractie uitgekoppeld vermogen van een OLED door een grating aan de overgang tussen electrode en glas. Ook wordt het vermogen in directe transmissie gegeven.

Figuur 4: Een rooster kan gebruikt worden aan zowel de overgang tussen electrode en glas als aan de overgang tussen glas en lucht.

extractie-efficïentie van 50%. Dus, de extractie efficïentie is 30% in plaats van 20%.

Verhogen van de effectiviteit

De effectiviteit van een lichtbron wordt gegeven door de verhouding van lichtstroom per stralingsstroom. De eenheid is lumens per Watt. Deze eenheid houdt rekening met de fysiologie van het menselijk oog en met het elektrische vermogen van de de lichbron. [14] Merk op, de meeste mensen zijn gevoeliger voor golflengtes die we ervaren als 'groen' licht dan voor golflengtes in het 'blauw' of 'rood'. Aan de andere kant heb je wel golflengtes in het 'blauw' en 'rood' nodig om wit te verkrijgen. Dus, het kiezen van het juiste spectrum kan de effectiviteit van je lichtbron verhogen.

In dit werk hebben we verder gebouwd op werk van D.L. MacAdam. Zijn werk geeft het spectrum met de maximale lichtstroom per stralingsstroom voor een gegeven chromaticiteit. [15] Voor een lichtbron met het warme wit 'illuminant A' wordt het spectrum met de grootste effectiviteit gegeven door twee monochromatische lichtbronnen. Deze twee lichtbronnen stralen uit op 450 nm ('blauw') en 580 nm ('oranje'). De kwaliteit van het licht-uitgedrukt in kleur reproducibeerbaarheid index [16]- is evenwel ver beneden de vereiste 80. In dit werk hebben we evenwel aangetoond dat het spectrum van figuur figuur 5 zowel een voldoende hoge kwaliteit heeft als de effectiviteit van de lichtbron verhoogt met 30%.

We hebben ook gekeken naar de effectiviteit van een lichtbron in functie van de golflengte-afhankelijke eigenschappen van een OLED. Hierbij hebben

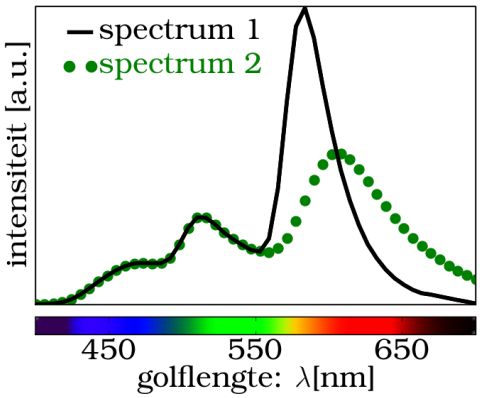

Figuur 5: Beide spectra geven dezelfde witte chromaticiteit. Spectrum 2 komt van een OLED met 3 emitters. [17] Evenwel spectrum 1 heeft een grotere effectiviteit dan spectrum 2: 429 lm/W tegenover 305 lm/W.

we twee stellingen gestaafd. De eerste stelling toont aan dat een witte lichtbron met een diep blauwe inefficiente emitter even effectief kan zijn als een witte lichtbron met een twee keer zo efficiente licht blauwe lichtbron. Hierbij hebben beide lichtbronnen hetzelfde chromaticiteit. De tweede stelling bevestigt dat je de extractie efficïentie moet afstemmen op het spectrum. In het geval van een RC^{2}LED die 'warm wit licht' uitstraalt, dien je vooral je extractie efficïentie af te optimaliseren voor de rode emitter.

Conclusie

In dit werk hebben we zowel de uitkoppelefficientie als de effectiviteit van witte OLEDs bestudeerd. Voor de extractie efficïentie zijn twee zaken duidelijk geworden. Allereerst kan een OLED met interferentielagen tussen de electrode en glas twee keer meer licht uitkoppelen dan een OLED zonder deze lagen. Evenwel deze verbetering is slechts over 75 nm. Dit is een zesde van het spectrum dat nodig is voor wit licht. Als tweede, om de uitkoppelefficientie correct te berekenen moeten de meerdere reflecties in de glas laag wel degelijk in rekening worden gebracht. Ook blijkt dat een rooster gelegen tussen elektrode en glas de licht uitkoppeling vooral verbetert door het licht uit het substraat uit te koppelen.

Voor de effectiviteit hebben we gekeken naar de spectra die een hogere lichtstroom per stralingsstroom geven dan de standaard OLED spectra. We hebben een spectrum gegeven met een hogere effectiviteit en een voldoend hoge kleur reproduceerbaarheids index.

English summary

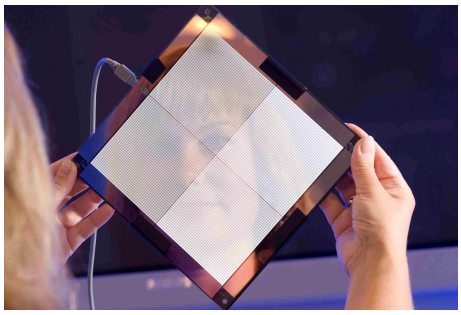

Figure 1: This lamp is based on Organic LEDs. We see a surface which gives light. (source: OLLA project, [1])

The focus of this work is a new illumination technology, which is potentially energy efficient: the White Organic Light Emitting Diode (OLED).

We use a lot of energy. A few numbers can already give an idea of the possible savings. According to research in the EU and the USA, about 20% of all electrical energy is used for illumination. [2] [3] For example, Europe uses 7 exajoules per year for illumination. This is roughly the equivalent of burning each second the oil in one olympic swimming pool. Moreover, the extremely inefficient incandescent light bulb is used for about 40% of the domestic illumination. [4] Incandescent light only converts 5% of the total electrical power for illumination, the other 95% is dissipated. Replacing these bulbs would already be very beneficial.

A new class of energy efficient illumination is solid state illumination. One class is the OLED. This light source can be seen as a large tile which emits diffuse light, figure 1. Another class of solid state illumination is the LED, which is a point source with very bright light from one small surface.

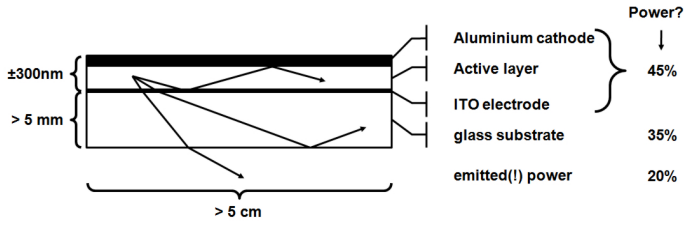

(a)

Figure 2: The OLED consists of several thin layers on top of a glass substrate. However, light with a too oblique angle can not go from organic layers to glass. The same is true for too oblique light from glass to air. In total, only 20% of the total generated light can escape.

Because of their properties, both classes are very complementary.

Figure 2 shows the simplified structure of an OLED. On a glass plate of a few hundred square cms, several layers of a few ten nms are deposited[2] : a **transparent** anode, usually ITO; organic layers and a metal cathode, usually Aluminium.

After applying a voltage difference between anode and cathode, an electrical current flows through the organic layers. These layers contain emitters which emit light. The field of research has intensified since 1987, when the first OLED with low voltage and sufficiently intens light was published. (then: < 10V, now: < 3.5V) [5] [6] In 1994 the first white OLED was published. This OLED gives white light with 3 types of emitters with different colors. [7] Since 1998, a new class of emitters became available. These emitters can convert 100% of the electrical current in light [8] These results show the (potentially) high efficiency of OLED for illumination.

The focus of this work are two aspects of the optical behavior of an OLED. The first aspect is the extraction **efficiency** of the light from an OLED. This extraction efficiency shows how much of the total generated light can escape the OLED. Figure 2 shows that only 20% of all light is extracted. The second aspect is the **efficacy** of an OLED. This property depends on how the human eye reacts on light. The eye is more sensitive for green than for blue or red. We need less green than blue to get the same sensation of intensity. However, white light requires blue and red. The second aspect is about finding the most effective spectrum.

[2] A human hair has a thickness between 20000 nm to 180000 nm. Also, the deviation of the thickness of the organic layers over the entire area can be at most a few percentages.

Increasing the extraction efficiency

Increasing the extraction efficiency means extracting as much light as possible. This work has investigated three designs with increased extraction efficiency. To optimize these three designs, a novel simulation method has been developed. For the first and second designs, several prototypes have been made and measured.

Figure 2 shows why the extraction efficiency is low. Between the interface of anode and glass, light under a too oblique angle is completely reflected. This is also called Total Internal Reflection. This is also true for the interface between glass and air. The main reason is the speed of light which is different in each of these materials. Snellius' law states that light which goes from a material with low light speed to a material with a higher light speed is totally reflected if its angle is more oblique than a critical angle.

To optimize the OLED design, we have developed a numerical method which can model a structure with layers where we model light as coherent and as incoherent. Indeed, because the thickness of the organic layers is about the same as the wavelength of light (450-700nm), light in these layers has to be coherently modeled. Because the thickness of the glass plate is much larger than the wavelength of light, light has to be incoherently modeled. The method uses rigorous coupled wave analysis and eigenmode expansion. [10] [9]

The first design, figure 3(a), uses three extra layers between anode and glass to increase light extraction. Because the organic layer stack and these 3 layers both are optical cavities, we call this design a RC^{2}LED. [11] Optimization of the layers shows in figure 3(b) the relative improvement in function of the wavelength. The relative improvement is the extraction efficiency of the RC^{2}LED compared to the extraction efficiency of this OLED without the three extra layers. Experimental verification compares the spectral power from the RC^{2}LED to the spectral power of this OLED without these three extra layers. Experiments and simulations show an improvement of 100% over a wavelength range of 75 nm.

The second design, figure 4(a), shows a grating which is between the glass substrate and air. Note, Total Internal Reflection (TIR) comes from the 'flatness' of the interface between these two materials. Thus, roughening this interface eliminates the TIR between glass and air. Simulations give a relative improvement of 50%. (results not shown!) Simulations and experiments show that this approach has no better extraction efficiency when compared to other corrugations of the glass-air interface. [12]

The third design also uses a grating similar to the one of figure 4(a). However, the grating is placed between anode and glass. Figure 4(b) shows the extraction efficiency. The extraction efficiency with grating is increased from 20% to 30%. Note, the developed numerical method can simulate the light which can escape the first time, in 'direct transmission' and light which

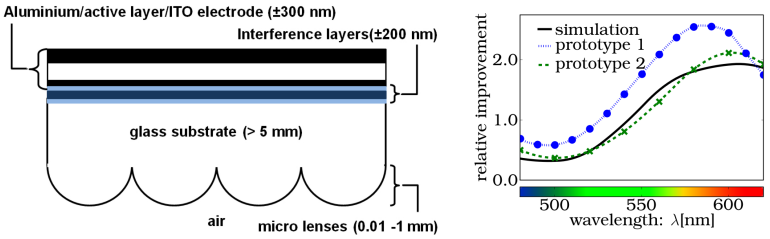

(a) (b)

Figure 3: (a) Adding extra layers between anode and glass creates interference effects which increase the extraction efficiency. (b) Relative improvement when using these extra layers.

can escape after 'multiple round trips'. Note, several papers, such as [13], only simulate the light in direct transmission. This last approach neglects the light which is trapped in the glass substrate. However, 4(b) shows that the main increase of the extraction efficiency comes from the extraction of the light in the substrate.

Increasing the efficacy

The efficacy of a light source is given by the luminous power efficiency, the ratio of luminous flux per required power. This unit considers both the properties of the eye and the electrical power of the light source. Note, the human eye is more sensitive for 'green' than for 'blue' and 'red'. However, you need blue and red to get white. [14] Thus, optimizing the spectrum can increase the efficacy.

This research extends the work of D.L. MacAdam. [15] The highest luminous power efficiency for warm white light ('illuminant A') is generated by 2 monochromatic sources. One source is monochromatic blue (450 nm), the other is monochromatic orange (580 nm). However, the color quality, which can be expressed by the Color Rendering Index [16], is far below the required 80 for illumination. Figure 5 shows an increase of the luminous power efficiency by 30% with a high CRI of 90.

We also have investigated the luminous power efficiency in function of wavelength dependent properties of an OLED, such as the extraction efficiency and the internal quantum efficiency. We have proved two statements. First, a white light source with deep blue inefficient emitter can have the same efficacy as a white light source with a two times more efficient light blue emitter. Both light sources have the same white chromaticity. The second statement: the optimum wavelength dependent extraction efficiency

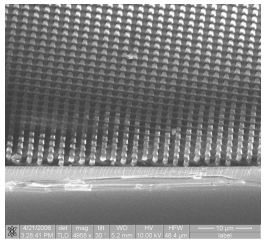

(a) The grating periodically repeats pillars. (Period = 2000nm, Height = 300nm)

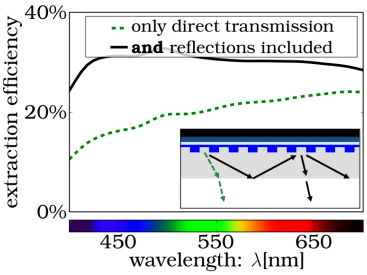

(b) This figure shows how much light is extracted when a grating is placed between anode and glass. We also give the power which can escape the first time, 'direct transmission'.

Figure 4: A grating can be used between anode and glass and between glass and air.

depends on the spectrum. For example, in a RC^{2}LED which emits 'warm white', the extraction efficiency should be the optimized for the red emitter.

Conclusion

This work investigates the extraction efficiency and the efficacy of white OLEDs. Concerning the extraction efficiency, we can make two statements. First, an OLED with interference layers between anode and cathode, such as the RC^{2}LED, can give two times more light than that OLED without these layers. Note, this improvement is limited to a wavelength range of 75 nm. Second, to calculate the extraction efficiency, we need to consider multiple round trips in the substrate. Neglecting these multiple round trips underestimates the extraction efficiency. Also, we have seen that a grating between anode and substrate does not increase the amount of light extracted from the organic layers.

Maximum efficacy can be achieved by approximating the spectrum by the spectrum which is given by the MacAdam limit. We have found a spectrum with an increased efficacy and with a sufficiently high color rendering index.

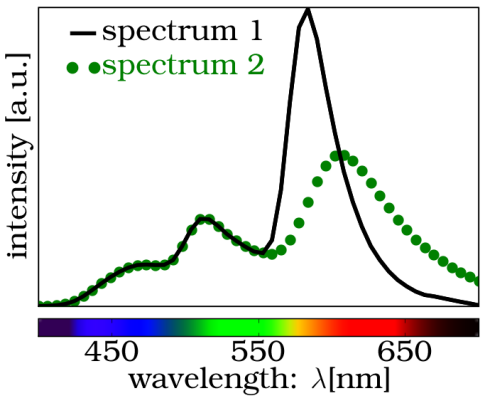

(a)

Figure 5: Both spectra have the same chromaticity. Spectrum 2 comes from an OLED with 3 emitters.[17] However, spectrum 1 has a much higher efficacy than spectrum 2: 429 lm/W compared to 305 lm/W.

1 Introduction

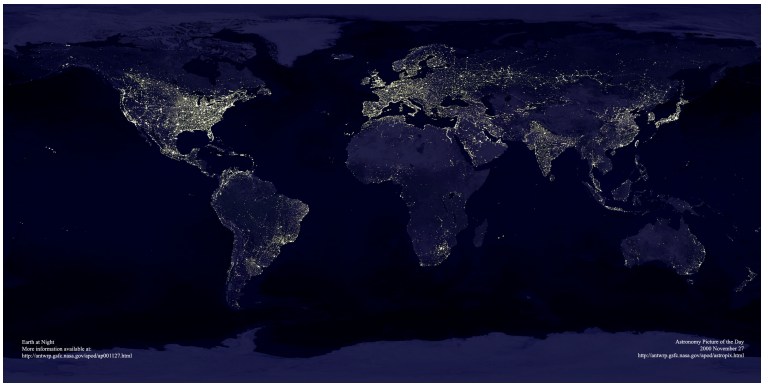

Figure 1.1: Earth by night. (source: NASA, 7th November 2000)

Roughly speaking, this work is about the optimization of optical designs of Organic Light Emitting Diodes (OLEDs) for lighting by using novel simulation tools. The focus of this chapter is to show the need for OLEDs for lighting and the need for good optical designs of OLEDs. Therefore, the first section shows the need for efficient lighting. Then, the second section is about Solid State Lighting (SSL) devices, which is a category of lighting under which OLEDs fall. To show the need of a good optical design of an OLED, the third section shows how a conventional design of a OLEDs gives a low efficiency. To find better designs, you need sufficiently accurate and fast simulation tools. Therefore, a short overview on simulation techniques is given in the subsequent section. To conclude, we present how this work fits in with the issues described in this chapter.

1.1 Energy consumption

Cold light, light generated by a device which has a high conversion of electricity to visible light, can save a lot of energy. Probably, lowering the energy consumption per person is the only way to give everybody the same share of the earth's natural resources without compromising on the quality of life. However, using an inefficient source such as the light bulb wastes a lot of energy. Although there have been some alternatives around for quite some time now, these alternatives never had the same success as the light bulb. This section illustrates these statements with some numbers.

According to the Energy Information Administration of the U.S. Government, the total energy consumption on this planet in 2006 was around 460 EJ (46 10^{19} J). More than 80% of this energy comes from burning fossil fuel. [18]. According to the Flemish Institute for Technological Research, VITO, Flanders has used 1266 PJ (1266 10^{1}5J) in 2005. [19] Depending on the source you consult, Flanders thus uses around 0.3-0.5% of the global energy consumption. To put these numbers in perspective, consider this: the global energy consumption is equivalent to burning a few million liters of oil, each second.

Although our planet can support this energy consumption [18], we will need to lower the energy consumption per person. More people than ever are living and consuming today. This is one of the factors of the large increase of the price of oil during the last decade. Moreover, creating awareness of the problem of global warming by human contribution to the green house effect has resulted in the Noble Peace Prize in 2007, [20].

Of course, the global energy consumption is more than lighting. Transport and heating account for the largest fraction of the global energy consumption. Still, in the U.S. and E.U., 20% of the **electrical** energy is used for lighting. [21] [2] In absolute numbers, the U.S. alone uses 7 EJ per year for lighting.

Though using energy for lighting is often necessary, using energy for inefficient lighting is an unnecessary waste, figure 1.1. The omnipresent light bulb only converts 5% of the electrical energy to visible light. The rest of the energy is infrared light, i.e. heat. Although recent research suggests that using a photonic crystal Tungsten filament in a light bulb might be used to suppress the infrared light, this is only a research concept. [22] A few recent documents show the omnipresence of the light bulb. A report of November 1999 by l'Agence de l'Environnement et de la Matrise de l'Energie of France showed that more than 60% of domestic lighting was generated by incandescent lighting. [23] Note that these bulbs convert at most 5% of the electrical energy to visible light. Another document by Photonics21, a consortium of European partners, mentions that even now (2007) 40% of lighting in the world is based on incadescent lamps. [4] 'Ban the bulb' would be a step in a more durable future.

Recently, Australia, Canada and the E.U. have announced they intend

Light source	Luminous power efficiency	Power	Luminous flux	Lifetime	CRI
light bulb	6-18 lm/W	100W	>1.300lm	1.000h	95
low voltage halogen	8-20 lm/W	50 W	900lm	2.000h	95
high voltage halogen	13-29 lm/W			95	
light saving bulb	60-70 lm/W	35 W	>3.000lm	>10.000h	60-85
fluorescent tube	70-90 lm/W	11 W	>500lm	>10.000h	60-85

Table 1.1: Properties of some popular light sources. The luminous power efficiency indicates the efficiency at which visible light is generated. The power is the amount of power used by one of these light sources. The luminous flux gives an idea of the amount of visible light. The Color Rendering Index (CRI) indicates how good colors can be reproduced with this light source. A good CRI is from 80 to 100, which is the maximum. (source: [25])

to ban the bulb. Moreover, Philips and General Electric, two of the world's top manufacturers of light bulbs, plan to phase out the incandescent light bulb. [24].

Although alternatives for the light bulb are widely available, these alternatives never have had the same success as the light bulb. These alternatives are given in table 1.1. Moreover, most incentives to replace the bulb have come from governments. Therefore, energy efficiency probably is not the deciding factor for domestic lighting. Other factors, such as perceived cost, functionality, ease of use and lifetime, come into play. For example, [25] states an old technology is replaced because of a **paradigm shift**. Thus, not only should the performance be better, meaning more efficient light generation, but the new technology should allow functionality which previously was impossible.

The ideal light source should be a cold light source which means that all electrical energy should be converted in light. Its lifetime should be extremely long. The shape of this light source should be easily changeable. Solid State Lighting (SSL), both Organic Light Emitting Diodes (OLEDs) and Light Emitting Diodes (LEDs) have the possibility to achieve these properties.

1.2 Solid State lighting

One crude definition of Solid State Lighting (SSL) might be: a light source which is composed of at least two bulk materials. Also, the electrical properties of at least one of these two bulk materials have to be that of a semiconductor. Then, the interface between these two materials can generate light if a current is applied. Because of the solid state of these two materials, this approach appears to be more stable compared to light generated by a Tungsten light filament or a gas discharge. This section gives two technologies which classify as SSL and a short review of their history. One of these two will be the Organic Light Emitting Diode (OLED). To conclude this section, we give some companies which commercialize technology of OLEDs.

Depending on the materials used to create the component, you have either inorganic Light Emitting Diodes (LEDs) or OLEDs. The properties of the used materials will influence the way the components are fabricated and more importantly the size of the area in which light is generated, table 1.2 . This distinction is illustrated by figure 1.2. A LED is especially suited for applications where a small dot with extremely bright light is desired. On the other hand, an OLED is especially suited for large area diffusive lighting. Nevertheless, it is possible to make a diffusive light with LEDs. For example, think of the back light of some LCD screens. [26] Although this work is mainly focused on lighting, other application areas where OLEDs might excel are display applications. [27] Of these two types, the inorganic LED has the longest history.

Light generation in a solid material had already been observed in the beginning of the 20th century by two independent researchers. [28] However, only in 1962, the semiconductor theory had advanced sufficiently to create a red LED. This was done by Nick Holonyak Jr. Nevertheless, white light with this technology only became possible by the development of a sufficiently bright blue LED, for which a patent was filed in 1993. [29] An excellent overview of the evolution of the field of LEDs can be found in paper. [25] The first OLED came later, in 1987. [5] Then, in 1994, the first White OLED was created. [7] However, a more complete overview of the history of the OLED will have to wait until section 2.2.

A few of the companies which are commercializing LEDs and OLEDs for lighting are Cree, Nichia, Seoul Semiconductor, OSRAM Opto Semiconductors and Philips Lumileds. Although Flanders has no companies which fabricate LEDs or OLEDs, some small and middle sized companies are specialized in designing fittings for lightings. Moreover, Flanders has a center where research is more directed toward application of existing and commercially available technology. [30]c

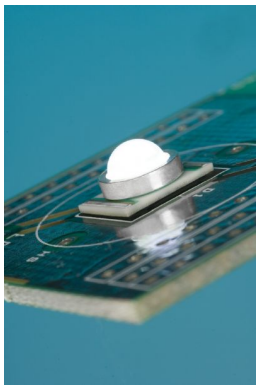

(a) A white LED emits bright light from an area smaller than a few mm^2. (source: Cree)

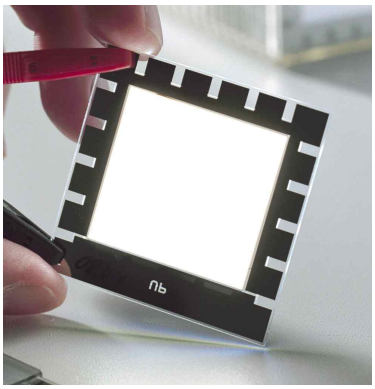

(b) A thin WOLED emits diffusive light from an area of around 5 by 5 cm^2 (source: Philips Research)

Figure 1.2: LEDs and OLEDs have different properties, which can be applied for different lighting applications, see table 1.2.

property	LED	OLED
luminous power efficiency	130 lm/W[1]	25lm/W
output power	25 lm	$>$ 1000 lm/m^2
lifetime	$>$ 10000h	$>$ 10000h
CRI	$>$ 90	$>$ 90
size	1000μm^2	30 cm * 30 cm

Table 1.2: Comparison between state of the art Solid State Lighting (SSL) devices. Properties come from literature.

1.3 Extraction efficiency and spectrum of a White Organic LED

Crudely stated, a White OLED (WOLED) for lighting has to have a high luminous power efficiency. Therefore, the WOLED has to satisfy three conditions. Firstly, we need to have a good conversion of electrical energy to photons. Secondly, most of these photons have to escape the lighting device. The fraction of photons which can escape the OLED is given by the extraction efficiency. Thirdly, the human eye needs to be as sensitive as possible for the wavelengths of these photons. Thus, the spectrum of the OLED has to match the eye sensitivity. Though the focus of this work are the last two conditions, chapter 2 also gives background on the first condition.

Let us now focus on the second condition. Light has to escape the OLED. To estimate the extraction efficiency, we start with the simplified structure of figure 1.3(a). This OLED is a large area glass substrate on which a stack of organic layers has been deposited. Basically, this OLED is a large thin tile which emits light. However, its planar structure is the reason for a low extraction efficiency. Why? Light can not go under an oblique angle from organic layers to the glass substrate **and** light can not go under an oblique angle from glass to air. This is known as Total Internal Reflection (TIR): Light under a too oblique angle can not pass a **planar** interface to go from a material with high refractive index to a material with a low refractive index. Because of TIR, only 20% of the generated light is extracted. In theory, corrugating the two interfaces eliminates TIR. Thus, this corrugation might give an increase of the extraction efficiency. At the end of this chapter we show that this work discusses several designs with corrugated interfaces and numerical methods to simulate these structures.

The third condition sounds trivial: the wavelength of the generated photons should match with the sensitivity of the human eye. The more sensitive the eye is to a particular wavelength, the less power you need to get the same 'experience'. If your OLED generates wavelengths for which the eye is sensitive, the more **effective** your OLED. Thus, using wavelengths for which the human eye is relatively insensitive should be avoided. However, the human eye is especially sensitive for green, not for blue and red. We experience green light as ten times more **bright** than blue or red light, even though the radiant fluxes are equal. Thus, the trade off is the following. On the one hand: you want as much green as possible to have a bright source. On the other hand, you need wavelengths in the blue and green to create white light, figure 1.3(b). However, depending on the 'blue' and 'red' wavelengths, you can make a more **effective** OLED. Thus, another topic of this work is to create an effective OLED by choosing the correct spectrum.

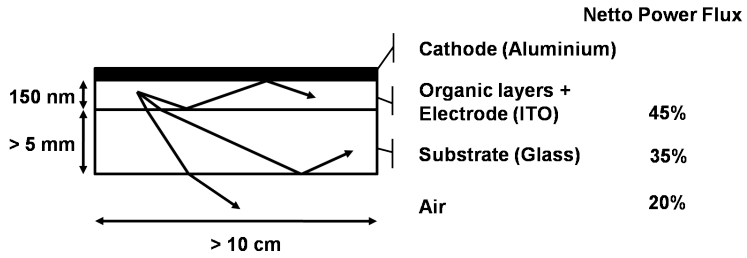

(a) This sketch shows a substrate emitting OLED of which the organic layers generate light. Light at oblique angles is reflected at some interfaces. Only 20% of the generated light can escape. (derivation in section 2.4.1)

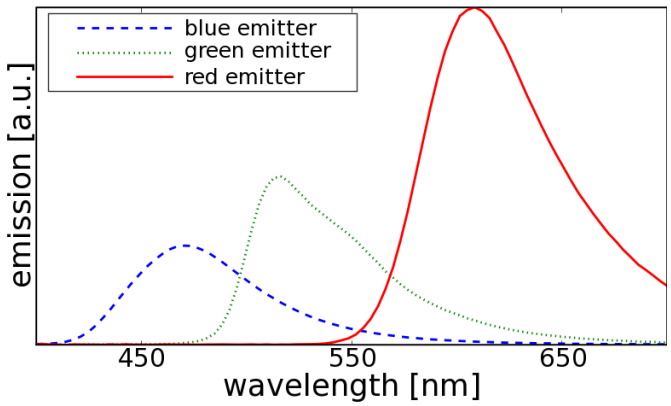

(b) The sum of these 3 spectra (blue, green and red) give a warm white light.

Figure 1.3: Two important properties of an OLED are its extraction efficiency and the spectra of its emitters.

1.4 Simulation tools for OLEDs

Simulation tools solve the equations of a **numerical model** which represents a real world device. By preference, the numerical model represents a 3d device. We use simulation tools to minimize the amount of costly prototypes by eliminating 'bad' designs in an early stage. In our case, we want an OLED design which has an extraction efficiency for light as high as possible. Thus, we start with a numerical model of the OLED. Then, we solve the equations of this model with a simulation tool. We will show that there are two types of numerical models to model optical behavior. We show that both numerical models are needed to model a substrate emitting OLED. However, a combination of these two types of numerical models did not exist. This is the contribution of our work.

To model the optical behavior of an OLED, we start with the integration of Maxwell's equations for the device of figure 1.3(a). Except for simple structures, an analytical solution does not exist. Therefore, a numerical model is required to numerically integrate Maxwell's equations. Depending on the thickness of the layer in the OLED, we classify two types of numerical models. The first type models layers which have a thickness of many wavelengths, such as the glass substrate. Then, light can be considered as incoherent plane waves. The combination of two plane waves is simply the sum of the energy flux of these two plane waves. The second type is used for layers which have a thickness of at most a few wavelength, such as the stack of organic layers. Then, light is considered as coherent plane waves. For coherent light, the sum of two plane waves depends on their phase, these two plane waves can 'cancel' each other out. In chapter 3, we will show that a combination of both types is required to model OLEDs which have a corrugation on either side of the substrate.

1.5 This work

The focus of this work is to increase the luminous power efficiency of a White OLED (WOLED). To increase the overall luminous power efficiency, we have looked at the two questions of section 1.3. The first question is how to increase the **efficiency** by increasing the light extraction. The second question is how to increase the **efficacy** by matching the spectrum to the sensitivity of the human eye.

The solution of the first question, how to increase light extraction efficiency, requires a design which has a corrugation of either the interface between organic layers-glass or between the interface between glass-air. (section 1.3) To simulate such a structure, a simulation tool has to combine the properties of two types of numerical models, coherent and incoherent, such as described by section 1.4. To the best of our knowledge, chapter 3 is the first to combine coherent and incoherent numerical models to numerically

integrate OLEDs .

To elaborate further on the first question, the previously described simulation tool has been used to optimize three structures with respect to the extraction efficiency. The first design has interference layers between the stack of organic layers and the glass substrate. This design is the RC^{2}LED, both simulation and experimental results will be the topic of chapter 4. Although this design already has been proposed for inorganic LEDs, this work describes the first experimental results. The second design has a grating between glass substrate and air. According to figure 1.3(a), the increase of extraction efficiency is due to the elimination of TIR at the interface between glass and air. The third design has a grating between organic layers and glass. Both numerical and experimental results are given in chapter 5. The main novelty in this last chapter are the simulation results which show the importance to include both coherent and incoherent waves.

A possible solution of the second question, how to increase the efficacy, is given in chapter 6. This chapter starts by showing the most optimal spectrum with respect to the luminous efficacy of a light source for a given chromaticity. This work is the first which gives the impact of the spectrum on the luminous power efficiency of an OLED with respect to the other properties of an OLED.

Chapter 7 stands slightly apart from the previous chapters. This chapter describes a numerical called 'complex Jacobi iteration' which was an alternative to the numerical model of chapter 3. Although it was less suited to simulate OLEDs, this model proved to be interesting to model non-linear optical components.

Finally, the basic conclusions and some perspectives of this work are described in chapter 8.

Because all chapters can stand on their own, some repetition between the different chapter may occur.

1.6 Publications

The work done during this thesis has led to some publications in international journals and also to presentations at national and international conferences.

1.6.1 Publications in international journals

- P. Vandersteegen, G. Schwartz, P. Bienstman, R. Baets, 'Luminous power efficiency optimization of a white organic light-emitting diode by tuning its spectrum and its extraction efficiency ', Applied Optics, 47(13), May 2008.
- P. Bienstman, P. Vandersteegen, R. Baets, 'Modeling gratings on either side of the substrate for light extraction in light-emitting diodes',

Optical and Quantum Electronics, 39(10-11), p.797-804, 2007.

- P. Bienstman, L. Vanholme, W. Bogaerts, P. Dumon, P. Vandersteegen, 'Python in Nanophotonics Research',Computing in Science & Engineering, 9(3), pp.46-47, 2007.

- P. Vandersteegen, B. Maes, P. Bienstman, R. Baets, 'Using the complex Jacobi method to simulate Kerr non-linear photonic components', Optical and Quantum Electronics, 38(1-3), pp.35-44, 2006.

- B. Luyssaert, P. Bienstman, P. Vandersteegen, P. Dumon, R. Baets, 'Efficient Nonadiabatic Planar Waveguide Tapers',Journal of Lightwave Technology, 23(8), pp.2462-2468, 2005.

- B. Luyssaert, P. Vandersteegen, D. Taillaert, P. Dumon, W. Bogaerts, P. Bienstman, D. Van Thourhout, V. Wiaux, S. Beckx, R. Baets, 'A Compact Horizontal Spot-Size Converter Realized in Silicon-on-Insulator',IEEE Photonics Technology Letters, 17(1), pp.73-75, 2005.

1.6.2 Publications in international conferences

- P. Vandersteegen, S. Mladenovski, V. van Elsbergen, G. Gaertner, P. Bienstman, K. Neyts, R. Baets, 'Luminous power efficiency of a white organic light-emitting diode by tuning its spectrum and its extraction efficiency' ,accepted for publication in SPIE Optics & Photonics 2007, United States, 2007.

- P. Vandersteegen, Angel Ullan Nieto, Carl Van Buggenhout, S. Verstuyft, P. Bienstman, P.P.P. Debackere, Kristiaan Neyts, R. Baets, 'Employing a 2D surface grating to improve light out coupling of a substrate emitting organic LED' ,Photonics West 2007: Integrated Optoelectronics Devices, 6486, United States, pp.64860H, 2007.

- P. Bienstman, P. Vandersteegen, R. Baets, 'Modeling light extraction in 3D organic LEDs containing photonic crystals',OWTNM, Denmark, pp.73, 2007.

- P. Vandersteegen, C. Van Buggenhout, A. Ullan Nieto, S. Verstuyft, P. Bienstman, K. Neyts, R. Baets, 'Increasing light extraction of a substrate emitting OLED using a 2D surface grating' ,2006 IEEE LEOS Annual Meeting Conference Proceedings , Canada, pp.502-503, 2006.

- P. Bienstman, P. Vandersteegen, B. Maes, R. Baets, 'Modeling methods for high-index contrast linear and non-linear nanophotonics' ,NUSOD 2006 (Numerical Simulation of Optoelectronics Devices) (invited), Singapore, 2006.

- P. Vandersteegen, P. Bienstman, R. Baets, 'Extensions of the Complex Jacobi Iteration to simulate Photonic Wavelength Scale Components',European Conference on Computational Fluid Dynamics (ECCOMAS CFD 2006), Netherlands, 2006.
- P. Vandersteegen, P. Bienstman, R. Baets, A. Dewandre, M. Haelterman, 'Simulations of Kerr based non linear optical components with the Complex Jacobi iteration',ICTON (COSTP11 training school), p.We.P.14, 2006.
- P. Vandersteegen, C. Van Buggenhout, P. Bienstman, R. Baets, 'Numerical Investigation of a 2D-Grating for Light Extraction of a Bottom Emitting OLED',ICTON, p.We.C.2.6, 2006.
- P. Vandersteegen, B. Maes, P. Bienstman, R. Baets, 'Simulating nonlinear third order effects with the adapted complex Jacobi iteration method' , IEEE/LEOS Symposium Benelux Chapter Proceedings, Belgium, pp.193-196, 2005.
- G.R.A. Priem, P. Vandersteegen, P. Bienstman, G. Morthier, R. Baets, 'Ultrafast, all-optical regeneration functionalities inside a Kerr-nonlinear platform' ,LEOS ANNUAL 2005, Australia, p.WF4, 2005.
- P. Bienstman, B. Maes, P. Vandersteegen, R. Baets, 'Modelling of nonlinear nanophotonic devices', OWTNM (invited), Australia, pp.32, 2005.
- P. Vandersteegen, P. Bienstman, R. Baets, 'Extending the Complex Jacobi Iteration method to simulate Kerr non-linear effects', OWTNM 2005, France, 2005.
- B. Luyssaert, P. Vandersteegen, W. Bogaerts, P. Dumon, P. Sanchis, J. Marti, R. Baets, 'A Versatile Optical Spot-Size Converter Design', European Conference on Optical Communication (ECOC), We(3), Sweden, pp. 468-469, 2004.
- B. Luyssaert, P. Vandersteegen, W. Bogaerts, V. Wiaux, J. Wouters, S. Beckx, R. Baets, 'Compact Photonic Spot-Size Converter', Photonic and Electromagnetic Crystal Structures (PECS-V), Japan, p.193, 2004.

1.6.3 Publications in national conferences

- P. Vandersteegen, P. Bienstman, R. Baets, 'Extension of a complex jacobi iteration technique to simulate wavelength scale photonic components', 5th FTW PHD Symposium, paper nr. 18, Belgium, 2004.
- B. Luyssaert, P. Vandersteegen, R. Baets, 'Compact Photonic Spot-Size Converters', FTW PhD symposium, Belgium, pp.57, 2003.

Imagine wallpaper that lights up.

Website of General Electric

2

Efficient Organic Light Emitting Diodes

Research into the White Organic Light emitting Diode (WOLED) for illumination is really multidisciplinary. During the last two decades, the increase of efficiency has required progress in physics, chemistry, optics and optometry. This chapter gives a general overview of the published research. Because of the central role of the extraction efficiency in this work, one section completely focuses on optics.

Overview

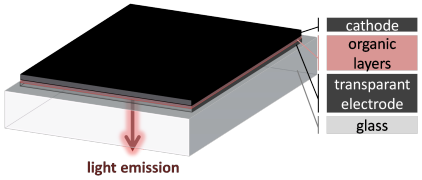

Figure 2.1: This perspective and cross section of a substrate emitting OLED shows that light is generated in the stack of organic layers. A top view of an OLED gives a large area of more than 100 square cm.

2.1 Structure and working principle of the OLED

This chapter starts with a simplified structure of an Organic Light Emitting Diode (OLED). As we will see, this structure is sufficiently general to describe a large class of OLEDs. Therefore, this simplified structure can be used as a starting point for the other sections. In this section, we also briefly discuss organic electronics and organic solar cells.

The OLED of figure 2.1 generates light in a thin stack of organic layers if a voltage is applied between the cathode and the transparent anode. Note that this sketch is not to scale. Thus the organic layers, cathode and anode combined are only in the order of a few hundreds nm, while the glass substrate is a few mm. Also, the area on which the stack of organic layers is deposited can be a few 100 square cm. Thus, the ultimate goal would be a fabrication by cheap deposition of an efficient OLED stack over a large area.

Applying a voltage gives an electrical current which is conducted by electrons and holes. These recombine to a photon through an intermediate state called the exciton. Though this description is quite general, it can be applied to most OLEDs, both used for illumination and as pixel in a display. [31][32][33][34][3]

Of course, the use of advanced organic materials is not restricted to OLEDs. Indeed, section 2.3 shows that the electrical properties of the materials in an OLED are similar to those of semiconductors. Therefore, organic solar cells [35] have been made, OLEDs have been integrated with 'classical semiconductor electronics' [36] and cheap organic electronics have been created. [37] All these applications have principles similar to inorganic semiconductors.

2.2 Important landmarks

It now has been little more than 20 years, since the first article of a bright green OLED with reasonable voltage (<10 V) was published in 1987. [5] Because of the small organic molecules used, vapor deposition was required for fabrication. Three years later, a green OLED with polymer organic molecules, which are larger than the small molecules and which were deposited from solution, was published by [38]. Moreover, conjugated polymer chains with high conductivity have already resulted in a chemistry Noble prize. [39] Because both approaches, the small molecule OLED (sm-OLED) and the Polymer OLED, each have typical advantages and disadvantages, both approaches will be addressed in section 2.3.3. Moreover, each approach has its own field of research.

In 1993, an article of the first White OLED (WOLED) was published. The white light was created by three different emitters which were in their own layer of the same stack of organic layers. Each emitter had its own color. Although the luminous power efficiency was lower than 5% of that of an incandescent light bulb, this was another important achievement. [7]

The increase of the electrical efficiency on the OLED has been the subject of two complementary approaches, both have been published in 1998. The first approach is doping of some of the organic layers by either a metal or an organic molecule, respectively [40] and [41]. This approach decreases the voltage at which the OLED can operate. The advantage of organic molecules compared to metal dopants is the higher stability of the OLED. The second approach is using dyes in the organic layers which can convert almost the energy of all electron-hole pairs into a photon. [8] These dyes are called phosphorescent emitters, compared to the previously used fluorescent emitters, which only have a conversion of 25%. More details on these approaches are given by respectively section 2.3.4 and 2.3.4.

An efficient blue phosphorescent emitter is at the moment of writing still one of the major problems to achieve high internal efficiency. However, a white OLED with a blue fluorescent emitter and a green and red phosphorescent emitter with a conversion of 100%, has recently been pusblished, [42]. More details can be found in section 2.3.6.

As stated earlier, today the OLED is considered to be a technology for efficient diffuse lighting sources or for bright displays and TVs. Although adoption of OLEDs for displays has been slower than predicted in a roadmap of 2004, [27], the first OLED-TV of Sony has hit the market at the end of 2007. To conclude, we mention two press releases on OLEDs for general illumination. Firstly, the European funded OLLA-project has demonstrated a lighting tile of 30 by 30 cm^2 with a luminous power efficiency of 50 lm/W at 1000cd/m^2. The lifetime is 10000 hours. [1] Secondly, Universal Display recently has claimed 102 lm/W at1000 cd/m^2, but the press release does not mention lifetime and size. [43] Note, no commercial light source to date exist. However, given the progress in the field, it is more than likely that

the OLED technology will find its way in mainstream applications.

2.3 Converting electrical power to photons

2.3.1 Introduction

The properties of the organic layer stack are important for both electrical and optical properties. The organic layer determines how much electrical energy is converted to photons. Also, the organic layer stack determines how light propagates in an OLED. Because of the central role of the organic layer stack in light propagation, this will dealt be with in a separate section, section 2.4. But this section starts with the structure and the electrical properties of the organic layer stack. Often, the design freedom of the structure of the organic layers is limited by its electrical properties. Thus, understanding electrical properties helps to understand the limitations on techniques which can be used to increase the extraction efficiency and the luminous power efficiency.

This section has four topics. Firstly, section 2.3.2 shows a simplified model on how current is converted to photons. Secondly, section 2.3.3 gives two main classes of OLEDs: polymer OLEDs and small molecule OLED (sm-OLED). In this section, we will see how each class influences the optical design. Increasing the conversion of electrical energy to photons is discussed in the next two sections. So, the third section, section 2.3.4 is about doping with dyes and section 2.3.5 is about doping the transport layers.

2.3.2 Band diagram of an OLED

For this work, a simplified model of the electrical properties of an OLED suffices. This model gives an idea how current is converted to photons. Thus, this model can be used as a starting point to understand the band diagrams which are found in literature. As we will see, this model is quite similar to the models used for inorganic LEDs. For example, the minimal voltage to create light can be estimated based on this model. To start, let us look at figure 2.2.

This figure shows the electrical band diagram of an ideal OLED to which a voltage of 2.6 V has been applied. This voltage is just big enough to straighten the energy levels of the band diagram. These energy levels are the lines in figure 2.2. If a voltage is applied, negatively charged electrons go from the cathode through the Lowest Unoccupied Molecular Orbit (LUMO) of the organic layers to the anode. Also, positively charged holes go from anode through the Highest Occupied Molecular Orbit (HOMO) of the organic layers to the cathode. Electrons can not have energies between LUMO and HOMO.

Electrons and holes form an intermediate exciton and decay radiatively. If the distance between LUMO and HOMO is given, both the minimal

voltage of the OLED and the wavelength of the photon are known. For example, the energy distance between LUMO and HOMO is $\Delta E = 5.4 - 2.8eV = 2.6eV$. Then, dividing the energy in eV by the elementary charge gives the corresponding voltage: 2.6 V. Also, the relation between energy and the wavelength of the photon is given by the well known equation:

$$\Delta E = h\mu = hc/\lambda \tag{2.1}$$

Starting from this equation, the external quantum efficiency of an OLED, $\eta_{external}$, can be estimated. [6] This external quantum efficiency gives the amount of power needed to generate optical power:

$$\eta_{external} = b_1 \frac{h\mu}{\Delta E} \eta_{recomb} \eta_{optical} \tag{2.2}$$

Three electrical parameters in this equation are the fractions of excitons formed by electron-hole pairs (b_1), the needed electrical energy (ΔE) and the amount of excitons which decay to a photon η_{recomb}. Moreover, the two optical parameters are the frequency of the photons (μ) and the extraction efficiency ($\eta_{optical}$). For an ideal OLED, we would $b_1 = 1$, $\eta_{recomb} = 1$ and $\Delta E = h\mu$.

Again, the previously described model is a simplification. However, this model is a starting point to understand the band diagrams which are commonly used in literature. Literature shows how conversion decreases due to mismatch between energy levels, no exciton formation ($b_1 < 1$), non radiative decay of the exciton (η_{recomb}) or Ohmic losses (V too high) can decrease conversion. Each of these topics will be addressed in the next subsections.

2.3.3 Small molecule OLEDs versus Polymer OLEDs

As stated in the introduction, the fabrication methods for small molecule OLEDs (sm-OLEDs) and Polymer OLEDs are different. The different fabrication methods give different layer structures and different properties, as can be seen on figure 2.3. Much more complicated multilayer stacks are possible for sm-OLEDs than for Polymer OLEDs.

Let us begin with a detailed comparison of the fabrication technologies. Then, the difference of the organic layer stack properties are discussed where we put special emphasis on the optical behavior.

On the one hand, fabrication of sm-OLEDs requires vacuum deposition. [44] On the other hand, fabrication of Polymer OLEDs can be done from solution. Thus, spin-coating and even printing on flexible metal foils is possible. [45] [36] As we will see, the first methods might result in higher efficiency, while the second might be cheaper.

The vacuum deposition techniques give a large control over the thickness of a layer which is deposited. Solution based techniques do not have this

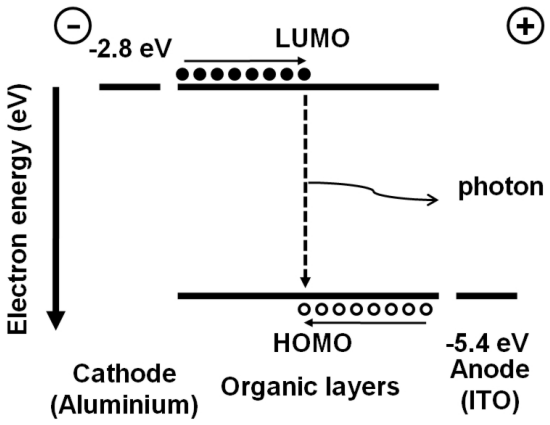

Figure 2.2: Band diagram of an ideal OLED. Applying a voltage gives an electrical. In the organic layers, you have electrons in the Lowest Unoccupied Molecular Orbit and holes in the Highest Occupied Molecular Orbit. Recombination of electrons and holes give a photon via an intermediate exciton.

control. Thus, in sm-OLEDs, higher control over the electrical behavior than the Polymer OLEDs fabrication is possible. Also, because of the control over electrical properties, the recombination and emission zone can be located at an optically optimal position. Thus, sm-OLED have better extraction efficiency. A complex multilayer structure might even be absolutely necessary to achieve ultrahigh luminous power efficiencies. [46] Although this paper also refers to methods to make more complex layer structures with solution-processed devices, this is not common practice. On the other hand, Polymer OLEDs can have anisotropic properties. [47] For example, anisotropy can give a larger fraction of in plane dipoles, which is beneficial for the extraction efficiency. To the best of our knowledge, this route has not been explored further.

Solution based fabrication of Polymer OLEDs appears to be more suited for mass fabrication than the vacuum deposition of sm-OLEDs, due to the possible lower cost. However, inline fabrication can achieve high vacuum throughput while maintaining the precise control needed for the layer thicknesses. Inline fabrication has been presented in 2004. [48] A full color device followed shortly. [49] [50] Finally, the inline evaporation of an advanced efficient device also has been presented. [51] Thus, a lot of effort is put in making mass fabrication of sm-OLEDs.

In conclusion, though in theory the Polymer OLED is more suited for mass fabrication than the sm-OLED, the sm-OLED outperforms the Polymer OLED in terms of luminous power efficiency. The main reason might be

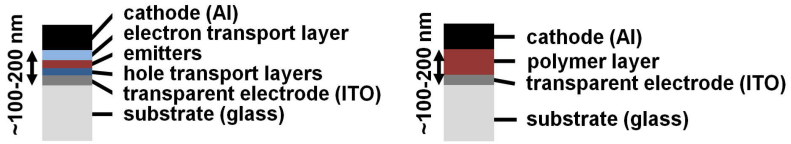

(a) The layer structure of a small molecule OLED

(b) The layer structure of a Polymer OLED

Figure 2.3: The layer structure of a small molecule OLED is more complex than the layer structure of a Polymer OLED. Note that these figure are not on scale, the substrate thickness is at least a few mm.

the precise control over electrical properties and the location of the emission zone.

2.3.4 Doping the emissive layer with dyes to improve internal quantum efficiency

Using dyes can greatly increase the fraction of excitons which excite a photon. Two types of dyes exist. Both types are used in either Polymer OLEDs or small molecule OLEDs (sm-OLEDs). On the one hand, we have fluorescent emitters of which the Internal Quantum Efficiency (IQE) is limited to 25%. This IQE gives the fraction of photons to electron-hole pairs. On the other hand, we have phosphorescent emitter which can have an IQE of 100%.

At time of writing, stable green and red phosphorescent emitters have been identified, a stable blue phosphorescent emitter not. This section aims to show the difference between these two types of dyes. At the end of this section, we also give an overview of companies which sell dyes.

Photon generation in an OLED requires two steps. Firstly, an electron-hole pair forms an intermediate state, the exciton. Then, this exciton has to radiatively decay to give a photon. Let us first look at exciton generation in detail. Then, we will show that for the second step dyes are needed.

Excitons are formed by one electron and one hole. Therefore, the total spin angular momentum of the exciton is either S=0 or S=1. These excitons are respectively singlets and triplets. If we have a spin-independent exciton formation, every exciton state has equal chance of being formed. Because figure 2.4 shows four possible states, the chance of each state is 25%. Note that the assumption of spin-independent exciton formation is only correct for sm-OLED. Indeed, the singlet-triplet ratio of Polymer OLED can go to 50%-50%. [52]. So, in an OLED, the singlets, which have spin angular momentum = 0 make up 25% of the total excitons.

However, radiative decay of an exciton to a photon only happens if the

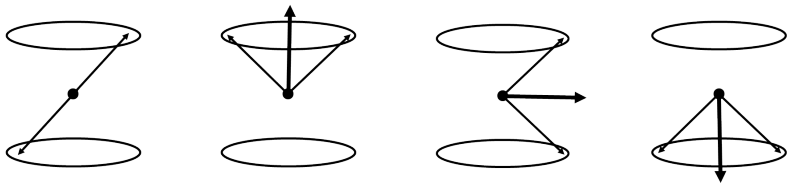

(a) Singlet state (S = 0, $M_S = 0$) (b) Triplet state (S = 1, $M_S = +1$) (c) Triplet state (S = 1, $M_S = 0$) (d) Triplet state (S = 1, $M_S = -1$)

Figure 2.4: Singlet versus triplet states

spin angular momentum is 0. Even then, dyes are needed to convert these 25% of the excitons. These dyes, which we call fluorescent emitters, increase the rate of radiant decay. This gives a decrease of the fraction of singlets which decay non-radiatively. However, a paper of 1998 showed dyes which gave a radiative decay of triplets in a small molecule OLED. [8] These dyes are called phosphorescent emitters. Later work even resulted in an IQE of almost 100%. [53] For Polymer OLEDs, phopshorescent emitters with an internal quantum efficiency of 100% were published in 2006. [46]. So, phosphorescent emitters are needed to achieve high efficiency.

As said before, only **stable** phosphorescent emitters for green and red have been identified. Although we have a blue phosphorescent emitter, FIrpic, [54] [55] a deep blue **stable** phosphorescent emitter still is outside reach. [56]. However, having no stable blue phosphorescent emitter can be circumvented for white OLEDs. We will come back on this remark in section 2.3.6.

A few companies can be found to buy dyes from. For example, Universal Display Coorporation, Merck and Kodak sell fluorescent and phosphorescent dyes for small molecule OLEDs. Cambridge Display Technology and Merck are producing fluorescent and phosphorescent dyes for polymer OLEDs. Note that only in July 2007 Cambridge Display Technology has been bought by Sumitomo Chemical.

2.3.5 Doping the transport layers to lower the voltage

Doping the transport layers in an OLED stack lowers the voltage, which directly improves the efficiency. Let us start with the lowest voltage needed. Equation 2.1 shows that a 'perfect' OLED requires about 2.4-2.8V, depending on the wavelength of the light. The lowest voltage is limited by the thermodynamical limit. [57] We will now discuss the influence on optical and electrical properties of doping the transport layers.

To optimize optical extraction, doped transport layers can help to place

the emissive layer at the most optimal location of the optical design, without negatively influencing the electrical properties. Indeed, because of the higher conductivity, the thicknesses of the doped layers can be varied with minimal impact on the electrical behavior. This optimal location of the emissive design will be addressed in section 2.4.

The other advantages result in an improvement of the electrical properties, as described by [40]. This paper describes doping the transport layers with metal particles. For stability, molecular doping however is superior. [41]. The improvement of the electrical properties is caused by two effects. The first effect is the much higher bulk conductivity of the hole transport layers. This results in a lower driving voltage of the OLED, which directly influences the efficiency. Decreasing the voltage by a certain factor automatically gives a efficiency increased by that factor. Of course, the lowest voltage you can have for an OLED is in relation to the most energetic photon which this OLED emits. ($eV = h\mu$, [6]) The second effect is the improvement of the electrical behavior at a metal/organic interface. A high doping of the organic interface leads to an efficient injection of holes at the metal/organic interface, similar to highly doped Schottky contact at an inorganic semiconductor surface acts as a Ohmic contact. Thus, adaptability to various substrates becomes possible.

Commercialization of these techniques has been done by NOVALED with their PIN-technology. Electron Transport Materials have been commercialized by Sanyo and Hole Transport Materials by Xerox.

2.3.6 Generating white light with OLEDs

Different OLED structures can be used to generate white light. Usually, white light requires at least two different colors. Generating at least two colors in one structure can be done with a wide variety of structures. These structures are discussed in this subsection.

First, we look at structures which can be applied for both sm-OLED stacks and polymer OLED stacks. Then, we will look at structures which use more complex layer stacks. Then, a sm-OLED needs to used.

Figure 2.5 shows three approaches which can use a less complex organic layer stack for white light.

First, the OLED stack of figure 2.5(a) emits light over a short bandwidth. Then, a downconversion layer, most often a phosphorescent layer, absorbs and re-emits light with a longer wavelength. Thus, an efficient blue emitter has to be used. [58] Note, an efficient blue *stable* emitter is still to be found. Secondly, the structure of figure 2.5(b) combines the light of three **distinct** OLEDs. [34] Thirdly, the structure of figure 2.5(c) uses one layer stack which generates white light.

Now, let us compare these three approaches. The structures of figures (a) and (b) are already commonly used in inorganic LEDs for illumination. Also, these approaches can have higher efficiency than the approach of (c),

mainly due to the higher efficiency of an OLED with a limited bandwidth range, compared to an OLED optimal over a large bandwidth range. For example, we will see in chapter 4 that the extraction efficiency is much easier to optimize for a small bandwidth range. The first structure also has the advantage of low differential aging. Differential aging means that two different colors of a structure shave a different degradation time. If the phosphor of the down conversion layer has a long lifetime with respect to the lifetime of the blue emitter, the color of the structure will be quite stable. The third structure generates all colors in one stack. Thus, different dopants can have different aging. However, this color shift has recently been addressed. [59]

The optical design of the structure of figure 2.5(c) has the advantage that its fabrication process only requires deposition of one stack organic layers on one substrate. However, designing an efficient stack of organic layers is no small feat. Different types of stack of organic layers can be used to produce white light. For polymer OLEDs, all emitters need to be embedded in the only layer of that OLED. For sm-OLEDs, more approaches exist as can be seen from figure 2.6.

Figure 2.6(a) shows how light is generated in **one** emissive layer. Either multiple dyes may be used in one emissive layer [7] or one single dopant can give white light. [60] The approach of figure 2.6(b) uses an emissive layer for each dye. This approach allows to place the emissive layer of each color at their own ideal optical place. The most efficient WOLEDs in literature use either a complete phosphorescent device or a blue fluorescent dye in combination with fluorescent green and red emitters. For example, [33] discusses an OLED with three phosphorescent dyes. However, because the low lifetime of the blue phosphorescent emitter, a stable structure has been presented with a blue fluorescent dyes and green and red phosphorescent dyes. [17] Note that the internal quantum efficiency is limited by the blue fluorescent emitters. However, only recently, some layer stacks with a blue fluorescent emitter can circumvent this low internal quantum efficiency. [42] [61] The singlet excitons decay radiatively on the fluorescent dye, the triplets however go to the phosphorescent dye.

Figure 2.6(c) can be seen as a concatenation of the stacks of figure 2.6(a) and 2.6(b). A commonly used name for this approach is the multistack OLED. [62] Note this approach makes it difficult to place the emissive layers at their optimized optical place. However, this approach is beneficial for efficiency and lifetime. Indeed, this OLED requires less current to achieve the same brightness. If each set of emissive layers gives a brightness of I, then using n sets of layers, gives a total brightness of nI, but for the same current as one set of emissive layers. This lower current has a positive effect on lifetime and efficiency. However, additional layers have to be inserted between the two emissive to ensure a proper generation of electrons and holes. Moreover, the voltage of this structure scales linearly with the number of emissive sets. Having n sets gives a voltage of nV, where V is the voltage

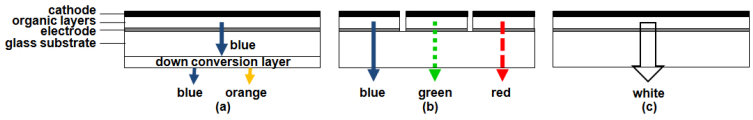

Figure 2.5: Different device structures to generate white light. (pictures adapted from [34]) (a) Some of the generated blue light is downconverted to orange/red. [58] (b) Each color is generated by a separate OLED-pixel. (c) White light is generated in one stack of organic layers. (see also figure 2.6)

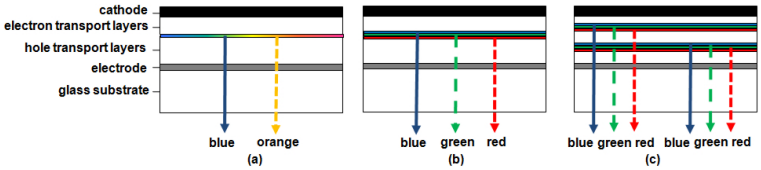

Figure 2.6: White light is generated in **one** stack of organic layers. (a) All dyes in one emissive layer (b) Each dye, its own emissive layer. (c) Stacking multiple sets of emissive layers allows to lower the current while keeping the same brightness.

over one set.

This section has given different approaches to create white light. Regardless of the structures, we can formulate some rules of thumb. Generating only one color per stack gives the highest flexibility to improve optical and electrical properties, figure 2.5(a) and 2.5(b). These structures can be used for both polymer OLEDs and sm-OLEDs. If we generate multiple colors in one stack, the dyes are best placed in their own emissive layer, figure 2.6(b). This approach however is restricted to sm-OLEDs. In the following section, the optimal location of the dipole is determined for an OLED. Depending on the type of OLED used, figure 2.5, it might be difficult to pinpoint the emissive layer at that specific location.

2.4 Extracting photons

2.4.1 Introduction

Light extraction plays a key role to achieve OLEDs with a high luminous power efficiency. For example, equation 2.2 already shows how the radiant flux linearly scales with the extraction efficiency. However, the extraction effic This section derives this crude estimation with some basic assumptions.

organic layer	47 %
substrate	34 %
air	19%

Table 2.1: Fraction of light in each layer

To estimate the extraction efficiency, the simplified OLED of figure 2.7(a) is used. As stated before, the low extraction efficiency is caused by TIR. TIR happens when light which is under a too oblique angle, goes from a material of high refractive index to a material of low refractive index. At the interface between these materials, light under a too oblique angle is completely reflected. The smallest angle for which TIR happens, can be calculated by substituting $\theta_2 = \pi/2$ in Snellius' law:

$$n_1 \sin(\theta_1) = n_2 \sin(\theta_2) \tag{2.3}$$

This smallest angle θ_1 then is the **critical** angle θ_c. Now, to simplify the situation, we make **two** assumptions. First assumption: if light is incident under an angle $\theta_1 < \theta_c$, we have **full** transmission. And, if light is incident under an angle $\theta_1 \geq \theta_c$, we have TIR. Second assumption: light emission in the organic layer is completely uniform.

With the refractive indices of the simplified OLED of figure 2.7(a), we now find for the extraction efficiency:

$$\frac{2\pi(1 - \cos(\arcsin(\frac{\theta_2}{\theta_1})))}{4\pi} = \frac{2\pi(1 - \cos(\arcsin(\frac{1.0}{1.7})))}{4\pi} = 19\% \tag{2.4}$$

Also, we can calculate with these assumptions the values for table 2.1, which gives the fraction of energy in each of the layers.

Note that we only consider the first and last layer of figure 2.7(a) to find the angle of total internal reflection. That extraction efficiency does not depend on the intermediate layers comes from the second assumption. As long as these intermediate layers have a sufficiently high refractive index and low losses to support light transmission, these layers can be ignored. Thus, even an almost perfect AR-coating, such as the one described by [63], would not improve the extraction efficiency.

To increase the extraction efficiency, we can distinguish two strategies. Firstly, interference effects can change the angular emission in glass and thus the amount of light inside the extraction cone of the substrate. Then, these interference effects can be introduced by adding interference layers between organic layers and substrate. Secondly, figure 2.8 shows how corrugations can eliminate TIR at each interface.

Although the main focus of this work is increasing extraction efficiency, the angular emission of an OLED will also be discussed. This property is usually expressed in radiant intensity which gives the power per unit solid

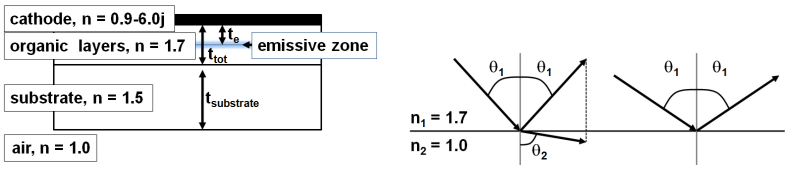

(a) The 3 main regions of a simplified OLED and their representative refractive indices.

(b) Total Internal Reflection happens when oblique light travels from high index material to low index material

Figure 2.7: An OLED is limited by total internal reflection.

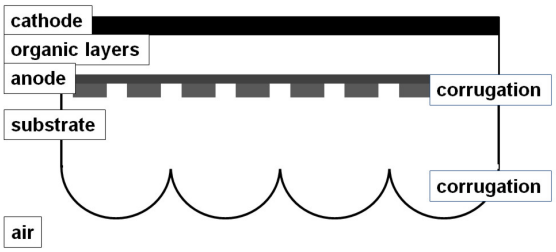

Figure 2.8: A corrugation can be placed at the interface between the organic layers-substrate and the interface between the substrate and air.

angle, which is emitted by an effective area. For a diffuse light source, we aim to have Lambertian emission. [64] For an observer, this gives a surface which has the same brightness regardless of the viewing angle. Thus, the radiant intensity has to vary with the cosine of the angle between view angle and the direction perpendicular to the surface.

To conclude, for a simplified OLED, we estimate an extraction efficiency of 19%. The following seven sections will now discuss the extraction efficiency in more detail. The first two sections, 2.4.2-2.4.3, will discuss the shortcomings of the simplified model of this section. Then, section 2.4.4 discusses a principle to determine the contribution of multiple round trips to the extraction efficiency. To finish, sections 2.4.5 to 2.4.8 discuss techniques to increase the extraction efficiency.

2.4.2 Refractive indices of the OLED stack

To determine the propagation of an electromagnetic wave, the refractive indices in which this wave propagates, are necessary. Thus, any optical model of an OLED uses the refractive indices as a starting point. Therefore, this section gives some representa

Roughly speaking, we can distinguish four regions: the cathode, the stack of organic layers, the anode and the substrate. In each of the regions, the refractive index is more or less the same.

Our first focus is the refractive index of the stack of organic layers. In most of the papers we refer to, these layers are assumed to have a refractive index of around 1.7-1.8. Moreover, these papers assume **isotropic** refractive indices. This is valid for OLEDs based on small molecule OLEDs, but this may not be true for polymer OLEDs. Section 2.3.3 already showed that the difference is due to the fabrication method. In a sm-OLED, the deposition of the molecules gives no preferential direction. For polymer OLEDs, solution based fabrication gives a preferential direction in which the molecules are laid down. In turn, the optical properties will be **anisotropic**. Moreover, this anisotropy is **uniaxial**, which means the value of the refractive index perpendicular to the interfaces is different from the refractive index parallel to the interfaces. [65]

The cathode and the anode can impact the optical behavior of an OLED, besides the impact on the electrical properties. Although for the cathode a number of options exist, most papers discuss either Silver (Ag) or Aluminium (Al), mostly in combination with a very thin LiF layer for better electron injection. The main optical difference between these cathodes is the better reflectivity for red light of the silver cathode compared to the aluminium cathode. The exact refractive index depends on the fabrication process. Therefore, the refractive indices will be discussed later on.

The most used anode for substrate emitting OLED is Indium Tin Oxide (ITO). Because of the grown popularity of ITO in displays and detectors, the price of Indium has steadily increased during the last decade. So, ITO's

increasing price has been the incentive to find replacements. One promising alternative for ITO, PEDOT:PSS formulation Baytron PH500, has been synthesized by Starck and has been succesfully applied for OLEDs. [66] Optical absorption of PEDOT:PSS however is a few orders of magnitude larger than the highly transparent ITO. This disadvantage will be addressed in chapter 5. Another alternative, ZnO, also has been published, [67]. Both alternatives have a refractive index which is lower than the refractive index of ITO: $n_{ITO} = 1.9, n_{PEDOT} = 1.47$.

The previously mentioned anodes and cathodes are mostly used for substrate emitting OLEDs. For top emitting OLEDs, the cathode can also be Ag or Al. However, for top emitting OLEDs, the anode usually is a thin semi-transparent metal layer of around 10-20nm sits between the organic layers and air. [68]

To conclude, the refractive indices of figure 2.7(a) are sufficient for the simplified model of section 2.4.1. However, to rigorously model an OLED, more accurate refractive indices have to be used.

2.4.3 Interference effects to determine the optimal dipole location

This section refines the simple model of section 2.4.1 by taking into account Fresnel reflections at interfaces. The simple model of section 2.4.1 assumed to have either full transmission or to have total reflection at an interface. However, the reflection at the interface between two materials varies with the incident angle. This section discusses the impact of Fresnel reflections.

Figure 2.9 shows an important consequence of light reflection: interference effects can occur. A plane wave makes multiple round trips. During each round trip, we have either constructive or destructive interferences which in turn give a higher or lower angular emission in a given direction. Then, an increase of the angular emission in the extraction cone increases the extraction efficiency. The focus of this section is to optimize the extraction efficiency by tuning two parameters: the location of the emissive zone and the thickness of the organic layers.

Now, to calculate the extraction efficiency, we use the simplified OLED of figure 2.9. A dipole is placed inside the organic layers at a certain distance z_e with respect to the cathode. We assume the cathode to be a perfect reflector. The refractive indices of the organic layers and the substrate are given by respectively $n_{org} = 1.7$ and $n_{sub} = 1.5$ Also, the thickness of the organic layers is given by t_{org}. Now, figure 2.10 gives the extraction efficiency in function of these two parameters. The calculation has been performed by calculating the total light inside the extraction cone of the substrate with the tool of chapter 3. We see that the extraction efficiency is maximal at:

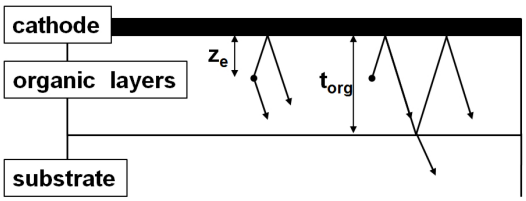

Figure 2.9: Interference effects happen because of reflection at two interfaces: cathode-organic layers and organic layers-substrate. These reflections determine the optimal position of the emissive zone and the thickness of the stack of organic layers. (adaptation of [69])

$$\begin{aligned} \frac{z_e n_{org}}{\lambda} &= \frac{1}{4} + \frac{n}{2} \\ \frac{t_{org} n_{org}}{\lambda} &= \frac{3}{4} + \frac{n}{2}, \; n \in I\!N \end{aligned} \tag{2.5}$$

The optimal distance of the dipole with respect to the cathode is a quarter of the effective wavelength and the optimal thickness of the organic layers is around three quarters of the effective wavelength. The effective wavelength is defined as the ratio of wavelength to refractive index. The first condition of equation 2.5 sometimes is called wide-angle interference, the second condition sometimes is called multiple-beam interference. [69]

For these two conditions, we have **constructive interference**. Indeed, a plane wave which starts from the dipole of figure 2.9 travels $\lambda/4n_{org}$ in the perpendicular direction before reaching the mirror. This is a phase difference with respect to the source of $\pi/2$. Then, the perfectly reflecting mirror gives an additional phase shift of π. If this plane wave is back in the emissive region, it has total phase difference of 2π. A similar reasoning gives constructive interference for the second condition of equation 2.5. Thus, these conditions directly follow from the assumption that we need constructive interference in the perpendicular direction.

In both cases, every round-trip of a perpendicular traveling plane wave, constructive interference happens, and thus this direction is favored above other directions. More light is emitted in the extraction cone and less light is emitted off-axis, which in turn gives an increase of the extraction efficiency. A similar reasoning can be used for off axis interference effects, as will be discussed in chapter 4.

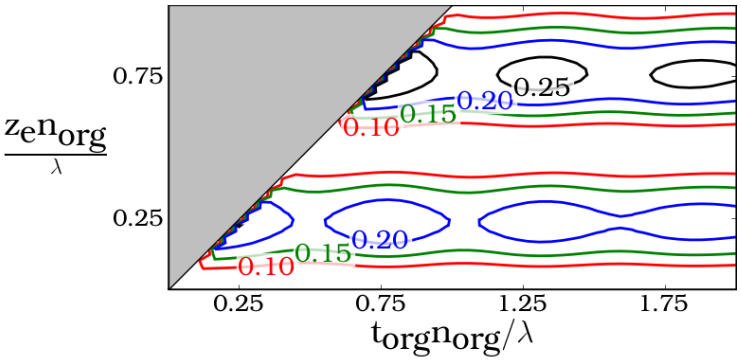

Figure 2.10: The extraction efficiency is given in function of the dipole location with respect to the cathode (z_e) and the thickness of the organic layers (t_{org}). (adaptation of [69])

2.4.4 Direct transmission through the substrate of an OLED

This section discusses the maximal **direct** transmission through a lens on top of the substrate of an OLED. Here, direct transmission means the light which directly passes through the substrate. Thus, this light does not make multiple round trips in the substrate before extraction. Though we use a lens, the principle of this section is also valid for other extraction techniques. The reason for this section is to make a clear distinction between light extraction by direct transmission and by multiple round trips in the substrate. Both mechanisms can increase the extraction efficiency. For example, we can use instead of one big lens an array of micro lenses. However, the size of the lenses determine how much of the extraction efficiency is contributed by direct transmission and how much by multiple round trips. Thus, estimating the maximal direct transmission helps to distinguish between light which is extracted in direct transmission and light which is extracted by multiple round trips.

Let us begin with the increase of the extraction efficiency by using a lens on top of the substrate. Table 2.1 showed that about 34% of the total generated light is trapped in the substrate by Total Internal Reflection (TIR). Only 19% escapes to air. To eliminate TIR, we can place a large lens on top of the OLED. Then, all light is incident on the curved surface under an angle smaller than the critical angle (θ_c). Now, almost all light can pass the substrate in direct transmission. Thus, we have an extraction efficiency of almost 34% + 19%. However, this conclusion uses two assumptions. Firstly, light is perpendicular indicent on the surface of the lens. Secondly,

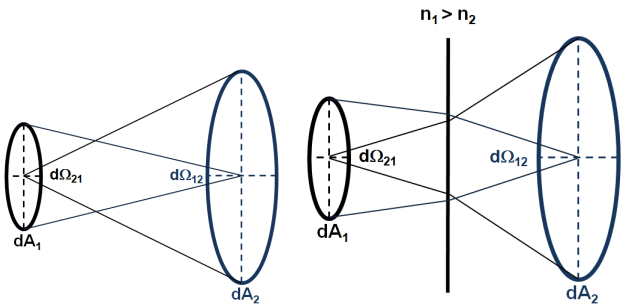

(a) in a homogeneous medium (b) at the interface between two materials with different refractive indices

Figure 2.11: Conservation of étendue can be used to express the limitations in direct transmission.

we neglect losses due to Fresnel reflections.

Thus, to extract all light in direct transmission, we need a very large lens. Indeed, the relation between the size of the lens and the fraction of light which passes the substrate in direct transmission directly follows from conservation of étendue. [70] Etendue gives the relation between the area of a surface through which a ray passes, dA_1, and the solid angle under which the illuminated surface is seen, $d\Omega_{12}$.

$$dA_1 d\Omega_{21} = dA_2 d\Omega_{12} \tag{2.6}$$

Without going into details, this definition indicates that conservation of etendue is related to conservation of radiance. Also, étendue is especially useful for optical systems which are much larger than the wavelength of light. Then, we may use basic ray optics to describe the optical behavior for the system. Conservation of étendue implies that étendue never increases, only decreases, regardless of the optical system.

Although equation 2.6 is trivial to prove for the system of figure 2.11(a), this equation is valid for any optical system, regardless of the number of lenses between the two surfaces. If the two surfaces dA_1 and dA_2 are at locations with different refractive indices, this equation has to be adjusted as can be seen from figure 2.11(b):

$$n_1^2 dA_1 d\Omega_{21} = n_2^2 dA_2 d\Omega_{12} \tag{2.7}$$

Now, let us apply conservation of étendue to determine the minimal size of a lens to have maximal direct transmission through the substrate. For

numerical values, we use figure 2.7(a). So, we have light which comes from a surface of dA_1 in a refractive index $n_1 = 1.5$. We want this light to go **in direct transmission** to an area dA_2 with a refractive index $n_2 = 1.0$. Because light can be under any angle at both sides:

$$d\Omega_{21} = d\Omega_{12} = 2\pi \tag{2.8}$$

Thus, equation 2.7 shows that **for direct transmission** through the substrate, the area after the lens (dA_2) has to be at least 2.25 times larger than the active region (dA_1) of the OLED. Note that this area after the lens is equal to the 'flat' bottom of the lens, not the curved surface. Important, we learn that an array of micro lenses will **not** increase light extraction by improving the fraction of light in direct transmission. Instead, a large fraction of light will be reflected at the lens-air interface. Extraction only happens through scattering after multiple round trips.

In conclusion, conservation of étendue helps to estimate the minimal size of a lens to have direct transmission through the substrate. If we do not wish to use such a large lens, multiple round trips will play a key role to determine the extraction efficiency.

2.4.5 A high refractive index substrate

One simple way to eliminate Total Internal Reflection (TIR) at the interface organic layers-substrate is by matching the refractive indices of organic layers and substrate. In section 2.4.1, we already saw that the interface between organic layers and substrate limited the extraction efficiency to 50%. The refractive indices are respectively 1.7 and 1.5. Thus, using a high refractive index substrate increases the fraction of light which can escape to the substrate. [71]

A high refractive index substrate increases the amount of light which is trapped in the substrate. For a planar OLED, the actual extraction efficiency is not increased. Only indirectly, the extraction efficiency can be increased by using lenses. Indeed, according to section 2.4.1, the estimated extraction efficiency of a planar OLED does not depend on the intermediate substrate layer. However, lenses might be used to extract light which is trapped in the substrate. If we use lenses, we again can use equation 2.7 of section 2.4.4 to estimate the fraction of light which is extracted in direct transmission. We see that using a substrate of higher refractive index lowers the fraction of light which can escape in direct transmission.

So, using a substrate with higher refractive index increases the amount of light which can escape to the substrate. Lenses then can extract this light. However, a higher refractive index substrate requires more multiple round trips for the light to be extracted. To the best of our knowledge, the referred paper is one of the few which mentions this route.

2.4.6 Interference layers

Multiple layers with different refractive indices between the organic layers and the substrate can increase the extraction efficiency by changing the angular emission.

The angular emission strongly depends on the amplitude and phase of the reflection at the anode *and* at the cathode. Then, constructive and destructive interference changes the angular emission in the substrate. However, if we increase the fraction of light inside the extraction cone, the extraction efficiency can be increased. Note that interference effects are highly wavelength dependent. Thus, depending on the angle, the color of the OLED may shift. Also, we still have Total Internal Reflection (TIR) at the interface substrate-air. This section gives an overview of the different approaches described in literature.

Let us begin with one interlayer at the transparent side of an OLED. For a substrate emitting OLED, we can use an interlayer between anode and substrate. Then, the interference layer can have a refractive index either higher or lower than the substrate. [70] [72] For example, a thin silver layer between anode and substrate theoretically gives a relative improvement of more than 2. [70] The relative improvement of other high refractive index materials as interlayers is much lower, because of the lower reflectivity. If we use an aero-gel with a low refractive index of n = 1.03 (!), experiments show an improvement of the extraction efficiency by a factor of 1.8. [72] However, simulations do not show this improvement. [70] This article claims that the increase of extraction efficiency is caused by scattering as opposed to micro cavity effects. The extraction efficiency of a top emitting OLED also benefits from one interference layer at the transparent cathode. [73] Strictly speaking, light intensity in the forward direction increases by a factor of 1.7. However, these experiments show a change of the emission spectrum of the green OLED. This change indicates a wavelength dependent extraction efficiency.

Other papers use a more complex set of interlayers at the transparent side of the OLED. One of the most well know set of interference layers is the Bragg mirror for a substrate emitting OLED. This mirror is created by an alternation of layers of low refractive index and high refractive index. Because the thickness of these layers is a quarter wavelength, a very strong reflecting mirror can be created. High reflectance is needed for high interference effects. One of the first papers with such a complex mirror use this mirror as a highly wavelength dependent filter. [74] At three peaks, a minor improvement is noticed. However, at others wavelengths, light extraction is strongly decreased. For lighting applications, which require a very broad wavelength range, a filter is disadvantageous. However, display application may make good use of this behavior. Filtering the correct colors gives very saturated colors, which are beneficial to create a large gamma of colors. Nevertheless for lighting applications, no overall improvement of

the extraction efficiency is noticed. A similar approach has been used in [75]. Three peaks give an increase of the brightness of 1.6. However, the extraction efficiency is decreased at other wavelengths.

Wavelength dependence of the angular emission can be decreased by sacrificing some of the increase of the extraction efficiency. [76] Numerical simulations show how the dispersive properties of the refractive index of the interference layers improve the angular dependence.

Now, we can also tune the extraction efficiency by using a different cathode in a substrate side OLED. [77] Mostly, an Al-cathode is used. However, different cathodes, such as silver (Ag) and Aluminium (Al), have a different reflectivity. Thus, the extraction efficiency depends on the cathode **and** on the interference layers at the anode-substrate side. [77] shows that the extraction efficiency of an OLED **without** interference layers at the anode side does not depend on the cathode. But, the increase of the extraction efficiency for an OLED **with** interference layers depends on the cathode. For two OLEDs with the same interference layers and Al or Ag cathode, the relative increase of the external quantum efficiency is 15% and 60% respectively. Two remarks. Note the improvement of only 15% is not in contradiction with the results of the previously described papers. This paper averages the external quantum efficiency out over the total emission spectrum of the red emitter. The previously described papers focus on one wavelength. Secondly, the better result of the OLED with Ag-cathode is limited to red. The reflectance of silver is only higher for wavelengths in the red. For other wavelengths, such as blue and green, the reflectance of a silver or aluminium cathode is almost equal. Thus, for red, an Ag cathode gives a higher extraction efficiency than an Al-cathode. But, averaging over a wide wavelength range limits the increase of the extraction efficiency for both cathodes.

In conclusion, the maximum relative improvement for one wavelength of an OLED with interlayers is around 70%. However, this positive effect is mostly cancelled out by the decrease of the extraction efficiency at the other wavelengths. Based upon these findings, chapter 4 will discuss a novel type of interference layers for OLEDs: the RC^{2}LED. This section also has shown that a highly reflective cathode such as Ag can improve the extraction efficiency. However the two most commonly used cathodes, Ag and Al, have equal reflectance for blue and green emission. For red emission, Ag shows an increase of the extraction efficiency compared to Al. A more detailed discussion of corrugations like microlenses in combination with interference layers will be in section 2.4.7.

2.4.7 Corrugation of the interface between substrate and air

A corrugation of the interface between substrate and air increases the extraction efficiency by eliminating Total Internal Reflection (TIR) at this in-

terface. Note that TIR always is present, even if the 'perfect' Anti-Reflection coating of [63] is placed between substrate and air. Only a corrugation of an interface can eliminate TIR. For example, figure 2.8 shows a sketch of an array of micro lenses on top of the substrate. These micro lenses typically have a base area of a few tens of micrometers by a few tens of micrometers. Thus, the size of this corrugation is much larger than the wavelength we want to extract. Micro lenses have been extensively discussed in literature. The main reason for their popularity is their easy attachment to an OLED. We simply attach a foil which has micro lenses on top of a flat OLED with a refractive index matching gel.

Let us first determine how light extraction works for an array of micro lenses. Indeed, section 2.4.4 was on direct transmission through the substrate in function of the size of the base area of the lens. The base area of a lens has to be at least 1.5^2 times the active area to extract all light by direct transmission through the substrate. If the base area of the lens(es) is smaller, light has to make multiple round trips before leaving the substrate. Thus, for micro lenses or other corrugations of the substrate, scattering after multiple round trips will be the main mechanism for light extraction.

One article gives a relative improvement of 50 % for an OLED with microlenses of 10 μm. [78] Another paper theoretically and experimentally verified that the optimal base surface of micro lenses is around 10 μm. [79] However, an experimental improvement of 80% was found.

The increase of the luminance in function of the ratio of the base surface of the lens area to the total area has also been investigated. [12] A relative improvement of 60% is found if there is no distance between microlenses.

Finally, micro lenses can be used in combination with interference layers. For more information on interference layers, see section 2.4.6. One OLED with interference layers and micro lenses shows an improvement of 80%. The irregular spacing of the microlenses showed that a precise design is not so important. Moreover, the OLED with interference layers and microlenses had a much better angular dependence of the spectrum compared to the OLED with only interlayers. [80]

In conclusion, micro lenses can increase the extraction efficiency by about 80% over a wide wavelength range. The size of these microlenses is much larger than the wavelength we want to extract. Moreover, microlenses can eliminate the angular dependence of the spectrum of OLEDs with interference layers. The major advantage of microlenses is their easy attachment to an OLED by attaching a foil with microlenses to a flat OLED and with a refractive index matching gel.

2.4.8 Corrugation of the interface between organic layers and substrate

A corrugation of the interface between organic layers and substrate increases the extraction efficiency by eliminating Total Internal Reflection (TIR)

at this interface. Section 2.4.1 shows that approximately 50% of light is trapped by TIR. This section discusses several key results from literature. Note that **metal** gratings which use plasmons are rarely mentioned. Most articles are on **dielectric** gratings at this interface. Although we give an extensive overview of fabrication methods of dielectric gratings, we also focus on the possible mechanisms which contribute to the extraction efficiency.

Metal corrugations of the interface between organic layers and substrate have been rarely mentioned in literature. These metal gratings have been proposed to increase light extraction by a two-tier mechanism. First, the generated light couples to a plasmon. Then, the grating couples light to an angle inside the extraction cone of the substrate. [81] So far, this principle only has been verified for an OLED under photoluminescence. No electroluminescent OLED has been demonstrated so far.

As stated before, dielectric gratings have been extensively mentioned in literature. Note, these gratings usually have a period which is in the same order as the wavelength we want to extract. We now give the main experimental results. To the best of our knowledge, simulation results are either rare or not in line with the experimental data.

The most common fabrication technique is interference lithography. This technique is also known as two beam holography. Two coherent rays create an interference pattern in resist which gives after development a grating. After etching, this pattern is transferred to the glass substrate. Because a large area can be patterned at one moment, the technique is suited for mass fabrication.

Four subsequent papers of the same authors use this fabrication method for small molecule OLEDs (sm-OLEDs). [82] [83] [84] [13] The first three papers conclude that a planarization layer between ITO and grating avoids a negative effect on the electrical behavior by the grating. The grating itself is made by holes which are etched in the glass substrate (SiO_2). These holes then are filled and planarized with SiN_x. Thus, a thin layer of SiN_x is between the grating and the ITO anode. The relative improvement of this design is around 50-60%. The last paper however creates a higher refractive index contrast by replacing SiO_2 by Spin on Glass. The refractive indices are respectively 1.5 and 1.25. For this last paper, first a thin layer of SiN_x is deposited on top of glass. Holes are fabricated in this layer after which a planarization with Spin-on-Glass is done. Because of the low refractive index of Spin-on-Glass, the distance between grating and ITO has to be as small as possible. Otherwise light which is trapped in the organic layers is not affected by the grating. This last design shows a relative improvement of 80%. A design with SiN_x and Spin-on-glass also has been shown to give a relative improvement of 200% for polymer OLEDs. [85]

Direct patterning of the ITO anode of a polymer OLED gives a relative improvement of 30%. [86]. A grating in the ITO-layer also means that the organic layers follows the pattern. The second fabrication technique is nano imprint. A relative improvement of 50% has been found. [87]

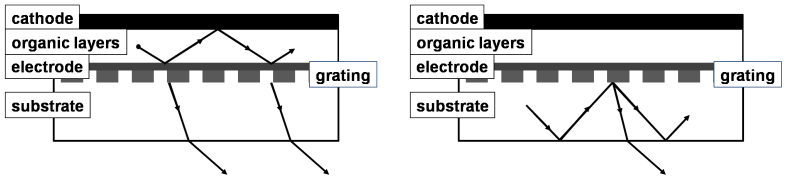

(a) *Direct transmission*: Direct transmission of light which normally is trapped in the organic layers

(b) *Multiple pass transmission*: Light which is reflected at the substrate-air interface, can be scattered to an angle smaller than the critical angle

Figure 2.12: A grating at the interface between organic layers and substrate has two mechanisms to increase light extraction.

So far, we have mentioned the fabrication techniques and the relative improvements of the extraction efficiency. Now, we focus on two mechanisms which might explain the increase of the extraction efficiency. As stated in section 2.4.1, about 50% of the generated light is trapped in the organic layers. Most authors claim that the extraction efficiency increases by increasing the fraction of light in direct transmission. This mechanism is illustrated by figure 2.12(a). The grating diffracts light to diffraction orders inside the extraction cone. For that reason, most simulation tools focus on the angular emission in the glass substrate. The larger the angular emission in the glass substrate, the larger the extraction efficiency is.

However, the mechanism of figure 2.12(b) also increases extraction efficiency. Light which normally is trapped in the substrate can be extracted by the grating after this light has been reflected by the substrate-air interface. This reflected light is scattered at the grating after the first, second, third, ... incidence.

In conclusion, gratings increase the extraction efficiency by 80% depending on the refractive index contrast. This effect has been experimentally demonstrated for polymer OLEDs and sm-OLEDs. Because all these experiments have been performed for OLEDs with one emitter, the effect for white OLEDs remains to be seen. In the papers we refer to, most authors contribute the increase of the extraction efficiency to the increase of light which can escape the substrate in direct transmission. The scattering of light after multiple round trips in the glass substrate is usually neglected. Chapters 3 and 5 show how and why our work takes into account these multiple round trips.

2.4.9 Conclusion

A planar OLED has an extraction efficiency of about 20%. The remainder of the light can be found in the organic layers (50%) and the substrate

(30%) The main reason for this low extraction efficiency is Total Internal Reflection (TIR). Only light which is almost perpendicular on an interface can escape. Light which is under a too oblique angle, is totally internally reflected.

In literature, we find four different approaches to increase the extraction efficiency.

Firstly, using a high refractive index substrate can increase the amount of light which can travel from organic layers to the substrate. Then, micro lenses can extract this light.

Secondly, using interference layers increases the extraction efficiency by changing the angular emission in glass. The experimental relative improvement is about 80% for a limited wavelength range. As long as we use planar interfaces, we always will have TIR.

Thirdly, we can apply micro lenses at the interface between substrate-air. Experiments show a relative improvement of about 60% for a large wavelength range.

Fourthly, a dielectric grating can be placed between organic layers and substrate. The experimental relative improvement of about 80% has only been verified for a limited wavelength range. Note that for these gratings, most authors claim that an increase of the direct transmission through the substrate is the reason for the extraction efficiency. Scattered light after multiple round trips usually is fully neglected. In the next chapters, we will explain how and why we have taken into account these multiple round trips.

3

Eigenmode expansion to model OLEDs with gratings

This chapter shows how eigenmode expansion models OLEDs with gratings. This numerical model is especially suited for substrate emitting OLEDs, because multiple round trips in the substrate are calculated. This is the main novelty of this work.

The model can integrate Maxwell's equations for a 3D OLED with a grating for one wavelength. The grating can be on either side of the substrate: either at the interface between the organic layers and the substrate or at the interface between the substrate and air. The organic layers are in the order of a wavelength, thus these are modeled as coherent. Because the substrate is optically thick, light propagation is modeled as incoherent. To the best of our knowledge, modeling of coherent and incoherent light is the new part.

This chapter gives results for simplified OLEDs. More complex OLEDs are discussed in chapter 5.

Overview

3.1 Mechanisms which contribute to light extraction

The goal of this chapter is to numerically analyze OLEDs with gratings. We show two mechanisms which contribute to a relative increase of the extraction efficiency. Note that the second mechanisms is overlooked by the commonly used FDTD. [13]

Let us look at the limitations of an OLED with planar interfaces. Figure 3.1(a) shows how Total Internal Reflection (TIR) traps most of the light. TIR happens for a large fraction of light which goes from a material from a high refractive index layer to a low refractive index layer. All light which is incident to their interface under a too oblique angle is fully reflected, regardless of polarization. What we mean by too oblique is defined by Snellius' laws, equation 2.3. Note that if light under a certain angle is not fully reflected by TIR, this light is almost completely transmitted.

Of course, a correct calculation of each interface requires Fresnel's equations. Still, this point of view suffices for an OLED with planar interfaces. We will now show that this point of view does not hold up if the OLED has a corrugated interface.

Figure 3.1(b) shows a grating at the interface between substrate and air. This approach is similar to using micro lenses. [88] [78] Light which is fully reflected at a planar interface, now can be extracted. Figure 3.1(b) also shows that if extraction does not happen after first incidence, light extraction might happen after the second, third, ... incidence. The rough estimate of table 2.1 shows that roughly 50% of all the generated light can be found in the substrate and air. To simulate this, we need to take into account multiple round trips.

Also, because of the thickness of the substrate, light has to be treated as temporal incoherent. For micro lenses, one very known numerical method is ray tracing. [79] Ray tracing uses geometrical optics to propagate a set of rays of light through a lens system. To the best of our knowledge, a numerical model to calculate multiple round trips of light in the substrate of an OLED with a grating does not exist.

Figures 3.1(c) and 3.1(d) show a grating at the interface between organic layers and substrate. These figures show two mechanisms which contribute to the extraction efficiency. First, more light escapes from the organic layers to the substrate, figure 3.1(c). Increasing the amount of light inside the extraction cone of the substrate increases the extraction efficiency. So, we see an increase in **direct** transmission through the substrate.

To calculate *direct* transmission from substrate to air, a very popular simulation technique is FDTD. [82] [83] [84] [13] The angular emission in glass is calculated. Then, the fraction of light in the extraction cone is assumed to be extracted. This approach overlooks the mechanism of figure 3.1(d). Light with a too oblique angle still undergoes TIR at the interface

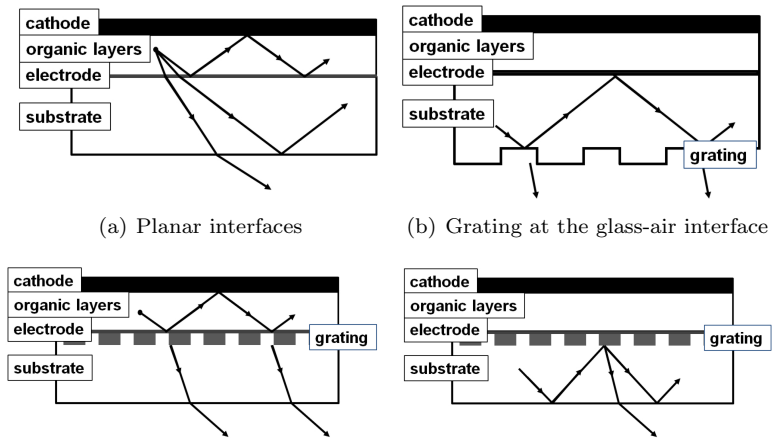

(a) Planar interfaces

(b) Grating at the glass-air interface

(c) Grating at the organic layers-glass interface

(d) Grating at the organic layers-glass interface

Figure 3.1: (a) At each interface, a fraction of the light not escape because of total internal reflection. Light which is incident at a too oblique angle is not transmitted. (b) A grating at the interface between substrate and air increases the fraction of light which can escape the substrate. Light which is not transmitted the first time, may have a second chance. (c)-(d) A grating at the interface between the organic layers and the substrate increases light extraction by two mechanisms. (c) The grating increases the amount of light which is extracted from the organic layers. (d) Light which is incident on the substrate-air interface at a too oblique angle gets a second chance by scattering.

substrate-air.

Thus, figure 3.1(d) shows the second extraction mechanism. Light extraction might occur after a few round trips if light scattering is good. Though FDTD can not model this, the approach in this chapter is able to take this effect into account.

In conclusion, we see that round trips in the substrate contribute to the extraction efficiency. Modeling of light in the substrate has to consider two properties. First, light can make several round trips before it is extracted. Second, light in the substrate has to be modeled as incoherently.

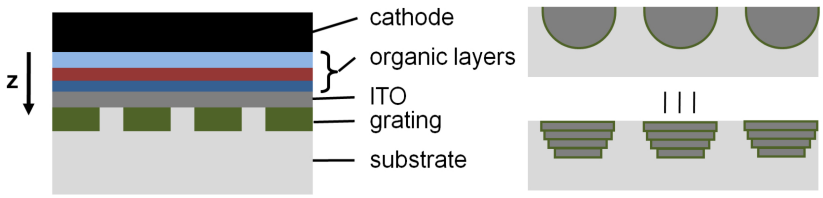

Figure 3.2: (a) An OLED can be described as a concatenation of z-invariant layers. (b) Also, a grating with non straight edges can be approximated by a grating of z-invariant layers.

3.2 Eigenmode expansion to model OLEDs

3.2.1 Seeing an OLED stack as a concatenation of z-invariant layers

Figure 3.2 shows how we can describe an OLED stack as a concatenation of z-invariant layers. So, both planar layers and gratings are z-invariant layers. Now, the electromagnetic field in each layer can be described as a summation of eigenmodes. [89] [9] Then, the transmission and reflection at an interface can be described by eigenmodes and an S-matrix formalism. Thus, eigenmodes and S-matrices are the **building blocks** to describe the propagation of the electromagnetic field. Note that these building blocks will be used later on in section 3.3. This last section combines coherent and incoherent propagation, which is necessary for propagation in the substrate. Here, we discuss the building blocks.

The next subsection gives a basic introduction of the simulation technique in subsection 3.2.2. Each subsequent section gives more details. This basic introduction shows how to calculate the field of a dipole which is placed in an OLED with only planar interfaces. Note that **eigenmodes** in the layers of a planar OLED are **plane waves**. Then, we discuss more about these eigenmodes, the excitation of eigenmodes by a dipole and how we need to treat the interface between two z-invariant layers. Each of these topics will be discussed in respectively subsection 3.2.3, subsection 3.2.4 and subsection 3.2.5.

To calculate an OLED with a grating instead of a planar OLED, we need the eigenmodes of the grating layer, subsection 3.2.6. Then, subsection 3.2.7 and subsection 3.2.8 give two properties of the numerical model, which can be exploited to speed up the calculation. Lastly, the goal of our numerical model is to calculate the extraction efficiency. For that purpose, we use the equations of subsection 3.2.9.

3.2.2 Dipole in a stratified medium

This subsection shows how eigenmode expansion can be used to calculate the electromagnetic field of a dipole which has been placed in a stratified medium. This approach calculates the field **for one given frequency**. Note that for planar structures, the eigenmodes in each layer correspond with plane waves. This subsection is the starting point for the numerical model of stacks with gratings.

Because we calculate the field for one frequency, this work **always** uses a phasor notation. For example, the electric component then is the complex vector $\mathbf{E}(\mathbf{r})$ instead of the real vector $\mathbf{e}(\mathbf{r}, t)$. These two vectors are connected by a phase term which varies harmonically in time:

$$\begin{aligned} \mathbf{e}(\mathbf{r}, t) &= \Re(e^{j\omega t}\mathbf{E}(\mathbf{r})) \\ \omega &= 2\pi\nu \end{aligned} \tag{3.1}$$

The frequency of the time harmonic field is ν. By convention, in this work, the sign of the time variation is positive: $e^{+j\omega t}$.

For the remainder of this work, we will assume that the field by a dipole corresponds with light generation by the radiative decay of an exciton. [90] If this field is known, the radiant flux in the direction perpendicular to the emissive zone can be calculated. A comparison between the radiant flux in the organic layers and air gives valuable information about the extraction efficiency. The simulation technique calculates the total field in three steps. [69]

First, we have a fourier transform of the field of the dipole in the plane of the emissive layer. The field of the dipole is the field in a homogeneous space with a refractive index equivalent to the plane of the emissive layer. This fourier transformation shows how eigenmodes are excited by a dipole. These eigenmodes are either propagating plane waves of evanescent waves, which propagate in the positive or negative z-direction. Second, we propagate these components through the structure. Thirdly, once we have the total field of the upper and lower propagating fields in a given direction, an inverse fourier transformation of these components gives the electromagnetic field which satisfies Maxwell's equations in the stratified medium.

Now, let us describe these steps in more detail.

First step: the fourier transformation of a dipole. The total field can be written as the sum of plane waves. Each eigenmode then will have the form $e^{-j(k_z z + k_x x + k_y y)}$. As we will see later on, only the phase ($e^{-jk_z z}$) of the field of an eigenmode changes in the z-direction. Again, this form gives for real values of the wavevector (k_x, k_y, k_z), a propagating plane wave. For more information on the form and the amplitude of each eigenmode, see respectively subsection 3.2.3 and 3.2.4.

Second step: figure 3.3 shows how the summation of the upward and downward propagations of the given eigenmode gives the total radiant flux.

For a specific direction, we have to consider the excitation of one downward component and one upward component. Indeed, for planar interfaces, the angle of an eigenmode is preserved in one layer, regardless of the reflections. For sake of argument, we assume that the amplitude of these components *at the location of the dipole* is given by respectively $A_{do,0}$ and $A_{up,0}$. The complex values of the reflectivity coefficients R_{bot} and R_{top} **fully** describe the optical behavior of the respectively lower and upper stack of layers. Both the phase difference and the magnitude are in these values. After one round trip, the amplitude and phase of the returning component *at the location of the dipole* is respectively $R_{bot}A_{do,0}$ and $R_{top}A_{up,0}$.

Because everything is referred at the same plane, the plane of the dipole, we have:

$$\begin{aligned} A_{do} &= (\ A_{do,0} + R_{top}A_{up,0}) + (R_{top}R_{bot}A_{do,0} + R_{top}R_{bot}R_{top}A_{up,0}) \\ &\quad +(\ R_{top}R_{bot}R_{top}R_{bot}A_{do,0} + R_{top}R_{bot}R_{top}R_{bot}R_{top}A_{up,0}) \\ &\quad +\ \ldots \\ &= (I - R_{bot}R_{top})^{-1}(A_{do,0} + R_{top}A_{up,0}) \end{aligned} \tag{3.2}$$

Now, to find the emission in the substrate, we can multiply this amplitude with the amplitude transmission T_{bot}.

Third step: once we have the total field of the upper and lower propagating fields in a given direction, an inverse fourier transformation of these components gives the total field which satisfies Maxwell's equations in the stratified medium. This inverse fourier transformation is an integration over the complex plane of the propagation vectors (k_x, k_y). Another name for this inverse transformation is Sommerfeld integral. To avoid an integration over the complex plane, you can use the trick of subsection 3.2.7.

In conclusion, the algorithm uses 3 steps: determine how eigenmodes such as propagating plane waves are excited. Then, each of these eigenmodes is propagated through the system. Thirdly, a summation over all eigenmodes gives the total field. Each of these 3 steps will be explained in more detail in the next sections.

3.2.3 The general form of eigenmodes for planar layers and gratings

The goal of this subsection is to show the general form of the field in a planar layer or a grating. The electromagnetic field in these layers can be written as a sum of eigenmodes. Again, our simulation method numerically integrates Maxwell's equations for one specific wavelength. This section is about the form of these eigenmodes.

Because of the mathematical elegance of symmetries, we will briefly mention this principle. Symmetries allow to write down the general form of

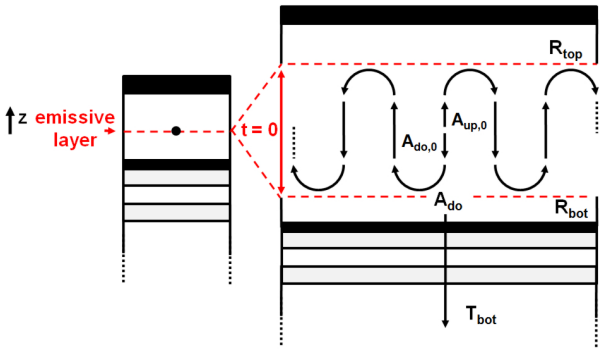

Figure 3.3: The optical behavior of an OLED can be described in terms of eigenmodes. For each of these eigenmodes, the extraction efficiency can be determined. (figure adapted from [9])

the electromagnetic field based on what the structure looks like. However, a more mathematical derivation is outside the scope of this work. [91].

Symmetry means that Maxwell's equations do not change under a coordinate transformation. For example, in a homogeneous medium, Maxwell's equation do not change under any translation.

$$\epsilon(x + d_x, y + d_y, z + d_z) \quad = \quad \epsilon(x, y, z), \ \forall d_x, d_y, d_z \in \mathbb{R} \tag{3.3}$$

Then, it is possible to derive that a possible solution of Maxwell's equations has the form:

$$\begin{aligned} \mathbf{E}(x, y, z) &= \mathbf{E}' e^{-jk_z z} e^{-j(k_x x + k_y y)} \\ \mathbf{E}' &= \mathrm{C}^{\mathrm{te}} \end{aligned} \tag{3.4}$$

Note the sign of the phase of the complex field. Again, this sign follows from our convention for the time factor: $e^{j\omega t}$.

The idea behind using symmetries is the following. Based on the symmetry, a symmetry operator can be constructed. This symmetry operator can be seen as an eigenvalue problem. Then, the most general solution of the symmetry operator automatically is a solution of Maxwell's equations. So, symmetries quickly give the form of a general solution of Maxwell's equations.

We now give the form of the electromagnetic field in a z-invariant layer for **one wavelength**. A z-invariant layer has a refractive index which is independent of z: $\epsilon(x, y)$.

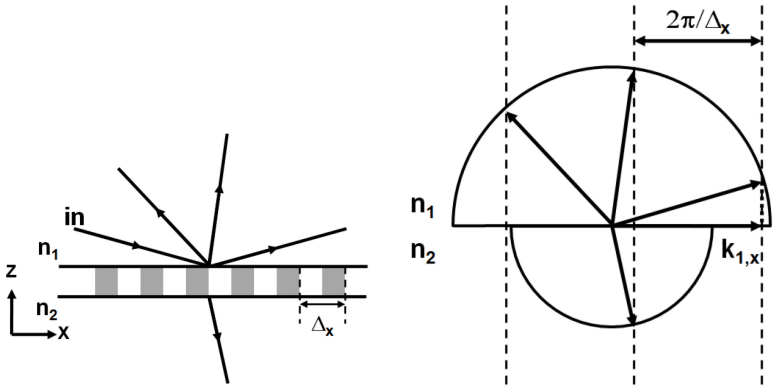

(a) Plane wave incident on a periodically corrugated interface

(b) K-vector diagram corresponding with (a).

Figure 3.4: The k-vector diagram shows which propagating plane waves are reflected and transmitted for a given incident plane wave. The transverse component k_x has to satisfy the Bragg-condition of equation 3.7. The total magnitude of the wave vector $\mathbf{k}$ in a homogeneous medium is given by a circle.

$$\epsilon(x,y,z+d) = \epsilon(x,y,z),\ \forall d \in \mathbb{R} \tag{3.5}$$

$$\Longrightarrow \quad \mathbf{E}_{mode} = \mathbf{E}(x,y)e^{-jk_z z} \tag{3.6}$$

For a grating, with periodicity in the x- and y-direction (Δ_x, Δ_y), we have:

$$\epsilon(x+n\Delta_x, y+m\Delta_y, z) = \epsilon(x,y,z),\ \forall n,m \in \mathbb{Z}$$

$$\Longrightarrow$$

$$\mathbf{E} = \sum_{i,j} \mathbf{E'}_{i,j} e^{-jk_z z} e^{-j(k_{x,i}x + k_{y,j}y)} \tag{3.7}$$

$$k_{x,i}, k_{y,j} = k_{x,0} + i\frac{2\pi}{\Delta_x}, k_{y,0} + j\frac{2\pi}{\Delta_y} \tag{3.8}$$

$$\mathbf{E'} = \mathrm{C}^{\mathrm{te}}$$

Note that in literature, the propagating modes of equation 3.7 are also referred to as Bloch modes.

It is quite easy to find the Bragg condition from equation 3.4 and 3.7. If we impose boundary conditions on the interface between a planar stack

and a grating, we need to find a linear combination of the solutions of equation 3.4 in the planar layer and a linear combination of the solutions of equation 3.7. This boundary condition imply that the phase factor $e^{-jk_x x}$ and $e^{-jk_y y}$ need to be present in the solution of both layers, see figure 3.4. If we assume that the plane wave is incident with the transverse components of the wave vector equal to $(k_{x,0}, k_{y,0})$, we have that in both layer the following components need to be present:

$$k_x, k_y = k_{x,0} + i\frac{2\pi}{\Delta_x}, k_{y,0} + j\frac{2\pi}{\Delta_y}, \quad i, j \in \mathbb{Z} \tag{3.9}$$

Note, equation 3.7 is fully equivalent with the Floquet Theorem. [10]

So, in this section, we have described the electromagnetic field in a layer or grating as a linear combination of eigenmodes. The form of eigenmodes in a planar layer or a grating are given by respectively equation 3.4 and equation 3.7. We have given the hint that these forms can be easily found with symmetries. However, such a derivation was outside the scope of this work.

3.2.4 Fourier transform of a dipole in homogeneous space

The first step of the numerical model determines the excitation of the eigenmodes by the dipole. [92] [10] Concretely, we want the amplitudes of the propagating plane waves and the evanescent waves.

The amplitudes of the eigenmodes are given by $\mathbf{E}(k_x, k_y, k_z)$. Then, the actual field of a dipole at a given location is given by:

$$\mathbf{E}(x, y, z) \quad = \quad \int\int \left[\mathbf{E}(k_x, k_y, k_z) e^{-jk_x x - jk_y y}\right] e^{-jk_z z} dk_x dk_y \tag{3.10}$$

In a homogeneous medium with refractive index n, these eigenmodes which have a free space wavelength λ should satisfy:

$$\left(\frac{2\pi}{\lambda} n\right)^2 \quad = \quad k_x^2 + k_y^2 + k_z^2 \tag{3.11}$$

Note that if all components of the propagation vector ($\mathbf{k} = k_x, k_y, k_z$) are real, the eigenmode is a propagating plane wave. Note that the angle of a plane wave changes when the wave travels to a medium of different refractive index. However, k_x, k_y does not change. This handy property will be exploited later on. If one of the components of the propagation vector is a complex number, the component will be an evanescent wave.

Now, the components $\mathbf{E}(k_x, k_y)$ are key. These components $\mathbf{E}(k_x, k_y)$ are given in density per unit $k_x k_y$. The dipole, which we assume to be in the origin (0,0,0), then has the phasor notation $\delta(x, y, z)\mathbf{p}$.

Let us discuss the classification used in the 2 by 2 table 3.1. First, depending on the orientation of the dipole, we have two options: parallel to the emissive layer: $p_{||}$ or perpendicular to the emissive layer: $p_{\perp}$. Second, we can use the polarization of plane waves, because we use (mostly) a stratified structure. Therefore, we have TE and TM polarizations. Planar interfaces keep TE and TM if a plane wave is incident on that planar interface. Figure 3.6 gives the convention of TE and TM polarized plane waves. In conclusion, the amplitudes of eigenmodes $\mathbf{E}(k_x, k_y)$ are given by table 3.1.

As we can see from this table, the sign shift of the electrical field of the vertical dipole shows that the electrical field is discontinuous at the emissive layer. Of course, this comes from the source we have introduced. Similarly, the magnetic field of the horizontal dipoles are also discontinuous. Though a detailed derivation is not given, the discontinuity comes from the vector products in Maxwell's equations.

The remainder of this section shows how the values of table 3.1 relate to the angular emission of a dipole and its far field pattern. So far, the eigenmodes have been expressed in density per unit (k_x, k_y). However, literature usually gives the decomposition of a dipole in eigenmodes in function of a density per unit solid angle $\mathbf{E}'(\theta, \phi)$: [92]

$$\mathbf{E}(x,y,z) = \int\int \mathbf{E}'(\theta,\phi) e^{-jk_x x - jk_y y - jk_z z} d\Omega \tag{3.12}$$

$$d\Omega = \sin(\theta) d\theta d\phi \tag{3.13}$$

$$(k_x, k_y, k_z) = k_0 n (\cos(\phi)\sin(\theta), \sin(\theta)\sin(\phi), \cos(\theta)) \tag{3.14}$$

Actually, this last paper is the basis for the amplitudes of table 3.1 . Therefore, we use the same normalisation of the amplitudes: $\mathbf{E}'(\theta, \phi)$ has been normalised with respect to the total radiant flux of the dipole. Note, the normalised amplitude $\mathbf{E}'(\theta, \phi)$ will be referred to as $A'(\theta, \phi)$. To ensure that the amplitude of plane waves is so that the total emitted flux of **one** dipole is 1, the following equation has to be valid:

$$\int\int |A'_s(\theta,\phi)|^2 + |A'_p(\theta,\phi)|^2 d\Omega = 1 \tag{3.15}$$

To go from the parameters $(\theta, \phi\ )$ to (k_x, k_y), we use $d\Omega = \sin(\theta) d\theta d\phi = dk_x dk_y / k_0 n_e k_z$, thus:

$$\mathbf{E}(k_x, k_y) = \frac{\mathbf{E}'(\theta,\phi)}{k_0 n_e k_z} \tag{3.16}$$

Figure 3.7 shows this radiant flux in function of solid angle $(dP/d\Omega)$. Also, we see at which directions the dipole emission will be maximal. We also see that the radial symmetry is around the axis of the dipole. Maximal

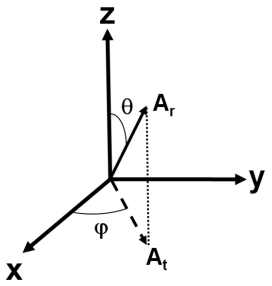

Figure 3.5: This figure gives the axis convention, used in table 3.1.

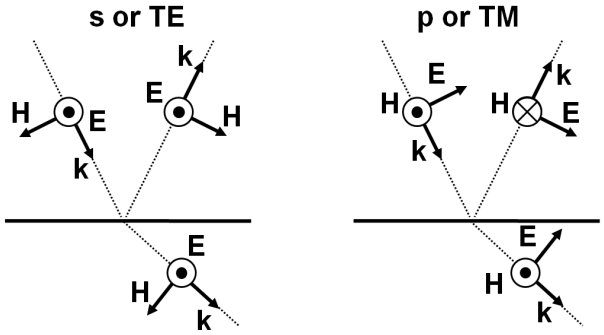

(a) (b)

Figure 3.6: Plane wave which are incident on an interface, can be classified in two types. The **H**-component of a p or TM polarised plane wave is parallel to the interface. The **E** component of a s or TE polarised plane wave is parallel to the interface.

	s polarization (TE)	p polarization (TM)
Vertical dipole (p_z)	$A'^{v}_{s\uparrow\downarrow}(\theta,\phi) = 0$ $A^{v}_{s\uparrow\downarrow}(k_x,k_y) =$ 0	$A'^{v}_{p\uparrow\downarrow}(\theta,\phi) = \pm\sqrt{\frac{3}{8\pi}}\sin(\theta)$ $A^{v}_{p\uparrow\downarrow}(k_x,k_y) =$ $\pm\sqrt{\frac{3}{8\pi}}\frac{k_t}{n_e k_0}\frac{1}{k_0 n_e k_z}$
Horizontal dipole (p_x)	$A'^{x}_{s\uparrow\downarrow}(\theta,\phi) = \sqrt{\frac{3}{8\pi}}\cos(\phi)$ $A^{x}_{s\uparrow\downarrow}(k_x,k_y) =$ $\sqrt{\frac{3}{8\pi}}\frac{k_x}{k_t}\frac{1}{k_0 n_e k_z}$	$A'^{x}_{p\uparrow\downarrow}(\theta,\phi) = \sqrt{\frac{3}{8\pi}}\cos(\theta)\sin(\phi)$ $A^{x}_{p\uparrow\downarrow}(k_x,k_y) =$ $\sqrt{\frac{3}{8\pi}}\frac{k_y}{k_t}\frac{k_z}{k_0 n_e}\frac{1}{k_0 n_e k_z}$
Horizontal dipole (p_y)	$A'^{y}_{s\uparrow\downarrow}(\theta,\phi) = -\sqrt{\frac{3}{8\pi}}\sin(\phi)$ $A^{y}_{s\uparrow\downarrow}(k_x,k_y) =$ $-\sqrt{\frac{3}{8\pi}}\frac{k_y}{k_t}\frac{1}{k_0 n_e k_z}$	$A'^{y}_{p\uparrow\downarrow}(\theta,\phi) = \sqrt{\frac{3}{8\pi}}\cos(\theta)\cos(\phi)$ $A^{y}_{p\uparrow\downarrow}(k_x,k_y) =$ $\sqrt{\frac{3}{8\pi}}\frac{k_x}{k_t}\frac{k_z}{k_0 n_e}\frac{1}{k_0 n_s k_z}$

Table 3.1: The decomposition of a dipole depends on its orientation and its polarization. The polarization and orientation of the dipole are defined by figure 3.7. The relation between $A'(\theta,\phi)$ and $A(k_x,k_y)$ is given by equation 3.16. (source: [92], [93])

emission is in the plane perpendicular to the dipole orientation. The total radiant flux of a dipole which emits in a homogeneous medium is:

$$P_{tot} = \frac{k^2 p^2 \sqrt{\frac{\mu}{\epsilon}}}{12\pi} \tag{3.17}$$

Mathematically, we find that the electric field lies in a plane which is formed by the dipole and its propagation vector ($\mathbf{k}$). Also, the radiant flux vanishes according to $\sin^2(\theta)$ for $p_\perp$. Basically, this already indicates that the a vertical dipole $p_\perp$ will emit no TE plane waves, as indeed can be found in table 3.1.

In conclusion, table 3.1 gives the excitation of eigenmodes by a dipole in a homogeneous medium. These amplitudes can be expressed per unit (k_x,k_y) or per unit solid angle (θ,ϕ). In a stratified medium, (k_x,k_y) of plane wave is invariant. Thus, amplitude per unit (k_x,k_y) is more easy to use. However, for insight, amplitude per unit solid angle is more beneficial. This statement is illustrated by the far field pattern of figure 3.7.

3.2.5 Concatenating different layers with eigenmode expansion and a S-matrix scheme.

To calculate the field in an OLED, we need to know the reflection and transmission at either side of the emissive layer, see equation 3.2. By using

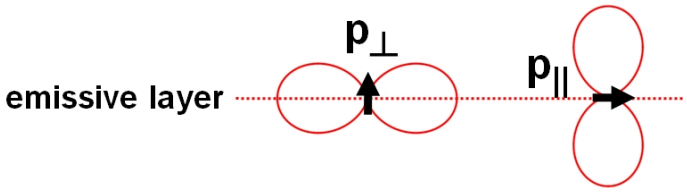

Figure 3.7: The orientation of the dipole is defined in function of its orientation compared to the interfaces. The polarization of the resulting plane waves also is defined in function of the interfaces. This figure shows the direction at which the angular radiant flux is maximal.

eigenmode expansion, the optical behavior of these stacks is completely given by the eigenmodes of the emissive region and the S-matrices of the stacks. [9] [94] [89]

To use eigenmodes, z-invariant layers are required. Thus, the refractive index in one layer does not change with z. Then, the S-matrices of the stacks at either side of the emissive layer gives the total field of an OLED by using equation 3.2. In this section, we describe how eigenmodes propagate through a stack with z-invariant layers.

Let us start with the propagation of an eigenmode through one z-invariant layer. To make eigenmodes a little more concrete, keep in mind that eigenmodes can be plane waves for planar layers. Section 3.2.3 has shown us that **any** eigenmode in a z-invariant layer has the general form:

$$\begin{aligned} \mathbf{E}(\mathbf{r}) &= \mathbf{E'}(x,y)e^{-jk_z z} \\ \mathbf{H}(\mathbf{r}) &= \mathbf{H'}(x,y)e^{-jk_z z} \end{aligned} \tag{3.18}$$

Thus, the form of an eigenmode at any xy-plane is always $\mathbf{E}'(\mathbf{x},\mathbf{y})$, save a phase factor $e^{-jk_z z}$. Note that the sign of the z phase factor depends on the time convention mentioned in section 3.2.3. Again, **any** plane wave can be written under the form of equation 3.18.

Providing that we have a complete set of eigenmodes, the field at any given xy-plane is given by the summation:

$$\mathbf{E}(\mathbf{r}) = \sum A_i \mathbf{E_i}(\mathbf{r}_t)e^{-jk_{z,i}z} \tag{3.19}$$

$$\mathbf{H}(\mathbf{r}) = \sum A_i \mathbf{H_i}(\mathbf{r}_t)e^{-jk_{z,i}z} \tag{3.20}$$

Basically, the representation of the field at a given xy-plane then is given by an expansion in eigenmode coefficients $[A_i]$ instead of its field components

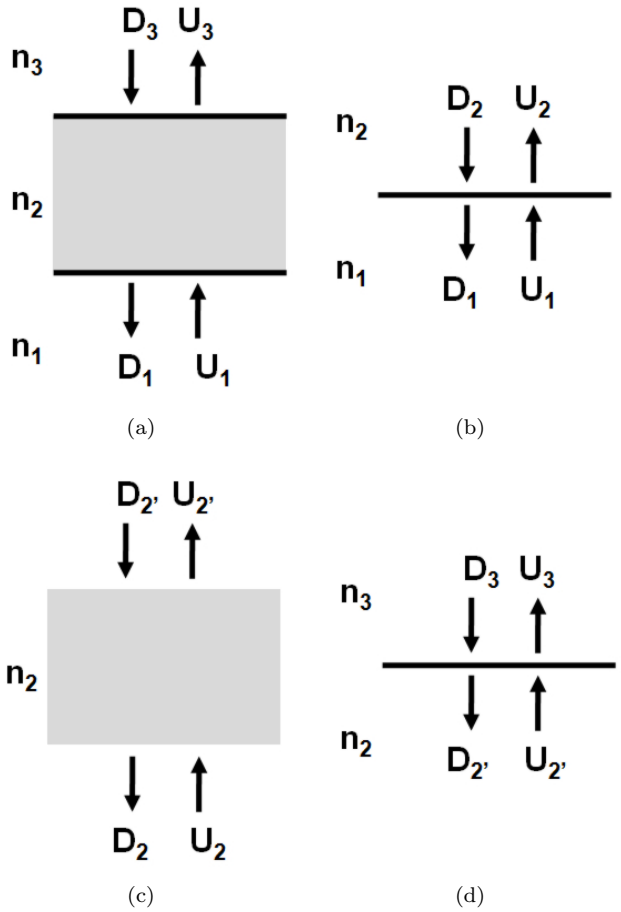

Figure 3.8: (a) A part of a propagating plane wave incident from medium 1, which goes to medium 3, is either reflected or transmitted. The calculation of this setup is a combination of three part-setups. (b) The transmission and reflection at the interface between medium 1 and medium 2 is calculated by Fresnell's equations. (c) Plane wave propagation in medium 2 gives an additional phase to the field amplitude. (d) Similar to (b).

$(\mathbf{E}(\mathbf{r}), \mathbf{H}(\mathbf{r}))$:

$$(\mathbf{E}(\mathbf{r}), \mathbf{H}(\mathbf{r})) \Longleftrightarrow \mathbf{A} = [A_i] \tag{3.21}$$

Now, any stack can be written as a concatenation of the stacks of figure 3.8. Either light propagates in one z-invariant layer (figure 3.8 (c)) or light has to pass through the interface between two z-invariant layers (3.8 (c)). Both cases or for that matter, any concatenated stack can be described by a transfer matrix;

$$\begin{bmatrix} \mathbf{U}_j \\ \mathbf{D}_i \end{bmatrix} = \begin{bmatrix} t_{i,j} & r_{j,i} \\ r_{i,j} & t_{j,i} \end{bmatrix} . \begin{bmatrix} \mathbf{U}_i \\ \mathbf{D}_j \end{bmatrix} \tag{3.22}$$

The submatrices $\mathbf{t}_{i,j}$ and $\mathbf{t}_{j,i}$ give respectively the amplitude transmission from interface i to interface j and vice versa. A similar notation is used for the amplitude reflection.

Now, for example, take the propagation in one layer of figure 3.8(c). Then, the propagation in one of the layers of the stack is given by:

$$\begin{bmatrix} \mathbf{U}_{2'} \\ \mathbf{D}_2 \end{bmatrix} = \begin{bmatrix} diag(e^{-j\beta_i z}) & 0 \\ 0 & diag(e^{-j\beta_i z}) \end{bmatrix} . \begin{bmatrix} \mathbf{U}_2 \\ \mathbf{D}_{2'} \end{bmatrix} \tag{3.23}$$

Note that the eigenmodes in the diagonal matrices $\mathrm{t}_{2,2'}$ and $\mathrm{t}_{2',2}$ have their own β_i. Also, we have $\mathrm{r}_{2,2'} = \mathrm{r}_{2',2} = 0$. In case of the planar interface between two z-invariant layers of figure 3.21(b), the matrices $\mathrm{t}_{1,2}$, $\mathrm{t}_{2,1}$, $\mathrm{r}_{1,2}$ and $\mathrm{r}_{2,1}$ are given by Snellius' laws.

The general case is more complex. For the transition between two more general z-invariant sections, the matrices $\mathrm{t}_{1,2}$, $\mathrm{t}_{2,1}$, $\mathrm{r}_{1,2}$ and $\mathrm{r}_{2,1}$ do not have to be diagonal. For example, a propagating plane wave incident on a grating can excite other propagating plane waves! To calculate these matrices, overlap integrals between the field profiles of the eigenmodes in each z-invariant layer are required.

To concatenate these transfer matrices, it turns out to be numerically advantageous to work with scattering matrices. Fore more details, we refer to [9] and[95].

The main point is that we describe the optical behavior at either side of the emissive layer in terms of eigenmodes of the emissive layer and S-matrices.

Now, we need to rewrite equation 3.2, which was used for an OLED with only planar interfaces. The form of the more general equation is the same:

$$\mathbf{A}_{do} = (\mathbf{I} - \mathbf{R}_{bot}\mathbf{R}_{top})^{-1}(\mathbf{A}_{do,0} + \mathbf{R}_{top}\mathbf{A}_{up,0}) \tag{3.24}$$

In this equation, the symbols represent matrices whereas equation 3.2 used scalars. Here, the matrices contain **all** eigenmodes. For example, $\mathbf{A}_{up,0}$

represents the decomposition of the dipole in **all** plane waves. Section 3.3 discusses this equation in more detail. Of course, in the case of an OLED with only planar interfaces, equation 3.24 reduces to equation 3.2 because $\mathbf{R}_{top}$ and $\mathbf{R}_{bot}$ are diagonal. For more general structures, this will no longer be the case.

In conclusion, the behavior of both stacks at either side of the emissive layers can be described as an S-matrix and the eigenmodes of the emissive layers. The field in one xy-plane can always be described as a summation or integration of eigenmodes.

3.2.6 Eigenmodes of a grating with Rigorous Coupled Wave Analysis

This section shows how to find the eigenmodes of a grating with Rigorous Coupled Wave Analysis (RCWA). As we will see, the eigenmodes are found in two steps. First, we have a fourier transform of the periodic refractive index of the grating and then we solve an eigenvalue problem. We restrict this section to Transverse Electric (TE) waves in a 1D grating. [96] For Transverse Magnetic (TM) waves and gratings in 2D, some additional convergence issues need to be resolved. However, these topics are outside the scope of this work. [97] [98] [10] We only wish to illustrate the general method to find the eigenmodes of a grating. Then, if we have the eigenmodes of the grating, the equations of section 3.2.5 can calculate the S-matrix.

Let us begin with equation 3.7 of section 3.2.5, which gives the general form of **any** eigenmode in an 1D z-invariant grating:

$$\begin{aligned} E &= \sum_i {E'}_i e^{-jk_z z} e^{-j(k_{x,0}+i\frac{2\pi}{\Delta_x})x} \\ \mathbf{E'}_i &= \mathrm{C}^{\mathrm{te}} \end{aligned} \tag{3.25}$$

The wave vector $k_{x,0}$ can be interpreted as the wave vector of the incident plane wave, which can excite this eigenmode, figure 3.4. Note that the form of equation 3.25 can be satisfied by any wave vector which satisfies the Bragg condition, equation 3.9. Now, we have two types of unknowns: the wavevector k_z and the **scalar** amplitudes E'_i.

The unknowns k_z and E'_i can be found by substituting equations 3.28 and 3.25 in the scalar Helmholtz equation for TE polarization: [94] [89]

$$\begin{aligned} \nabla^2 E(x) + (k_0^2 - k_z^2)E(x) &= 0 \\ \frac{\partial^2}{\partial_x^2} E(x) + (k_0^2(x) - k_z^2)E(x) &= 0 \\ k_0^2 &= \left(\frac{2\pi}{\lambda}\right)^2 \epsilon(x) \end{aligned} \tag{3.26}$$

Note that the field E is a scalar. For more detail on the Helmholtz equation, we refer to equation 7.1 of chapter 7. Now, we will show that equation 3.26 basically is an eigenvalue problem in k_z.

Because of the peridiocity of the permittivity, we have:

$$\begin{aligned} \epsilon(x + n\Delta x) &= \epsilon, \quad n \in \mathbb{Z} && (3.27) \\ &= \sum_i \epsilon_i e^{j(\frac{i2\pi x}{\Delta x})} && (3.28) \end{aligned}$$

After substituting equation 3.25 and equation 3.28 in equation 3.26, each term $e^{-j(i\frac{2\pi}{\Delta_x})}$ has to be equal to zero. First, let us simplify two terms. Without going into detail, for the full derivation we need Laurent's rule of factorization to simplify the product of the electrical permittivity and eigenmode. This rules states that for two functions $f(x) = \sum_i f_i e^{j(i2\pi/\Delta_x)}$ and $g(x) = \sum_i g_i e^{j(i2\pi/\Delta_x)}$, the fourier component h_n of the product h(x) can be written as :

$$\begin{aligned} h(x) &= f(x)g(x) \\ h(x) &= \sum h_i e^{j(i2\pi/\Delta_x)} \\ h_n &= \sum_{i=-\infty}^{+\infty} f_{n-i} g_i \end{aligned} \qquad (3.29)$$

This procedure results in an infinite series. Thus, we have to truncate the series. Then, we have a finite number of unknowns: the wavevector k_z and the **scalar** amplitudes E_i'. Again, each term $e^{-j(i\frac{2\pi}{\Delta_x})}$ has to give zero. Then, equation 3.28, equation 3.25 and equation 3.26 can be rewritten as:

$$\mathbf{A}.\mathbf{E}' = k_z^2 \mathbf{E}' \qquad (3.30)$$

This is an eigenvalue problem in k_z. Each eigenmode has an eigenvector $\mathbf{E}'$ with the truncated series of coefficients of equation 3.26 and with the corresponding eigenvalue k_z^2.

Note that for TM polarization and 3D structures, equation 3.26 is no longer correct, a more involved analysis is needed to deal with numerical instabilities. [97] [93] [10]ties. [97] [93] [10]

In conclusion, finding the eigenmode problem comes down to a fourier transformation of the refractive index. Then, we can substitute this refractive index and the eigenmode as an fourier expansion in the Helmholtz equation. After truncation of the infinite series, we find an eigenvalue problem in k_z. Solving this equation finally gives the eigenmodes of the grating. This way of working applies to all gratings. Nevertheless, some additional issues have to resolved for TM waves or 2D gratings.

3.2.7 Simplifying the inverse Fourier transform

Using a reference layer of high refractive index as emissive layer can simplify the inverse fourier transform in the presented algorithm. Subsection 3.2.2 showed that the third step in the algorithm is an integration over the **complex** (k_x, k_y)- plane. This subsection shows a 'trick' which simplifies the integration to the **real** plane (k_x, k_y). [99]

So far, we have seen two steps of the three step algorithm in respectively subsections 3.2.4 and 3.2.5. First step: the dipole excites eigenmodes of the emissive layer. Second step: S-matrices and eigenmodes describe the optical behavior of stacks at either side of this emissive layer. Now we discuss the third step. To find the complete field, we have an inverse fourier transform over a complex (k_x, k_y) plane. This inverse transform is also known as a Sommerfeld integration. If we only consider real values for the wavevector in the emissive region ($\mathbf{k} = (k_x, k_y, k_z)$), we only include propagating plane waves and we exclude evanescent waves.

To illustrate the importance of inclusion of evanescent waves in the emissive region, the extraction efficiency of a simplified OLED calculated with and without evanescent waves is given in figure 3.9. This simplified OLED consists of a cathode (refractive index n = 0.9-6.0j), an organic layer (n = 1.7, thickness t_{tot}) and a glass substrate (n = 1.5). The distance between emissive layer and cathode is z_e.

A comparison of figures 3.9(a) and figure 3.9(b) illustrates following statement. The evanescent modes of dipoles which are close to the cathode are more critical than evanescent modes of dipoles which are further from the cathode.

The reason is the exponential decay of the evanescent waves. Mathematically the decay comes from a complex propagation constant. If a dipole is placed in bulk material, the exponential decay of the evanescent waves can not influence the far field pattern. However, this is not true if the dipole is placed close to a metal or any other material with a higher refractive index than the dipole's surrounding material. Then, a propagating plane wave in the material of high refractive index can be generated by an evanescent wave. Figure 3.10(a) also illustrates this behavior. Propagating plane waves in emissive layer can excite propagating plane waves in the high refractive index material. However, also evanescent waves in the emissive region can excite propagating plane waves in the high refractive index material.

Now, figure 3.10 illustrates the trick we use. We want to excite the propagating plane waves in the materials with higher refractive index. However, we do not want to use evanescent waves to ease numerical implementation. Note again that evanescent waves are the ones with a complex wave vector (k_x, k_y, k_z). Therefore, we use an infinitesimal thin reference layer which has a larger refractive index than any of the surrounding high index layers. A propagating plane wave in this reference layer can excite a propagating plane wave in the high refractive index material!

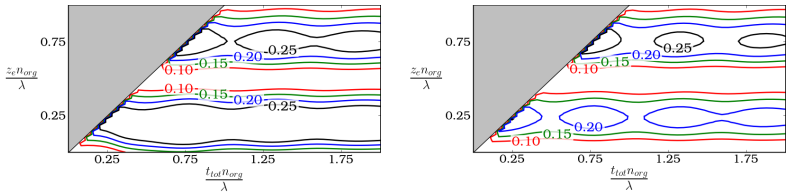

(a) Calculation only considers propagating plane waves in the emissive layer.

(b) Calculation considers propagating plane waves and evanescent waves in the emissive layer.

Figure 3.9: Extraction efficiency of a simplified OLED in function of two parameters. The structure is: cathode: refractive index n = 0.9-6.0j, organic layer: n = 1.7, thickness t_{tot}, substrate: n = 1.5. Distance between emissive layer and cathode is z_e.

Using a high refractive index reference layer, the simulation method only requires an integration over all the propagating plane waves in the reference layer. Thus, we limit the integration over the real k_x, k_y, k_z-plane of the reference layer.

Now, we give a remark on rescaling the radiant flux. Indeed, the total power emission P_0 of a dipole located in an infinitesimal thin layer of refractive index n_{ref} is changed because of microcavity effects. However, this dipole's angular emission is unchanged. A rigorous derivation of the following equations can be found in section 3.3.4.2 of [99]. Depending on the orientation of the dipole with respect to the interfaces, the total emitted power changes.

For a dipole which is parallel to the interface, the total emitted power $P_{||}$ is given by:

$$P_{||} = \frac{n_{org}}{n_{ref}} P_0 \tag{3.31}$$

For dipole perpendicular to the interface, the total emitted power $P_\perp$ is given by:

$$P_\perp = \left(\frac{n_{org}}{n_{ref}}\right)^5 P_\perp \tag{3.32}$$

Thus, if you use a reference layer, you need to rescale the total power emitted by the dipole:

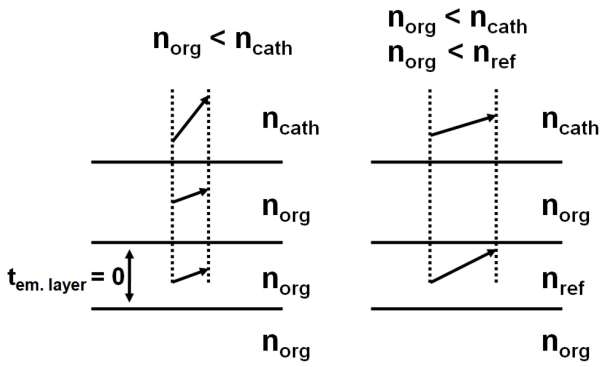

Figure 3.10: The propagating plane wave vectors are shown in each of the layers of an OLED. If we only use the propagating plane waves of the n_{org}-material, some propagating plane waves of oblique incidence in the n_{cath}-material can not be excited by a propagating plane wave . In (b), the emissive layer has a high refractive index, so propagating plane waves of oblique incidence can be excited by evanescent modes. The propagation vector k of these evanescent mode is imaginary, thus it is not shown in the n_{org}-material of (b).

$$\begin{aligned} P_0 &= \frac{n_{ref}}{n_{org}} P_{||} \\ P_0 &= \left(\frac{n_{ref}}{n_{org}}\right)^5 P_{\perp} \end{aligned} \tag{3.33}$$

Let us finish by discussing the refractive index of the reference layer we need to choose. Figure 3.11 gives the extraction efficiency in function of the refractive index of the reference layer for the simplified OLED with $\frac{z_e n_{org}}{\lambda} = 0.25$ and $\frac{t_{tot} n_{org}}{\lambda} = 0.75$. Because a reference layer with a refractive index $n_{ref} = 1.7$ corresponds with the 'default' propagating plane wave expansion, power dissipation to the cathode is underestimated. The higher n_{ref}, the more accurate we consider this power dissipation. As can be seen from figure 3.11, for an infinitesimal thin layer with $n_{ref} > 2.1$, convergence is reached.

Let us finish with two remarks. First, this convergence analysis is best redone for every z_e. For an emissive layer which is several wavelengths from the cathode $n_{ref} = 1.7$ suffices. However, figure 3.11 gives $n_{ref} > 2.1$ as minimal refractive index for this case. Thus, the minimal refractive index indeed depends on the distance from the cathode.

Second, a reference layer with a very high refractive index also has its disadvantages. As always, the algorithm can only use a finite set of propagating plane waves. Using the same number of equidistant propagating plane waves, would decrease the number of propagating waves in the organic layer if the refractive index was too high. So, we need to use the lowest refractive index for the reference layer for which we see convergence of the extraction efficiency.

In conclusion, the third step in our algorithm requires an inverse fourier transform over a complex k_x, k_y-plane. Using a high refractive index reference layer as the emissive layer, an integration over a real k_x, k_y-plane suffices. The refractive index of this reference layer has to be high enough to reach convergence of the extraction efficiency.

3.2.8 Grouping eigenmodes by using the Bragg condition

Figure 3.1 shows how light makes multiple round trips in an OLED with a grating before extraction. After each round trip, one propagating plane wave which is incident on the grating excites other propagating plane waves. Thus, you might expect a large bookkeeping of propagating plane waves after multiple round trips. This is not correct. This section shows how the Bragg condition results in a small number of propagating plane waves for one starting plan wave, even after an infinite amount of round trips! Mathematically, this reduces the dimensions of the matrices of equation 3.24.

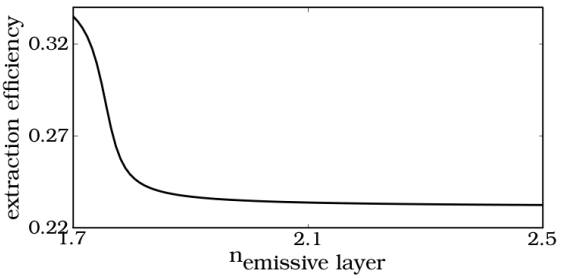

Figure 3.11: The extraction efficiency is plotted in function of the refractive index of the infinitesimal thin emissive layer. If this layer has a refractive index similar to the refractive index of the surrounding layers, the extraction efficiency is underestimated.

Let us begin with an arbitrary propagating plane wave which is incident on the grating, figure 3.4. This propagating plane wave has a wave vector of which the transversal components are $(k_{x,0}, k_{y,0})$. For a grating with period (Δ_x, Δ_y), the wavevectors of all excited eigenmodes are given by the Bragg-condition:

$$k_x, k_y \quad = \quad k_{x,0} + n\frac{2\pi}{\Delta_x}, k_{y,0} + m\frac{2\pi}{\Delta_y}, \quad n, m \in \mathbb{Z} \tag{3.34}$$

The main property of this set eigenmodes is the following: each eigenmode set can only excite other eigenmodes which satisfy equation 3.34! Let us call these eigenmodes a **subset** of the full set of all eigenmodes. No eigenmodes outside the subset will be excited.

This is a powerful statement. Mathematically, round trips of eigenmodes are described by equation 3.24:

$$\mathbf{A}_{do} \quad = \quad (\mathbf{I} - \mathbf{R}_{bot}\mathbf{R}_{top})^{-1}(\mathbf{A}_{do,0} + \mathbf{R}_{top}\mathbf{A}_{up,0}) \tag{3.35}$$

Here, we do not have to do an inversion any more over matrices which relate to **all** eigenmodes. Because of the Bragg condition, we can split up this calculation in sub-matrices of one subset. In practice, such an implementation is much faster.

For completeness, we also discuss the concept of the first Brillouin zone. Because of equation 3.34, each wavevector $\mathbf{k}$ of an eigenmode is directly related to a wavevector $\mathbf{k}$ in the first Brillouin zone. Indeed, the Brillouin zone of a square lattice is defined as the area in k-space, for which the following conditions are fulfilled:

$$-\frac{2\pi}{2\Delta_x} \leq k_x < \frac{2\pi}{2\Delta_x} \quad -\frac{2\pi}{2\Delta_y} \leq k_y < \frac{2\pi}{2\Delta_y} \tag{3.36}$$

Thus, once you have all the reflection and transmission matrices of the components in the first Brillouin zone, all components outside the first Brillouin zone are also known.

In conclusion, we have shown that multiple round trips of an eigenmode do not result in a large number of excited eigenmodes. Indeed, we only need to consider eigenmodes which satisfy the Bragg condition, even after an infinite amount of multiple round trips. Mathematically, this means that inverse operations of the smaller **S**-matrices are much faster.

3.2.9 From field amplitudes to radiant flux in the z-direction

So far, the previous sections were about numerically integrating the field, which gave the amplitudes of eigenmodes. However, to quantify OLEDs, we need the extraction efficiency, which is the ratio of the total radiant flux in air to the total radiant flux emitted by the dipole in the emissive region. Thus, to calculate the extraction efficiency we need the radiant flux. We calculate this as:

$$P_{tot} = \int\int \frac{dP(k_x, k_y)}{dk_x dk_y} dk_x dk_y \tag{3.37}$$

We approximate this integral by a discrete sum. This integration is done over (k_x, k_y) in the first Brillouin zone.

Let us begin with the radiant flux to the substrate. Now, we will need the Poynting vectors in the z-direction, $S_{z,i}[W/m^2]$, of all eigenmodes. As in the previous sections, the z-direction is defined as the propagation direction of the eigenmode, figure 3.3. So far, we have calculated the excitation of all eigenmodes in the emissive region, which are given by vectors with the elements $A_{do,i}(k_x, k_y)$ and $A_{up,i}(k_x, k_y)$. Now, the radiant flux in the **substrate** of figure 3.3 can be calculated: [9]

$$\begin{aligned} \mathbf{A}_{sub} &= \mathbf{T}_{sub}\mathbf{A}_{do} \\ P_{sub} &= \sum_i S_{z,i}|A_{sub,i}|^2 \end{aligned} \tag{3.38}$$

Note, $\mathbf{T}_{sub}$ is a matrix, because one eigenmode in the emissive region with wave vector (k_x, k_y) can excite an eigenmode with a different wave vector.

One factor, which needs more explanation, is the 'normalisation factor' S_z. The parameter $\mathbf{S}_z$ is the radiant flux in the z-direction for one eigenmode which has an amplitude of 1. Thus, the radiant flux of an eigenmode in the substrate with amplitude E, will be $|E|^2.S_z$ for a surface perpendicular on the direction of propagation.

Let us now give two comments concerning the eigenmodes we take into account. Computations limit the amount of eigenmodes. First, we only consider propagating plane waves in the emissive region. Thus, the other possible eigenmodes which are evanescent modes are neglected. Section 3.2.7 gives some more background on this topic. Second, we only work with a discrete set of eigenmodes. Thus, which propagating plane waves do we need to consider? In our work, we use an adaptive algorithm based on the Composite Simpson's rule. For a given propagating plane wave k_x, k_y, it is possible to calculate the radiant flux. Now, the algorithm selects the propagating plane waves which need to calculated.

Let us now discuss the radiant flux in the emissive layer. Now, we need to consider the **net** radiant flux to both the bottom and the top stack of figure 3.3. Because of bidirectionality, simply using equation 3.38 would give a wrong result. The net flux away from the emissive region - to both top and bottom stack - has to give the total radiant flux in the emissive region.

To find the **net** flux which goes to the bottom stack P_{bot}, we require two vectors. The first vector gives the eigenmodes which go toward the bottom stack, $\mathbf{A}_{bot,\downarrow}$. The second vector gives the eigenmodes which come from the bottom stack, $\mathbf{A}_{bot,\uparrow}$. Thus, with the notations of figure 3.3, we have:

$$\mathbf{A}_{bot,\downarrow} = (\mathbf{I} - \mathbf{R}_{top}\mathbf{R}_{bot})^{-1}(\mathbf{A}_{do,0} + \mathbf{R}_{top}\mathbf{A}_{up,0}) \tag{3.39}$$

$$\mathbf{A}_{bot,\uparrow} = \mathbf{R}_{bot}\mathbf{A}_{bot,\downarrow} \tag{3.40}$$

Finally, the net flux $P_{bot}$to the bottom stack is given by:

$$P_{bot} = \sum_i S_{z,i}.(|A_{bot,\downarrow,i}|^2 - |A_{bot,\uparrow,i}|^2) \tag{3.41}$$

For the net flux to the top stack, we have a similar derivation, which leads to:

$$P_{top} = \sum_i S_{z,i}.(|A_{top,\uparrow,i}|^2 - |A_{top,\downarrow,i}|^2) \tag{3.42}$$

Note that for a perfect cathode reflector, the net flux to the top stack P_{top} is 0.

Now, the total power emitted by the dipole is the sum of equation 3.41 and equation 3.42:

$$P_{org} = P_{top} + P_{bot} \tag{3.43}$$

Using this method has some advantages compared to other methods. Most papers use the radiant flux per solid angle $dP(\theta, \phi)/d\Omega$ to calculate the total emitted power P_{tot}. [100] Then, we have:

$$P_{tot} = \int\int \frac{dP(\theta,\phi)}{d\Omega} d\Omega \tag{3.44}$$

This approach has the advantage of being intuitive. Indeed, the radiant flux $P(\theta,\phi)$ can be directly measured with a detector, if we place the detector in the far field of an OLED. Thus, the angular emission of figure 3.7 can be directly measured. But, the disadvantage of this approach is the integration over the solid angle $d\Omega$. For each layer, the parameter over which you integrate, (θ,ϕ) changes, which complicates integration.

In our approach, we have chosen over an integration over (k_x,k_y) in equation 3.37. The advantage is the conservation of (k_x,k_y) when moving between different layers. Thus, using (k_x,k_y) simplifies bookkeeping.

This section has shown how to go from the field and the corresponding amplitudes of the propagating plane waves to the extraction efficiency. The main issue is to calculate the total emitted power in each layers. We have shown how you can go from the decomposition in eigenmodes to a radiant flux in the z-direction.

3.2.10 Location of the dipole with respect to the grating

Dipoles in an OLED with a grating can have a different position with respect to this grating. In theory, we have to calculate the field for each possible location in the emissive region. In practice, we only calculate a finite number of dipoles. This section shows the dipole distribution we have used most of the time in this work.

Figure 3.12 gives the three different positions for which we calculate the field. Then, to calculate the field at a different location in the triangle spanned by these three positions, we use a linear interpolation.

Now, let us use this interpolation to calculate the extraction efficiency. First, for each dipole we calculate the total radiant flux in the z-direction at two locations inside the OLED: the generated power in the organic layers and the power extracted to air. Section 3.2.9 has shown how to calculate the total radiant flux. Now, $P_{org,1}$ is the notation for the total radiant flux in z-direction in the organic layers by a dipole on location 1. Similar notations can be applied for substrate and air, dipoles 2 and 3.

Then, to find the radiant flux in the organic layers for a dipole at a normalized location (x,y) in the emissive layer $P_{org}(x,y)$, we use a linear interpolation:

$$P_{org}(\mathbf{r}) = P_{org,1} + x(P_{org,2} - P_{org,1}) + y(P_{org,3} - P_{org,2}) \tag{3.45}$$

Now, an integration over the dipole positions can be used to calculate the total radiant flux per area in the organic layer. Similar, we calculate the

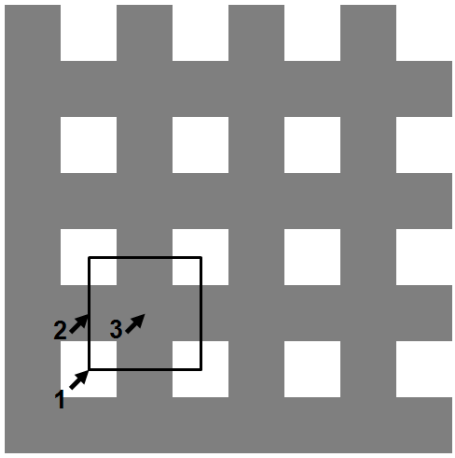

Figure 3.12: The dipole is placed on 3 different locations. For our implementation, this means that you recalculate the OLED with a different elementary cell to calculate the generated power.

total radiant flux in air. Working out the integration, we find the extraction efficiency η_e:

$$\eta_e = \frac{\sum_{i=1,2,3} P_{z,air,i}}{\sum_{i=1,2,3} P_{z,org,i}} \tag{3.46}$$

The extraction efficiency of all dipoles simply is the ratio of the average emission in air of three dipoles to the average emission in the organic layers of the three dipoles.

Remark: to come to equation 3.46, the excitons were modeled as dipole radiators. Another way to model is the following: the extraction efficiency is the chance that a generated photon is extracted. Then, the total extraction efficiency η_e is the average of the extraction efficiency of all locations. Thus, $\eta_e = \sum_{i=1,2,3} P_{z,air,i}/P_{z,org,i}$. Because the refractive index contrast in an OLED is small, we have : $P_{z,org,1} \approx P_{z,org,2} \approx P_{z,org,3}$. There is no clear advantage for either point of view.

In conclusion, this work uses a linear interpolation for the three calculated points as defined by figure 3.12. Then, in this work, the extraction efficiency of all dipoles in the emissive region is given by equation 3.12.

3.3 Multiple round trips in the substrate with a grating on either side of the substrate

To model a dipole in a substrate emitting OLED with a grating, we model coherent **and** incoherent light propagation of propagating plane waves. Figures 3.1(b) and (d) already have illustrated how multiple reflections are important for gratings at either side of the substrate. Note, these two setups are in this algorithm mathematically equivalent.

To explain how we model the substrate, we first have to make a distinction between coherent and incoherent light. So far, we have implicitly assumed coherent light propagation in the organic layers. For example, a propagating plane wave can have constructive or destructive interference after a round trip in the organic layers. In practice, we use the summation of field amplitudes to model this behavior. This model is no longer valid for the substrate which we may consider to be optically thick. Thus, a summation over field amplitudes is no longer valid. For an optically thick layer, we need to use use the radiant flux in z-direction of light instead of its field amplitude to model the substrate.

The algorithm uses a two step algorithm. The first step calculates coherent light propagation of propagating plane waves to the substrate. Here, we can use the algorithm of section 3.2 and of figure 3.13(a). This section is about the second step of figure 3.13(b). To calculate the multiple incoherent round trips in the substrate, we use the angular radiant flux in the z-direction **to the substrate**.

To calculate the radiant flux in the z-direction in air -$\mathbf{P}_{z,air}$-, we use:

$$\mathbf{P}_{z,air} = \mathbf{T}^P_{out}(\mathbf{I} - \mathbf{R}^P_{bot}\mathbf{R}^P_{top})^{-1}(\mathbf{P}^P_{z,sub}) \tag{3.47}$$

Now, where does this equation come from? First, note that the form of this equation is similar to the form of equation 3.35. However, instead of field amplitudes, the radiant flux in the z-direction is used.

The radiant flux of the first step -$\mathbf{P}_{z,sub}$- is used as the 'source' of equation 3.47, the second step. Thus, the power reflectance of the bottom stack and top stack of figure 3.13 are respectively defined by the matrices $\mathbf{R}^P_{bot}$ and $\mathbf{R}^P_{top}$ The transmittance to air is defined by the matrix $\mathbf{R}^P_{bot}$. This equation again holds for a **set** of propagating plane waves as defined by subsection 3.2.8.

This subsection has shown how we model incoherent propagation of propagating plane waves. Combined with decomposition of a dipole to propagating plane waves over the entire (k_x, k_y)-space and addition over this entire space, we now have all the building blocks to model light extraction.

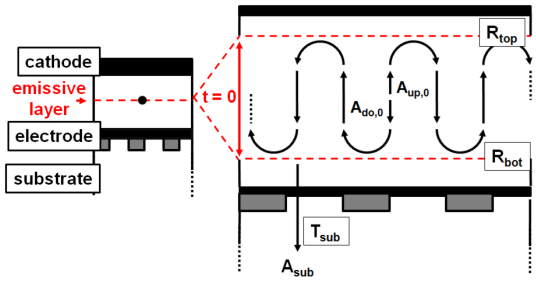

(a)

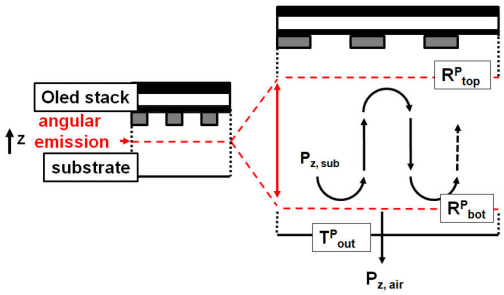

(b)

Figure 3.13: This figure defines the notation which is used in equation 3.47 (a) Plane wave decomposition of a dipole is used to calculate the angular radiant flux to glass. (b) Multiple reflections in the substrate.

3.4 Overview of the Rigorous Coupled Wave Analysis algorithm

In this subsection, we summarize **all** the steps of the complete numerical model for multiple round trips. So far, each step has been explained in section 3.3 and 3.2. The level of detail might have been too high to make it easy to keep an overview. Also, this subsection shows the changes of the algorithm depending on the location of the grating.

As stated before, the numerical model in this work is very similar to the algorithm of subsection 3.2.2, which is used to calculate the field of a dipole in a stratified medium. However, adding a grating and an optically thick substrate requires some changes.

1. Describe the OLED as a stack of z-invariant layers. Then, the eigenmodes of subsection 3.2.3 can be used. The eigenmodes are identified by their polarisation (TE or TM) and the part of the wave vector which is parallel to the emissive region (k_x, k_y).

2. Calculate the excitation of the eigenmodes of the emissive region by the dipole with subsection 3.2.4.

3. Calculate the coherent propagation of eigenmodes in the organic layers by using subsections 3.2.5 and 3.2.6.

4. We now have the field amplitudes. Use subsection 3.2.9 to calculate the radiant flux in the z-direction to the substrate. [1]

5. Use equation 3.47 of subsection 3.3 to calculate the incoherent propagation of eigenmodes in the substrate. [2]

6. Calculate the extraction efficiency. Divide the total radiant flux to air to the total radiant flux in the organic layers, see also equation 3.46 or subsection 3.2.9. Note that we need to calculate for more than one dipole position if the grating is close to the emissive region.

In conclusion, this subsection has given an overview of all steps which we need to model multiple round trips. The end result of our calculations is the extraction efficiency of the OLED.

[1] In theory, we need to use the complete **set** of eigenmodes in a specific layer. However, subsection 3.2.8 shows how to group eigenmodes to make matrix calculations more manageable.

[2] To find the total radiant flux in the z-direction for a given point, we need to sum over **all** eigenmodes. Use the trick of subsection 3.2.7 to simplify the integration over a complex k_x, k_y-space to an integration over a real k_x, k_y-space.

3.5 Convergence analysis of the numerical model

This section gives some numbers on the two parameters which influence accuracy and simulation time. The first parameters is the number of diffraction orders we use for the Rigorous Coupled Wave Analysis (RCWA) algorithm. Equation 3.9, the Bragg condition, shows us that for each incident component, an infinite amount of diffraction orders exists. However, we need to restrict the amount of orders. The second parameter is the resolution Δk we use to perform the integration over in the first Brillouin Zone.

Let us start with the first parameter, the number of diffraction orders. Figures 3.14(a) and 3.14(b) give respectively the convergence and the simulation time in function of the number of diffraction orders. Table 3.2 gives the layer structure. Each figure uses an x-axis with the number of diffraction orders as parameters. In our implementation, the total number of diffraction orders we calculate in one dimension is always given by $2N + 1$, where N is a positive integer. Thus, if we consider a diffraction order +1 in our calculations, we also consider diffraction order -1. Because we work in two dimensions, we only calculate a total number of orders equal to $N_{orders} = (2N + 1)^2$.

Let us now consider accuracy by looking at figure 3.14(a). Only for a sufficient number of orders does the result converge. For the extraction efficiency of the substrate, only considering the first diffraction order (N=9) has a relative difference of 10% with the result where we also consider the second diffraction order (N=25). This comes at a price. Figure 3.14(b) shows that going from 9 orders to 121 orders, increases the simulation time by 10^3. The bottle neck is caused by matrix inversions. Thus, **simulation time scales with the third power of the number of orders.**

As a rule of thumb, we at least take all the propagating plane waves into account. The required number of orders to achieve this is given by:

$$\begin{aligned} k_{tot} &= \frac{2\pi}{\lambda} n_e \\ k_{\Delta_x}, k_{\Delta_y} &= \frac{2\pi}{\lambda_x}, \frac{2\pi}{\lambda_y} \\ N_x &= \left\lfloor \frac{k_{\Delta_x}/2 + k_{tot}}{k_{\Delta_x}} \right\rfloor \\ N_y &= \left\lfloor \frac{k_{\Delta_y}/2 + k_{tot}}{k_{\Delta_y}} \right\rfloor \end{aligned} \tag{3.48}$$

In this equation, we have an emissive region with refractive index n_e and an incident propagating plane wave with wavelength λ. The period of the grating the x and y-direction is given by respectively Δ_x and Δ_y. Let us now derive equation 3.48 by using figure 3.15.

In this equation, $-k_{\Delta_x}/2$ gives the smallest wave vector of the first

Brillouin zone. If we consider this point as the incident propagating plane wave, all other **propagating** diffraction orders have to lie within a circle with radius k_{tot}. For more details, see section 3.2.6. Then, the total number of propagating orders within this circle are given by equation 3.48. Thus, in the example of above, to include all propagating plane waves, we have $N_x = N_y = 2$. Therefore, as a rule of thumb, the minimal orders to include all propagating orders. Of course, it is good practice to confirm calculations by doing a convergence study.

The second parameter is the resolution Δk we use to numerically integrate the radiation profile. This determines the number of propagating plane waves we consider in the **first** Brillouin zone. More background information on Brillouin zones is in subsection 3.2.8. Figure 3.14(d) shows that an increase of the k points by a factor 10 ^{2}, in **each** dimension by a factor of 10, also increases the simulation time by about 10^2. So, we have a linear relation between the amount of $\mathbf{k}_t$- vectors and the simulation time. Beyond $(N_{k_x}, N_{k_y}) = (20,\ 20)$, we see that the results fluctuate by about 3%.

In conclusion, these results show that our implementation depends on two simulation parameters for which we find a trade-off between accuracy and simulation time. The first parameter is the number of diffraction orders N_{orders}. Our implementation scales by the third power. We also have shown that as a rule of thumb, we should at least include all propagating plane waves. The second parameter is the amount of discrete $\mathbf{k}_t$-vectors in the first Brillouin zone, N_k. Simulation scales linearly with this parameter. For this parameter, we have given no rule of thumb. In theory, to make sure you have sufficient accuracy, a convergence analysis has to be carried out for all simulations.

3.6 Extraction efficiency for a model with or without multiple round trips.

The reason to develop this simulation tool is to model the multiple round trips in the substrate. To the best of our knowledge, all other simulation techniques only model the light in the substrate which can escape the substrate directly. Thus, all light which only escapes the substrate after multiple round trips is ignored. This section gives three examples to illustrate the underestimation of the extraction efficiency if we only consider **direct transmission**.

The three examples are given by table 3.3. The three simplified OLEDs are respectively a stratified OLED, an OLED with a grating at the organic layers-substrate interface and an OLED with a grating at the substrate-air interface.

Let us consider the first example in figure 3.16(a): an OLED with only planar interfaces. We see a difference between direct transmission and

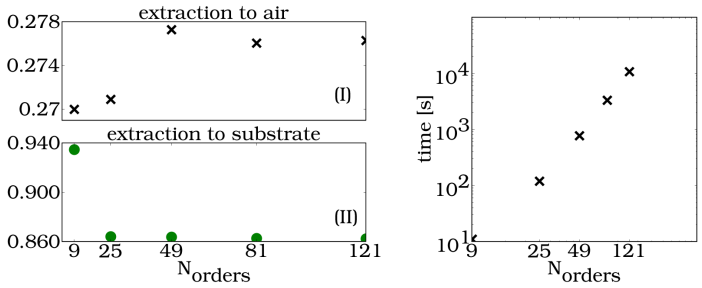

(a) (b)

Extraction efficiency in function of the number of orders N_{orders}: (a) result (b) timing. The extraction efficiency has been calculated to air (I) and substrate (II).

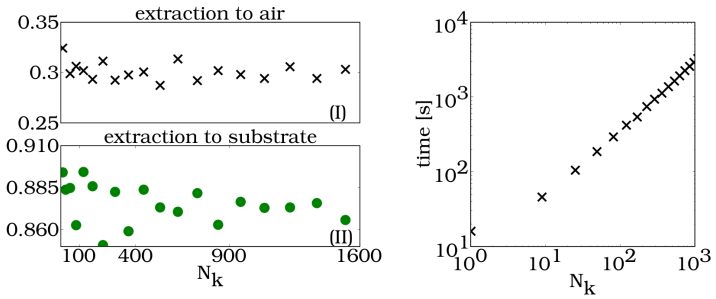

(c) (d)

Extraction efficiency in function of the number of discrete k-steps in the first Brillouin zone N_{k}: (c) result (d) time. The extraction efficiency has been calculated to air (I) and substrate (II).

Figure 3.14: Convergence of the extraction efficiency depends on two parameters. The number of orders and the amount of discrete k-vectors in the first Brillouin zone. The structure has been defined by table 3.2.

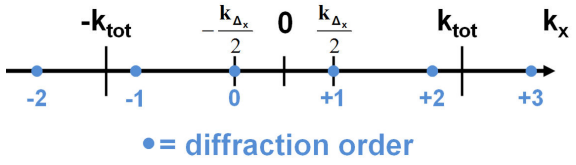

Figure 3.15: The k-diagram helps to derive the minimal number of diffraction orders we require to include all propagating orders. More details can be found in the derivation of equation 3.48. ($k_{\Delta x} = 2\pi/\Delta x$)

Material	Refractive index	thickness
Al	0.87 - 6.5j	100 nm
Electron Transport Layer	1.74	80 nm
emissive layer	1.74	0 nm
Hole Transport Layer	1.78	65 nm
ITO	1.8	150 nm
Grating		300 nm
substrate	1.5	N.A.

Grating

SiN_x-layer in which square holes with size 250 nm are placed on a square lattice with period 550 nm. These holes have been filled with Spin on Glass. The refractive indices are $n_{SiN_x} = 1.93$, $n_{SoG} = 1.28$.

Table 3.2: Layer structure which has been used to investigate convergence of the numerical model for $\lambda = 520nm$, see figure 3.14.

multiple round trips because of Fresnel reflections. In direct transmission, you only consider light which passes the glass-air interface the first time. Granted, considering Fresnel's equations we find that most light within the extraction cone can pass the first time. Nevertheless, a small fraction of light inside the extraction cone still is reflected. Also, some of this small fraction of reflected light can escape after one or multiple round trips. Therefore, we see a small relative difference of less than 5% between direct transmission and multiple round trips for a planar OLED.

Now, the situation changes if we no longer have planar interfaces. Then, a grating scatters one incident plane wave to other angles. Thus, after multiple round trips, light might escape. This is true regardless of the location of the grating. Thus, the extraction efficiency which only considers direct transmission should be much smaller than the extraction efficiency which also considers multiple round trips. Figures 3.1(b) and (c) indeed validates these conclusions. Here, we simulate the structures of table 3.3(b) and (c). These figures give the extraction efficiency in function of the wavelength. Note that the relative difference between the two graphs can be more than 75%. Thus, a model which takes into account multiple round trips gives a larger extraction efficiency.

Note that the absolute extraction efficiency in direct transmission of figure 3.16(c) is lower than for figure 3.16(a) and 3.16(b). Placing a grating between the organic layers and the substrate changes the micro cavity effects, so a deviation from the optimal position is possible in this case.

In conclusion, we have demonstrated that multiple round trips may be neglected for planar OLEDs. However, according to our numerical model, neglecting multiple round trips for an OLED with a grating underestimates the extraction efficiency. We will come back on this conclusion in chapter 5, which contains more accurate OLEDs structures.

3.7 Conclusion

This chapter has described a simulation technique which calculates the extraction efficiency of a substrate emitting OLED for one frequency. The OLED may have a grating at either side of the substrate. Either side of the substrate means either at the interface between the organic layers and the substrate or at the interface between the substrate and air. This technique is based on eigenmode expansion. The novelty of the presented technique is that we also model multiple round trips inside the substrate.

Our model uses two steps. First, we model the radiant flux from the organic layers to the substrate. Here, we assume that light propagation is coherent. Then, we model the multiple round trips in the substrate. Because of the thickness of the substrate, we assume light propagation to be incoherent.

In our last subsection we have shown that multiple round trips are im-

(a) planar interfaces	(b) grating at the substrate-air interface	(c) grating at the organic layers-substrate interface
	Cathode, n = 0.9-6.0j, t = 150 nm	
	Organic layer, n = 1.7, t = 81 nm	
	Emission zone, t = 0 nm	
	Organic layer, n = 1.7, t = 162 nm	
N.A.	N.A.	Grating*2
	substrate, n = 1.5, t = mm	
N.A.	Grating*1	N.A.
	air	

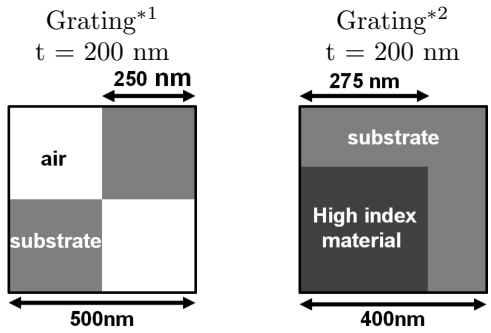

Table 3.3: This table gives the structure of three simplified OLEDs. The extraction efficiency of these OLEDs in function of the wavelength is given by figure 3.16. Notice that the emission zone is located a quarter wavelength of the cathode for a wavelength of 550 nm.

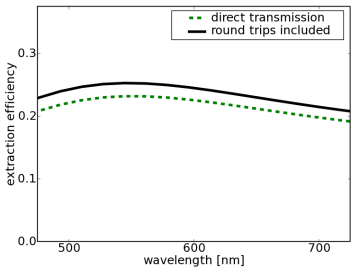

(a) Extraction efficiency of a simplified OLED with only planar interfaces

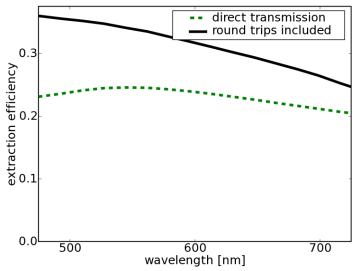

(b) Extraction efficiency of a simplified OLED with a grating at the substrate air interface.

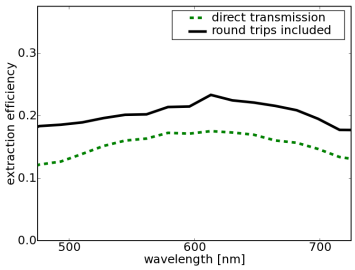

(c) Extraction efficiency of a simplified OLED with a grating at the organic layers-substrate interface.

Figure 3.16: This figure gives the extraction efficiency in function of the wavelength. This extraction efficiency can be calculated in either direct transmission or with multiple round trips. This figure shows a comparison for three different simulation setups: a planar OLED, an OLED with corrugated substrate and an OLED with a grating between organic layers and substrate. Table 3.3 gives the specifications of the simulated structures.

portant if the OLED has a grating. Then, light can be extracted in direct transmission or after multiple round trips. Ignoring these multiple round trips will underestimate the extraction efficiency. The same conclusion is true for a grating at the interface between organic layers and substrate. Light extraction can be increased because more light can be extracted to the substrate **and** because light can scatter at the grating after a few round trips.

4

The RC^{2}LED for increased light extraction

This chapter shows how to increase light extraction by using planar interference layers. The location of these interference layers is between the organic layers/ITO and the substrate. In the introduction chapter, we already have discussed OLEDs with interference layers, such as resonant cavity OLEDs. Here, we discuss the RC^{2}LED, which has two cavities. The first cavity is formed by the organic layers and the interference layers. The second cavity is formed **inside** the interference layers. This chapter basically consists of 3 parts. First, we discuss optical parameters of an optimized design. The second and third section discuss respectively the simulation results and the experimental results of a green OLED.

Overview

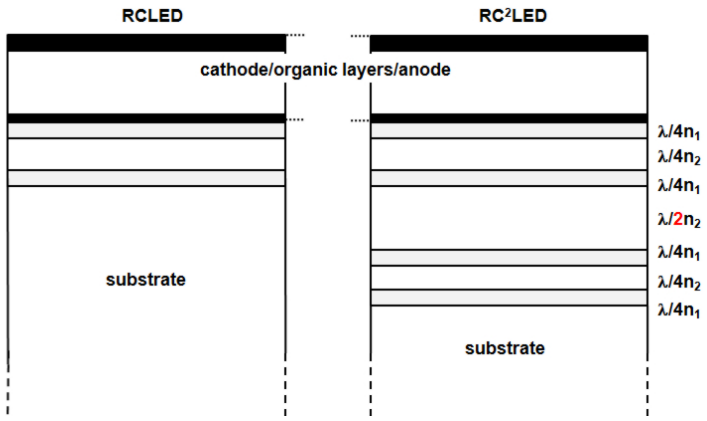

Figure 4.1: Figures (a) and (b) respectively give the structure of a RCLED and the structure of a RC²LED.

4.1 The RC²LED stack

4.1.1 Introduction

The angular emission of a planar OLED fully describes the extraction efficiency. Indeed, to calculate the extraction efficiency, we compare the angular emission over all angles and the angular emission over the angles within the extraction cone. Luckily, the angular emission can be changed with interference layers close to the organic layers. One type of interference layers is the RC²LED. This design originally was proposed for semiconductor LEDs. [11] Due to problems with current injection, the design was never tested. We will show that the design however works for OLEDs.

This section shows how to calculate the angular emission. A key role is for the reflectivity of the stacks at either side of the emissive layer. Therefore, subsection 4.1.3 gives some extra information on the reflectivity on the interference layers. The next section, section 4.2 then will optimize the extraction efficiency of the RC²LED by tuning the layer thicknesses.

As stated before, the angular emission can be changed by interference layers. To explain this behavior, the term **density of states** sometimes is used. The density of states gives the number of photon states to which an exciton can couple. According to Fermi's golden rule, the more states the photon can couple to, the higher the chance that a photon couples to these states. Thus, increasing the density of states inside the extraction cone increases the extraction efficiency. We however can find a direct relation

between density of states and the electromagnetic field. [10] Thus, from here on, we describe the extraction efficiency in function of the angular emission.

The interference layers we use in this chapter give a RCLED and a RC^{2}LED, figures 4.1(a) and (b). The interference layers of the RCLED form a Bragg mirror. The layer structure of the RC^{2}LED is given by figure 4.1(b). Here, two Bragg mirror enclose a cavity. Again, the organic layers and one Bragg mirror form the first cavity, the two Bragg mirrors and cavity form the second cavity.

The next subsection, subsection 4.1.2 repeats the main mathematical principles to calculate the angular emission. For sake of completeness, subsection 4.1.3 shows how the reflectivity of the interference layers change in function of parameters such as thickness.

4.1.2 Eigenmode expansion to calculate the angular emission of an OLED

In this subsection, we repeat how the numerical model of section 3.2.2 calculates the angular emission. Special focus is placed on how we mathematically describe the optical behavior of the interference layers.

We model a substrate emitting OLED by a monochromatic dipole which radiates in a stack of layers. The angular radiant flux requires a decomposition of the dipole field in free space in a continuum of eigenmodes. Note that these eigenmodes always are plane waves or evanescent waves if we have planar interfaces. The second step propagates each of these eigenmodes throughout the structure. The third and final step sums the upward and downward propagating plane waves to get the total radiant flux in a specific direction. This derivation gave us equation 3.2:

$$A_{do} = T_{bot}(I - R_{bot}R_{top})^{-1}(A_{do,0} + R_{top}A_{up,0}) \tag{4.1}$$

Now, the far field pattern follows from A_{do}. To calculate this amplitude for a specific direction, we have to consider the excitation of two plane waves by the source. Both a plane wave propagating downwards and a plane wave propagating the opposite direction are excited. For sake of argument, we assume that the amplitude of these plane waves *at the location of the dipole* is given by respectively $A_{do,0}$ and $A_{up,0}$. The complex values R_{bot} and R_{top} fully describe the optical behavior of the respectively lower and upper stack of layers.

To illustrate how R_{top} and R_{bot} depend on the dipole location and the reflectivity at both sides, we look at the angular emission in the perpendicular direction of a simplified OLED. The simplified OLED has a perfectly reflecting cathode, organic layers with a refractive index n_{org} and a substrate. For one plane wave, we assume that the angle between the normal

to the emissive region and its propagation direction is θ. Also, the thickness between cathode and dipole is z_e, the distance from the cathode and the total thickness of the organic layers is t_{org}. This gives:

$$\begin{aligned} R_{top} &= -\exp\left(-j2\frac{2\pi n_{org}}{\lambda} z_e \cos(\theta)\right) \\ R_{bot} &= R_{org/sub} \exp\left(j2\frac{2\pi n_{org}}{\lambda} t_{org} \cos(\theta)\right) \end{aligned} \tag{4.2}$$

In this equation, the amplitude reflectivity between organic layers and substrate is given by $R_{org/sub}$. The perfect reflector at the cathode gives a phase shift of π. For a maximal extraction efficiency in the **perpendicular direction**, two conditions have to be satisfied. First, the nominator - $A_{do,0}+A_{up,0}R_{bot,0}$ - should be maximal. Second, the numerator $I-R_{bot}R_{top}$ should be minimal. As already was described in section 2.4.3, this happens for positive interference between down and up propagating plane waves, as

$$\begin{aligned} \frac{z_e n_{org}}{\lambda} &= \frac{1}{4} + \frac{n}{2} \\ \frac{t_{tot} n_{org}}{\lambda} &= \frac{3}{4} + \frac{n}{2}, \; n \in I\!N \end{aligned} \tag{4.3}$$

In conclusion, the angular emission of an OLED follows from a decomposition of the dipole in plane waves. Then, the angular emission follows from equation 4.1. In this equation, the optical behavior of the interference layers is fully described by R_{bot}.

4.1.3 Reflectivity of the interference layers of a RCLED and a RC^{2}LED

The goal of this subsection is to give some extra information on R_{bot} of equation 4.1 for the interference layers of figure 4.2. Having some feel for this term can be interesting for the next section, section 4.2.

Let us begin by looking at the reflectivity of the two interference layers. Figure 4.2 and table 4.1 give the parameters of the interference layers of a RCLED and a RC^{2}LED. Figure 4.3 gives the power reflection.

The main resemblance between the two structures are the Bragg mirrors. These Bragg mirrors reflect perpendicular incident light. The wavelength of this reflection depends on λ_{res}. The bandwidth over which this reflection happens depends on number of layers and refractive index difference. This will be discussed in the remainder of this section.

The main difference between the two structures is the optical cavity in the RC^{2}LED. For the resonance wavelength λ_{res}, a spectrally narrow peak has a very high transmission. You could describe the interlayers of a

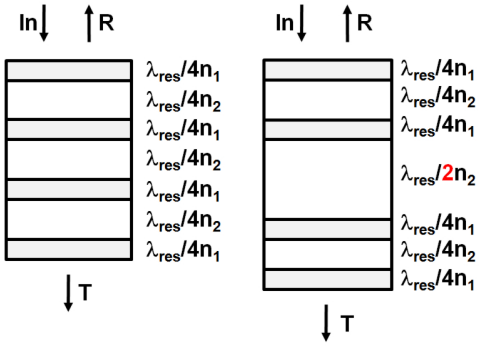

(a) RCLED (b) RC^{2}LED

Figure 4.2: The stack of a RCLED are quarter wavelength layers which form a mirror. However, the cavity in the stack of a RC^{2}LED allows perpendicular incident plane waves to pass. More details are in table 4.1.

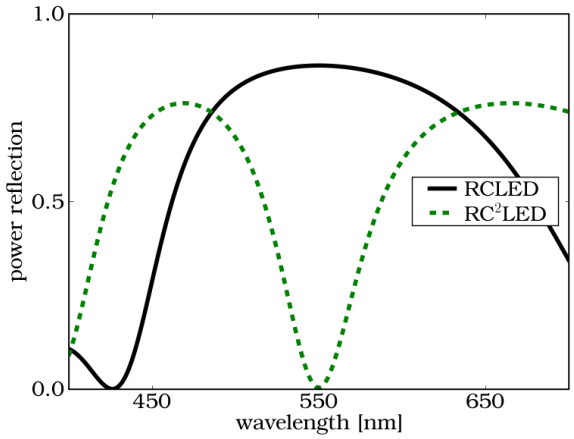

Figure 4.3: The reflection of a RCLED and a RC^{2}LED are very similar, except at the location of the resonance wavelength, λ_{res}. This figure uses the setup of figure 4.2 with the parameters of table 4.1

refractive index incident plane	1.7
refractive index of the high index layer, n_1	2.3
refractive index of the low index layer, n_2	1.5
resonance wavelength λ_{res}	550 nm

Table 4.1: Default parameters for the structure of figure 4.2. All figures of this section use these parameters, unless indicated otherwise

RC^{2}LED as an anti-reflection coating for the resonance wavelength. This resonance wavelength in the RC^{2}LED gives an extra degree of freedom with which we can optimize the extraction efficiency.

Figure 4.4 gives both magnitude as phase of the amplitude reflection in function of angle for a given wavelength. Both RCLED and RC^{2}LEDs interference layers have been investigated for different incident angles. The RCLED interference layers are a Bragg mirror at the resonance wavelength. Thus, we see very high reflection for perpendicular incident plane waves. However, reflection of the RC^{2}LED interference layers is minimal for a perpendicular incident angle!

As a rule of thumb, more number of layers for the Bragg mirror will make the angular emission much more resembling a block function. Increasing the refractive index contrast will make the 'block' for which we have high reflection will stretch over a larger region of angles. Also, increasing the refractive index will make sure that the reflection will be over a wider wavelength range. [91]

4.2 Optimization of the extraction efficiency of a RC^{2}LED

4.2.1 Introduction

The main focus of this section is the extraction efficiency in function of the wavelength for both a reference OLED and a RC^{2}LED. These OLEDs will also be discussed in the next section on experiment, section 4.3. The only difference between the reference OLED and the RC^{2}LED will be interference layers between ITO and the substrate. The thickness of these interference layers will be used to optimize the extraction efficiency of the RC^{2}LED. Both OLEDs use the same stack of organic layers.

The organic layer stacks of the OLEDs are given by table 4.2. Of these two, the extraction efficiency of the reference OLED already has been optimized. As we will see later on, its extraction efficiency is around 20% for all visible wavelengths. To optimize the RC^{2}LED, we have performed a **brute force scan** over two parameters: (t_{NbO_x}, t_{SiO_2}). Note that this can result in a different resonance wavelength for organic layer stack ($\lambda_{res,org}$ and the

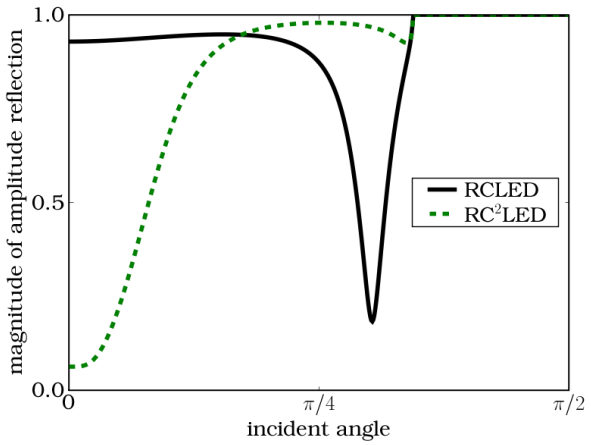

(a) Magnitude of the amplitude reflection

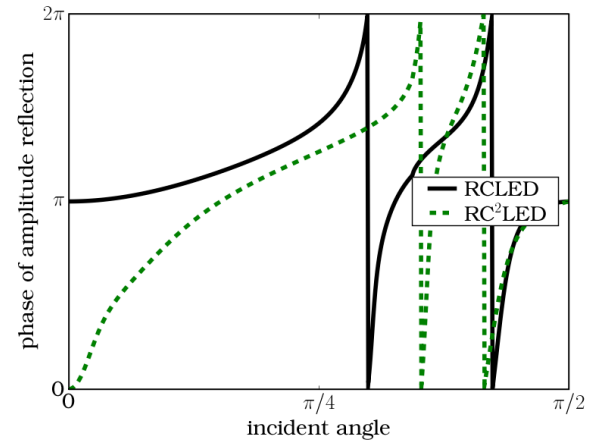

(b) Phase of the amplitude reflection

Figure 4.4: The amplitude reflection of the RCLED and the RC^2 LED differ both in magnitude and phase. These plots have been calculated in function of the incident angle of figure 4.2. The parameter values are in table 4.1.

Material	refractive index (@550 nm)	reference OLED	RC^{2}LED
Aluminium	0.96 - 6.69j	150 nm	150 nm
ETL	1.66	80 nm	20 nm
Emissive Layer*	1.66	40 nm	40 nm, $\lambda_{res,org} \neq$430 nm
HTL	1.81	20 nm	80 nm
ITO	1.82 - 0.01j	50 nm	50 nm
NbO_x	2.38	N.A.	45 nm $\lambda_{res,RC^2} \approx$ 430 nm
SiO_2	1.46	N.A.	146nm $\lambda_{res,RC^2} \approx$ 430 nm
NbO_x	2.38	N.A.	45 nm
glass	1.53	N.A.	N.A.
air	1.0	N.A.	N.A.

Table 4.2: The layer stack of the RC^{2}LED and the reference OLED only differ in the three additional layers. (*The emission takes place in the middle of the emissive layer. N.A.: not applicable)

RC^2 interference layers (λ_{res,RC^2}). The OLED we use for the experiments has one layer with a green dye. Therefore, as optimization criterium we have used the extraction efficiency around 550 nm.

Because the organic stack has been optimized for the reference OLED, the relative improvement of the RC^{2}LED might even be higher if both the stack of organic layers and the interference layers are optimized at the same time.

The next subsection, subsection 4.2.2 gives the extraction efficiency in function of wavelength. Also, we discuss the influence of some deviations from this design. So, this shows how robust our design is. To explain the wavelength dependent behavior, we look at the angular emission in subsection 4.2.3.

4.2.2 Extraction efficiency in function of the wavelength

In this section, we describe the extraction efficiency in function of the wavelength for both the reference OLED and the RC^{2}LED. An analysis has to wait until subsection 4.2.3. Note that the extraction efficiency usually refers to the extraction efficiency to air. As stated before, this parameter gives the fraction of photons which can go from emissive region to air. However, in this section we will also look at the extraction efficiency to the substrate. This extraction efficiency to the substrate is the fraction of photons which can escape from the organic layers to the substrate. Also, we look how

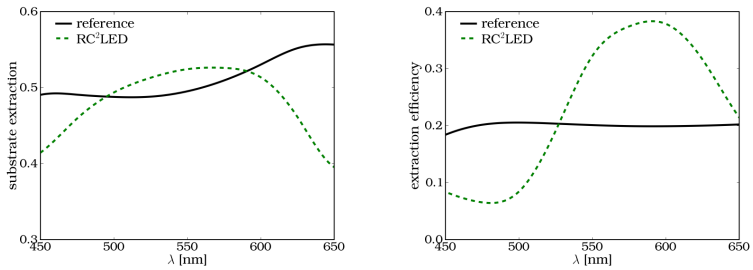

(a) fraction of generated photons which can escape to the substrate(!)

(b) fraction of generated photons which can escape to air

Figure 4.5: Extraction efficiency in function of wavelength, λ.. (structure: table 4.2)

robust our design is.

Figure 4.5(b) gives the extraction efficiency to air for both the reference OLED and the RC^{2}LED in function of the wavelength. From this figure it is clear that the extraction efficiency of the reference OLED is 20% over the full visible wavelength range. Not so for the RC^{2}LED. The RC^{2}LED has a maximal extraction efficiency of 40%. At other wavelengths, the RC^{2}LED has a much lower extraction efficiency than the reference OLED.

If we look in figure 4.5(a) at the extraction efficiency to the substrate, we see a different story. Between 500 and 600 nm, the reference OLED and RC^{2}LED have almost the same extraction efficiency to the substrate. However, the extraction efficiency to the substrate of the RC^{2}LED rapidly decreases outside this wavelength range.

To investigate how robust our design is, we vary three parameters. First, so far, we have used a dipole in the middle of the emissive zone. However, figure 4.6(a) shows that an off-set of the location of the emissive region does not change the location of the peak. Nevertheless, an off-set changes the magnitude of the extraction efficiency. The second parameter is the thickness of the emissive layer, figure 4.6(b). If we define the wavelength with the maximal extraction efficiency to air as λ_{peak}, then we find following equation: $\lambda_{peak}/t_{tot} \approx C^e$. If we consider that fabrication tolerances are well within these large variations, we expect a good agreement between simulation and experiment.

4.2.3 Angular emission for different wavelengths

The wavelength dependent extraction efficiency of the reference OLED and the RC^{2}LED,figure 4.5(b) can be explained with the angular radiant flux per solid angle for both OLEDs. Here, this will be done for two wavelengths:

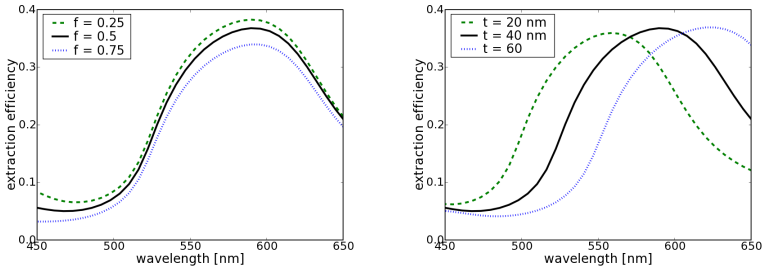

(a) Dipole location varies. The default is f = 0.5 the middle of the emissive layer. The fraction f = 0.25 means emissive layer is placed 10 nm from the ETL and 30 nm to the HTL.

(b) Different thicknesses of the emissive layer.

Figure 4.6: Extraction efficiency in air as a function of the wavelength for a variation of the parameters of table 4.2.

525 nm and 600 nm.

To explain the wavelength dependent extraction efficiency of figure 4.5(b), we use the angular radiant flux of figure 4.7. The angular radiant flux is given in glass. Thus, we have Total Internal Reflection (TIR) for all light which is incident under an angle more oblique than 41^o. First, the angular emission of the reference OLED does not change much in function of the wavelength. However, the angular radiant flux of the RC^{2}LED is more directional. This can be beneficial. Indeed, if the peak of radiant flux lies within the extraction cone, we have a high extraction efficiency. However, if the wavelength shifts, the peak of the radiant flux may shift outside the extraction cone. Conclusion, the highly directional radiation profile of the RC^{2}LED causes the wavelength dependent behavior of the extraction efficiency.

Remark: the highest extraction efficiency occurs for the angle of the radiant flux which is as oblique as possible while being smaller than the angle of TIR, θ_{TIR}. Indeed, to calculate the extraction efficiency, we need to integrate the radiant flux P(θ) over the solid angle, see equation 3.44. In this equation, more oblique angles have more impact due to the higher weight factor of the solid angle $d\Theta$.

To conclude, the wavelength dependent behavior of both the reference OLED and the RC^{2}LED can be explained with the angular radiant flux per solid angle for both OLEDs.

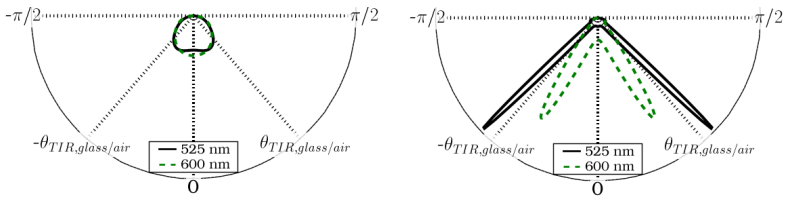

(a) reference OLED (b) RC^{2}LED

Figure 4.7: Angular radiant flux per solid angle P(θ) in **glass** for a reference OLED and an RC^{2}LED at 525 nm and 600nm. Total Internal reflection occurs for emission at angles larger than 41^o. (structure: table 4.2)

4.2.4 Conclusion

This section has tried to explain the wavelength dependent behavior of the RC^{2}LED. Although a relative improvement by a factor of two is possible, this improvement is only in a limited wavelength range. Another disadvantage might be the strong angular dependency. However, this might be solved by using a layer on top of glass, which scatters some of the incident light.

4.3 Experimental verification

4.3.1 Introduction

This section shows how measurements verify the simulations of the previous section, section 4.2. For the measurements, two sets of two OLEDs have been fabricated. Each set contains a reference OLED and a RC^{2}LED with the design parameters of 4.2. Thus, each set has been fabricated in a different run. However, each set contains the same two OLEDs by design.

For each set, the same organic layer stack has been deposited on two types of substrates. The first substrate is a normal glass substrate, which gives after deposition reference OLEDs. The second substrate however has 3 additional layers which gives after deposition RC^{2}LEDs. Fabrication of the 3 layers and the organic layer stack was done respectively by Philips Eindhoven and by Philips Research Aachen. As we will see, these devices have a relatively low voltage which is because the doping of the transport layers with dopants from NOVALED. Finally, the measurements of these devices has been done in collaboration with the 'Liquid Crystals and Photonics'-group of the Ghent University.

The remainder of this section is as follows: first, subsection 4.3.2 shows how to compare simulation and experimental results. Also, the way of measurement is explained and a short overview of the measurements results

is given. Then, for completeness, subsection 4.3.3 shows the influence of microlenses on top of the OLEDs. Using a microcavity OLEDs and microlenses is not unique, as was demonstrated in the literature overview of subsection 2.4.7. Finally, we conclude in subsection 4.3.4.

4.3.2 Comparison of simulations and measurements

A direct comparison of simulations and measurements would require absolute measurements. On the one hand, simulations give the wavelength dependent extraction efficiency. On the other hand, measurements of an OLED give its spectrum. Therefore, we have opted for a more indirect approach. Here, we eliminate the need for absolute measurement by using the relative improvement of the RC²LED to the reference OLED. Both OLEDs have been fabricated in the same run. Thus, though we start with absolute measurements, we assume the stack of both OLEDs to be sufficiently reproduceable for our measurements. Thus, from now on, we compare the relative improvement of simulations and measurements.

To find the relative improvement of the simulated RC²LED to the simulated reference OLED, their respective extraction efficiencies, $\eta_{e,RC^2LED}(\lambda)$ and $\eta_{e,\text{reference OLED}}(\lambda)$ are divided:

$$\text{relative improvement}_{\text{simulations}}(\lambda) = \frac{\eta_{e,RC^2LED}(\lambda)}{\eta_{e,\text{reference OLED}}(\lambda)} \quad (4.4)$$

To find the relative improvement of the measured RC²LED to the measured reference OLED, their respective spectral emission, $E_{e,RC^2LED}(\lambda)$ and $E_{e,\text{reference OLED}}(\lambda)$ are divided:

$$\text{relative improvement}_{\text{measurements}}(\lambda) = \frac{E_{e,RC^2LED}(\lambda)}{E_{e,\text{reference OLED}}(\lambda)} \quad (4.5)$$

This last equation is illustrated by the simulation result of figure 4.8. The electroluminescence spectrum of the organic layers is given by $\phi_{EL}(\lambda)$. Then, the actual emission of both the reference OLED and the RC²LED comes from the product of $\phi_{EL}(\lambda)$ and their respective extraction efficiency: $\eta_{e,RC^2LED}(\lambda)$, $\eta_{e,\text{reference OLED}}(\lambda)$. Thus dividing the spectral emission, cancels out the spectral behavior of the emitter from figure 4.8(a).

Strictly speaking, using equations 4.4 and 4.5 means that we implicitly have assumed that light generation in the organic layer is not influenced by the cavity. Let us first show how light generation can be influenced. For example, the Purcell effect tells us that the lifetime of the exciton can be influenced by the cavity. Now, suppose that the RC²LED increases the lifetime of the exciton compared to the lifetime of the exciton in the reference OLED. This does not make a difference if there all decays are radiative. However, if excitons can decay non-radiatively, then more excitons in the RC²LED would decay by non-radiative processes. This would mean that

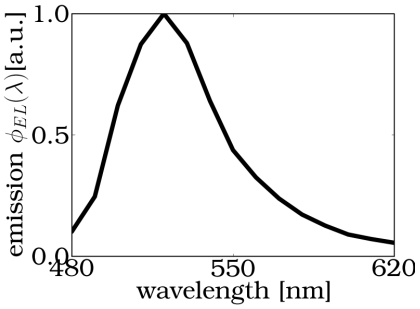

(a) Electroluminescence of the green emissive layer

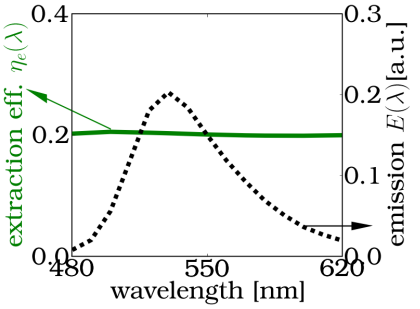

(b) Extraction efficiency and the spectrum of the reference OLED

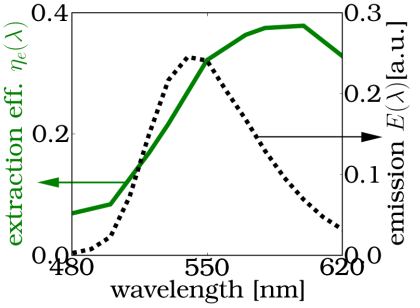

(c) Extraction efficiency and the spectrum of the RC^{2}LED

Figure 4.8: Multiplying the spectrum of the green emissive layer $\phi_{EL}(\lambda)$ in the organic layers and the extraction efficiency of a structure $\eta_e(\lambda)$ gives the spectrum of that structure: $E(\lambda) = \phi_{EL}(\lambda)\eta_e(\lambda)$.

(a) (b) (c)

Figure 4.9: (a)The OLEDs emit green light. (b) Using a foil with an array of microlenses can easily be applied. (c) Measurements can be done with an (optional) cover screen. (OLEDs and plastic foil with microlenses have been fabricated by Philips Aachen)

equations 4.4 and 4.5 would no longer be valid. However, the microcavity presented in this work is sufficiently weak to neglect the Purcell effect.

So far, we have discussed our way of comparing measurements with simulations. Now, let us focus on the actual fabrication and measurements of the OLEDs, which would have been impossible without the institutes mentioned in the introduction.

Figure 4.10 gives the measured spectrum of the second set of devices of figure 4.9(a). As stated before, the **same** stack of organic layers has been deposited on two substrates. The first substrate is a normal glass substrate on which the reference OLED is deposited. The second substrate however has 3 additional layers. These substrates have a size of 5 cm by 5 cm on which the organic layers have a size of 4 cm by 4 cm. Figure 4.8(a) shows that emission of the organic layer stack is focused in the visible green. Variations on the thicknesses of the organic layers is around 5%. Thus, roughly speaking, two consecutive fabrication runs of the same layer stack result in an emission with a relative deviation of up to 5%. The wavelength for which the cavity has been optimized wavelength turned out to be slightly different from the electroluminescent peak.

The actual measurements have been done with an integrating sphere of which the light is coupled to a monochromator. The integrating sphere of Bentham has a diameter of 15 cm, the monochromator is a DK 240 Digikröm 1/4 m monochromator. The OLEDs were driven with a Keithley 220 programmable current source of which the driving current was 5.5 mA. The voltages of table 4.3 were measured with a standard multimeter. As can be seen from figure 4.10, the spectrum of interest is between 480 nm and 620 nm. Outside this range, measurement errors are too high. The wavelength step between each measurement point is either 10 nm or 20 nm.

Now, figure 4.11 gives an overview of the relative improvement for both simulations and experiments, respectively figure 4.5 and 4.10. In this fig-

	reference OLED	RC^2LED
set 1, I = 5.5 mA	6.2 V	5.4 V
set 2, I = 5.5 mA	5.8 V	6.0 V

Table 4.3: Driving current and measured voltage of the different OLEDs in set 1 and set 2.

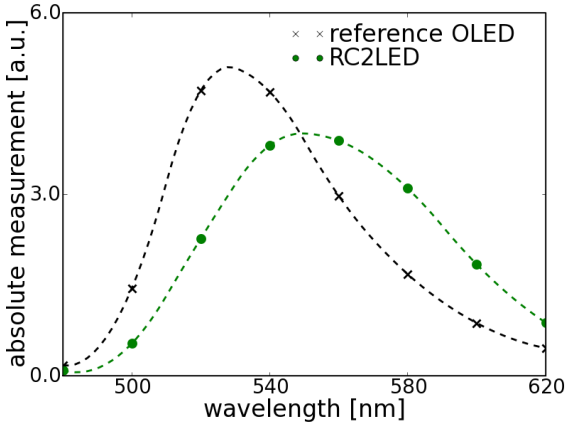

Figure 4.10: Absolute emission in air of the second fabricated set of OLEDs, both the RC^2 LED and the reference OLED. (Dots and Crosses indicate measurement points, lines are interpolated values.)

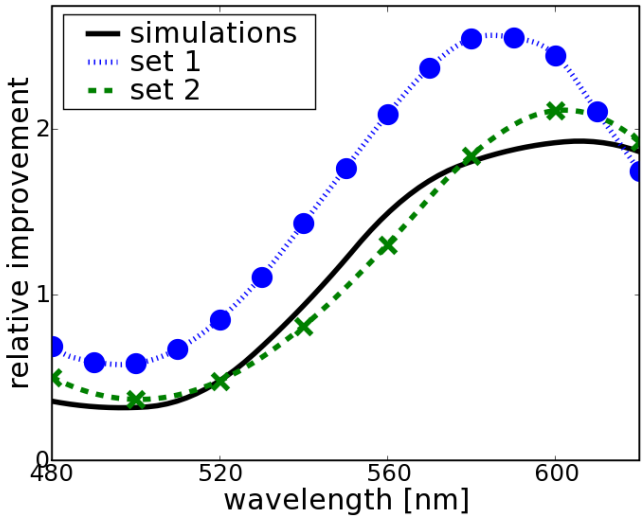

Figure 4.11: A good agreement of the relative improvement for two different sets of fabricated samples and the simulation results has been demonstrated.

ure, the peak of the simulated relative improvement differs by 10 nm from the experimental data. This could be caused by fabric deviation of layer thicknesses which can be 5%. Apart from this, both a good quantative and qualitative agreement is between simulations and experimental data. Moreover, a relative improvement of almost a factor of 2 for a limited wavelength range has been demonstrated with the RC^{2}LED.

4.3.3 Addition of microlenses on the OLED surface

To conclude this section, we also give the relative improvement of the device of set 1 with and without microlenses in figure 4.12. Both the reference OLED and the RC^{2}LED are used, the microlenses are shown in figure 4.9.

Microlenses can be used to increase light extraction from the glass substrate. Adding such a foil of microlenses is done by applying a refractive index matching gel between the substrate of the OLED and the planar side of the foil with an array of microlenses. Figure 4.12 clearly shows that the extraction efficiency of the reference OLED increases by 30% by applying a microlens foil. Also, this relative improvement is quite wavelength independent. Not so for the RC^{2}LED! A microlens foil does not improve extraction efficiency at 600 nm. However, at other wavelengths, we see an improvement up to a factor of 2.5. To explain, take figure 4.11. The maximal relative

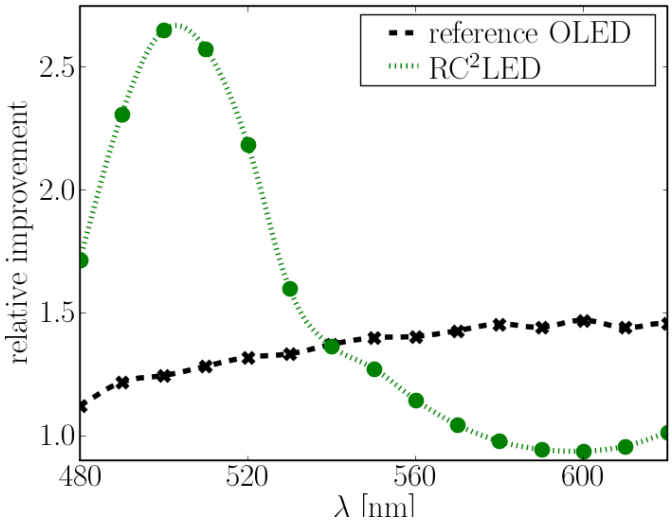

Figure 4.12: Using an array of microlenses on top of either a reference OLED or a RC^{2}LED can increase the amount of power measured. This figure shows the relative improvement between a device with microlenses and one without microlenses.

improvement of the RC^{2}LED to reference OLED is at 600 nm.

Here, the RC^{2}LED already extracts a large amount of the light in the substrate. Thus, the improvement that can be gained with microlenses is minimal. At off-resonances where the RC^{2}LED is not effective, more light remains trapped in the substrate. This light can be extracted with microlenses. Thus, at non-resonance wavelengths, this microlens foil has a higher relative extraction than the microlens foil on a reference OLED.

It is safe to say that microlenses mitigate the wavelength dependence of the RC^{2}LED somewhat. We come back on these results in the simulation results of section 5.2.4.

In conclusion, a microlens foil improves the extraction efficiency of both the reference OLED and the RC^{2}LED. However, the actual improvement is almost negligible for the RC^{2}LED at the wavelength with its highest extraction efficiency. The microlens foil however gives a small compensation of the lower light extraction of the RC^{2}LED at non resonance wavelengths.

4.3.4 Conclusion

In conclusion, the experiments qualitatively verify the simulations of RC^{2}LED. We find a peak of the extraction efficiency around 600 nm. Nevertheless, a

small deviation of the location of the peak was found between simulations and experiments. The quantitative results have quite good agreement. Experiments give a relative improvement between a factor of 2-2.5. The simulations give a relative improvement of slightly less than 2.

Adding a foil of microlenses does not increase light extraction at the resonance wavelength of the RC^{2}LED. The microlens foil however gives a small compensation of the lower light extraction of the RC^{2}LED at non resonance wavelengths.

Oh sure. Even communism works. In theory.

Homer Simpson

5 Gratings in OLEDs to increase light extraction

This chapter shows how gratings in an OLED can increase light extraction. The location of the grating can be on either side of the substrate. Thus, the grating is either between active stack and substrate or between substrate and air. Simulation results by using the the numerical model of chapter 3 are given. Also, some experimental results on a grating between substrate and air are presented. During the optimization of the grating, we highlight the necessity to model multiple round trips in the substrate to correctly model the extraction efficiency.

Overview

5.1 Introduction

Placing a grating at an interface with TIR can increase the extraction efficiency, see chapter 2. First, we give a more rigorous definition of a grating. Then, we define two different **figures of merit**, one for each interface, to quantify 'how good' a grating is.

First, a grating is a structure which is composed by a motif which repeats periodically in two dimensions. For example, figure 5.1 gives four gratings. The first three examples, figures 5.1(a), (b) and (c), use motifs which repeat on a rectangular lattice. The last example, figure 5.1, has a motif on a hexagonal grid.

The first location where we can place a grating is the interface between substrate and air, section 5.2. Now, we can determine the **relative improvement** of an OLED with grating and that same OLED without grating. This proves to be a directly measurable quantity. How? We first measure the spectrum of an OLED. Afterward, we can measure that same OLED with a grating, which has been attached with a refractive index matching gel. This way of working assumes that the grating is not fabricated in the same glass plate supporting the organic layers. Of course, the planar OLED already should already be optimized for a high extraction efficiency. There is no point in increasing light extraction of an OLED which has a badly located emissive region. In conclusion, results of gratings at this interface will be expressed in terms of relative improvement.

The second location where we can place a grating is between the active region and substrate, section 5.4. As active region, we define the stack with cathode, organic layers and ITO. The quantity we are interested in, is the **extraction efficiency**. This extraction efficiency gives the ratio of photons in air to the total emitted photons. Note there are at least two reasons for not using relative improvement as quantity to express our results. First, compared to a grating between substrate and air, the relative improvement in this setup is much more difficult to measure. Second, it is difficult to discern the relative improvement which is caused by microcavity effects and the relative improvement which is caused by the grating. Thus, results of gratings at this interface will be expressed in terms of the extraction efficiency.

5.2 Grating at the substrate-air interface: simulations

5.2.1 Introduction

A grating at the interface between substrate and air helps us to extract light which would normally be trapped in the substrate. Another corrugation at this interface is an array of microlenses. As stated in chapter 2, publications

Rectangular lattice

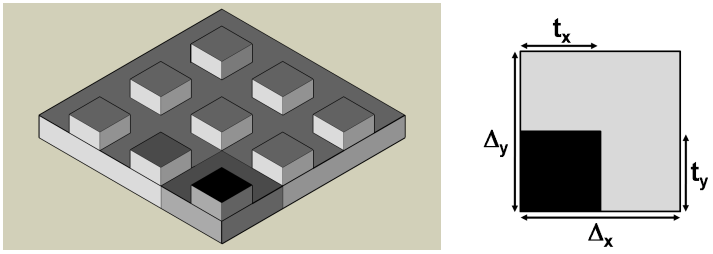

(a) Pillars (perspective and top view of an elementary cell)

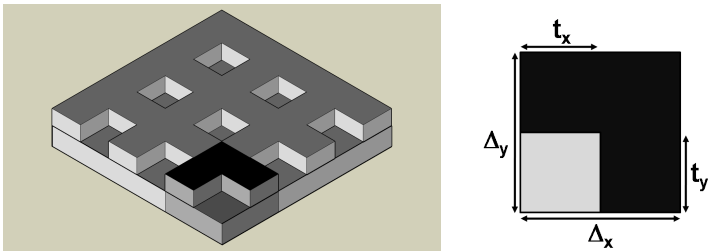

(b) Holes (perspective and top view of an elementary cell)

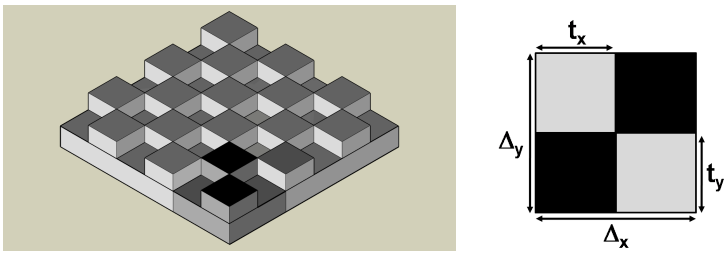

(c) Chess-board (perspective and top view of an elementary cell)

Hexagonal lattice

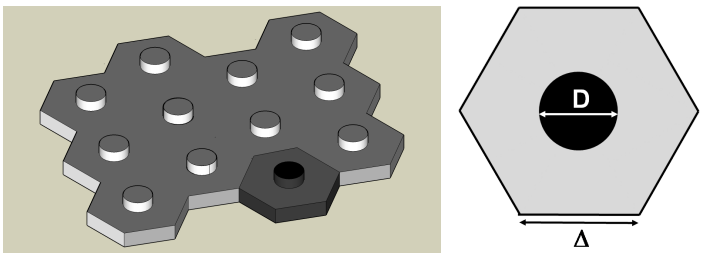

(d) Pillar (perspective and top view of an elementary cell)

Figure 5.1: We distinguish 3 types of gratings on a rectangular lattice and one type of grating on a hexagonal grating.

show an increase of 50-100% by microlenses. Note that neither corrugation, grating or microlenses, extracts light from the stack of organic layers. Thus, measurements give the increase of light which is extracted from the glass substrate.

Our discussion on the simulation results of a grating at the substrate-air interface is spread out over the next three subsections. In subsection 5.2.2, we will determine the optimal parameters for several gratings. Because the focus of this work is the white OLED, special attention is given to the wavelength dependency. Then, subsection 5.2.3 uses the optimized grating to show the influence of round trips in the substrate. This work is similar to the work of subsection 3.6. Because multiple round trips in the substrate prove to be very important, we will also look at the influence of the organic layer stack on multiple reflections in section 5.2.4.

The next section, section 5.3 gives an overview of a few experimental results. This section also includes a comparison between gratings and microlenses.

5.2.2 Parameter optimization

To optimize the gratings, we start from the layer stack of table 5.1. The extraction efficiency of a planar OLED with this stack is given by figure 5.2. This stack will also be used for the experiments of subsection 5.3. Moreover, we investigate the gratings of figure 5.1. We can already see that each grating on a square lattice has 5 parameters. Indeed, the parameters of figures 5.1 (a)-(c) are: Δ_x, Δ_y, t_x, t_y and the height of the corrugation.

To find an optimum, we have performed a local optimization. Meaning, the optimum of the first parameter is found by brute force. At the same time, the other four parameters are kept constant. Then, the optimum of the second parameter is found by brute force. And so on, until the optimum of the last parameter is found. In our experience, this local optimization already gives a good indication for the global optimum. In the parameter range around the local optimum, each grating parameter influences the extraction efficiency largely independently. Thus, best performance is achieved for symmetrical structures, i.e. period and fill factor are equal in both direction of figures 5.1(a) to (c).

Let us now discuss each parameter.

Both depth and period show saturations in figure 5.3. The relative improvement flattens. Here, the minimal depth is 500 nm, the minimal period is 1400 nm. Although figure 5.3 shows the saturation of the relative improvement of a grating of pillars - figure 5.1(a) - , the depth should be at least 500 nm for the other gratings of figure 5.1. Important: the optimal parameters are roughly independent from the wavelength. Of course, this does not mean that the relative improvement is wavelength independent. Only, the value for the optimal parameter is wavelength independent.

material	refractive index	thickness
Al	1.0-6.9j	150 nm
Electron Transport Layer	1.66	55 nm
Emissive layer	1.66	0 nm
Hole Transport Layer	1.80	45 nm
ITO	1.80 - 0.01j	120 nm
SiON	1.62	100 nm
glass	1.52	

Table 5.1: Layer structure which has been used in section 5.2.2 to optimize a grating at the substrate air interface

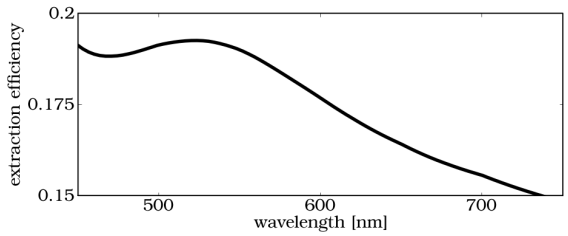

Figure 5.2: Extraction efficiency in function of the wavelength for the OLED defined by table 5.1. This OLED has a maximal emission at 550 nm.

According to figure 5.4, the fill factor is the only parameter which gives a different optimum depending on which grating of figure 5.1 you use. With the notation of figure 5.1, the fill factor is given by:

$$\text{fill factor}_x, \text{fill factor}_y \quad = \quad \frac{t_x}{\Delta_x}, \frac{t_y}{\Delta_y} \tag{5.1}$$

With this definition, figure 5.4 gives the parameter sweep of this parameter. Again, the optimal fill factor is the same for all three wavelengths.

In conclusion, we have found optimal values for each parameter. The depth and period have to be at least respectively 0.5 and 1.4 μm. The fill factor depends on the motif. See figure 5.4 for the optimal fill factor. Moreover, these optimal values prove to be wavelength independent. Note that the maximal improvement is about 1.5. However, the actual relative improvement is dependent on the wavelength.

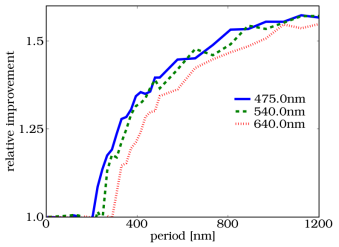

(a) Relative improvement in function of the grating period: cut off value at 400 nm

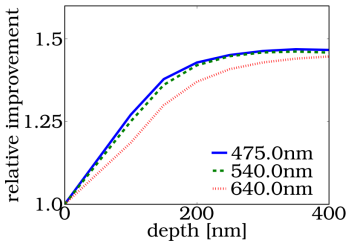

(b) Relative improvement in function of the depth

Figure 5.3: Optimal parameters for the period and depth of the pillars of figure 5.1(a). Similar figures can be found for the chess-board and the holes of figures 5.1(b) and 5.1(c).

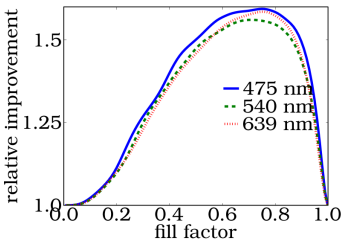

(a) Pillars

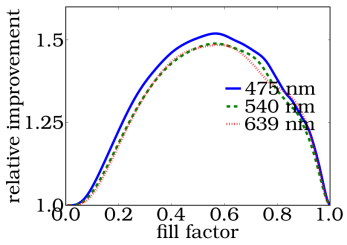

(b) Holes

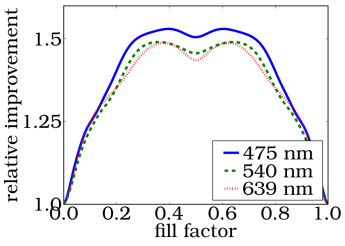

(c) Chess-board

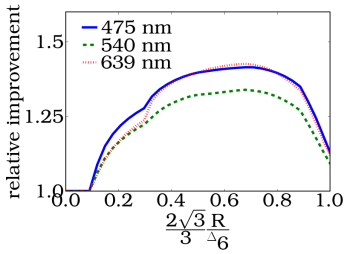

(d) Hexagonal lattice with circular pillars

Figure 5.4: The relative improvement in function of fill factor is given for different wavelengths for the four gratings of 5.1. The optimal location of the fill factor is wavelength independent.

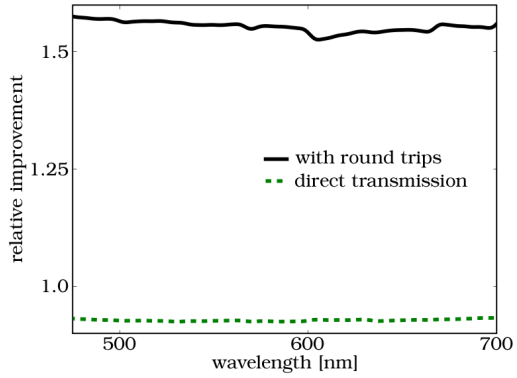

Figure 5.5: The relative improvement of the grating has been calculated for both direct transmission as well as for multiple round trips.

5.2.3 Direct transmission versus multiple round trips

This section highlights the importance of modeling multiple round trips in the substrate. These results are similar to the ones of section 3.6.

To look into the effect of multiple round trips, we again use the relative improvement. This relative improvement is the ratio of the extraction efficiency of the OLED with the grating to the extraction efficiency of the OLED without grating. The extraction efficiency of the OLED without grating takes into account multiple round trips. Note, a fraction of the light inside the extraction cone requires multiple round trips before extraction. The Fresnel reflections reflect part of light. However, after one round trip, this light has another chance to escape. The extraction efficiency of the OLED with grating can be either with or without multiple round trips. The OLED stack is given by table 5.1. The grating are the symmetrical pillars of figure 5.1(a) with a height of 600 nm. The period of the grating is 1.0 μm and the fill factor is 70%.

Figure 5.5 indeed shows that the relative improvement is exclusively due to the multiple round trips. This result was to be expected due to the conservation of etendue, see section 2.4.4. Because the size of the corrugation is the same as the size of the active area, roughly only $1.0/1.5^2$ of the light can escape by direct transmission.

5.2.4 Relative improvement of a grating on a RC^{2}LED

In this subsection, we will discuss the relative improvement of a RC^{2}LED with a grating. This subsection is in close relation with the experimental measurements of a RC^{2}LED with microlenses, see figure 4.12 of section

4.3.3.

The specifications of these stacks are given by table 4.2. Figure 5.6(a) shows the relative improvement for both the reference OLED and the RC^{2}LED. Here, the reference OLED has a relative improvement of about 80%. Note, this relative improvement is higher than the one of subsection 5.2.3. The reason is the thinner ITO layer of this OLED. Indeed, the thinner the ITO is, the less absorption happens after each round trip.

Now, let us focus on the relative improvement of the RC^{2}LED. There is almost no relative improvement for the wavelength range around 600 nm. This can be explained with figure 5.6. This figure shows the extraction efficiency of a planar reference OLED and of a planar RC^{2}LED. Though the RC^{2}LED has a much higher extraction efficiency around 600 nm, the total amount of radiant flux to the substrate is almost the same for both OLED Thus, the RC^{2}LED already extracts a lot of light around 600 nm whereas the reference OLED has more room for improvement.

To conclude, at wavelengths with the highest extraction efficiency for the RC^{2}LED, the grating can not improve the extraction efficiency.

5.3 Grating at the substrate-air interface: experimental results

5.3.1 Introduction

To experimentally verify the influence of a grating, several gratings have been fabricated. Then, measurements have been done in collaboration with the 'Liquid Crystals and Photonics'-group of Ghent University. Note that most of this work has been done in the context of the master thesis of Carl Van Buggenhout.

We take the ratio of the spectral emission of a reference OLED with grating to the spectral emission of that same OLED without a grating. To avoid Total Internal Reflection (TIR) at the interface between the substrates of the reference OLED and the grating, we use a refractive index matching gel. Since we have used a separate substrate to fabricate the grating in, adding a grating is as simple as attaching the substrate of a planar OLED to a planar substrate with a grating. A similar procedure has been used to measure that reference OLED with microlenses.

The remainder of this section is divided in the three parts. First, we describe the grating fabrication in subsection 5.3.2. The second part is about the measurem

5.3.2 Fabrication of the gratings

In this subsection, we list the steps to fabricate a grating on a glass substrate. We have used interference lithography to define the pattern. Com-

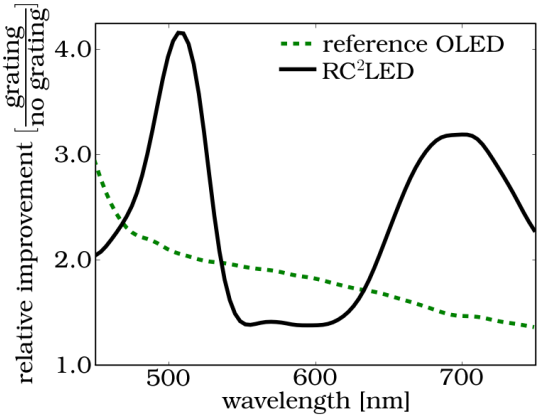

(a)

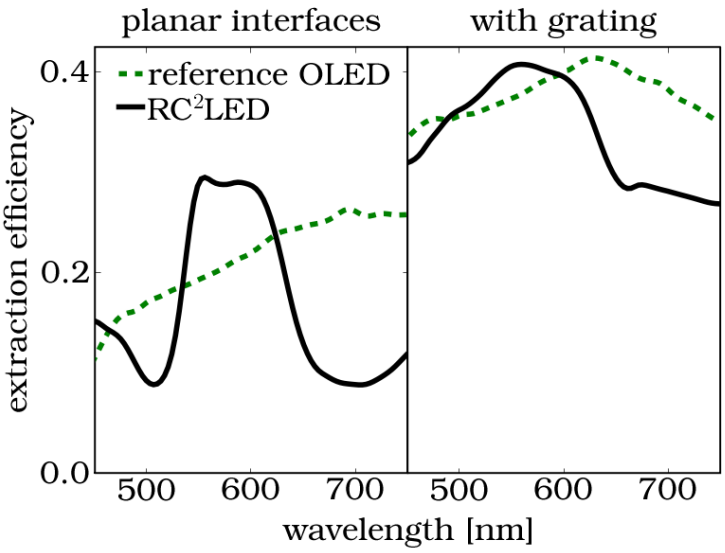

(b) (c)

Figure 5.6: The extraction efficiency depends on the reflectance of the stack of organic layers. These figures use either the reference OLED or the RC^{2}LED of table 4.2: (a) relative improvement of the extraction efficiency by using a grating (b) extraction efficiency without grating (c) with grating .

pared to e-beam lithography, interference lithography can pattern an entire area in one step.

To fabricate a grating in a planar glass substrate by interference lithography, we have three steps: (I) deposition of a SiO_x-layer on top of the glass, (II) making a pattern in resist on top of the SiO_x layer and (III) etching the pattern in the resist in the SiO_x-layer. Generation of the pattern in the resist is done by using a Lloyd mirror setup with an Argon laser. [10]

Table 5.2 gives a detailed overview of all the fabrication steps.

Because of the limitations of our interference lithography setup, the maximal width of the grating W_{max} is given by:

$$W_{\max} = W_{\text{mirror}} \frac{\lambda_{\text{LASER}}}{\sqrt{4\Delta^2 - \lambda_{\text{LASER}}^2}} \tag{5.2}$$

In our setup, we use an Argon laser with a wavelength of $\lambda_{\text{LASER}} = 363.8\text{nm}$. The width of the mirror is $W_{\text{mirror}} = 5$ mm. Depending on the period of the grating, which is defined by Δ, we find a maximal size of a grating in the order of a few millimeter. For a square grating, this means a maximal area of a few millimeters by a few millimeters. Also, the filling factor of our gratings is limited to 50%. If we look at the simulation result of figure 5.4(a), this fill factor gives a slightly lower relative improvement than the optimal value.

After fabrication, some electron microscope pictures, such as figure 5.7(a), show nicely fabricated gratings.

5.3.3 Measurement results

In this subsection, we will discuss the measurements of one OLED on which we attach different gratings. Thus, each measurement always uses the same planar OLED on which we attach a different grating with a refractive index matching fluid. Each of these setups has been measured in an integrating sphere. For each grating, we measure the relative improvement.

The measurements have been done with a reference OLED with an emitting area of 9 mm^2. Fabrication of this **green** OLED was done by Philips Research Aachen. PRA has deposited a organic layer stack, which is similar to the one of table 5.1. Note, the size of the OLED is in the same range as the size of our fabricated gratings. The actual measurements have been done with an integrating sphere of which the light is coupled to a monochromator. The integrating sphere of Bentham has a diameter of 15 cm, the monochromator is a DK 240 Digikröm 1/4 m monochromator. The OLEDs were driven by a Keithley 220 programmable current source to ensure reproduceable measurements.

Figure 5.8(a) shows the two measurements we perform to quantify each grating. First, we measure the 'reference' OLED without grating. Then, the reference OLED is measured with grating. Because of the small size of

(I)	Deposition a SiO_x-layer on top of glass.

This layer is roughly 500 nm thick.

(II)	Making a pattern in photo resist (6 sub-steps)

Deposition of layers

1. Deposition of anti-reflection coating
   XHRiC anti reflection coating is spincoated by 3000 rpm to get a thickness of 200 nm.
   Baking of the ARC is for 60 s at 175^{o}C on a hot plate.
2. Deposition of the **positive** resist
   AZ MiR 701 is spincoated by 3000 rpm to get a thickness of 1.0 μm.
   Baking of the resist is for 60 s at 90 ^{o} C on a hot plate.

Interference lithography

3. Use a Lloyd's mirror setup to generate the pattern.
   To get a square lattice, the sample has to be rotated over 90^o.
4. Post-exposure baking for 60 s at 110 ^{o}C.

Development

5. Place the exposed sample in AZ 726 MIF development fluid for 30 s.
6. Clean afterward with Deionized water and dry with N_2.

(III)	Dry Etching (4 sub-steps)

1. Reactive Ion Etching of the Anti-reflection Coating
2. Inductively Coupled Plasma etches the pattern of the positive resist in SiOx.
3. Remove remaining resist with aceton
4. Reactive Ion Etching of the remaining Anti-reflection Coating

Table 5.2: Detailed overview of the different steps to create a grating in a SiO_x- layer in glass.

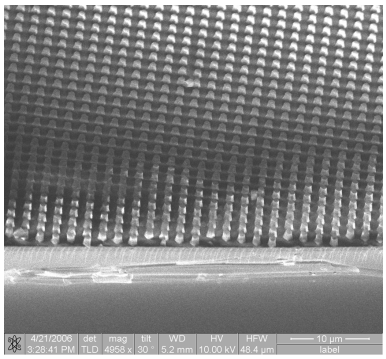

(a) Grating fabricated with interference lithography, round pillars

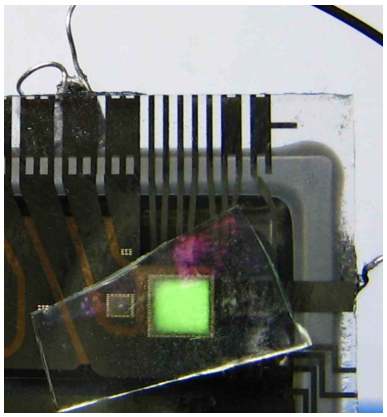

(b) The grating is placed on a small 3 by 3 mm green reference OLED. (fabricated by Philips Research Aachen). Note: the grating is only slightly bigger than the green area of the OLED.

Figure 5.7: Fabrication and measurements have been performed on a green OLED on which we attach a grating with refractive index matching gel

the OLED, the noise on these absolute measurements is around 0.1 [a.u.]. Dividing the spectrum gives the spectral relative improvement. This procedure is repeated for different gratings.

Figure 5.8(b) shows that a grating with a depth of 450 nm outperforms a grating with a depth of 125 nm. We see a qualitative agreement between the experimental relative improvement and the simulated relative improvement of figure 5.3(b). However, we only find a maximum relative improvement of about 25%, whereas simulations show a relative improvement of over 50%. Different reasons may be found to explain this difference. First, the organic layer stack might be more absorbing than we have assumed. This can lower the relative improvement. Another reason is that we were limited to a fill factor of 50% whereas the optimal value is 70%.. Thus, we see a qualitative but no quantitative agreement between simulations and measurements.

Figure 5.8(c) shows that a grating with a period of 1200 nm outperforms a grating with a period of 600 nm. However, we do not find a qualitative agreement between the experimental relative improvement and the simulated relative improvement of figure 5.3(a). One possible reason might be the fabrication deviation.

In conclusion, several gratings have been fabricated and measured. The experimental relative improvement is limited to 25%, whereas simulations predict an improvement of 50%.

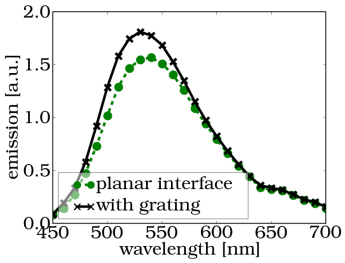

(a) Emission in function of wavelength for an OLED with and without grating

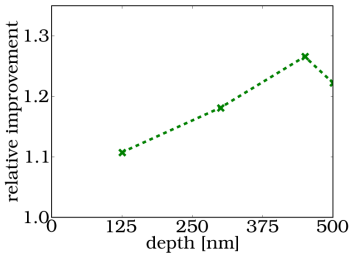

(b) Relative improvement in function of the depth for $\lambda = 500nm$

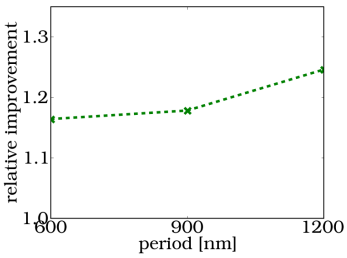

(c) Relative improvement in function of the period for $\lambda = 500nm$

Figure 5.8: Experimental results for fabricated gratings. All measurements have used the same OLED on which we attach a grating with a refractive index matching gel.

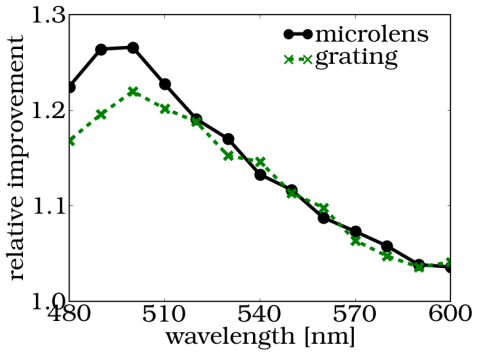

Figure 5.9: Relative improvement in function of the wavelength. The OLED has either a grating or microlenses attached.

5.3.4 Comparison of an OLED with grating to an OLED with microlenses

In this subsection, we compare gratings to microlenses with respect to the extraction efficiency. These experiments follow from the question: do gratings give a sufficiently higher relative improvement than microlenses to justify the extra fabrication effort? With the same measurement setup as the previous paragraphs, figure 5.3.4 shows both the relative improvement of a grating and of a substrate with microlenses.

We should remark that both setups had deviations from an ideal setup. For the microlenses, we can not guarantee that all light can travel from the OLED substrate to grating substrate. Indeed, the microlenses have been fabricated on PMMA by Philips Research Aachen. Because, the refractive index of this PMMA is $n_{\text{PMMA}} \approx 1.48$, some reflection occurs at the interface between OLED and grating. To estimate the amount of light which can pass this interface, we can use the assumption of random emission in glass. Then, by using a similar reasoning as in subsection 2.4.1, you can estimate that about over 85% of all light can go from glass to PMMA. Note that the refractive index of the refractive index matching gel is higher than glass. Thus, there will be no angles for which TIR happens. For the gratings, our fabrication setup is incapable to fabricate gratings with the optimal theoretical value. However, though the fill factor was limited to 50%, this grating had an optimal depth of 450 nm and a optimal period of 2.0 μm. Anyhow, for both setups, these fabrication imperfections can underestimate the relative improvement by about 15-20%

However, we still can state that in our measurements we see no distinctive advantage for either grating or microlenses with respect to the relative improvement.

5.4 Grating at the active region-substrate interface: simulations

5.4.1 Introduction

This section is about gratings which are placed between the active region and the substrate. By active region, the stack cathode/organic layers/ITO is meant. The aim of a corrugation at this interface is to extract light which is trapped in the active region. As has been stated in section 2.4.8, a few publications present experimental verification of increased extraction efficiency by using such a grating. In this work, we will focus on numerical results to gain insight and to find optimal parameters of such a grating.

To quantify the simulation results, most figures give the extraction efficiency in function of the wavelength. Using the extraction efficiency as key parameter has two reasons. First, it is impossible to determine whether a relative improvement comes from the scattering effect of the grating or from microcavities. Therefore, we use a parameter which takes into account both. Second, in contrast to the previous section (2.4.8), it is difficult to find an experimental setup to compare absolute measurements of an OLED without grating and that same OLED with a grating. Thus, the extraction efficiency will be used to express the results.

Similar to section 5.2, the discussion is spread out over different subsections. First, subsection 5.4.2 gives the optimal parameters for different types of gratings. Special care is given to the wavelength dependent behavior. Then, subsection 5.4.3 compares two different motifs. One motif has round holes, the other has square holes. Next, subsection 5.4.4 discusses the angular emission. This subsection will lay the foundation for the the comparison between hexagonal lattices versus square lattices in subsection 5.4.5. Subsection 5.4.6 uses one optimized grating to show the influence of round trips in the substrate. Here, we also show how well in the presence of a grating light extraction from the active region is increased. To conclude this section, we will look at the absorption of the electrode in 5.4.8.

5.4.2 Optimization of the grating parameters

To optimize the grating, we first have to define the organic layer stack and which type of grating we use. The organic layer stack is defined in table 5.3. For the grating, we analyze both the pillars or the holes of respectively figure 5.1(a) and figure 5.1(b). Then, we need to optimize 5 parameters: Δ_x, Δ_y, t_x, t_y and the height of the corrugation.

The optimization procedure for the grating is similar to the one of subsection 5.2.2. Again, we have performed a local optimization for each parameter while keeping the other parameters constant. In steps, we first find the optimum of the first parameter by brute force. At the same time, the other four parameters are kept constant. This procedure is repeated for the

material	refractive index @550 nm	thickness
Al	1.0-6.7j	150 nm
Electron Transport Layer	1.76	75 nm
Emissive layer emission in the middle	1.79	20 nm
Hole Transport Layer	1.66	10 nm
ITO	1.82 - 0.01j	100 nm
Planarisation layer	1.93	700 nm
	Grating	300 nm
glass	1.52	N.A.

Grating
This symmetric grating has a period Δ of 400 nm. Pillars of glass with a width of 275 nm have been surrounded by material of the planarisation layer.

Table 5.3: This layer stack has been used to the gratings of figure 5.1(a)-(b) at the interface between active region and substrate. This table also gives the default parameters used for the grating.

other 4 parameters. This local optimization already gives a good indication for the global optimum. Indeed, a parameter sweep over two parameters shows that these two parameter change the extraction efficiency largely independently. Also, this implies that a symmetric grating gives the highest extraction efficiency.

Figure 5.10 shows the extraction efficiency in function of corrugation height and period. Optimum parameters are: corrugation height $>$ 300 nm, period $>$ 350 nm and fill factor $\approx$ 60%. Then, figure 5.11 gives the optimal value for the fill factor. Similar to figure 5.4, the optimal value depends on the motif of the grating.

In conclusion, an OLED with a grating of optimal parameters gives an extraction efficiency of 30% as compared to the 20% of an OLED without grating.

5.4.3 Circular pillars versus square pillars on a square lattice

This subsection shows which extraction efficiency we might expect if we have round pillars instead of rectangular pillars. Using rectangular pillars is easier to implement and these give a faster simulation time, whereas

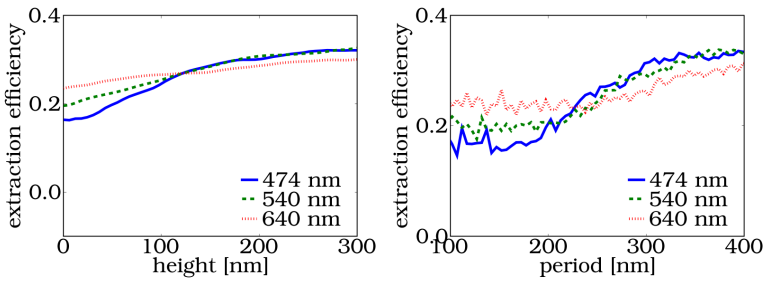

(a) Pillar height (b) Period

Figure 5.10: Optimal parameters of the pillars of figure 5.1(a). The structure has been defined by table 5.3

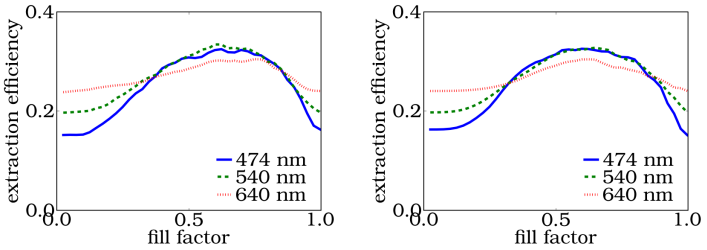

(a) Pillars (b) Holes

Figure 5.11: The optimal value of the fill factor is wavelength independent. Nevertheless, the optimal value depends on the actual grating structure, see also figure 5.1

round pillars will be more realistic. Indeed, fabrication of gratings usually gives more rounded edges. Now, we compare the extraction efficiency of a rectangular pillar and a round pillar.

To simulate a round structure with our implementation, we subdivide a circle in different rectangular stacks. Of course, the coarser the subdivision, the worse the approximation of a circle. The approximation of figure 5.12 uses a subdivision of rectangles of 10 nm. This corresponds to 1/40th of the period.

Figure 5.12 gives the extraction of both rectangular pillars and round pillars. There only is a small difference between the results obtained with square holes and round pillars. So, a square pillar with a width of 275 nm gives almost equal results as a circular pillar with a diameter of 275 nm.

5.4.4 Angular emission of an OLED with grating

This subsection shows how to analyze the angular emission in glass of an OLED which has a grating with a square lattice. For this purpose, we will introduce Wave Vector Diagrams (WVDs) and the reciprocal lattices to analyze the angular emission. Then, these concepts will be used in subsection 5.4.5 where we compare between OLEDs with a grating on a square lattice and OLEDs with a grating on a hexagonal lattice.

In this subsection, we show how the radiant intensity in glass depends on the angle. Note that the unit of the radiant intensity is power per unit solid angle. Moreover, most papers we refer to in 2.4.1 use the radiant intensity to quantify the angular emission. In practice, to measure this parameter, a big lens can be attached to the surface to avoid multiple round trips.

Let us start by discussing the Wave Vector Diagram (WVD), which gives us the radiant intensity for all propagating waves. To identify a propagating wave, we use the part of the wave vector in the plane of the emissive layer: $\mathbf{k}_t$. Let us illustrate with an example. Figure 5.13(a) and figure 5.13(b) give the WVD for two different gratings. The axes of these figures use $\mathbf{k}_t = (k_x, k_y)$. Any propagating wave lies within a circle with the length of the total wave vector of that medium. Thus, for a glass substrate with a refractive index n_{glass}, we have $\|\mathbf{k}_t\| < \|2\pi n_{glass}/\lambda\|$.

After looking at how to interpret the WVD, we now discuss how to determine the angles with higher radiant intensity. The advantage of the WVD is the easy way to visualize the Bragg condition. How? Because any direction is expressed as a wave vector in a WVD, summation of wave vectors is quite easy. Then, let us recapitulate equation 3.9, which gives the Bragg condition for a square lattice:

$$k_x, k_y \quad = \quad k_{x,0} + i\frac{2\pi}{\Delta_x}, k_{y,0} + j\frac{2\pi}{\Delta_y}, i, j \in \ \in \mathbb{Z} \tag{5.3}$$

Now, figures 5.13 (c) and (d) show how to combine the WVD and the

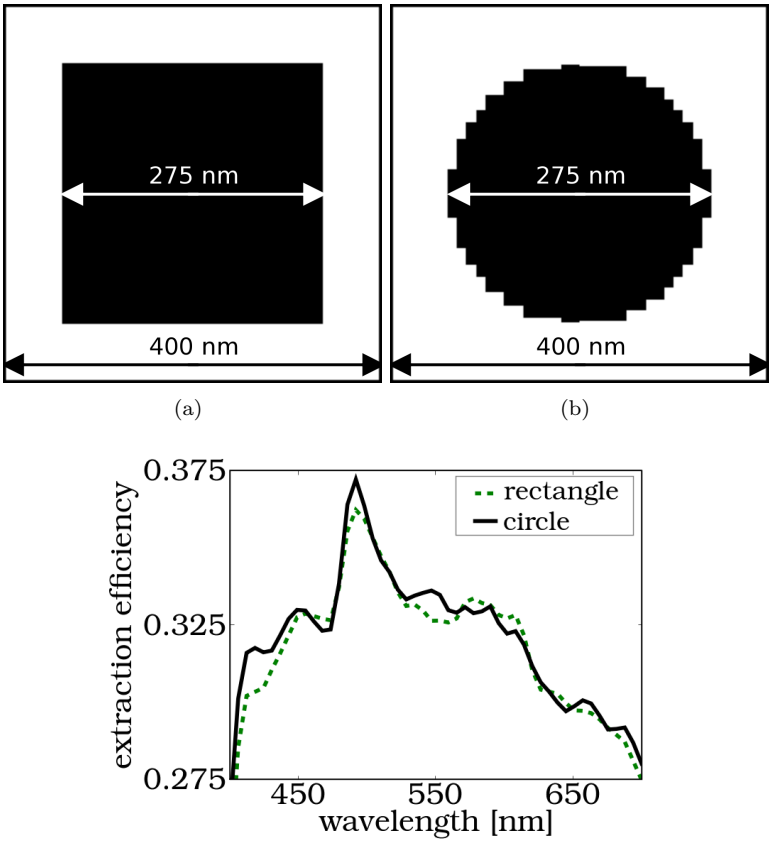

Figure 5.12: Calculations with the structure of table 5.3 have been done with two gratings on a square lattice. Either the grating has (a) square pillars or (b) round pillars. Figure (c) shows a relative difference of at most 2% between both types.

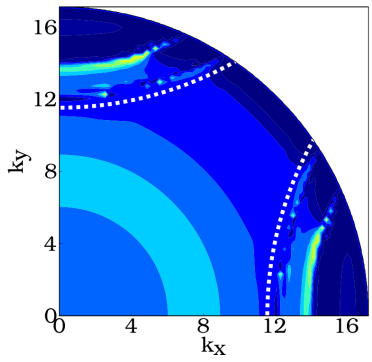

(a) $\lambda = 550nm$, $\Delta_{x,a} = 200$ nm

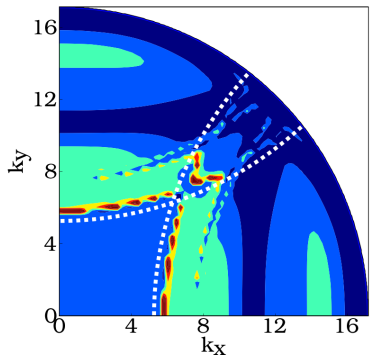

(b) $\lambda = 550nm$, $\Delta_{x,b} = 250$ nm

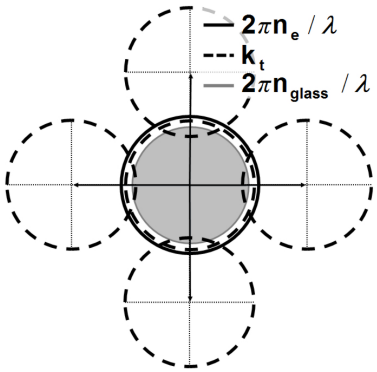

(c) $\lambda = 550nm$, $\Delta_{x,a} = 200$ nm, see a.

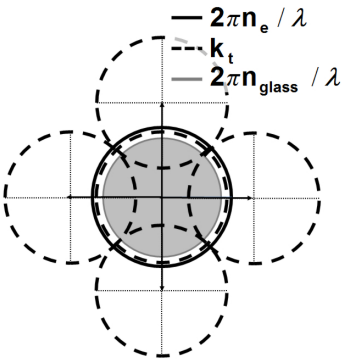

(d) $\lambda = 550nm$, $\Delta_{x,b} = 250$ nm, see b.

Figure 5.13: Figures (a) and (b) show how the angular dependency of the radiant intensity changes in function of the grating period. The bigger the grating period is, the smaller (k_x, k_y) are for which the first diffraction order gives a higher radiant intensity. The dotted lines of figures are merely to show how the angles of higher radiant intensity shift. Figures (c) and (d) show how to use the addition of wavevectors to check this conclusion with the Bragg condition in the WVD. The OLEDs of table 5.4 Some details on the grating: the symmetric rectangular grating has holes in SiN_x, which have been filled with Spin on Glass. Fill factor is 60% and $n_{SiN_x} = 1.93$, $n_{SoG} = 1.28$.

material	refractive index @550 nm	thickness
Al	0.86 - 6.5j	150 nm
Electron Transport Layer	1.74	60 nm
Emissive layer emission in the middle	1.74	20 nm
Hole Transport Layer	1.79	65 nm
ITO	1.8	150 nm
	Grating	300 nm
glass	1.5	N.A.

Table 5.4: The organic layer stack has been used for the figures of subsection 5.4.4.

Bragg condition. Take all wavevectors with a length of $\|\mathbf{k}_t\|$. Next, the first orders under diffraction are found by a translation over either $2\pi/\Delta_x$ or $2\pi/\Delta_y$.

The last question is: which $\|\mathbf{k}_t\|$-values gives the angles of higher radiant intensity? As a rule of thumb, we find that they occur in:

$$\frac{2\pi}{\lambda} n_{\text{glass}} \leq \|\mathbf{k}_t\| \leq \frac{2\pi}{\lambda} n_{\text{emissive layer}} \tag{5.4}$$

Light under these angles would have been trapped by Total Internal Reflection (TIR) without grating. With a grating, this light now gives a higher radiant intensity. The hot spots on figure 5.13 are the overlapping points of the circles.

To generalize this way of working to other lattices, we can use the reciprocal lattices of figure 5.14. Indeed, equation 5.3 is completely equivalent to adding the in plane wave vector $\mathbf{k}_{t,0}$ with a vector from the reciprocal lattice!

In this section, we have shown that WVD help to visualize the angular emission in glass. To generalize the Bragg condition, we can use reciprocal lattices. With these, a quick estimate of the angles with higher radiant intensity can be done.

5.4.5 Hexagonal lattice versus a square lattice

In this subsection, we compare between gratings with a square lattice and gratings with a hexagonal lattice. To start, we explain how a hexagonal lattice can be transformed in a square lattice. This step is necessary for our numerical model, which is based on a square lattice. Then, this subsection

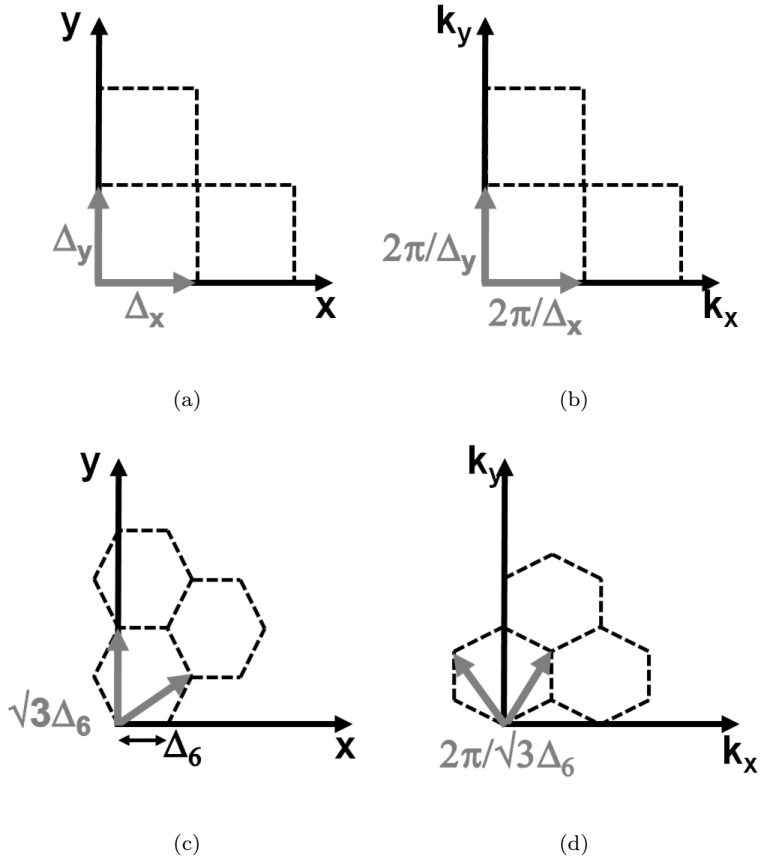

(a) (b)

(c) (d)

Figure 5.14: The Bragg condition can be visualized using the reciprocal lattice. Any incident plane wave with in plane wave vector $\mathbf{k}_{t,0}$ is diffracted. To find these diffracted orders, sum $\mathbf{k}_{t,0}$ with the vectors of the reciprocical lattice! (a)-(b): rectangular lattice. (a) Any of the **vertices** of the rectangular lattice are a linear combination of two perpendicular vectors. (b) The corresponding reciprical lattice of (a). (c)-(d): hexagonal lattice (c) Any of the **vertices** of the hexagonal lattice are a linear combination of two perpendicular vectors. (d) The reciprocical lattice of (c) is also hexagonal, but rotated over 30^o.

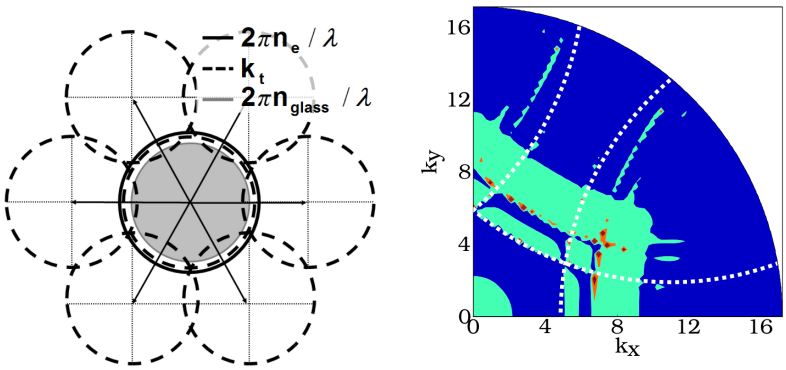

(a) (b)

Figure 5.15: Radiant intensity for a hexagonal lattice. See figure 5.16 on how to interpret. The WVD of (a) indicates how the radiant intensity of (c) looks like. Note: the dotted lines are merely to show the curvature of the k-vectors with the highest radiant intensity. Some more details on the simulation: OLED-stack is in table 5.4. The grating is made from holes in SiN_x, which have been filled with Spin on Glass, $n_{SiN_x} = 1.93$, $n_{SoG} = 1.28.$, $\lambda = 550nm$, $\Delta_6 = 165nm$

investigates the angular dependency of both lattices. Also, the extraction efficiency of an OLED with these lattices will be investigated.

Figure 5.16 shows the relation between a hexagonal lattice and a larger square lattice. Using this method, simulation results for a hexagonal lattice have been obtained.

The WVD of an OLED with a square lattice and the WVD of an OLED with a hexagonal lattice are given by respectively figure 5.13(a)&(b) and figure 5.15(b). The radiant flux of the OLED with a hexagonal lattice, figure 5.15(b), is more symmetrical than that of an OLED with a square lattice, figure 5.13(b). This can be understood with their reciprocal lattices figure 5.14.

So far, we only have looked at the reciprocal lattice of a square lattice. Now, a grating with a hexagonal lattice of figure 5.14(c) has a reciprocal lattice of figure 5.14(d). The reciprocical lattice of a hexagonal lattice again is a hexagonal lattice, but rotated over 30^o with respect to the original lattice, figure 5.14(d).

Now, we see that the hexagonal reciprocical lattice is more symmetrical than the square reciprocal lattice. Also, we can use the technique described in the previous subsection. With these two statements, we can also state that the WVD of a hexagonal lattice is much more symmetrical than that of a square lattice.

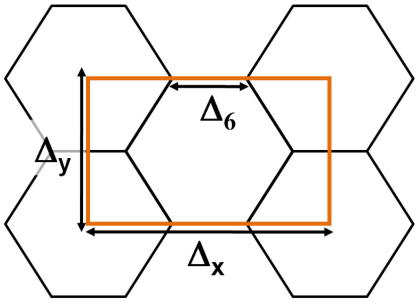

Figure 5.16: To simulate a grating with a hexagonal unit cell, we can make a grating with square cells. Note that: $\Delta_x = 3\Delta_6$ and $\Delta_y = \sqrt{3}\Delta_6$

We will now give two comments on these figures.

The angular dependence is wavelength dependent. Thus, the color will also shift. The question will be: how do the 'hot spots' shift in function of the wavelength? This question also has been addressed in [101]. The shift between one order to another order only depends on the period of the grating, equation 5.3 and figures 5.13(c)&(d). However, the in plane wave vector of a mode $\mathbf{k}_t$ depends on the wavelength. The actual color shift depends on the order you are investigating.

To have maximum extraction efficiency, we need a period of at least 400 nm. Here, we only use a period of $\Delta_{x,a} = 200nm$ or a period of $\Delta_6 = 165nm$. These periods have been chosen to clarify how to use the WVDs. Only first order diffraction orders are considered. However, with a period of 400 nm, we have up to the third order diffraction orders. Therefore, the hot spots of figures 5.13(a)&(b) and figure 5.15(b) will be much more spread out. Thus, the higher symmetry of a hexagonal lattice will be less pronounced for higher periods.

The extraction efficiency of an OLED with a hexagonal lattice does not differ from the extraction efficiency of an OLED with a rectangular lattice. Both have been optimized according to the method described in subsection 5.4.2. The optimum values for period and depth of the hexagonal lattice are similar to the one of the rectangular lattice. The fill factor however is 60%, similar to the fill factor of figure 5.4(d). In both cases, we have found an extraction efficiency of 30%.

For small periods, a hexagonal grating has a higher symmetry than a rectangular grating. However, the previous sections also have shown that maximal extraction efficiency requires much larger periods. Then, higher order diffraction orders will play an important role, which limits the ease of the quick analysis by the WVD. Also, the extraction efficiency of an OLED with a hexagonal lattice does not differ from the extraction efficiency of an

OLED with a rectangular lattice. Thus, the hexagonal lattice does not offer any benefit over a square lattice for this application.

5.4.6 Direct transmission versus multiple round trips

Similar to subsection 5.2.3, we wish to highlight the importance of multiple round trips in the substrate for a grating at the interface between active region/substrate.

As stated before, direct transmission **and** multiple round trips need to be considered when calculating the relative improvement. However, most papers which are mentioned in section 2.4.8 neglect multiple round trips in the substrate. The reasoning to neglect is as follows: if light is incident on the interface glass/air under an angle which is too oblique, this light is considered to be lost because of Total Internal Reflection (TIR). This assumption neglects that light travels back up, can be scattered at the grating and have a second chance of escaping. This assumption is mostly done because of the difficulty to model optically thick substrates by a method such as FDTD.

So, this subsection will address two questions. First, how important are multiple round trips? Second, does the increase of the extraction efficiency come from light of the active region or from light of the substrate?

To answer the first question, look at figure 5.17(a). This figure already shows the difference between an approach which includes multiple round trips and one that does not. This figure gives the extraction efficiency in function of the grating depth for the structure of 5.3. If we only consider direct transmission, the increase of the extraction efficiency is completely negligible for using a deeper grating. However, considering multiple round trips gives an increase of the extraction efficiency from 20% to 30%. Thus, multiple round trips play a key role.

To answer the second question, we use figure 5.17(b). This figure shows the fraction of photons which can go from the active region to the substrate. Indeed, we see an increase. However, the fraction only goes from 50% to about 56%. So, this means that the increase of the extraction efficiency from 20% to 30% does not come from the increase of light of the active region. So, the main mechanism to increase light with a grating at the interface between glass and the active region are multiple round trips.

In conclusion, multiple round trips are necessary to determine the extraction efficiency. Moreover, the main mechanism to increase light extraction are the multiple round trips. Thus, though the main idea of using a grating is to increase light extraction from the active region, this effect only plays a minor role in the overall extraction efficiency increase.

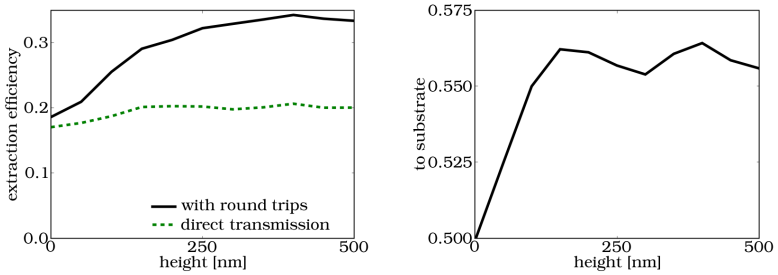

(a) Extraction efficiency in function of the pillar height.

(b) Fraction of generated photons which go to the substrate in function of the pillar height

Figure 5.17: This figure gives the fraction of the generated photons which get to air or to the substrate. Figure (a) gives the extraction efficiency; the fraction of generated photons which get to air. Figure (b) shows that adding a grating does not change much the fraction of photons which can escape from the organic layers to the substrate.

5.4.7 Orientation of the dipole

In this section, we will address the influence of the orientation of the dipole. Though small molecule OLED (sm-OLED) have a random dipole orientation, the dipole orientation in polymer OLEDs can be changed by stretching the long molecules. [47] For example, this stretching may come from spin casting from solution. Thus, we investigate if tuning dipole orientation might be interesting for polymer OLEDs.

To investigate the influence of the dipole, we will look at the fraction of photons which go to the substrate and which go to air. This has been done for both a planar OLED and for an OLED with grating at the substrate-air side. To find the extraction efficiency, we use the following equation:

$$\eta_e = \frac{f P_{air,\ par} + (1-f) P_{air,\ per}}{f P_{tot,\ par} + (1-f) P_{tot,\ per}} \tag{5.5}$$

This equation gives the extraction efficiency η_e in function of the fraction of dipoles which are **parallel** to the emissive region. We call the orientation of these dipoles in-plane. Also, this equation requires both total emitted power as well as the power in air by parallel dipoles and perpendicular dipoles with respect to the emissive region. To find the extraction efficiency of a randomly orientated dipole, we simply need to fill in $f = 2/3$.

Additional remark: microcavity effects may cause $P_{org,\ par}$ to be different from $P_{org,\ ver}$. Therefore, we use equation 5.5 instead of a weighted average of the extraction efficiency.

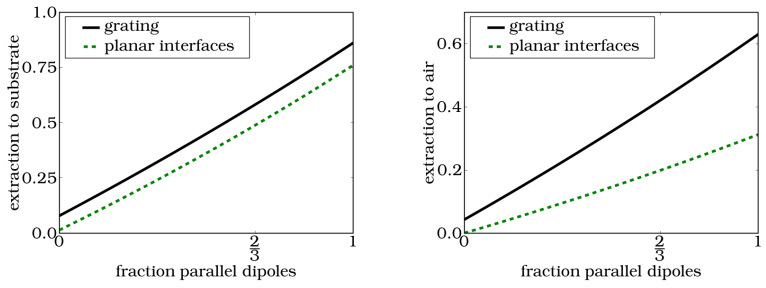

(a) (b)

Figure 5.18: Extraction to either substrate or air depends on the orientation of the dipole. Parallel is parallel to the emissive layer. Some paper refer to this orientation as in-plane. As can be expected from figure 3.7, the parallel dipoles have the highest extraction.

Figure 5.18 shows that both devices would have the highest efficiency if only in-plane dipoles are used. Also, figure 5.18(b) shows that the extraction efficiency of perpendicular dipoles benefits the most from the grating. Without grating, almost no light of the perpendicular dipoles is extracted. With grating, 10% of the light of these dipoles is extracted. However, the highest extraction efficiency always comes from in-plane dipoles, as could be expected from figure 3.7. Thus, in absolute terms, the more light of parallel dipoles, the better.

In conclusion, an OLED with only dipoles which are parallel to the emissive region show the highest extraction efficiency. Using only parallel dipoles instead of random dipoles gives about an relative improvement of 50% for the extraction efficiency, with or without grating.

5.4.8 Extraction efficiency for different electrodes

This section shows the influence of the anode absorption on the extraction efficiency. Special focus goes to the multiple round trips in an OLED with grating. Indeed, the previous section 5.4.6 has shown the impact of multiple round trips. Therefore, a minimal loss of light after one round trip will certainly increase the extraction efficiency.

One key dissipation mechanism is the cathode which absorbs 10% to 20% of all incident light. However, the anode is also lossy compared to the rest of the organic layers. Section 2.4.2 gives different anodes for OLEDs. This section looks at the extraction efficiency of planar OLEDs and OLEDs with a grating at the interface between active region and substrate in function of two anodes ITO and PEDOT:PSS^{TM}formulation Baytron PH500 from H.C. Starck. Its commercial name is Clevios^{TM}. This last anode will here

Material	refractive index @ 550 nm	thickness
Al	1.0-6.7j	150 nm
Electron Transport Layer	1.77	75 nm
Emissive region	1.78	0 nm
Electron Blocking Layer	1.66	10 nm
Hole Transport Layer	1.75	135 nm
anode	$\mathbf{n_{anode}}$	$\mathbf{t_{electrode}}$
A 150 nm thick square grating with holes in glass which have a period of 450 nm.The holes have been filled by AlN, $n_{AlN} = 2.1$		
glass	1.52	N.A.

Table 5.5: The anode of this layer structure can be either ITO or PEDOT:PSS formulation Baytron PH500 from H.C. Starck. This structure is used to look at the influence of the loss of the anode on the extraction efficiency in section 5.4.8.

after be referred to as PH500.

Figure 5.19 gives the extraction efficiency in function of the thickness of both electrodes for the OLED of table 5.5. Note that a thickness of 100 nm is quite common. Figure 5.19(a) shows an extraction efficiency of about 20% for the planar OLED with a nominal thick ITO. Except for the small increase for a thickness of 70 nm which is caused by micro cavity effects, this extraction efficiency is quite constant. If we look at the extraction efficiency of the OLED with grating at the active region-substrate interface, we see that the extraction efficiency slightly decreases for thicker electrodes.

A similar reasoning can be held for the OLEDs with PH500 anode of figure 5.19(b) . However, we also see the impact of the low refractive index of the anode. The anode of low refractive index is placed between organic layers and the grating, which both have a high refractive index. Thus, a thicker anode of low refractive index decreases the light which 'feels' the grating. However, we are also interested in the impact of the loss of the anode on the extraction efficiency of an OLED with grating. Then, the more lossy PH500 influences the extraction efficiency much more negative than ITO, especially for the corrugated structure.

In conclusion, a lossy anode negatively impacts the extraction efficiency. This is especially so for an OLED with a corrugation, because of the multiple round trips.

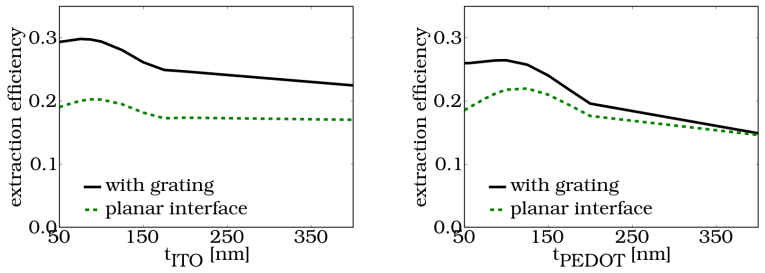

(a) (b)

Figure 5.19: Extraction efficiency in function of the thickness of the anode for (a) ITO and (b) PEDOT ^{TM}(commercial name: Clevios^{TM}). The refractive indices are respectively n_{ITO} = 1.82-0.01j and $n_{PH5000^{TM}}$ = 1.41-0.04j.

5.5 Conclusion

This chapter has given an overview of the simulations which have been performed for a grating at either side of the substrate.

For a grating at the substrate-air interface, simulations give wavelength independent optimal values for the design of the grating. These values are a minimal depth of 500 nm and a minimal period of about 1.4 μm. The fill factor is a parameter which depends on the motif, which can be pillars, holes or chess board. The optimal wavelength independent fill factors are respectively 70%, 60% and 35%. For each motif, we find a theoretical relative improvement of 50%. We also saw that the relative improvement depends on the organic layer stack. Experiments have been performed on gratings at the interface substrate-air. Here, the relative improvement is about 25%. Also, the relative improvement of an OLED with grating does not differ from the relative improvement of an OLED with microlenses.

For a grating at the organic layers-substrate interface, we also have looked for gratings which give the maximal absolute extraction efficiency. Thus, here the figure of merit is the extraction efficiency. Our simulations give wavelength independent optimal values for the design of the grating: a minimal depth of 300 nm, a minimal period of about 350 nm and a fill factor of about 60%. This last parameter is less dependent from the motif as the grating at substrate-air interface. The increase of the extraction efficiency again is 50%. We also have used the Wave Vector Diagram (WVD) to explain the highly angular dependent emission of our simulation results. Again, we saw the importance of multiple round trips in the substrate.

The grating does not increase much the fraction of light which can be extracted from the organic layers. Thus, the increase of the extraction efficiency comes from light which would normally have been trapped in the

substrate.

Of course it is happening inside your head, Harry, but why on earth should that mean it is not real?

Dumbledore, Harry Potter and the Deadly Hallows

6 Optimization of the luminous power efficiency

The focus of this chapter is the luminous power efficiency. This parameter consists of two questions. The first question is: how efficient is the conversion of electrical power to optical power? The second question is: how does the eye react to the light? In other words, is the generated light effective? So far, the focus of this work has been the extraction efficiency. Thus, we have only considered the first question. However, how the eye reacts is also important to quantify a light source. For example, we will see that two equally efficient OLEDs with the same color can still have a different luminous power efficiency. So, in the next chapter we will start with a numerical model to calculate the luminous power efficiency. With this model, we will make three statements on the luminous power efficiency to illustrate the trade off between efficiency and efficacy.

Overview

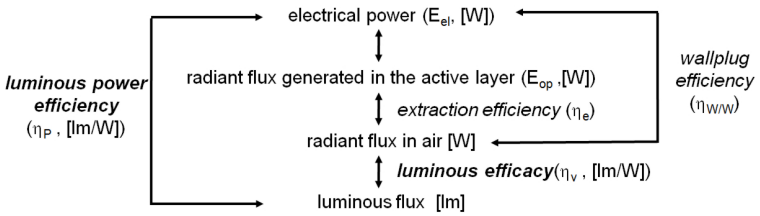

Figure 6.1: The relation between luminous efficacy and luminous power efficiency is given by this figure, as well as the relation with the other parameters of this chapter.

6.1 Introduction

To quantify a light source, the luminous power efficiency has a central role. The **luminous power efficiency** (η_{P}, [lm/W])is the ratio of luminous flux (F, [lm]) to the electrical power ($\mathrm{P_{el}}$, [W]). [64] For a given light source with given chromaticity, we want this parameter to be as high as possible. Thus, the light source has to be as bright as possible with minimal input of electrical power. A small introduction on color related properties such as luminous flux and chromaticity are in Appendix A. In this section, we look at the upper limit of the luminous power efficiency of a perfect light source. Thus, what is the maximal luminous flux [lm] for one Watt of radiant flux? Then, we briefly introduce the other sections, which look at more realistic white OLEDs

Let us first stress the difference between two parameters: the luminous power efficiency and the luminous efficacy, figure 6.1. The luminous efficacy (η_{V}, [lm/W]) is the ratio of luminous flux to the radiant flux ($\mathrm{P_{opt}}$, [W]). To calculate this last parameter, only the spectrum is needed. So, we can see that luminous power efficiency and luminous efficacy are related by the wall plug efficiency ($\eta_{W/W}$, [W/W]). This last parameter gives the efficiency at which electrical power is converted to radiant flux. So, the remainder of this section uses the luminous efficacy. Important: the upper limit of the luminous efficacy for one chromaticity automatically is the upper limit for the luminous power efficiency of any light source.

To find the maximal luminous efficacy, we use two properties of the interaction between visible light and the human eye. First, many spectra can have the same chromaticity. This is called metamerism. Different spectra however have a different luminous efficacy. Second, only one spectrum can give the highest luminous efficacy. This highest luminous power efficiency is the MacAdam limit. [15] Thus, the MacAdam limit gives the highest luminous power efficiency achievable for one color point. Figure 6.2 gives this limit for all chromaticities. For example, the MacAdam limit for 'illuminant

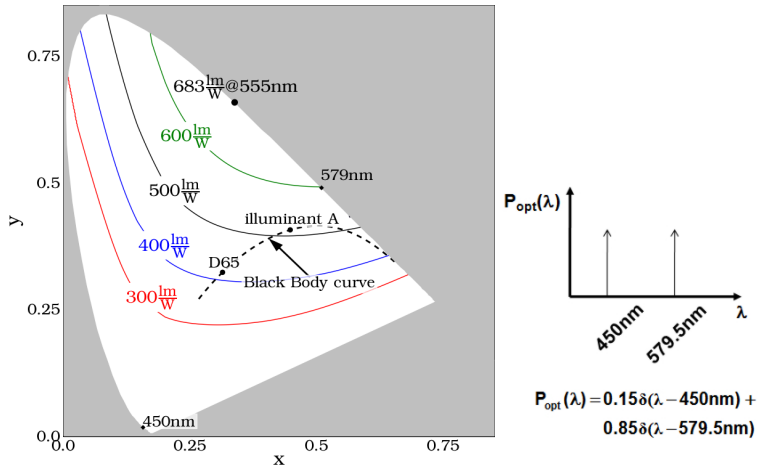

(a) (b)

Figure 6.2: (a) This figure shows the maximal luminous efficacy of any color point in CIE 1931 xy color space. (b) For example, the given spectrum for color point illuminant A achieves 512 lm/W. (Source: [15])

A' is 512 lm/W. The corresponding spectrum has 15% of its radiant flux emitted at 450 nm and 85% at 579.5 nm! Note that the spectra of most WOLEDs do not look like this spectrum. Subsection 6.3 comes back to this statement. Even more, the luminous efficacy of most OLEDs' spectra is at most 350 lm/W.

So far, we only have used a 'perfect' light source. Indeed, we have used the luminous efficacy which only considers the spectrum. However, in the remainder of this chapter we wish to model the luminous power efficiency of a more realistic OLED. Therefore, the remainder of this chapter is as follows. First, section 6.2 describes a numerical model to calculate the luminous power efficiency. Subsection 6.2 up to subsection 6.4 prove three statements on OLED properties which limit the luminous power efficiency.

6.2 A numerical model to calculate the luminous power efficiency of a 3 color WOLED

The goal of this chapter is optimize the luminous power efficiency. For this purpose, this section gives a numerical model of a 3 color WOLED. This model and some small variations of this model will be used in the remainder of this chapter.

As stated before, the luminous power efficiency (η_P, $[\frac{lm}{W}]$) is defined as the ratio of luminous flux (F, [lm]) to electrical power (P_{el}, [W]). Now, to calculate the luminous power efficiency, we use a generic model of a 3 color WOLED which requires 4 parameters.

The four parameters are: the internal quantum efficiency which gives the conversion of excitons to photons ($\eta_{int,i}$), the extraction efficiency of these photons ($\eta_{e,i}$) and the radiant flux of the emitters ($E_{el,i}(\lambda)$). See also figure 6.1. One last relevant parameter is the driving voltage of the OLED. The index i of each of the 3 emitters is either b(lue), r(ed) or g(reen). Typical values of η_{int} and the voltage are in respectively subsections 2.3.4 and 2.3.5. The extraction efficiency was discussed in section 2.4. For the spectra of the emitters, most articles mention emitters with a bandwidth of about 100 nm. Except Europium: Europium emitters emit in red with wavelength bandwidth of one fourth of the usual width. [102]

The model of subsection 6.2.1 and its small adapta

6.2.1 A 3 color white OLED with 3 emitters

In this subsection, we show how to calculate the luminous power efficiency of a White OLED with 3 emitters in one organic stack. The luminous power efficiency is calculated with the luminous flux (F_i) and electrical power ($P_{el,i}$) of each of the 3 emitters.

$$\eta_P = \frac{\sum_{i=b,g,r} F_i}{\sum_{i=b,g,r} P_{el,i}} \tag{6.1}$$

For a given chromaticity of the White OLED (WOLED), the contribution of each emitter automatically is fixed. Thus, the first step needs to determine the spectrum which corresponds with the given chromaticity. Also, the spectrum then gives the luminous flux. The emitted spectrum in air of each of the emitters is given by:

$$E_{op,i}(\lambda) = E_{el,i}(\lambda)\eta_{e,i}(\lambda) \tag{6.2}$$

$$E_{op}(\lambda) = \sum_{i=b,g,r} A_i E_{op,i}(\lambda) \tag{6.3}$$

Each of these spectra corresponds to tristimulus values in the CIE color space of 1931, Appendix A or [14]:

$$\begin{aligned} X_i &= \int E_{op,i}(\lambda)\overline{x}(\lambda)d\lambda \\ Y_i &= \int E_{op,i}(\lambda)\overline{y}(\lambda)d\lambda \\ Z_i &= \int E_{op,i}(\lambda)\overline{z}(\lambda)d\lambda \end{aligned} \tag{6.4}$$

Given the addition properties of the color coordinates, the color coordinate of the WOLED, (X_w, Y_w, Z_w) has to satisfy:

$$\begin{aligned} X_w &= \sum_{i=b,g,r} A_i X_i \\ Y_w &= \sum_{i=b,g,r} A_i Y_i \\ Z_w &= \sum_{i=b,g,r} A_i Z_i \end{aligned} \tag{6.5}$$

To get a certain chromaticity, equation 6.5 tell us how to chose the prefactors A_i. The prefactors (A_b, A_g, A_r) determine the mutual ratio of radiant flux inside the organic layers. We assume that we can change these prefractors A_i without changing any other property or parameter of the OLED!

The luminous flux of one emitter then is given by:

$$F_i = 683.0 \int A_i E_{op,i}(\lambda)V(\lambda)d\lambda \tag{6.6}$$

Here, V(λ) is the eye sensitivity curve. Calculating the denominator of equation 6.1 is the next step. This equation is a function of the internal quantum efficiency and the power injected in the organic layers.

$$P_{el,i} = \int A_i E_{el,i}(\lambda)\frac{1}{\eta_{int,i}}\frac{qV\lambda}{hc}d\lambda \tag{6.7}$$

The parameter $\frac{1}{\eta_{int}}$ gives the amount of excitons needed to create one photon. The ratio $\frac{hc}{\lambda qV}$ gives the relation between the optical power of the photon and the energy of the creating exciton. [6] As stated in the introduction, one can use doped layers to minimize $P_{el,i}$ by minimizing the required voltage V.

6.2.2 A blue/green OLED with a down conversion layer

White light can be generated by the setup of figure 6.3. An OLED which generates blue or green light can have a layer which downconverts a fraction

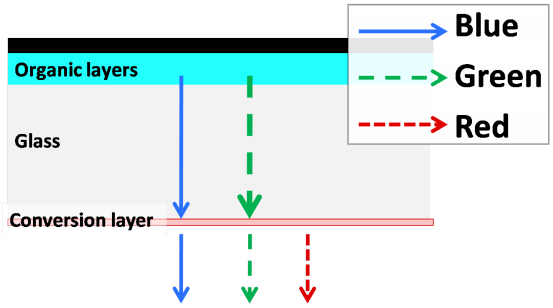

Figure 6.3: Downconversion of blue and green light to red light can result in white light

of this light to red light. For example, this concept is also used in fluorescent tubes. Materials for this downconversion can be found in [103].

To calculate the overall luminous efficacy of this structure, we will have to adapt equations 6.3 and 6.7 of subsection 6.2.1. A wavelength dependent absorption $Ab_{op}(\lambda)$ and an emission of the photons of the down conversion $E_{op,DC}(\lambda)$ have to be introduced in the total emitted spectrum E_{op}:

$$E_{op}(\lambda) = A_b E_{op,b}(\lambda) + A_g E_{op,g}(\lambda) - Ab_{op,DC}(\lambda) + E_{op,DC}(\lambda) \quad (6.8)$$

The relation between the absorption $Ab_{op,DC}(\lambda)$ and the Emission $E_{op,DC}$ of the downconversion layer is completely determined by the material of this layer. Because the 3 equations 6.5 have to be satisfied, three variables are required. Put otherwise, we need 3 variables to get the chromaticity we want. These variables are the radiant flux of the blue and green emitter (A_b, A_g) and the absorption $(Ab_{op,r})$. Again, we assume a fixed relation between absorption $Ab_{op,DC}(\lambda)$ and emission $E_{op,DC}$.

We model the absorption of the downconversion layer with a probability of absorption. The thicker the layer, the more chance a photon is absorbed. Then, the thickness T_{DC} of the downconversion layer is a free parameter which we can use to tune the color point.

One way to model the change of the probability that a photon with a certain wavelength (λ) after a distance T_r is absorbed is using an exponential dependence. The expression $(1\text{-}\exp(\text{-}\gamma_{ab}(\lambda)T_{DC}))$ then indicates the probability of absorption after a distance of T_{DC}. We now get from equation 6.3:

$$\begin{aligned} E_{op}(\lambda) = {} & (A_b E_{op,b}(\lambda) + A_g E_{op,g}(\lambda))\,(1 - (1 - \exp(-\gamma_{ab}(\lambda)T_{DC})) \\ & + E_{op,DC}(\lambda) \end{aligned} \quad (6.9)$$

Note, this equation neglects the angle under which light is incident. The electrical power used by the OLED now only is given by the blue and green emitter:

$$P_{el} = \sum_{i=\mathbf{b},\mathbf{g}} \int A_i E_{el,i}(\lambda) \frac{1}{\eta_{int,i}} \frac{qV\lambda}{hc} d\lambda \tag{6.10}$$

As already mentioned, the relation between $E_{op,DC}$ and the absorption of the downconversion layer is given by material constants. Equation 6.5 now can be solved by finding the correct values of (A_b, A_g, T_{DC}). This model will be used in subsection 6.3.2.

6.2.3 A 3 color White OLED of 3 monochrome OLEDs

White light can be generated with 3 monochrome OLEDs. This differs from the approach of subsection 6.2.1 where the three emitters are placed in the same organic layer stack. Generating white light with three distinct monochrome OLEDs has the advantage that each of the 3 emitters can be optimized independently. This principle is also known as a horizontally stacked WOLED. [34]

To calculate the luminous power efficiency, we use the spectra and the wall plug efficiency $(\eta_{W/W,i})$ of each of the 3 emitters. This wall plug efficiency of an emitter can be calculated if its spectrum and its luminous power efficiency $(\eta_{P,i})$ are known.

To calculate the luminous power efficiency of the complete WOLED, we first calculate the overall wall plug efficiency $(\eta_{W,W})$:

$$\eta_{W/W} = \frac{\sum_{i=b,g,r} A_i}{\sum_{i=b,g,r} \frac{A_i}{\eta_{W/W,i}}} \tag{6.11}$$

Note, the fraction of radiant flux of each emitter (A_i) is directly given by equation 6.5.

The luminous power efficiency finally is given by:

$$\begin{aligned} \eta_P &= \eta_V \eta_{W/W} \\ &= \frac{683 \int E_{op}(\lambda) V(\lambda) d\lambda}{\int E_{op} d\lambda} \eta_{W/W} \end{aligned} \tag{6.12}$$

The optical spectrum of the WOLED E_{op} is determined by the spectrum of each of the emitters $(E_{op,i})$ and their relative fraction (A_i). Here, $V(\lambda)$ is the eye sensitivity curve. This model is used in subsection 6.4.

6.3 A spectrum which looks like the spectrum of the MacAdam limit has the highest luminous power efficiency

The first subsection, subsection 6.3.1 gives more details on the MacAdam limit. Here we prove the following statement: to have a high luminous power efficiency, the spectrum of a light source has to look like the spectrum of the MacAdam limit. As stated before, the MacAdam limit is the upper limit of the luminous power efficiency which any light source can achieve. Also, we compare the spectrum of the MacAdam limit to spectra of real WOLEDs. One important property of a light source we also introduce is the color reproducibility.

The second subsection, subsection 6.3.2 shows one possible design to get a spectrum which resembles the spectrum of the MacAdam limit, while having a sufficiently high color reproducibility. We do this placing a red down conversion layer on top of a blue/green OLED.

6.3.1 Comparing the spectrum of the MacAdam limit with spectra of WOLEDs

In this section, we compare the luminous efficacy of the MacAdam limit with the luminous efficacy of WOLEDs. Also, we introduce color reproducibility by calculating the Color Rendering Index (CRI). Color reproducibility shows how good we can distinguish colors under a light source. As we will see, we need to make a trade-off between luminous efficacy and color reproducibility. In this discussion, we make a link with the luminous power efficiency. Thus, we use the luminous power efficiency of some OLEDs calculated with the model of subsection 6.2.1.

The luminous efficacy of the chromaticity 'illuminant A' is 512 lm/W. This is also the maximum luminous power efficiency. The corresponding spectrum has 15% of its radiant flux emitted by a monochromatic source at 450 nm and 85% by a monochromatic source at 579.5 nm. For more details and a derivation, we refer to figure 6.2 and [15]. On the other hand, a spectrum of a typical White OLED (WOLED) with this chromaticity is given by figure 6.4(a). The luminous efficacy of this spectrum is only 305 lm/W. Thus, this also is the upper limit of the luminous power efficiency. Figure 6.4(b) and table 6.1 give the luminous efficacy if we replace the red emitter of this last spectrum by a monochromatic emitter of 585 nm. The luminous efficacy of the WOLED becomes 454 lm/W! Here, a comparison between figure 6.4(b) and figure 6.2 shows that trying to match a spectrum to the MacAdam limit is beneficial for the luminous efficacy.

Another important parameter of a light source besides its luminous power efficiency is its color reproducibility. Therefore, we will now discuss the trade-off between luminous power efficiency and color reproducibility.

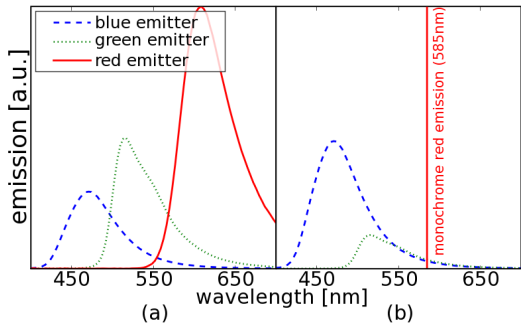

Figure 6.4: The total spectrum of the 3 emitters gives the chromaticity 'illuminant A'. (a) Spiro-DPVBi, Ir(ppy)3 in TCTA and Ir(MDQ)(acac) in α-NPD. (b) The red emitter has been replaced by a monochromatic emitter at 585 nm.

	Figure 6.4(a)	Figure 6.4(b)
η_V	305 lm/W	454 lm/W
η_P for $(\eta_{int,b}, \eta_{int,g}, \eta_{int,r}) = (1., 1., 1.)$	39 lm/W	66 lm/W
η_P for $(\eta_{int,b}, \eta_{int,g}, \eta_{int,r}) = (0.25, 1., 1.)$	30 lm/W	42 lm/W

Table 6.1: The luminous efficacy (F/P_{opt}) and the luminous power efficiency (η_P) for the spectra of figure 6.4 has been calculated for different internal quantum efficiencies. The driving voltage is 3.075V, the extraction efficiency is 20% for all wavelengths and all emitters.

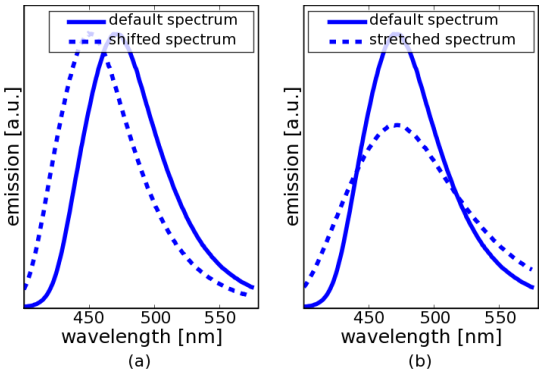

Figure 6.5: (Shifting (a) and stretching (b) of the spectrum of the blue emitter are given by respectively equation 6.13 and 6.14.

To measure the quality of a light source and to measure how good colors are reproduced when illuminated with that source, the Color Rendering Index (CRI) is often used, see appendix A. Recently, visual experience has shown that the current CRI based ranking of a set of light sources containing white LED light sources contradicts the visual ranking. [104]. Spectral narrow LEDs can have good light quality, but a low CRI. Nevertheless, because the CRI is widespread, we will classify a CRI of higher than 80 as good, even for a light source with a spectrum with narrow peaks. Note that the CRI of the WOLED with the monochromatic yellow emitter of table 6.1 is well below 80. It should be mentioned that a CRI of 80 is greater than that of the majority of fluorescent lamps.

Now, we want a spectrum which has a higher luminous power efficiency than the 'default' spectrum, but with a sufficiently high CRI. To achieve this, we vary the spectrum of one of the emitters. Two possible methods to change a spectrum of an emitter are shifting its peak position or narrowing this spectrum. The shift of a spectrum is given by figure 6.5(a) and equation 6.13, the narrowing of spectrum is given by figure 6.5(b) and equation 6.14.

$$\phi_i(\lambda) \quad \rightarrow \quad \phi\left(\lambda - \lambda_0\right) \tag{6.13}$$

$$\phi_i(\lambda) \quad \rightarrow \quad \phi\left(\lambda_{max} + \frac{\lambda - \lambda_{max}}{\text{narrowing factor}}\right) \tag{6.14}$$

The spectrum of an emitter is given by $\phi(\lambda)$, a shift by λ_0. A narrowing-factor of 0.5 means that the spectrum is half as wide in wavelength as the default spectrum.

Let us now define the parameters, we use in the equations of section 6.2 to calculate the luminous power efficiency (η_P) and the CRI. We choose an

extraction efficiency of 20% and a driving voltage of 3.075 V, which is close to the thermodynamical limit to emit deep blue. Moreover, the green and red emitters have an internal quantum efficiency of $\eta_{int,g} = \eta_{int,r} = 100\%$. Because no phosphorescent deep blue emitters with long lifetime are known, we make a distinction between a WOLED with a blue fluorescent emitter ($\eta_{int,b} = 25\%$) and a blue phosphorescent emitter ($\eta_{int,b} = 100\%$).

With the previous values, figure 6.6 shows the different luminous power efficiencies of the WOLED for the chromaticity 'illuminant A' (CIE xy 1931: 0.4475, 0.4074). In this figure, the variations of the blue and red emitter are shown. Because the luminous power efficiency and the CRI of the WOLED are almost independent on variations of the green emitter, these variations are not shown. Moreover, variations of the green spectrum are only significant when the shift is large enough to overlap with the spectrum of either blue or red emitter.

Varying the blue emitter is especially interesting for the WOLED with the blue fluorescent emitter. Indeed, a variation of the blue phosphorescent emitter of the WOLED with a blue phosphorescent emitter does not change the luminous power efficiency. The increase of the overall luminous efficacy is caused by a decrease of the amount of light emitted by the blue emitter, which is the least efficient emitter. This effect is discussed in more detail in section 6.4.

Varying the red emitter has the largest influence on the luminous efficacy and the luminous power efficiency, when compared with variations of the other emitters. The reason is the 'warm' chromaticity of the WOLED. We now compare two WOLEDs with a CRI above 80. These WOLEDs are the red emitter with its peak at 600 nm, and with a narrowing factor of 0.5 and the default red emitter. The narrower red emitter in the WOLED still gives a satisfying CRI of 80, but increases the luminous power efficiency ($\eta_P = 47 lm/W$) for a WOLED with a blue phosphorescent emitter. The default red emitter in a WOLED gives a CRI of 90. However, the luminous power efficiency is only 39 lm/W (phosphorescent blue), see also table 6.1. Although the improvement is smaller in a WOLED with a blue fluorescent emitter, we also see here a relative improvement. Again, a spectrum which resembles the MacAdam limit is beneficial for the luminous power efficiency.

In conclusion, the MacAdam limit plays an important role in this hypothetical WOLED. The maximal luminous power efficiency has been found by replacing the red emitter by a monochrome red emitter. The downside is the low CRI of a WOLED with monochromatic red. However, we find that we still can increase the luminous power efficiency by 15% and at the same we can have a CRI above 80 by using a red/orange emitter. The bandwith of this emitter, 50 nm, is less than most of the red emitters in literature.

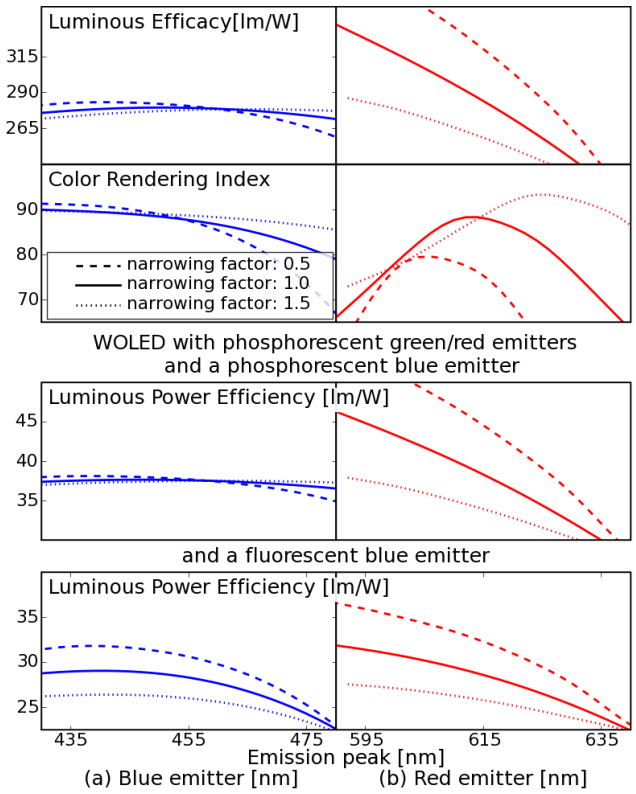

Figure 6.6: Variation of the spectral intensity of the blue and red emitter of figure 6.4(a). A white OLED with a more narrow red emitter with it's peak at 615 nm can still increase the luminous power efficiency by about 50% and with a CRI of 90. The variations are defined by figure 6.5. Varying the red or blue emitters affects the luminous efficacy, the Color Rendering Index and the luminous power efficiency of the white OLED.

6.3.2 Placing a red downconversion layer on top of a blue/green OLED

Subsection 6.3.1 has shown the importance of a spectrum which resembles the MacAdam limit. Another way to achieve this, is by placing a downconversion layer on top of an OLED with blue and green emitters to generate white light with the desired spectrum.

Figure 6.7 shows how the downconversion layer changes some fraction of the blue and green light in red light. A downconversion layer is already been adopted by fluorescent tubes and more recently in white LEDs. The phosphors which are commonly used in these devices usually convert ultraviolet or blue light in orange or red light. [105] Here, we propose a blue and green hypothetical OLED which has a spectrally broad absorption in the green region and a spectrally narrow emission in the red.

This approach has two direct advantages. First, an emission in the blue and green has a smaller bandwidth. Thus, this spectrum might be easier to extract than one which spans the entire visible spectrum. For example, if you try to increase light extraction at one wavelength with microcavity effects, the light extraction at other wavelengths decreases. Second, using a spectrally narrow red emitter is beneficial because of the MacAdam limit, as described in the previous subsection.

Remark: in our model, we also could have used an OLED with only a blue emitter. Then, we simply can use the phosphors which have been developed for blue LEDs. However, at present, most deep blue phosphorescent emitter are not stable enough. Therefore, our hypothetical OLED uses downconversion of green light, so we can use more stable fluorescent blue emitters. Note, blue fluorescent emitters can be used in combination with green phosphorescent emitters to achieve 100% internal quantum efficiency. [42]

Now, to quantify this design, we will compare it with the luminous power efficiency of the default OLED of figure 6.4(a) or table 6.2. To calculate the luminous power efficiency, we again use the numerical model of subsection 6.2.1. Both OLEDs, the default OLED and the one with downconversion layer, have an extraction efficiency of 20% and a driving voltage of 3.1V. For completeness, we again compare the luminous power efficiency of WOLEDs with a blue fluorescent or a blue phosphorescent emitter were calculated, because at present no stable deep blue phosphorescent emitter is known.

To calculate the absorption and emission of the downconversion layer are given by the following equations. First, the absorption ($\gamma_{ab}(\lambda)$) of equation 6.9 is modeled by the following equation:

$$\exp(-\gamma_{ab}(\lambda)T_{DC}) \quad = \quad \exp(-\exp(-\frac{(\lambda-\lambda_0)^2}{2\Delta\lambda^2})T_{DC}) \qquad (6.15)$$

Again, the parameter to tune the color point is T_{DC}. To calculate the emission, we also need a relation between absorption and emission. We'll

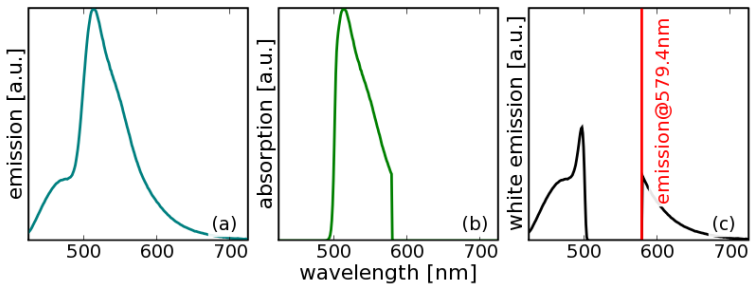

Figure 6.7: The absorption of green light is converted in red (almost) monochromatic light to create white light with the structure of figure 6.3. (a) The OLED emits blue and green light. (b) Mostly green light is absorbed. (c) Full white spectrum

assume that 100% of all absorbed photons are converted to a monochromatic red with wavelength λ_{em}. This also implies that a photon with wavelength λ only keeps $\frac{\lambda}{\lambda_{em}}$ of power. Thus, the total amount of power which will be emitted by the red monochromatic emitter is:

$$\int \left(A_b E_{op,b}(\lambda) + A_g E_{op,g}(\lambda)\right) \left(1 - \left(1 - \exp(-\gamma_{ab}(\lambda) T_{DC})\right) \frac{\lambda}{\lambda_{em}} d\lambda \quad (6.16)$$

The actual spectrum for chromaticity 'illuminant A' then is given by figure 6.7. This figure illustrates how most of the green light is absorbed and downconverted. In the end, we keep a blue emission and a yellow/red peak which resembles the spectrum of the MacAdam limit. In table 6.2, we see that the increase of the luminous power efficiency as compared to the default WOLED is at least 60%. This conclusion holds for both a WOLED with a blue fluorescent emitter and a WOLED with a blue phosphorescent emitter.

In conclusion, this section has given one possible design to achieve a spectrum which resembles the spectrum of the MacAdam limit. We use a red downconversion layer on top of a blue/green OLED. Using a downconversion layer has two advantages. First, light extraction of only blue/green light might be easier than to extract over a white spectrum. Second, we want to have a spectrum which resembles the spectrum of the MacAdam limit. In table 6.2, we indeed see an increase of the luminous power efficiency of at least 60% with this hypothetical design.

	Figure 6.4(a)	Figure 6.7(c)
$\frac{F}{P_{opt}}$	305 lm/W	464 lm/W
η_P for $(\eta_{int,b}, \eta_{int,g}, \eta_{int,r}) = (1., 1., 1.)$	43 lm/W	84 lm/W
η_P for $(\eta_{int,b}, \eta_{int,g}, \eta_{int,r}) = (0.25, 1., 1.)$	30 lm/W	49 lm/W

Table 6.2: Comparison between the 'default' WOLED of figure 6.4(a) and the WOLED with a downconversion layer of figure 6.7(c). In both cases, we use an extraction efficiency of 20% and a driving voltage of 3.1V.

6.4 A WOLED with a less efficient deep blue emitter outperforms a WOLED with a more efficient light blue emitter

In this section, we look at the relation between the internal quantum efficiency and the luminous power efficiency of a 3 color White OLED (WOLED). This internal quantum efficiency gives the conversion efficiency of an emitter of electron-hole pairs to photons by that emitter. We will prove that we may not automatically assume that increasing the internal quantum efficiency of one emitter automatically increases the luminous power efficiency.

To see a relation between internal quantum efficiency and luminous power efficiency, we use the following setup. We compare two almost identical WOLEDs. The only difference is the blue emitter. The fluorescent deep blue emitter of the first WOLED has an internal quantum efficiency which is two times less than the internal quantum efficiency of the phosphorescent light blue emitter of the second WOLED. The main conclusion will be: the luminous power efficiency of both WOLEDs is the same!

For this setup, we will use a hypothetical WOLED which combines 3 distinct monochrome OLEDs found in literature. To calculate the luminous power efficiency, we will use the equations of subsection 6.2.3. So, we start by calculating the wall plug efficiencies of the monochrome OLEDs. To do this, we divide the luminous power efficiency and the luminous efficacy. The luminous efficacy directly follows from the spectrum. Note that these OLEDs have driving voltages which are larger than 6V. Thus, lowering the driving voltage in these OLED, could already increase the wall plug efficiency by a factor of 2. Anyhow, figure 6.8 and table 6.3 gives the properties of the emitters we use in this section.

Note that this section makes conclusions based on a WOLED of 3 distinct monochrome OLEDs. However, we simply can replace in our reasoning the wall plug efficiency by the internal quantum efficiency. Thus, the conclusions of this section can easily be extended to a WOLED with one stack with 3 emitters.

Now, let us calculate the luminous power efficiency of the hypothetical

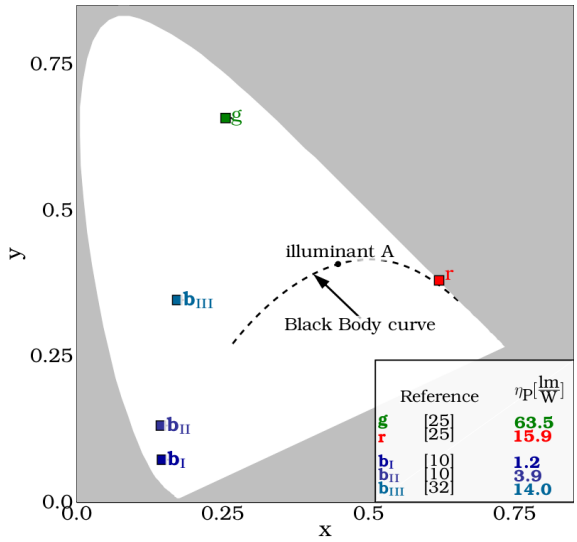

Figure 6.8: This figure shows the color points of monochrome emitters, which we find in literature. The color coordinates are placed on a CIE xy 1931 chromaticity diagram. The luminous power efficiencies of these emitters is also given.

b_I	b_{II}	b_{III}	g	r
undoped MADN	doped MADN with BD1	PhOLED		
Color coordinates in the CIE 1931 color space				
(0.15, 0.66)	(0.14, 0.13)	(0.17, 0.35)	(0.25, 0.66)	(0.62, 0.38)
Luminous Power Efficiency $\eta_{P,i}[\frac{lm}{W}]$				
1.2	3.9	14	63.5	15.9
Wall plug efficiency $\eta_{W/W,i}$				
0.01	0.03	0.05	0.13	0.06

Table 6.3: This table gives the properties of the emitters of figure 6.8.

Different blue emitters in a WOLED with the same green and red emitter, see table 6.3		
b_I	b_{II}	b_{III}
very deep blue	deep blue	light blue
Wall plug efficiency $\eta_{W/W}$ of the WOLED		
0.050	0.060	0.066
Luminous Power Efficiency (η_P) of the WOLED		
22.3 $\frac{lm}{W}$	26.6 $\frac{lm}{W}$	26.7 $\frac{lm}{W}$
Relative fraction of the emitters to create 'illuminant A' (A_b, A_g, A_r)		
(0.11, 0.27, 0.62)	(0.125, 0.255, 0.62)	(0.26, 0.13, 0.61)

Table 6.4: A White OLED (WOLED) with the color point 'illuminant A' can be created by combining a blue, green and red emitter. This table gives the luminous power efficiency of the three WOLEDs. These WOLEDs have the same green and red emitter of table 6.3. However, in each WOLED we use one of the three blue emitters of table 6.3.

WOLED with equations 6.11 and 6.12. Table 6.4 gives the results for the WOLEDs with either $\mathbf{b_I}$, $\mathbf{b_{II}}$ or $\mathbf{b_{III}}$.

Though the wallplug efficiency of the phosphorescent $\mathbf{b_{III}}$ is almost twice that of fluorescent $\mathbf{b_{II}}$, the luminous power efficiencies of the WOLED are equal. This mainly is caused by the lower fraction of blue which we need for a deep blue. It should be noted that a WOLED with a more efficient blue phosphorescent, such as recently presented in [106], would outperform both the WOLEDs of this section. Nevertheless, an increase of 1.66 in wall plug efficiency, 3% versus 5%, is compensated because of the lower fraction of the blue emitter in the radiant flux.

So, in conclusion, replacing one emitter with an emitter with higher internal quantum efficiency does not automatically give a higher luminous power efficiency. We have demonstrated that a deep blue fluorescent emitter outperforms a light blue phosphorescent emitter.

6.5 The extraction efficiency has to match the spectrum to get a higher luminous power efficiency

This last section shows the relation between the extraction efficiency and the luminous power efficiency. This sounds straightforward. For example, increasing the extraction efficiency by 50% for all wavelengths automatically increases the luminous power efficiency by 50%. However, the extraction efficiency is mostly wavelength dependent. Also, the internal quantum effi-

material	refractive index @ 550nm	thickness
Al	0.96-6.69j	100 nm
NET5	1.76	t_{NET5}
ETL	1.75-0.0092j	10 nm
blue emitter	1.80	10 nm
interlayer	1.78	5 nm
green emitter	1.78	3 nm
red emitter	1.80	10 nm
HTL	1.75-0.0092j	10 nm
NHT5	1.75-0.0092j	t_{NHT5}
ITO	1.82-0.0113j	90 nm
begin optional interference layers		
SiO_2	1.46	t_{low}
Nb_2O_5	2.38	t_{high}
SiO_2	1.46	t_{low}
end optional interference layers		
glass	1.52	mm
air	1.0	

Table 6.5: Typical stack of a 3 color White OLED. Each color is generated in a distinct layer. The electron and hole transport layer are respectively NET5, NHT5. The optional layers give a stronger wavelength dependent extraction efficiency than the basic stack. This basic stack simply does have no interference layers.

ciency plays a role. Indeed, we might have a trade-off. We could increase the extraction efficiency of a less efficient emitter at the expense of the extraction efficiency of a more efficient emitter. Thus, to increase the luminous power efficiency, the extraction efficiency has to match the other properties of the WOLED.

In section 2.4, we have mentioned different techniques to increase the extraction efficiency. However, most of these papers only discuss this increase for one wavelength or over a small wavelength range. However, any WOLED emits over 450 nm to 700 nm. This section's focus is matching a strong wavelength dependent extraction efficiency with the other properties of a WOLED. To get a strong wavelength dependent extraction efficiency, we will use a RC^2LED. More information on the RC^2LED and ways to calculate it can be found in chapter 4. The RC^2LED is defined by table 6.5.

To show the influence of the extraction efficiency and the internal quantum efficiency on the luminous power efficiency, we will compare four different WOLEDs. Two 'basic' WOLED have no interference layers between

ITO and glass, the other two WOLED have additional interlayers. The difference between the two 'basic' WOLED is their blue emitter, which is either a phosphorescent emitter ($\eta_{int,b} = 1.0$) or a fluorescent emitter ($\eta_{int,b} = 0.25$). The green and red emitters in both devices are phosphorescent emitters ($\eta_{int,g} = \eta_{int,r} = 1.0$). So, we compare the WOLEDs two by two. The 'basic' WOLED with fluorescent blue is compared to the RC^{2}LED with fluorescent blue. The 'basic' WOLED with phosphorescent blue is compared to the RC^{2}LED with phosphorescent blue.

How to optimize the two 'basic' OLEDs and the two RC^{2}LEDs? Because both 'basic' WOLED and both RC^{2}LEDs have different electrical properties, their optimization has to be done separately.

The global optimization of the two 'basic' WOLED is a brute force method where we simply scan for the highest luminous power efficiency in a two dimensional parameter space: (t_{NET5}, t_{NHT5}). Note, the calculation of the extraction efficiency of one OLED for one wavelength takes a few seconds on a system with an AMD Opteron Processor of 2 Ghz. Thus, a complete scan of the two dimensional parameter space takes at least one day.

To optimize the two RCLEDs, we have four parameters: $(t_{NET5}, t_{NHT5}, t_{low}, t_{high})$. Thus, a global optimization of four parameters would take too long. So, the two RC^{2}LEDs are only locally optimized. We start from the optimal thicknesses (t_{NET5}, t_{NHT5}) of the basic OLEDs. For example, for the RC^{2}LED with blue fluorescent emitter, we take the optimal thicknesses of the basic OLED with blue fluorescent emitter. Then, we search for the optimal parameters of the interference layers (t_{low}, t_{high}) by brute force. Finally, the results of the optimization of all four WOLEDs is given by table 6.6 and figure 6.9.

The main conclusion of table 6.6 is the following: adding interference layers on a basic WOLED increases the overall luminous power efficiency by at most 10%. This is true for both sets: the OLED and RC^{2}LED with fluorescent blue emitter and the OLED and the RC^{2}LED with phosphorescent blue emitter.

Let us now look in more detail at the extraction efficiency for the WOLEDs with the blue phosphorescent emitter. Figure 6.9(a) gives the 'basic' WOLED, figure 6.9(c) gives the RC^{2}LED and table 6.6 gives the luminous power efficiency. Though the difference of the luminous power efficiency is only 10%, the extraction efficiency is quite different. For some wavelengths, the relative change of the extraction efficiency is around 50%! The extraction efficiency for blue is decreased, but the extraction efficiency for red is increased.

Again, the increase of the luminous power efficiency is partly due to the large fraction of red for this warm 'chromaticity'. Important: if we would have designed the RC^{2}LED to have its maximal extraction efficiency at 500 nm, the luminous power efficiency would have been around 33 lm/W, a decrease of 30%. So, though the RC^{2}LED has only an increase of 10% for

Basic White OLEDs		
$\eta_{int,b}, \eta_{int,g}, \eta_{int,r} =$ 1.0, 1.0, 1.0 figure 6.9 (a)	t_{NET5}, $t_{NHT5} =$ 48 nm, 60 nm	$\eta_P = 48 lm/W$
$\eta_{int,b}, \eta_{int,g}, \eta_{int,r} =$ 0.25, 1.0, 1.0 figure 6.9 (b)	t_{NET5}, $t_{NHT5} =$ 45 nm, 30 nm	$\eta_P = 32 lm/W$
Basic White OLEDs with interference layers		
$\eta_{int,b}, \eta_{int,g}, \eta_{int,r} =$ 1.0, 1.0, 1.0 figure 6.9 (c)	t_{low}, $t_{high} =$ 125 nm, 90 nm	$\eta_P = 53 lm/W$
$\eta_{int,b}, \eta_{int,g}, \eta_{int,r} =$ 0.25, 1.0, 1.0 figure 6.9 (d)	t_{low}, $t_{high} =$ 190 nm, 80 nm	$\eta_P = 35 lm/W$

Table 6.6: Additional layers between ITO and glass increase the luminous power efficiency compared to the 'default' White OLED. The thicknesses and the overall luminous power efficiencies are given for two WOLEDs with different emitter's internal quantum efficiencies. The corresponding extraction efficiencies are given by figure 6.9.

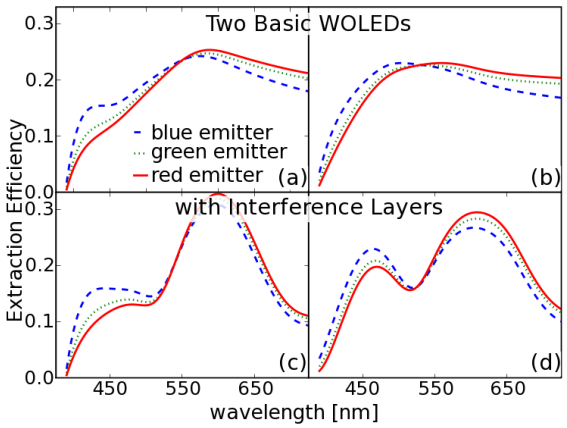

Figure 6.9: Wavelength dependent extraction efficiency corresponding with the values of tables 6.5 and 6.6 and for different stack configurations. Figures (a) and (b) give the basic WOLED, respectively with a blue phosphorescent emitter and a blue fluorescent emitter. Figures (c) and (d) give these WOLEDs with additional interference layers, respectively with a blue phosphosrescent and a fluorescent emitter. The green and red emitters are always phosphorescent emitters.

the luminous power efficiency compared to the basic OLED, the wavelength dependent extraction efficiency changes much. Also, a wrong design of the extraction would lead to a strong decrease of the luminous power efficiency.

We can also look at the extraction efficiency of the WOLEDs with the blue fluorescent emitter. Figure 6.9(b) gives the 'basic' WOLED, Figure 6.9(d) gives the RC^{2}LED Again, the RC^{2}LED has an increase of the luminous power efficiency by 10% compared to the basic WOLED. We also see that the much less efficient blue emitter requires an increase of extraction efficiency of the blue emitter.

In conclusion, we have shown the importance of tuning the extraction efficiency to some parameters of a WOLED. Indeed, we see an increase of 10% for the luminous power efficiency by using the RC^{2}LED. However, the extraction efficiency of a RC^{2}LED at some wavelengths is more than 50% compared to a extraction efficiency of the 'default' OLED. Placing this peak of maximal extraction efficiency at another wavelength can decrease the luminous power efficiency by 30%. Also, these conclusions have been made for RC^{2}LEDs.

Nevertheless, any technique of which the increase of the extraction efficiency is wavelength dependent, should be tuned to match the spectrum and the electrical properties.

6.6 Conclusion

We have shown the relation of the luminous power efficiency and the electrical and optical properties of a 3 color White substrate emitting OLED (WOLED). This luminous power efficiency is the main parameter to measure how efficient and effective a light source is.

We have started by introducing the MacAdam limit. This limit gives the maximum luminous power efficiency of any light source for a given chromaticity. We also saw that the spectrum of most WOLEDs does not look like the spectrum of this limit.

Therefore, to investigate the relation between efficiency and efficacy of a light source, we have made a numerical model to calculate the luminous power efficiency. This model uses optical and electrical properties. The optical parameters are the spectra and extraction efficiencies of the emitters, the electrical parameters are the driving voltage and the internal quantum efficiencies of the emitters. Then, we can prove three statements.

First, we have looked at variations of the spectrum. By changing the spectrum of an WOLED to look like the spectrum of the MacAdam limit, we can increase the luminous efficacy. So, the luminous power efficiency of the WOLED is increased by 30% while retaining a sufficiently high CRI of 80. Also, we have shown how we can make a WOLED with such a spectrum by using a blue/green OLED with a red downconversion layer.

The second statement is demonstrated by a comparison of two WOLED which generate white light with 3 distinct monochrome OLEDs. The WOLEDs are almost identical. The green and red emitter of both WOLEDs are phosphorescent emitters. The only difference is the blue emitter. The fluorescent deep blue emitter of the first WOLED has an internal quantum efficiency which is two times less than the internal quantum efficiency of the phosphorescent deep blue emitter of the second WOLED. The main conclusion will be: the luminous power efficiency of both WOLEDs is the same! Using a deep blue color requires less radiant flux from the blue emitter, while still getting the same chromaticity. This lower fraction compensates the lower efficiency of the deep blue emitter.

Thirdly, tuning the extraction efficiency with respect to the other parameters of a WOLED is needed to increase the luminous power efficiency. To demonstrate this, you can compare two WOLEDs: a basic 3 color WOLED and a RC^{2}LED. This RC^{2}LED has the same organic layers as the basic WOLED, but the additional interference layers give a strong dependency of the extraction efficiency on the wavelength. Conclusion, although the relative increase of the overall luminous power efficiency is limited to 10%, the increase of the extraction efficiency at some wavelengths is more than 50%. Placing this peak of the extraction efficiency at the wrong wavelength, can decrease the overall luminous efficacy by 35%. Although this example is limited to one method to increase extraction efficiency, it clearly shows the importance of tuning the extraction efficiency to the other parameters

of the WOLED.

7 The Complex Jacobi Method

This chapter discusses several extensions we have made to the Complex Jacobi Method (CJ). This technique numerically integrates Maxwell's equations for one frequency. Although the original idea was to use this technique as an alternative to the technique of chapter 3, the former proved to be less suited than the latter. With one extension it is possible to numerically simulate a few devices which include Kerr non linear materials.

Because this chapter is out of phase with the rest of this work, section 7.1 first explains when to use Kerr non linear materials. In the last three subsections, we discuss three examples, one in 1D, one in 2D and one in 3D.

Overview

7.1 Introduction

In this chapter, the main goal is an extension of the Complex Jacobi Method (CJ) to simulate optical components with materials which have the almost instantaneous non linear Kerr effect. In these materials, the refractive index linearly depends on the intensity. This change happens within ps. Thus, the state of such a component depends on the intensity. Moreover, by using feedback of optical resonators, the state of an optical device can become dependent on the previous history. An example of this is an optical flip-flop, a system of which the state depends on its history. Let us first explain the rationale to study these components. Then, this introduction gives an overview of other popular techniques to study components with this effect.

Present day telecom networks rely on lasers pulses which travel through optical fibers to transfer data from user to user. The start of this technology has been around since the seventies. [107] [108] [109] Only optical fibers have sufficiently high bandwidth to satisfy the ever growing need for higher bandwidth. The high bandwidth comes from modulating the optical signals at ever higher speeds and sending multiple signals on different wavelengths through one optical waveguide. [110]

Using optical flip flops might simplify the process of directing signals through the network. Indeed, in every node of the backbone of this optical network, optical signals are analyzed and redirected to ultimately reach the signal's destination node. Now, optical signals are converted to electrical signals which can be handled by ICs. Thus, handling of these signals costs energy and limits bandwidth. Therefore, a dream is an all optical network, where all routing happens in the optical domain.

To have all optical routing, we need optical components which change in function of the incident light. Moreover, switching has to be done as fast as possible. An optical effect with these properties is the almost instantaneous Kerr effect. Now, the refractive index of such a material (n) changes in function of the intensity (I) of the signal: $n = n_0 + n_2 I$. Also, because part of the dielectric field (D) changes by the third power of the electric field (E), we also refer to these materials as third order non linear materials. The time scale is a few femtoseconds (fs). One disadvantage of this effect is its small magnitude ($n_2 = 10^{-13} - 10^{-15} cm^2/W$). Although materials in combination with nanoparticles give higher values for this value, a high intensity still is required to have sufficient high change of the refractive index.

During the last few years, high intensity has been made possible. The components with high intensity are advanced dielectric structures, e.g. photonic crystals and photonic wires. These small waveguides guide light through a waveguide with a cross section of half a micrometer by a quarter of a micrometer. The fabrication of these structures has been made possible by recent advanced mass fabrication production techniques, normally used by CMOS. [111]

To numerically model such structures, the following techniques have been used: Finite Differences in Time Domain (FDTD), [112] [113], Beam Propagation Method (BPM), [114] and Eigenmode Expansion (EME), [115]. These techniques have been shown to simulate a wide variety of non-linear dielectric wavelength scale components. FDTD gives insight in the time-evolution of the fields by numerically integrating Maxwell's equations in the time domain. A steady state solution however requires all transient field effects to be extinct. The extinction rate of these transient field effects is completely dependent on the reflections in the structure. BPM only gives an accurate solution for the steady state fields if reflections are negligible. The lack of bidirectionality is a limiting assumption. EME is a bidirectional frequency domain method. Its main application area are dielectric structures which consist of a few z-invariant sections. Now, the technique of this chapter simulates structures in the frequency domain. Also, the technique is bid

The remainder of this chapter is as follows: we first discuss the linear CJ of [116] in section 7.2. The original paper discusses an iteration process which solves the Helmholtz equation if the fields at the simulation area's boundaries are given. This Helmholtz equation is the equivalent of Maxwell's equations in the frequency domain. To solve optical components with non linear Kerr materials, we however have added the three extensions of section 7.3 . The first extension is a field source based on Total Field/Scattered Field (TFSF) formalism, which is commonly used in FDTD. [112]. The second extension adds good absorption at the edge of the simulation by using Perfectly Matched Layers (PMLs). [117] These two extensions are also useful for linear optical components. The last extension is for materials with the non-linear Kerr effect.

The next three sections describe three components which have been analysed by these methods. Section 7.4 is a non linear optical cavity in 1D. A comparison with EME validates our results. Then, section 7.5 gives a soliton in 2D. Thirdly, section 7.6 is a OLED in 3D.

7.2 The Helmholtz equation & The Complex Jacobi Method

This section contains two topics on solving the Helmholtz equation. First topic, subsection 7.2.1 shows the discrete Helmholtz equation. Due to computational limitations, one usually has to make approximations. Here, we only solve the fields in a space with discrete points. Second topic, subsection 7.2.2 shows how to solve this discrete Helmholtz equation with the Complex Jacobi Method of [116].

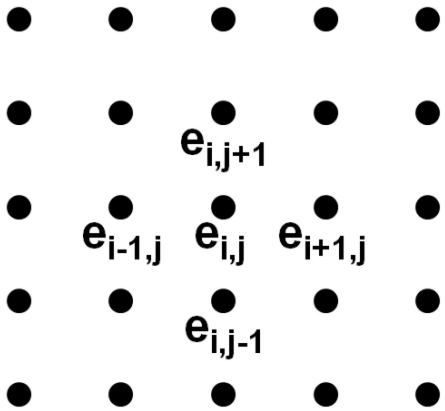

Figure 7.1: The complex Jacobi calculates the fields for points on an equidistant grid.

7.2.1 Discrete version of the Helmholtz equation

The Complex Jacobi Method solves the Helmholtz equation on a mesh. This is similar to Finite Differences in Time Domain (FDTD). In both cases, only the fields on equidistant points are calculated. Moreover, all derivations are replaced by central differences.

Before we give a short overview of the derivation of this technique, let us first discuss the Helmholtz equation. The Helmholtz equation is equivalent to Maxwell's equations, if we want to integrate for one frequency. [94] Some papers call these fields time harmonic fields. The Helmholtz equation is:

$$\epsilon(\mathbf{r})\nabla \times \frac{1}{\epsilon(\mathbf{r})}\nabla \times \mathbf{H}(\mathbf{r}) + \omega^2 \epsilon(\mathbf{r})\mu \mathbf{H}(\mathbf{r}) \quad = \quad 0 \tag{7.1}$$

Integration of this equation gives a complex field: $\mathbf{H}(\mathbf{r})$. This form has no time parameter. To show variations in time, we can use the following relation:

$$\mathbf{h}(\mathbf{r}, t) = \Re(\mathbf{H}(\mathbf{r})e^{j\omega t}) \tag{7.2}$$

Here, Maxwell's equations give a **real** time variant vector $\mathbf{h}$ for each point $\mathbf{r}$ and for every moment. The time harmonic factor has a positive sign by convention. Instead of $e^{j\omega t}$, we could also have chosen $e^{-j\omega t}$. Remark: if your time dependence is $e^{j\omega t}$, lossy materials will have $\Im\epsilon < 0$.

Now, let us look at the discrete variant of equation 7.1. First, simplify the equation 7.1 by only using 2D. Then, instead of a vector field $\mathbf{E}(\mathbf{r})$, we only need to numerically integrate **two independent** eigenvalue problems:

$$\epsilon(\mathbf{r})\nabla \times \frac{1}{\epsilon(\mathbf{r})}\nabla \times H(\mathbf{r}) + \omega^2\epsilon(\mathbf{r})\mu H(\mathbf{r}) = 0 \quad (7.3)$$

$$\nabla^2 E(\mathbf{r}) + \omega^2\epsilon(\mathbf{r})\mu E(\mathbf{r}) = 0 \quad (7.4)$$

In these equations E and H are **scalar** fields and the coordinate **r** is in 2 dimensions. The first equation -7.3- gives the transversal magnetic field (TM), the second equation -7.4- is transversal electric field (TE).

Numerical integration of the Helmholtz equation by the complex Jacobi method now makes the assumption that you only look at the field points on a equidistant mesh. So, for the electric field coordinates on a 2D mesh, these are the points $e_{i,j}$ of figure 7.1. The derivatives of equation 7.4 then are replaced by finite differences:

$$\begin{aligned} \frac{\partial}{\partial x}e(x,y) &\equiv \delta_x e_{i,j} \\ \delta_x e_{i,j} &= \frac{e_{i+1,j} - e_{i-1,j}}{2\Delta x} \\ \frac{\partial^2}{\partial^2 x}e(x,y) &\equiv \delta_x^2 e_{i,j} \\ \delta_x^2 e_{i,j} &= \frac{e_{i+1,j} - 2e_{i,j} + e_{i-1,j}}{\Delta x^2} \end{aligned} \quad (7.5)$$

Thus, difference operators, which use the notation $\frac{\partial}{\partial x}$ are replaced by finite differences, which use the notation δ_x. The field $e_{i,j}$ is located at the point $(i\Delta x, j\Delta y)$, i and j are integers, Δx and Δy are the discretization steps in x and y directions. This gives us the following scalar Helmholtz equation for a discrete mesh:

$$\begin{aligned} \nabla^2 e_{i,j} + k^2 e_{i,j} &\equiv \frac{e_{i+1,j} - 2e_{i,j} + e_{i-1,j}}{\Delta x^2} + \frac{e_{i,j+1} - 2e_{i,j} + e_{i,j-1}}{\Delta y^2} \\ &\quad +(k_0 n_{i,j})^2 e_{i,j} \\ &= 0 \quad (7.6) \\ n_{i,j} &= n(i\Delta x, j\Delta y) \\ k_0 &= \frac{2\pi}{\lambda_0} \end{aligned} \quad (7.7)$$

The wavelength in free space is λ_0, $n_{i,j}$ is the position dependent refractive index.

In conclusion, integration of Maxwell's equations for one frequency is equivalent to the integration of the Helmholtz equation. Also, we use the discrete Helmholtz equation instead of the continuous Helmholtz equation for numerical integration. Thus, the difference operators are replaced by finite differences.

7.2.2 The Complex Jacobi Method

Here, we briefly give the technique to numerically integrate the discrete Helmholtz equation of subsection 7.2.1. A derivation is outside the scope of this work, but can be found in literature. [116]

To solve the field on the points of this discrete mesh, one uses an iterative process. Thus, one starts with an estimate of the field. Then, every iteration this estimate is refined until a certain accuracy is achieved. Because of convergence issues, we use a two step iteration process. This two step iteration process refines the fields with a correction factor which depends on the previously found values:

$$e_{i,j}^{n+1} = e_{i,j}^{n} + \left(2\alpha_1\left(\frac{1}{\Delta x^2} + \frac{1}{\Delta y^2}\right)\right)^{-1} \left((\delta_x^2 + \delta_y^2 + (\frac{2\pi}{\lambda} n_{i,j})^2) e_{i,j}\right) \quad (7.8)$$

The superscript n is the iteration step. The iteration process consists of repeatedly updating the fields with this equation, first with α_1, then with α_2.

Note that this iteration process is performed for all mesh points, except the boundary points. Indeed, the values at these boundary points need to be known a priori to numerically integrate the Helmholtz equation. In section 7.3.1, we come back on this disadvantage.

Using $exp(j\omega t)$ for the time phase factor results in the following optimal constants: $\alpha_1 = \sqrt{3} + 1j$ and $\alpha_2 = -\alpha_1^*$. For $exp(-j\omega t)$, you get $\alpha_1 = \sqrt{3} - 1j$ and $\alpha_2 = -\alpha_1^*$. Derivation of these optimal values for α_1 and α_2 can be found in the original paper. [116]

7.3 Extensions of the Complex Jacobi Method

7.3.1 Introduction

In this section we show three extensions to the Complex Jacobi Method (CJ). To begin this introduction, why do we need these extensions?

The previous section, section 7.2 has shown how to numerically integrate the Helmholtz equation. Also, subsection 7.2.2 has shown the field had to be known on the boundary points. However, these points are usually the unknowns. Indeed, most numerical models have a source which has been placed somewhere in the simulation domain. Then, the field is calculated for these points. Thus, the first two extensions remove this disadvantage.

The first two extensions aim to include sources. These extensions are illustrated by figure 7.2. The first extension is a 'transparent' source field, subsection 7.3.2 . This transparent field source is very similar to Total Field/Scattered Field (TFSF), which is well known in FDTD. [112] Through this interface, we can inject any field. Also, reflections which occur in the

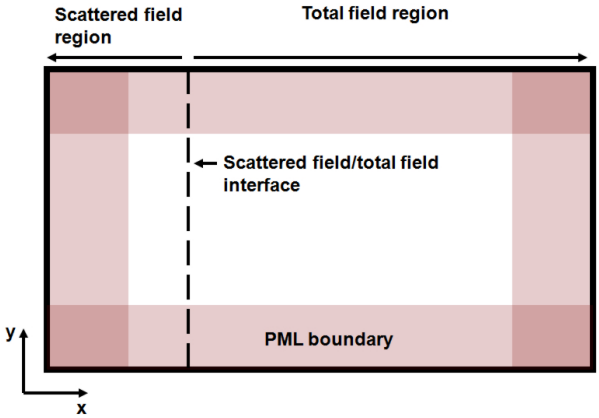

Figure 7.2: A simulation box with 'Total Field/Scattered Field' as field source and PMLs as absorbing boundary conditions.

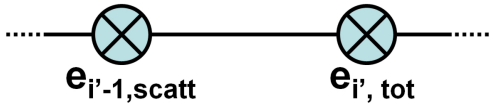

Figure 7.3: Interface between scattered field - total field.

right side of the figure can pass this interface without scattering. To absorb the radiation of this source, we use perfectly matched layers at the boundaries, subsection 7.3.3. In theory, any radiation is absorbed, regardless of angle of incidence or polarisation. [117]

Now, to numerically integrate components with the Kerr non linear effect, we need another extension, subsection 7.3.4. This last extension is an extra iteration step of the iteration process.

In conclusion, this section gives three extensions. The first two extensions remove the requirement of knowing the fields at the boundaries a priori. Then, the third extension adds Kerr non linear materials.

7.3.2 Total Field/Scattered Field

Total Field/Scattered Field (TFSF) helps to numerically model the injection of any desired wave in the simulation domain. Now, figure 7.2 shows how. First, notice that the interface divides the simulation domain in three areas: scattered field region, interface and total field region. Let us assume that the structure of interest is placed in the total field region. Now, through the interface, we can inject a propagating electromagnetic field which goes

from left to right. Then, after numerical integration, the total field region gives the scattered field and the injected field. The left side only gives the field which scatters back from the field.

Remark: this interface is called a transparent field source. See figure 7.9 for an illustration of this behavior. If we would have implemented a hard source, we set the field at the location of this hard source to a fixed value, which causes parasitic reflections. The remainder of this subsection shows how to implement this transparent field source.

Now, we first show how to calculate the field at either side of the interface of figure 7.2. Then, we will show how to calculate the fields at the interface.

At either side of the interface, equation 7.8 calculates $e^n_{(i,j)}$. In the total field domain, we have $e^n_{(i,j),tot}$ which is the sum of source field and scattered field. In the scattered field region, we have $e^n_{(i,j),scatt}$. Thus, the scattered field region has no source field. We do not need to numerically integrate the total field in the scattered field region, as long as we assume two conditions. First, the injected propagating field satisfies the Helmholtz equation. Then, superposition means that the scattered field also satisfies the Helmholtz equation. Second, superposition implies that non-linear materials have to be located in the total field region.

Now, we need to combine the fields -$e^n_{(i,j),scatt}$, $e^n_{(i,j),tot}$- at either side of the interface. The calculation of an amplitude at the interface between the regions is illustrated by figure 7.3.

$$\begin{aligned} e^n_{(i'-1,j),scatt} &= e^n_{(i'-1,j),tot} - e_{(i'-1,j),source} \\ e^n_{(i',j),tot} &= e^n_{(i',j),scatt} + e_{(i',j),source}, \forall n, \forall j \end{aligned} \tag{7.9}$$

The injected field amplitudes $e_{(i'-1,j),source}$ and $e_{(i',j),source}$ are the amplitudes of the exciting wave at respectively positions $(i'-1,j)$ and (i',j). Substituting equation 7.9 in the update equation 7.8 in order to calculate $e^n_{(i'-1,j),scatt}$ and $e^n_{(i',j),tot}$ gives the required update equations. The following equations have omitted the j-index of the y-direction for simplicity.

$$\begin{aligned} e^{n+1}_{i'-1,scatt} &= e^n_{i'-1,scatt} + \\ &\quad C(\frac{e^n_{i',tot} - e_{source,i'} + e^n_{i'-2,scatt} - 2e^n_{i'-1,scatt}}{\Delta x^2} - k^2 e^n_{i'-1,scatt}) \\ e^{n+1}_{i',tot} &= e^n_{i',tot} + \\ &\quad C(\frac{e^n_{i'+1,tot} + e^n_{i'-1,scatt} + e_{source,i'-1} - 2e^n_{i',tot}}{\Delta x^2} - k^2 e^n_{i',tot}) \\ C &= \left(2\alpha(\frac{1}{\Delta x^2} + \frac{1}{\Delta y^2})\right)^{-1} \end{aligned} \tag{7.10}$$

In conclusion, at either side of the interface, we use equation 7.8 to calculate the field. To calculate the field at the interface, where we inject

our field, we use equation 7.10. Then, the total field region shows how a structure scatters the field we have injected through the interface. Also, only in the total field region we may use non linear materials.

7.3.3 Absorbing Boundaries based on PML

Elimination of reflections at the boundaries of a finite simulation box is necessary to achieve physical simulation results. Every wave incident on these boundaries should be absorbed for any polarization and incident angle, without any spurious reflections. Here, we show how to implement Perfectly Matched Layers (PMLs).

One of the most efficient absorbing boundaries is the PML. Here, we show how we have extended the Complex Jacobi Method with a PML based on Complex Coordinate Stretching. Using Complex Coordinate Stretching to achieve PMLs has been around since 1994. [117] We use use this implementation of PML, because Complex Coordinate Stretching results in the easiest implementation of PML for the Complex Jacobi Method.

To implement Complex Coordinate stretching, the difference operators of equation 7.1 are adjusted as follows:

$$\left(\delta_x^2 + \delta_x^2\right) e \quad = \quad \frac{1}{s_x}\frac{\partial}{\partial x}\left(\frac{1}{s_x}\frac{\partial}{\partial x}e\right) + \frac{1}{s_y}\frac{\partial}{\partial y}\left(\frac{1}{s_y}\frac{\partial}{\partial y}e\right) \tag{7.11}$$

For $s_x = 1.0$, the previous formulae reduce to the classical Helmholtz equation. However, a complex function s_x gives absorption in the x-direction, a complex function s_y gives absorption in the y-direction!

A finite difference equivalent of equation 7.11 is:

$$\begin{aligned}
\delta_x^2 e \quad &= \quad \frac{1}{s_x}\left(\frac{\partial}{\partial x}\frac{1}{s_x}\right)\frac{\partial}{\partial x}e + \frac{1}{s_x^2}\frac{\partial^2}{\partial x^2}e \\
&= \quad \frac{1}{s_{x,i}}\left(\frac{\frac{1}{s_{x,i+1}} - \frac{1}{s_{x,i-1}}}{2\Delta x}\right)\left(\frac{e_{i+1} - e_{i-1}}{2\Delta x}\right) \\
&\quad + \frac{1}{s_{x,i}^2}\frac{e_{i+1} + e_{i-1} - 2e_i}{\Delta x^2}
\end{aligned} \tag{7.12}$$

In our experience, optimal absorption was achieved with linearly increasing PML from $s_x = 1.0$ to $s_x = 1.0 - 0.75j$ over 30 grid-points. Note, these complex coordinates implicitly assume the time dependent phase factor of the amplitudes is $\exp(j\omega t)$. For $\exp(-j\omega t)$, we would need to use a linearly increasing PML from $s_x = 1.0$ to $s_x = 1.0 + 0.75j$ over 30 grid-points.

7.3.4 An extra iteration step for Kerr non-linearities

Simulating structures with the instantaneous Kerr effect is quite straight forward. The basic idea is an extra update step of the refractive index

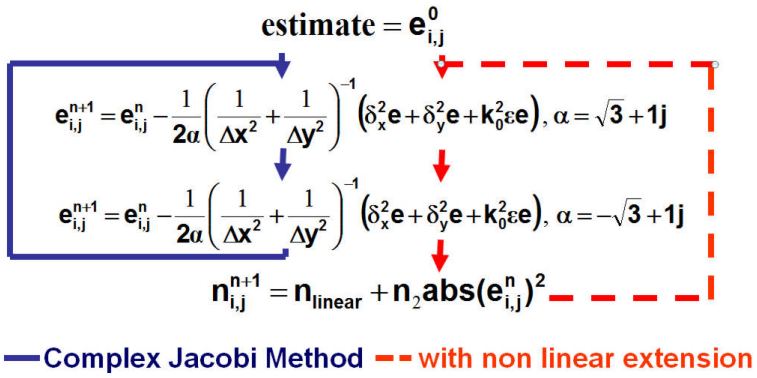

Figure 7.4: The non linear extension for the Complex Iteration Method is one extra step.

after each iteration step. Then, the instantaneous Kerr effect is modeled by $n = n_{lin} + n_2|E|^2$. As stated before, the Complex Jacobi Method (CJ) is a two step iteration. So, we use equation 7.8 with α_1, then we use equation 7.8 with α_2. After these two steps, we use:

$$\epsilon^{n+1}_{i,j} = \left(n_{i,j,lin} + n_{i,j,2}|e_{i,j}|^2\right)^2 \tag{7.13}$$

The extra step of equation 7.13 is also illustrated by figure 7.4.

In conclusion, after each second iteration step, the field at a certain location results in an adjusted refractive index.

7.4 Comparison with non-linear eigenmode expansion

7.4.1 Introduction

In this section, we compare the Complex Jacobi Method (CJ) with extensions of the non linear Eigenmode Expansion (EME). [115]

To compare, we use the 1D structure of figure 7.5. Here, we will introduce the linear behavior of the structure. Then, subsection 7.4.2 gives the comparison between the simulations results of CJ and EME. Both the linear and non linear behavior are discussed. To conclude, subsection 7.4.3 discusses the influence of the discretization step of the mesh.

To begin, look at the structure of figure 7.5. A complete study of this structure can be found in [118]. Moreover, experimental validation of a similar structure has been done. [119] The structure basically is a cavity which has been encapsulated by two Bragg mirrors. The cavity has a thickness

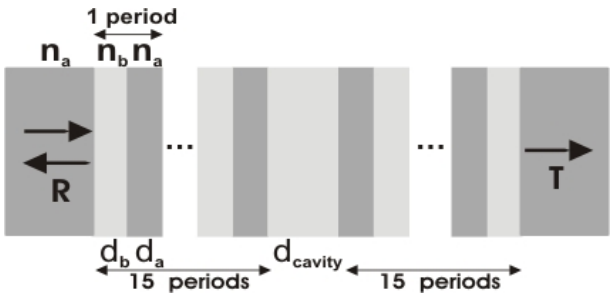

Figure 7.5: Two Bragg mirrors encapsulate a cavity. ($\lambda_{resonance} = 1.56\mu m$)

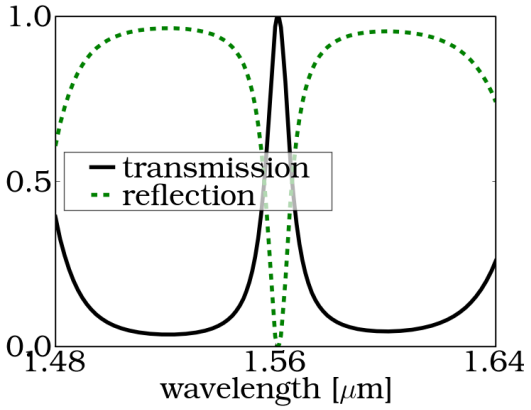

Figure 7.6: Power Transmission and Reflection, see structure in figure 7.5. For a similar behavior, you can also look at the structure of subsection 4.1.3.

of half the effective wavelength: $\lambda_{resonance}/2n_b$. The Bragg mirrors are a stack of alternating layers. Each layer has a thickness of one quarter the effective wavelength: $\lambda_{resonance}/4n_a$ and $\lambda_{resonance}/4n_b$.

The linear behavior of this structure is especially interesting for waves with a wavelength around $\lambda_{resonance}$. Figure 7.6 shows the reflection in function of the wavelength. Almost all plane waves with a wavelength between 1.48 μm and 1.64 μm are blocked. The large wavelength range over which we block light is sometimes referred as an optical band gap. . The only exception are plane waves with a wavelength which is around 1.56 μm. These have full transmission, due to the cavity.

So, we use a structure which blocks all light, except around the small wavelength range of 1.56 μm. Note that this only is the linear behavior.

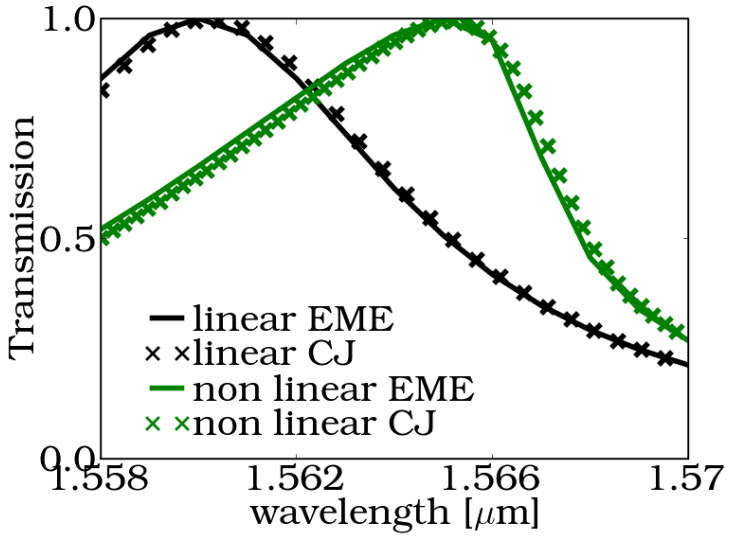

Figure 7.7: Power transmission for linear and non-linear cavity. ($\Delta x = 15nm$)

7.4.2 Comparison between Complex Jacobi Method and Eigenmode Expansion

This subsection compares the results of Complex Jacobi Method (CJ) with extensions to the results of non linear EME. First, let us check if the simulation results agree. Later on, we will address convergence and simulation time.

The parameters we have used for figure 7.5 are the following: $n_a = 2.6$, $n_b = 2.36$, $d_a = \lambda_{resonance}/4n_a$, $d_b = \lambda_{resonance}/4n_b$and $d_{cavity} = \lambda_{resonance}/2n_b$. To illustrate the non linear behavior, we need two extra parameters to quantify the refractive index change. First, the incoming plane wave has an amplitude $e = 1\frac{V}{m}$. Second, if we use n_2 of equation 7.13, the non-linear cavity has $n_2 = 5.10^{-3}\frac{m^2}{V^2}$.

Now, figure 7.7 shows a good agreement between the results of EME and the results of CJ. Both linear and non linear behavior are the same.

The shift of the peak can be explained by considering the interference condition at maximum transmission. Here, one round trip in the cavity will be one 'effective' wavelength: λ/n. Increasing the power means a higher refractive index. To satisfy this condition, the peak should be located at higher wavelength.

Before we discuss the differences between the simulation time, we give

some background on non linear EME. Non linear EME uses a lot of principles of linear EME. Linear EME -subsection 3.2.5- divides a structure in a stack of z-invariant layers. Then, non linear EME uses an iterative process for the non-linear sections. Each iteration, the refractive indices of the non-linear sections are refined until convergence. Thus, simulation time of EME depends on the size of the non-linear sections. Indeed, the linear sections only need to be calculated once. On the other hand, CJ also calculates the linear sections for each iteration step. Thus, EME has an advantage if large sections of the simulation space can be modeled as linear.

Convergence of our method is guaranteed even for a large non-linearity of $n_2 = 0.025\frac{m^2}{V^2}$ with the previously described simulation parameters. This results in an increase of refractive index of approximately $\Delta n \approx 0.6$. For higher non linearities, we however saw divergence of the fields. Thus, this numerical model is not unconditionally stable. Moreover, so far, it is not clear why some setups diverges. Note that this conclusion is also applicable to other setups, 1D and 2D. However, for this setup, if we had convergence, we did notice a significant decrease of convergence rate for these large non-linearities in this setup.

To finish, some small comparison with FDTD and BPM. Simulating the steady state solution of the previous problem with a time domain simulation method - e.g. FDTD - would require extremely long simulation times. This is especially the case for a structure with many reflections, as is the case for this example. So, CJ only gives the steady state solution. BPM can quickly be ruled out because of the bidirectionality of the component.

Therefore, our proposed extension to CJ is very well suited for structures where the non-linearity is present in a large portion of the simulation domain. In such a situation EME would not be very efficient.

7.4.3 Influence of discretization step

Using finite differences instead of derivatives always introduces numerical errors. This is true for FDTD, this is true for Complex Jacobi Method (CJ). Equation 7.5 already showed that finite differences depend on a discretization step. Here, we look at the errors we might expect.

Figure 7.8 gives the shift of the resonance peak in function of the discretization step. Remark, we only look at the linear setup of figure 7.6. Although in theory the peak should not change, CJ gives a different resonance wavelength. A coarser grid causes a resonance peak shift to higher wavelengths.

To explain this behavior, we can use numerical dispersion. Numerical dispersion shows that the speed of light in a dispersionless medium depends on its frequency. In a dispersionless medium, substitution of a plane wave ($e^{j\omega t - jkx}$) in equation 7.4 gives:

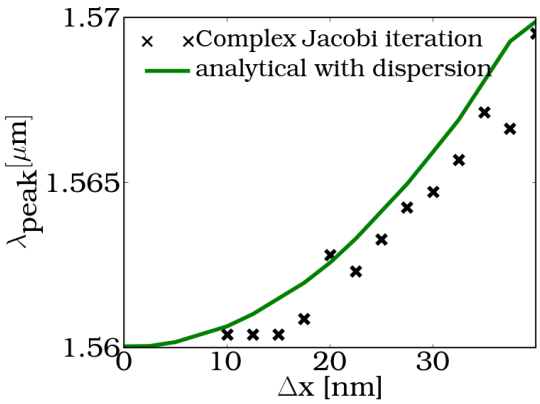

Figure 7.8: Resonance peak -cfr. figure 7.5- shifts in function of the discretization step. (The analytical dispersion model uses equation 7.15 to adjust n_a and n_b in the calculated structure.)

$$k_0 n = \frac{\omega}{c} \tag{7.14}$$

Here, k_0 is the amplitude of the wavevector in vacuum, n is the refractive index, c is the speed of light in vacuum and ω is the angular frequency.

However, substitution of $e^{j\omega t - kx}$ in equations 7.4 and 7.5 gives:tion of $e^{j\omega t - kx}$ in equations 7.4 and 7.5 gives:

$$\begin{aligned} \frac{4\sin^2(\frac{k_0 n_{eff}\Delta x}{2})}{\Delta x^2} &= \frac{\omega^2}{c^2} \\ n_{eff} &= \frac{\arcsin(\frac{k_0 n \Delta x}{2})}{\frac{k_0 \Delta x}{2}} \end{aligned} \tag{7.15}$$

The effective refractive index -$n_{eff} = \frac{\omega c}{k_0}$-, 'felt' by a plane wave in a discrete simulation space is different than the actual refractive index.

Now, we can analytically calculate the peak of the structure with the new refractive indices: $n_{eff,a}$ and $n_{eff,b}$. This peak is given in figure 7.8 by the 'analytical dispersion model'.

In conclusion, we have seen that the peak of the linear component shifts in function of the discretization step. This numerical error can be explained by numerical dispersion. Also, a small value Δ_x in 7.15 reduces n_{eff} to $n_{eff} = n$.

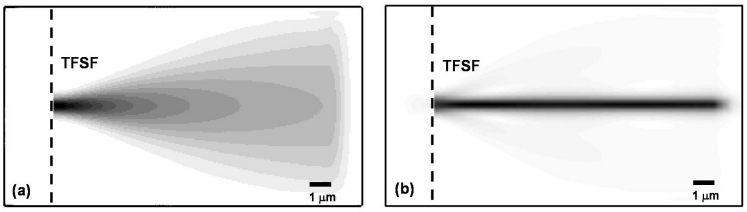

Figure 7.9: Injection of a gaussian field profile in a linear and non-linear medium. ((a): diffraction in linear medium, (b): soliton in non-linear medium)

7.5 Spatial Soliton in a non linear Kerr-material

Here, we will validate our extension by simulating the self-focusing of a gaussian beam in non-linear space.

In linear space, the injection of a gaussian field profile with Total Field/Scattered Field (TFSF) gives diffraction, figure 7.9(a). The gaussian field profile is described by $e = 1.0e^{\frac{x^2}{2*0.25^2}} \frac{V}{\mu m}$. The refractive index is $n = 3.6$.

The situation changes for Kerr non linear materials. Now, the increase of the refractive index gives a self focusing effect in the middle, figure 7.9(b). The parameters are the same as for the linear case, but with $n_2 = 0.2\frac{m^2}{V^2}$.

Now, non linear Eigenmode Expansion (EME) requires a large amount of eigenmodes to simulate the same straight forward simulation setup. The lack of linear regions, which should only be calculated once, takes away the main advantage of non linear EME.

7.6 An OLED with a grating

In this section, we show how to simulate an OLED with grating in 3D. All materials are assumed to be linear. Also, we compare the simulation time with the simulation time of the numerical model of chapter 3.

To simulate a corrugated OLED in 3 dimensions we need to numerically integrate equation 7.1, the vectorial Helmholtz equation. Thus, in 3D, each coordinate has 3 field components which need to be numerically integrated. To have an absorbing boundary condition, each of these three components has to satisfy equation 7.12.

Figure 7.10 gives the numerical integration of a simple corrugated OLED. The layer structure of this figure is as follows: Aluminium,n = 1.0-3.0j, t = 500nm / ETL, n = 1.66, t = 60 nm / emissive region / HTL, n = 1.807, t = 45 nm / ITO, n = 1.806 - 0.01j, t = 120 nm / SiON, n = 1.622, t = 100 nm / a square with a grating of pillars of SiON in air. The period of the grating is 800 nm. These pillars are made from SiON with a fill factor of

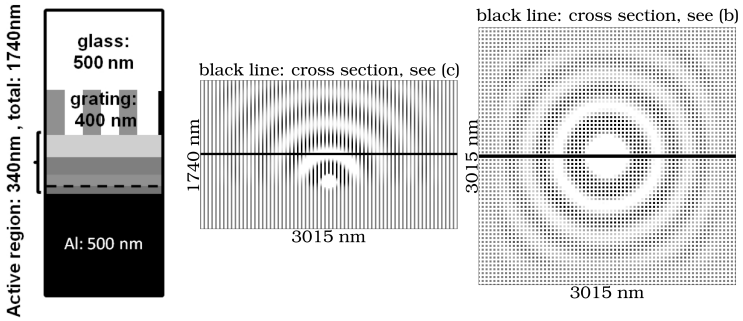

(a) (b) (c)

Figure 7.10: A 3d simulation of a corrugated OLED for which the horizontal dipole ($\mathbf{p} = (1., 1., 1.)$) emits at 550 nm is done in a simulation box with discrete steps of 15nm*45nm*45nm.In this figure $\Re(H_y)$ is given.

60%, t = 400 nm./ air. To determine the discretization step, we use a rule of thumb which commonly is used in FDTD. We use at least 10 points per effective wavelength. Thus, the setup of figure 7.10 has 166*65*65 points.

The simulation time for 20000 iterations is about 1 day on a opteron 2Ghz system for each wavelength, for each polarisation and each position of the dipole. This is much longer than the few minutes which are needed by the numerical model of chapter 3.

One additional remark concerning stability and convergence rate. Although this particular structure gave convergence, convergence is not automatically guaranteed. A simulation where we use a metal with a large complex part of the refractive index ($\Im\epsilon > 8$)gave divergence. Also, the convergence rate is not known a priori! Figure 7.11 shows how the error decreases in function of the iteration step. So far, it has not been possible to predict the actual convergence rate. This is in contrast with FDTD. With FDTD, you can estimate how much time steps the simulation requires. As a rule of thumb, you might state that if you increase reflections or decrease losses, the convergence decreases. Thus, it is impossible to anticipate the duration of a simulation.

In conclusion, although the algorithm can be used for 3D setups, the simulation method of chapter 3 proved to be better suited for the goals we initially anticipated. Also, convergence is not always guaranteed for highly lossy materials. Also, even if you have convergence, the convergence rate is unpredictable. Thus, before starting a simulation, it is quite difficult to anticipate when the simulation finishes.

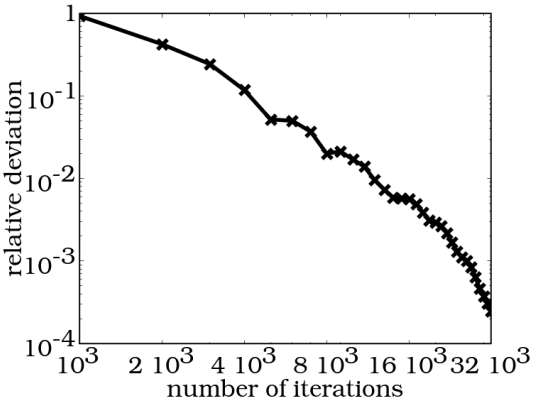

Figure 7.11: This figure shows the average relative error in function of the iteration step. (The relative error is the relative deviation from the field at iteration step 40000, which is the end of the simulation.)

7.7 Conclusion

Our extensions to the recently introduced complex Jacobi method allow the simulation of some 2D-components with Kerr-based materials in the frequency domain. Our proposed extension to the complex Jacobi method is very suited for structures where the non-linearity is present in a large portion of the simulation domain. We also have demonstrated simulations of a 3D structure.

To finish, we give some remarks on stability and convergence rate. First, stability is still an issue. The numerical model is not unconditionally stable. For large non linearities or very lossy materials, stability is not guaranteed. Second, estimating the simulation time beforehand is impossible. Only by running a simulation over several iterations, the convergence rate can be estimated. These two requirements should be addressed before this technique can be considered for device simulation.

Panel member: If you were to meet these Vegans, and were permitted only one question to ask of them, what would it be?
Ellie Arroway: Well, I suppose it would be, how did you do it? How did you evolve, how did you survive this technological adolescence without destroying yourself?

Contact, 1997

8 Conclusions and Perspectives

8.1 Conclusions

The goal of this work has been to improve the optical performance of White Organic LEDs for general illumination. Here, we give the main conclusions of this work.

Generally speaking, to achieve a better optical performance, two questions can be asked. The first question is: how can you increase the extraction efficiency? Increasing the extraction efficiency is key for efficient OLEDs. Thus, we have investigated designs which increase the fractions of photons which can escape to air. Also, numerical methods, simulations and experiments are addressed. The second question is: is the most efficient OLED automatically the most effective OLED? Here, we look at the relation between properties of the OLED and the eye sensitivity curves. The two questions are in respectively subsections 8.1.1 and 8.1.2.

8.1.1 How to increase the extraction efficiency?

Normally, an OLED has an extraction efficiency of 20% for the entire visible range from 350 nm up to 700 nm. The main reason for this low extraction efficiency is Total Internal Reflection. Oblique light can never go from a high refractive index material to a low refractive index material. In this work we have numerically analyzed three substrate emitting OLED designs which might increase the extraction efficiency. The first and second designs have also been fabricated and measured.

To numerically analyze these designs, we have developed a 3d numerical model for substrate emitting OLEDs, chapter 3. The interfaces between some of its layers can be either planar or a grating. Development of this numerical model is based on two other numerical techniques: eigenmode

expansion and rigorous coupled wave analysis. The main novelty of the numerical model is the way light propagation in the substrate of an OLED is modeled. The model includes multiple round trips in the substrate. After comparing the extraction efficiency with multiple round trips and the extraction efficiency without multiple round trips, the relative difference could be up to 75%.

Note that we originally planned to use a different numerical model, which was based on Complex Jacobi Method (CJ), chapter 7. Though this numerical model proved to be less useful for OLEDs, we have shown how to model optical components with non linear materials.

Now, let us look at the three OLED designs.

One conclusion which is valid for all three OLED designs relates to the orientation of the dipoles in the active region. A parallel orientation of the dipoles with respect to the emissive layer gives a much higher extraction efficiency than a vertical orientation of the dipoles.

The first OLED design is the RC^{2}LED. This design has three additional interference layers between the active region and the glass substrate. These additional interference layers have subsequently a high refractive index, low refractive index and a high refractive index. Both simulations and experiments show that our design increases light extraction by a factor of 2. The wavelength range for which the relative increase of the light extraction still is higher than 75% is 75 nm. Increasing the wavelength range will decrease the maximal extraction efficiency.

The second and third OLED designs have a grating at respectively the substrate-air interface and the active region-substrate interface. In both cases, we see a relative increase of light extraction by 50% for a wavelength range which spans the visible spectrum. Let us now focus on the conclusions specific for each approach.

The second design is an OLED with a grating at the interface between substrate and air. Here, we have locally optimized the grating parameters for one wavelength. For the depth and period, we found that the parameters had to be larger than respectively 200 nm and 800 nm. The other parameters depend on the motif of the grating. For pillars and holes, we can define a fill factor. The optimal values are respectively 70% and 55%. Also, small variations of these parameters show that these parameters are extremely robust. Also, the optimal parameters appear to be the optimal parameters over the entire visible wavelength range.

For the second design, we now can compare the extraction of a reference OLED without grating and that same OLED with grating. By reference OLED, we mean an OLED which has an extraction efficiency of about 20% over the entire wavelength range. Then, the simulated relative improvement is roughly 50%-80% for all wavelengths. Our experimental conclusions are largely qualitative, but we see a good qualitative agreement. The most important conclusion relates to the relative improvement by using gratings or microlenses. This relative improvement is roughly the same.

We conclude the second design with a more complicated layer structure. Here, the relative improvement is more wavelength dependent. For example, you can use a RC^{2}LED which already has an extraction efficiency of 40% for one wavelength. Then, the grating does not increase light extraction of specific wavelengths.

The third design is an OLED with a grating at the interface between active region and substrate and air. Again, we have locally optimized the grating parameters for one wavelength. For the depth and period, we found that the parameters had to be larger than respectively 200 nm and 600 nm. The other parameters depend on the motif of the grating. For pillars and holes, we can defined a fill factor. The optimal values are in both cases 60%. Note, small variations of these parameters show that these parameters are extremely robust. Also, the optimal parameters appear to be the optimal parameters over the entire range. We saw a relative improvement of the extraction efficiency of 50%.

To finish, we have tested three statements with the third design. First, multiple round trips are an important effect to determine the extraction efficiency. We stress this statement because most articles in literature do not consider this effect. To validate this statement, we can compare the extraction efficiency for which only direct transmission is considered and the extraction efficiency for which multiple round trips in the substrate are considered. The relative difference of the extraction efficiency is around 50%. Second, an electrode with high absorption severely limits the extraction efficiency. Indeed, if multiple round trips are important, reflection is important. We have shown that an OLED with ITO outperforms an OLED with Clevios$^{\text{TM}}$, a conductive polymer. The main reason is the higher absorption of Clevios$^{\text{TM}}$. Third, the grating helps to extract light from the substrate, not from the organic layers! Indeed, the amount of light which can go from the organic layers to glass only increases by 10%. However, because of multiple round trips and scattering in the substrate, the light extraction increases by 50%. Thus, the increase of light extraction comes from the light which would normally be trapped in the substrate, not from the light which is trapped in the organic layers.

We can summarize our results in table 8.1. Regardless of which of the three designs to extract light, the extraction efficiency is limited to about 40%.

8.1.2 Is an efficient OLED automatically an effective OLED?

Now, we will show that the design of an efficient White OLED (WOLED) and the design of an effective WOLED do not automatically coincide. The focus of the previous subsection is how to increase the efficiency. However, for illumination, the figure of merit is the luminous power efficiency. This luminous power efficiency shows how efficient light is generated and how

structure	extraction efficiency (simulation)
Planar OLEDs	
reference OLED	± 20%, all wavelengths
RC^{2}LED	± 40%, wavelength range of ± 100 nm
Grating at the substrate-air interface	
reference OLED with micro lenses	35%-40%, all wavelengths
reference OLED with grating	35%-40%, all wavelengths
RC^{2}LED with grating	35%-40%, all wavelengths
Grating at the organic layers-substrate interface	
reference OLED with micro lenses	> 25%-30%, all wavelengths

Table 8.1: An overview of all the simulated extraction efficiencies, we find for this work.

effective that light is. Thus, to make an OLED more effective, we have to match properties of the OLED with its spectrum and the eye sensitivity curves. Three statements have been proved by using three Gedanken experiments. To perform these Gedanken experiments, we have developed a numerical model.

First statement: if we can change the spectrum of an WOLED to look like the spectrum of the MacAdam limit, we increase the luminous efficacy. This luminous efficacy is the maximal luminous power efficiency. So, the luminous power efficiency of the WOLED is increased by 30% while retaining a sufficiently high CRI of 80. Also, we have shown how we can make a WOLED with such a spectrum by using a blue/green OLED with a red downconversion layer.

The second statement is demonstrated by a comparison of two WOLED which generate white light with 3 distinct monochrome OLEDs. The WOLEDs are almost identical. The green and red emitter of both WOLEDs are phosphorescent emitters. The only difference is the blue emitter. The fluorescent deep blue emitter of the first WOLED has an internal quantum efficiency which is two times less than the internal quantum efficiency of the phosphorescent light blue emitter of the second WOLED. The main conclusion: the luminous power efficiency of both WOLEDs is the same!

Third statement: tuning the extraction efficiency with respect to the other parameters of a WOLED is needed to increase the luminous power efficiency. To demonstrate this, you can compare two WOLEDs: a basic 3 color WOLED and a RC^{2}LED. This RC^{2}LED has the same organic layers as the basic WOLED, but the additional interference layers give a strong dependency of the extraction efficiency on the wavelength. Conclusion,

although the relative increase of the overall luminous power efficiency is limited to 10%, the increase of the extraction efficiency at some wavelengths is more than 50%. Placing this peak of the extraction efficiency at the wrong wavelength, can decrease the luminous power efficiency by 35%. Although this example is limited to one method to increase extraction efficiency, it clearly shows the importance of tuning the extraction efficiency to the other parameters of the WOLED.

These conclusions illustrate that extraction efficiency is important. However, in the end, the figure of merit is the luminous power efficiency.

8.2 Perspectives

For now, the best OLEDs already achieve 50 lm/W. If their luminous efficacy can be increased to 100 lm/W, even the most efficient fluorescent tubes are outperformed. Considering the other advantages, such as long lifetime and deposition on non planar shapes or even flexible substrates, this technology indeed might change the way we think about general illumination.

Is it possible that in our basically trichromatic species, a subset of females become tetrachromatic, enjoying an extra dimension of colour experience?

John Mollon

A Color Properties of a Light Source

A.1 Quantification of Color and Color Rendering

Color is a visual sensation, caused by electromagnetic waves which result in impulses in the brain. A quantification of color related properties is necessary to objectively determine the properties of a light source. This chapter summarizes two publications of Commission Internationale de l'Eclairage (CIE), which quantify the color sensations of a 'standard' person. [14] [16]

Two properties are important. First, which color should the light source emit? Warm white or cool white? Second, which colors can I discriminate when I illuminate an object with a given light source? Think of reading a map under streetlighting, it is even difficult to discriminate between blue and red lines. This second property is the Color Rendering Index (CRI).

Section A.2 shows the relationship between the spectrum of electromagnetic waves and color by introducing the concept of color spaces. Another way to quantify colors is the Correlated Color Temperature (CCT), section A.3. Then, section A.4 shows a metric which determines how good you can discriminate colors when you illuminate an object with a light source.

A.2 Color Spaces

To mathematically quantify a color, we can use its color coordinate in a given color space. Addition of colors can also be done if you use the correct addition rules for that specific color space. This section first gives some general remarks on the dimension of color spaces and the addition rules. These remarks apply to most color spaces. Then, sections A.2.1 and A.2.3

give two color spaces of which the first one is used throughout this work.

Each color corresponds with one point in a given color space. If and only if two colors have the same color coordinate, they are equal. Because most humans have three receptors with each recepter sensitive in its own wavelength range, humans are called trichromats. [120] The first color space which took this into account is the Munsell color space. In general, a color space of three dimensions suffices to express the stimulation of the three sets of receptors.

Now let us look at the addition of two colors. To begin, we start by explaining **metamerism**. . Two **different** spectra can give the same stimulation of these receptors, thus two different spectra can give the same color. However, **if two colors A and B are equal and C is another color, then the combination of color A with color C gives the same color as the the combination of color B and color C.** This is one of Grasmann's laws. However, this law is only valid for well-lit conditions. Under well-lit conditions, we speak of photopic vision. Under insufficient illumination, these Grasmann's laws are no longer valid and we speak of scoptopic vision. The implication for the addition of color coordinates is the following: under well lit conditions, adding colors can be described as the addition of their color coordinates.

A.2.1 The CIE XYZ 1931 color space and the luminous efficiency function

The XYZ color space has been defined by Commission Internationale de l'Eclairage (CIE) in 1931 for a standard observer. This standard observer is based on measurements which have been performed on a cross section of the population. In this section, we also show at which wavelengths the eye is most sensitive by introducing the luminous efficacy. This unit is directly related to this color space As the next subsections will show, most other color spaces can be derived from this color spaces.

As stated in the introduction, each color is expressed by three coordinates which are the color tristimulus (X,Y,Z):

$$\begin{aligned} X &= \int_0^\infty L_e(\lambda)\overline{x}(\lambda)d\lambda \\ Y &= \int_0^\infty L_e(\lambda)\overline{y}(\lambda)d\lambda \\ Z &= \int_0^\infty L_e(\lambda)\overline{z}(\lambda)d\lambda \end{aligned} \tag{A.1}$$

The right side equations are a convolution of the radiance (L_e) and the eye sensitivity curves ($\overline{x}(\lambda)$, $\overline{y}(\lambda), \overline{z}(\lambda)$) of figure A.2.1. These eye sensitivity curves of the CIE 1931 standard observer give the stimulation of the three receptors for a 2-degree field of observation. Similar to this color space

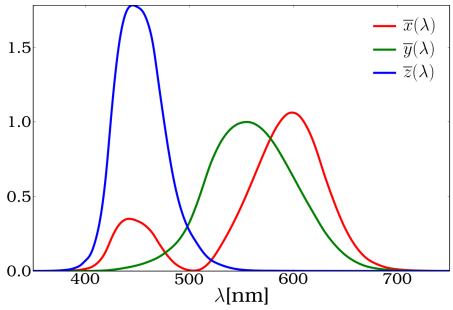

Figure A.1: Eye sensitivity curves ($\overline{x}(\lambda)$, $\overline{y}(\lambda), \overline{z}(\lambda)$)

is the CIE 1964 supplementary standard observer. This observer is based on measurements over a larger field of view (10 degrees) than the CIE 1931 XYZ color space, producing slightly different results. Instead of the radiance, also the spectral power distribution is commonly used to find the tristimulus values.

To find the luminous efficacy (F), we simply have to use the $\overline{y}(\lambda)$ color matching function. Indeed, this curve is equal to the photopic luminous efficiency function V(λ) for the 'CIE standard photopic observer' (CIE 1926). This curve gives the average sensitivity for a given wavelength. The human eye is more sensitive at 555 nm (green) than for lower (blue) or higher (red) wavelengths. Then

$$F = 683 \int_0^\infty \overline{y}(\lambda) J(\lambda) d\lambda \tag{A.2}$$

In conclusion, both the color coordinate (XYZ) as the luminous efficacy (F) follow from the CIE XYZ color space.

A.2.2 The CIE xy 1931 color space

To make a representation of the 3d CIE XYZ 1931 color space in 2d, one possible way is to remove the luminance information. Indeed, a color has a chromaticity and a luminance. This can be understood by comparing grey and white. They both can have a 'white' chromaticity, but they differ in brightness or luminance. Very dim white is experienced as grey. Thus, grey and white are two different colors. This section gives mathematical equations for the chromaticity. Also, we give the chromaticity diagram which is a well known way to represent chromaticity.

To go from the tristimilus values (X,Y,Z) to the CIE xy 1931 color space, we use the following definition:

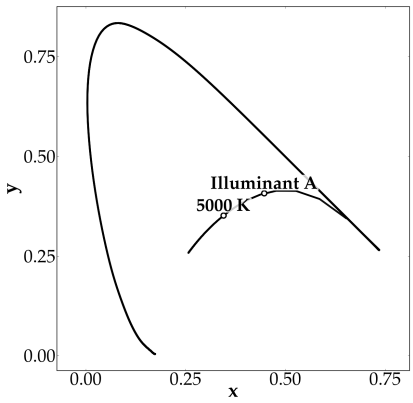

Figure A.2: The chromaticty diagram in CIE 1931 xy color space

$$\begin{aligned} x &= \frac{X}{X+Y+Z} \\ y &= \frac{Y}{X+Y+Z} \end{aligned} \tag{A.3}$$

These equations give the chromaticity by the values (x,y). Sometimes the information (x,y,Y) is given where Y is the luminance. Again, two colors can have the same chromaticity (x,y) , but they differ in brightness/luminance, Y.

To represent this two dimenstional color space, we use the chromaticity diagram of figure A.2.2. The boundaries of this chromaticity diagram is given by the spectral locus. To find the spectral locus, we calculate the color coordinates of monochromatic sources. These monochromatic sources emit at one wavelength.

As background information, we now give the main disadvantage of the CIE XYZ 1931 and the CIE xy 1931 color spaces. These color spaces have no correlation between the distance of two color coordinates and the discremination of the corresponding colors. Thus, there is no metric in these color spaces. For example, a person can discreminate two 'blue' colors which have a distance of 0.01. However, that person can not discreminate two 'green' colors which have a distance of 0.01. The correlation between color discrimination and color distance can be visualised with MacAdam Ellipses. A MacAdam ellipse is a region in a chromaticity diagram with colors which can not be discriminated. Therefore, The MacAdam ellipses in a color space with an intuitive correlation between color discrimination

and color relation would have to be circles with equal radius. The shape and size of these ellipses however varies throughout the entire xy1931 color space. For that reason, other color spaces have been developed. One color space where the MacAdam Ellipse are circles of equal radius is the CIE 1976 L*u*v* (CIELUV) colorspace.

A.2.3 uv 19630 color space

The main reason to include this color space is its application in the calculation of the Color Rendering Index (CRI) of section A.4. Note, except the calculation of the CRI, this space is no longer used.

This color space is a 2 dimensional color space with chromaticity coordinates (u',v') which are given by:

$$\begin{aligned} u' &= \frac{4X}{X+15Y+3Z} = \frac{4x}{-2x+12y+3} \\ v' &= \frac{6Y}{X+15Y+3Z} = \frac{6y}{-2x+12y+3} \end{aligned} \tag{A.4}$$

Note that these (u',v') chromaticity coordinates are closely related to (u',v') chromaticity coordinates of the CIE 1976 L*u*v* (CIELUV) color space.

A.3 Correlated Color Temperature

The Correlated Color Temperature (CCT) of a light source gives the temperature of a black body radiator which has the 'closest' chromaticity to that of the light source. The spectrum of a black body radiator is fully determined by its temperature T. There are two applications for the CCT. First, the chromaticity of a light source is sometimes indicated by its CCT. Of course, the accuracy of this representation depends on its distance to the black body curve of figure A.2. The second application of the CCT is to use it as reference light source in the calculation of the Color Rendering Index (CRI). We will come back on this in section A.4.

A black body emitter at a temperature of T (Kelvin) has the following spectral radiation (I(λ)):

$$I(\lambda) = \frac{8\pi hc}{\lambda^5} \frac{1}{e^{\frac{hc}{\lambda kT}} - 1} \tag{A.5}$$

The wavelength is given by λ, h, c and k are respectively Planck's constant, the speed of light and Boltzmanns constant.

To determine the black body radiator with the 'closest' chromaticity, you need to specify your color coordinate system. For the CCT, you use

the uv 1960 color space of section A.2.3 Then, you minimize the distance between the color coordinate of your light source and the color coordinate of a black body radiator by varying T. The metric to determine the distance (Δ) between two color coordinates ((u'_0, v'_0) and (u'_1, v'_1))is the well known Euclidian distance:

$$\Delta = \sqrt{(u'_0 - u'_1)^2 + (v'_0 - v'_1)^2} \tag{A.6}$$

A.4 Color Rendering Index

A light source with a high Color Rendering Index (CRI) means that that light source can reproduce an object's color almost as good as a reference source. This CRI is a scale up to 100, where 100 is the value of the reference light source. For example, street light has a low CRI. Reading a map under a street light surely is not an easy task. This scale is defined in a publication of the CIE. [16]. We will now briefly give the mathematical implementation of this scale.

The first version of the CRI used the 8 standard samples of which the reflectance is given by figure A.3(a). These eight samples were both illuminated by a reference light source and by the test source. The color difference between the color you see under these two illuminations is used to determine the CRI of that sample. Averaging the CRI of these samples then gives the averaged CRI. However, 6 additional samples have been added to the CRI to correctly quantify fluorescent tubes. These tubes could have a high CRI, but with low color quality. Figure A.3 shows the spectral reflectance of these 14 samples. Although this scale now has been widely adopted to quantify color quality and color reproducibility of a light source, this scale has been critized during the last decade. Recently, visual experience has shown that the current CRI based ranking of a set of light sources containing white LED light sources contradicts the visual ranking. [104]. Spectral narrow LEDs can have good light quality, but a low CRI.

Let us know look at the CRI of a test light source (k). To get a color difference, we need to define one reference light source and a color space. We let the reference light source (r) of this light source (k) depend on the Correlated Color Temperature (CCT) of the light source (k). If that temperature is below 5000 K, the reference light source is a Planckian radiator with the CCT of (k). Above 5000 K, one of a series of SPDs corresponding to phases of daylight are used. The color space is the W*U*V* 1964 color space. In this space, we will look at the color coordinates of the samples illuminated by (k) and (r).

The first step is to determine the chromaticities of both light sources (k) and (r) in 1960 uv color space, A.2.3. This gives respectively (u'_k, v'_k) and u'_r, v'_k

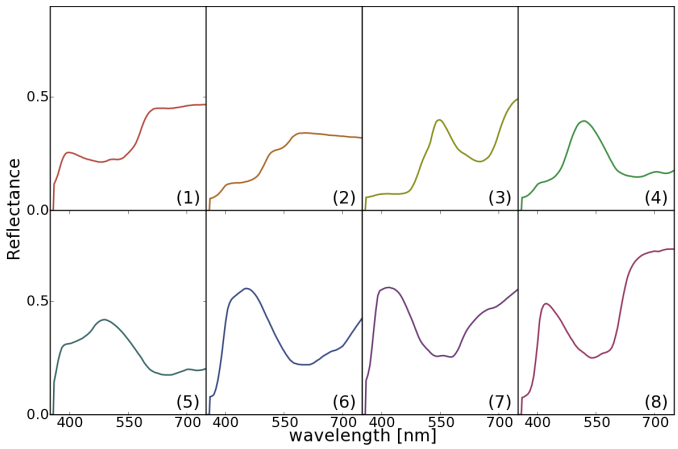

(a) Reflectance of the original 8 samples

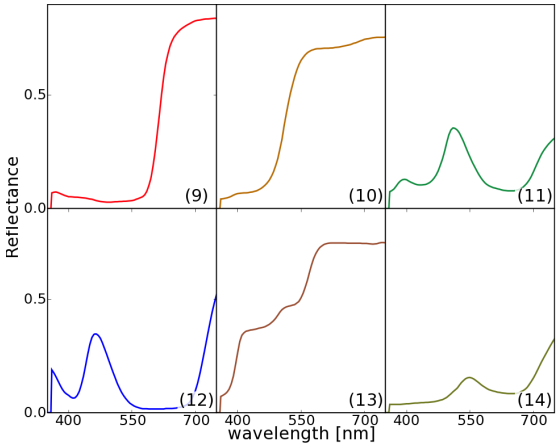

(b) Reflectance of the extra 6 samples

Figure A.3: The Color Rendering Index uses 8 + 6 samples as reference.

The second step is the color points of the sample (i) under illumination by these two light sources, (k) and (r). For the sample under illumination by the reference light (r) source, we have $u'_{k,i}, v'_{k,i}$. For the sample under illumination by the light source (k), additional steps need to be used to calculate the color coordinate $u'_{r,i}, v'_{r,i}$. These steps are necessary because of chromatic adaptation. In a room with yellow illumination, a yellow surface will look less yellow than when that same surface is illuminated by daylight. The eye adapts to the chromaticity of the light source.

To find $(u'_{r,i}, v'_{r,i})$, we first calculate the following intermediate results:

$$\begin{aligned} c_r &= \frac{4 - u_r - 10v_r}{v_r} \\ d_r &= \frac{1.708v_r + 0.404 - 1.481u_r}{v_r} \end{aligned} \tag{A.7}$$

$$\begin{aligned} c_k &= \frac{4 - u_k - 10v_k}{v_k} \\ d_k &= \frac{1.708v_k + 0.404 - 1.481u_k}{v_k} \end{aligned} \tag{A.8}$$

$$\begin{aligned} c_{k,i} &= \frac{4 - u_{k,i} - 10v_{k,i}}{v_{k,i}} \\ d_{k,i} &= \frac{1.708v_{k,i} + 0.404 - 1.481u_{k,i}}{v_{k,i}} \end{aligned} \tag{A.9}$$

Then, the chromaticity under the light source (k) is:

$$\begin{aligned} u'_{k,i} &= \frac{10.872 + 0.404\frac{c_r}{c_k}c_{k,i} - 4\frac{d_r}{d_k}d_{k,i}}{16.518 + 1.481\frac{c_r}{c_k}c_{k,i} - \frac{d_r}{d_k}d_{k,i}} \\ v'_{k,i} &= \frac{5.520}{16.518 + 1.481\frac{c_r}{c_k}c_{k,i} - \frac{d_r}{d_k}d_{k,i}} \end{aligned} \tag{A.10}$$

Background information: if we would have used the equations for chromatic adaptation for the reference source (r), this would not have changed $u'_{r,i}, v'_{r,i}$. Indeed, the parameters $(c_{k,i}, d_{k,i})$ in the equations A.10 would have been replaced by (c_k, d_k). The chromaticity of the light source (u'_k, v'_k), after chromatic adaption is the chromaticity of the reference light source (r): (u_r, v_r).

Before the calculation of the actual color coordinates in 1964 W*U*V* color space, we need to determine a **relative** illuminance for the samples under illumination. The illuminance corresponding with a color coordinate is the Y-coordinate of this color point in CIE 1931 color space. Both the light source (k) and the reference light source (r) will be normalized to 100.0. The illuminance of the color of the test sample under illumination needs to be adapted accordingly.

With the previous information, the coordinates in 1960 uv space and the normalized luminance, the color coordinate of the test sample under illumination by the test source (k) and the reference source (r) now can be calculated:

$$\begin{array}{lllllll} W^*_{r,i} & = & 25\,(Y_{r,i})^{\frac{1}{3}} - 17 & & W^*_{k,i} & = & 25\,(Y_{k,i})^{\frac{1}{3}} - 17 \\ U^*_{r,i} & = & 13W^*_{r,i}\,(u_{r,i} - u_r) & & U^*_{k,i} & = & 13W^*_{k,i}\left(u'_{k,i} - u'_k\right) \\ V^*_{r,i} & = & 13W^*_{r,i}\,(v_{r,i} - v_r) & & V^*_{k,i} & = & 13W^*_{k,i}\left(v'_{k,i} - v'_k\right) \end{array} \quad \text{(A.11)}$$

Note that the color coordinate of the light source k, (u'_k, v'_k) is equal to (u_r, v_r).

Then the difference between these 2 color points is given by:

$$\Delta E_i = \sqrt{\left(\Delta U^*_i\right)^2 + \left(\Delta V^*_i\right)^2 + \left(\Delta W^*_i\right)^2} \quad \text{(A.12)}$$

Finally the special Color Rendering Index, R_i of each sample (i) is given by:

$$R_i = 100.0 - 4.6\Delta E_i \quad \text{(A.13)}$$

The general Color rendering Index which refers to an average of the first eight samples is given by :

$$R_a = \frac{\sum_{i=1to8} R_i}{8} \quad \text{(A.14)}$$

References

[1] http://www.olla-project.org. *Olla project delivers final milestone.*

[2] http://www.iaeel.org/iaeel/Archive/Right_Light_Proceedings/DELight/DELight.html . *European DELight study, Domestic Efficient Lighting*, 1998.

[3] An OIDA Technology Roadmap. *Organic Light Emitting Diodes (OLEDs) for General Illumination, Update 2002.* http://www.OIDA.org, August 2002.

[4] Photonics 21. *Towards a Bright Future for Europe, Strategic Research Agenda in Photonics.* http://photonics21.org/.

[5] C.W. Tang and S.A. Van Slyke. *Organic electroluminescent diodes.* Applied Physics Letters, 51(12):913–915, 1987.

[6] K. Walzer, B. Maennig, M. Pfeiffer, and K. Leo. *Highly Efficient Organic Devices Based on Electrically Doped Transport Layers.* Chemical Review, 107:1233–1271, 2007, 107.

[7] J. Kido, K. Hongawa, K. Okuyama, and K. Nagai. *White light-emitting organic electroluminescent devices using the poly(N-vinylcarbazole) emitter layer doped with three fluorescent dyes.* Applied Physics Letters, 6(7):815–817, February 14 1994.

[8] M. A. Baldo, D. F. OBrien, Y. You , A. Shoustikov, S. Sibley, M. E. Thompson, and S. R. Forrest. *Highly efficient phosphorescent emission from organic electroluminescent devices.* Nature, 395:151–154, September 1998.

[9] Peter Bienstman. *Rigorous and efficient modelling of wavelength scale photonic components.* PhD thesis, Universiteit Gent, 2001.

[10] Danae Delbeke. *Design and fabrication of a highly efficient light-emitting diode: The Grating-Assisted Resonant-Cavity Light-Emitting Diode.* PhD thesis, Ghent University, 2002.

[11] P. Bienstman and R. Baets . *The RC2LED: a novel resonant-cavity LED design using a symmetric resonant cavity in the outcoupling reflector.* IEEE Journal of Quantum Electronics, 36(6):669–673, 2000.

[12] Mao-Kuo Wei, I-Ling Su, Yi-Jia Chen, Ming Chang, Hong-Yi Lin, and Tung-Chuan Wu. *The influence of a microlens array on planar organic light-emitting devices.* Journal of Micromechanics and Microengineering, 16:368374, 2006.

[13] Yoon-Chang Kim, Sang-Hwan Cho, Young-Woo Song, Yong-Jae Lee, Yong-Hee Lee, and Young Rag Do. *Planarized SiNx/spin-on-glass photonic crystal organic light-emitting diodes.* Applied Physics Letters, 89:173502–1–3, 2006.

[14] Colorimetry 3rd edition. www.cie.co.at, publication: 15:2004.

[15] DL MacAdam. *Maximum attainable luminous efficiency of various chromaticities.* Journal of the Optical Society of America, 40:120, 1950. printed: article which gives an idea of the maximum achievable efficacy for a given color point... mentioning of the concept metameric...

[16] CIE 13.3-1995. *Method of Measuring and Specifying Colour Rendering Properties of Light Sources.* ISBN: 3 900 734 57 7.

[17] Gregor Schwartz, Karsten Fehse, Martin Pfeiffer, Karsten Walzer, and Karl Leo. *Highly efficient white organic light emitting diodes comprising an interlayer to separate fluorescent and phosphorescent regions.* Applied Physics Letters, 89:0835092006, 2006.

[18] *http://www.eia.doe.gov/ Energy Information Administration, Official Energy Statistics of the U.S. Government.* last visit: January 2008.

[19] *http://www.emis.vito.be Energie en Milieu Informatie Systeem voor het Vlaamse Gewest*, last visit: January 2008.

[20] *http://nobelprize.org/.*

[21] Optoelectronics Industry Development Association. *Organic Light Emitting Diodes (OLEDs) for General Illumination, Update 2002, An OIDA Technology Roadmap.* http://www.OIDA.org, August 2002.

[22] J. G. Fleming, S. Y. Lin, I. El-Kady, R. Biswas, and K. M. Ho. *All-metallic three-dimensional photonic crystals with a large infrared bandgap.* Nature, 417:52–55, 2002.

[23] Ademe (Agence de l'Environnement et de la Matrise de l'Energie). *L'eclairage dans votre logement*, November 1999.

[24] BBC news. *Lights out for GE bulb factories.* online.

[25] Jeff Y. Tsao. *Solid State Lighting.* IEEE Circuits & Devices Magazine, N.A.:28–37, May/June 2004.

[26] K. Kalantar, S. Matsumoto, and T. Onishi. *Functional light-guide plate characterized by optical micro-deflector and micro-reflector for LCD backlight.* IEICE Transactions on Electronics, E84C:1637–1646, November 2001.

[27] James Norman Bardsley. *International OLED Technology Roadmap.* IEEE Journal of Selected Topics in Quantum Electronics, 10(1):3–9, 2004.

[28] Nikolay Zheludev. *The life and times of the LED a 100-year history.* Nature Photonics, 1:189–192, 2007.

[29] S. Nakamura, T. Mukai, and M. Senoh. *Candela-Class High-Brightness InGaN/AlGaN Double-Heterostructure blue light-emitting diodes.* Applied Physics Letters, 64(13):1687–1689, March 1994.

[30] www.lichttechnologie.be. *Laboratorium voor Lichttechnologie.*

[31] N.K. Patel, S. Cina, and J.H. Burroughes. *High-Efficiency Organic Light-Emitting Diodes.* IEEE Journal on Selected Topics in Quantum Electronics, 8(2):346–361, 2002.

[32] Stephen R. Forrest. *The road to high efficiency organic light emitting devices.* Organic Electronics, 4:45–48, 2003.

[33] S. R. Forrest B. W. D'Andrade, R. J. Holmes. *Efficient Organic Electrophosphorescent White-Light-Emitting Device with a Triple Doped Emissive Layer.* Advanced Materials, 16(7):624–628, April 2004.

[34] Aparna Misra, Pankaj Kumar, M. N. Kamalasanan, and Subhas Chandra. *White organic LEDs and their recent advancements.* Semiconductor science and Technology, 21:R35–R46, 2006.

[35] Michael Niggemann. *Fundamental investigations on Periodic Nano- and Microstructured Organic Solar Cells.* PhD thesis, Albert-Ludwigds-Universitat, 2005.

[36] C. C. Wu, S. D. Theiss, G. Gu, M. H. Lu, J. C. Sturm, S. Wagner, and S. R. Forrest. *Integration of Organic LEDs and Amorphous Si TFTs onto Flexible and Lightweight Metal Foil Substrates.* IEEE Electron Device Letters, 18(12):609–612, December 1997.

[37] Stephen R. Forrest. *The path to ubiquitous and low-cost organic electronic appliances on plastic.* Nature, 428:911–918, April 2004.

[38] J. H. Burroughes, D. D. C. Bradley, A. R. Brown, R. N. Marks, K. Mackay, R. H. Friend, P. L. Burns, and A. B. Holmes. *Light-emitting diodes based on conjugated polymers.* Nature, 347:539541, 1990.

[39] Alan J. Heeger, Alan G. MacDiarmid, and Hideki Shirakawa. *"for the discovery and development of conductive polymers".* The Nobel Prize in Chemistry 2000.

[40] Junji Kido and Toshio Matsumoto. *Bright organic electroluminescent devices having a metal-doped electron-injecting layer.* Applied Physics Letters, 73(20):2866–2868, November 1998.

[41] J. Blochwitz, M. Pfeiffer, T. Fritz, and K. Leo. *Low voltage organic light emitting diodes featuring doped phthalocyanine as hole transport material.* Applied Physics Letters, 73(6):729–731, August 1998.

[42] Yiru Sun, Noel C. Giebink, Hiroshi Kanno, Biwu Ma, Mark E. Thompson, and Stephen R. Forrest. *Management of singlet and triplet excitons for efficient white organic light-emitting devices.* Nature, 440:908–912, 2006.

[43] *Press Release: Universal Display Corporation's white OLED technology exceeds 100 lm/W (102lm/W).*

[44] Stephen R. Forrest. *Ultrathin Organic films grown by organic molecular beam deposition and related techniques.* Chemical Reviews, 97(6):1793–1896, September/October 1997.

[45] H. Sirringhaus, T. Kawase, R. H. Friend, T. Shimoda, M. Inbasekaran, W. Wu, and E. P. Woo. *High-Resolution Inkjet Printing of All-Polymer Transistor Circuits.* Science, 290:2123–2126, December 2000.

[46] Xiaohui Yang, David C. Mller, Dieter Neher, and Klaus Meerholz. *Highly Efficient Polymeric Electrophosphorescent Diodes.* Advanced Materials, 18:948–954, 2006.

[47] J.A.E. Wasey, A. Safonov, I.D.W. Samuel, and W.L. Barnes. *Effects of dipole orientation and birefringence on the optical emission from thin films.* Optics Communications, 183(1-4):109–121, September 2000.

[48] M. Schreil, M. Eritt, J. Amelung, K. Leo, U. Hoffmann, and M. Bender. *50.1: OLED Devices Manufactured Using a Vertical In-Line Concept.* SID International Symposium Digist of Technical papers, 35(2):1376–1379, 2004.

[49] U. Hoffmann, M. Bender, M. Campo, and E. Sommer. *Vertical Inline Deposition Technology for Full-Color OLED Production.* SID International Symposium Digist of Technical Papers, 36(2):1204–1209, 2005.

[50] J. Amelung, M. Toerker, C. Luber, M. Eritt, Y. Tomita, H. Cholewa, R. Hermann, F. Loeffler, C. May, U. Vogel, G. Bunk, A. Heinig, W. Jeroch, H.J. Holland, and K. Leo. *Second generation OLED devices and systems: inline evaporation, highly efficient OLED devices, and novel driver/controller ASICs.* In Building European OLED Infrastructure. Edited by Pearsall, Thomas P.; Halls, Jonathan. Proceedings of the SPIE, Volume 5961, pp. 47-57, 2005.

[51] M. Toerker, J. Amelung., M. Eritt, D. Hill, C. Luber, F. Lffler, Ch. May, Ch. Zschippang, and K. Leo. *In-line deposition of high-efficiency p-i-n organic light-emitting devices.* In Organic Optoelectronics and Photonics II. Edited by Heremans, Paul L.; Muccini, Michele; Meulenkamp, Eric A.. Proceedings of the SPIE, Volume 6192, pp. 619203., 2006.

[52] J. S. Wilson, A. S. Dhoot, A. J. A. B. Seeley, M. S. Khan, A. Khler, and R. H. Friend. *Spin-dependent exciton formation in π-conjugated compounds.* Nature, 413:828–830, October 2001.

[53] Chihaya Adachi, Marc A. Baldo, E. Thompson, and Stephen R. Forrest. *Nearly 100% internal phosphorescence efficiency in an organic light emitting diode.* Journal of Applied Physics, 90(10):5048–5051, November 2001.

[54] R. J. Holmes, B. W. D'Andrade, S. R. Forrest, X. Ren, and and M. E. Thompson J. Li. *Efficient, deep-blue organic electrophosphorescence by guest charge trapping.* Applied Physics Letters, 83(18):3818–3820, 2003.

[55] S.J. Yeh, M.F. Wu, C.T. Chen, Y.H. Song, Y. Chi, M.H. Ho, S.F. Hsu, and C.H. Chen. *New dopant and host materials for blue-light-emitting phosphorescent organic electroluminescent devices.* Advanced Materials, 17(3):285–288, Februari 2005.

[56] Cheng-Han Yang, Yi-Ming Cheng, Yun Chi, Chia-Jung Hsu, Fu-Chuan Fang, Ken-Tsung Wong, Pi-Tai Chou, Chih-Hao Chang, Ming-Han Tsai, and Chung-Chih Wu. *Blue-Emitting Heteroleptic Iridium(III) Complexes Suitable for High-Efficiency Phosphorescent*

OLEDs. Angewandte Chemie International Edition, 46:2418–2421, 2007.

[57] SPIE, editor. *Highly efficient organic light emitting diodes (OLED) for displays and lighting*, volume 6192 of *Organic Optoelectronics and Photonics II*.

[58] Benjamin C. Krummacher, Vi-En Choong, Mathew K. Mathai, Stelios A. Choulis, Franky So, Frank Jermann, Tim Fiedler, and M. Zachau. *Highly efficient white organic light-emitting diode*. Applied Physics Letters, 88:113506, 2006.

[59] Malte C. Gather, Ronald Alle, Heinrich Becker, and Klaus Meerholz. *On the Origin of the Color Shif tin White-Emitting OLEDs*. Advanced Materials, 19:4460–4465, 2007.

[60] V. Adamovich, J. Brooks, A. Tamayo, AM Alexander, PI Djurovich, BW D'Andrade BW, C. Adachi, SR Forrest, and ME Thompson. *High efficiency single dopant white electrophosphorescent light emitting diodes*. New Journal of Chemistry, 26(9):1171–1178, 2002.

[61] G. Schwartz, M. Pfeiffer, S. Reineke, K. Walzer, and K. Leo. *Harvesting triplet excitons from fluorescent blue emitters in white organic light-emitting diodes*. Advanced Materials, 19:3672–3676, 2007.

[62] Hiroshi Kanno, Noel C. Giebink, Yiru Sun, and Stephen R. Forrest. *Stacked white organic light-emitting devices based on a combination of fluorescent and phosphorescent emitters*. Applied Physics Letters, 89:023503, 2006.

[63] J.-Q. Xi, Martin F. Schubert, Jong Kyu Kim, E. Fred Schubert, Minfeng Chen, Shawn-Yu Lin, W. Liu, and J.A. Smart. *Optical thin-film materials with low refractive index for broadband elimination of Fresnel reflection*. Nature Photonics, 1:176–179, March 2007.

[64] Stephen R. Forrest, Donald D.C. Bradley, and Mark E. Thompson. *Measuring the efficiency of Organic Light-Emitting Diodes*. Advanced Materials, 15(13):1043–1048, 2003.

[65] D. McBranch, I. H. Campbell, D. L. Smith, and J. P. Ferraris. *Optical determination of chain orientation in electroluminescent polymer films*. Applied Physics Letters, 66(10):1175–1177, March 1995.

[66] Karsten Fehse, Karsten Walzer, Karl Leo, Wilfried Lvenich, and Andreas Elschner. *Highly Conductive Polymer Anodes as Replacements for Inorganic Materials in High-Efficiency Organic Light-Emitting Diodes*. Advanced Materials, 19:441–444, 2007.

[67] Yuto Tomita, Christian May, Michael Toerker, Joerg Amelung, Michael Erit, Frank Loeffler, Claus, Karl Leo, Karsten Walzer, Karsten Fehse, and Qiang Huang Q. *Highly efficient p-i-n-type organic light emitting diodes on ZnO : Al substrates.* Applied Physics Letters, 91(6):063510, August 2007.

[68] Myung-Gyu Kang and L. Jay Guo. *Nano imprinted Semitransparent Metal Electrode sand Their Application in Organic Light-Emitting Diodes.* Advanced Materials, 19:1391–1396, 2007.

[69] Kristiaan A. Neyts. *Simulation of light emission from thin-film microcavities.* Journal of Optical Society of America A, 15(4):962–971, 1998.

[70] Kristiaan Neyts. *Microcavity effects and the outcoupling of light in displays and lighting applications based on thin emitting films.* Applied Surface Science, 244:517–523, 2005.

[71] M. H. Lu and J.C. Sturm. *Optimization of external coupling and light emission in organic light-emitting devices: modeling and experiment.* Journal of Applied Physics, 91(2):595–604, 2002.

[72] Tetsuo Tsutsui, Masayuki Yahiro, Hiroshi Yokogawa, Kenji Kawano, and Masaru Yokoyama. *Doubling Coupling-out Efficiency in Organic Light-Emitting Devices Using a Thin Silica Aerogel Layer.* Advanced Materials, 13(15):1149–1152, August 2001.

[73] H. Riel, S. Karg, T. Beierlein, W. Rie, and K. Neyts. *Tuning the emission characteristics of top-emitting organic light-emitting devices by means of a dielectric capping layer: An experimental and theoretical study.* Journal of Applied Physics, 94(8):5290–5296, 2003.

[74] A. Dodabalapur, L. J. Rothberg, and T. M. Miller. *Color variation with electroluminescent organic semiconductors in multimode resonant cavities.* Applied Physics Letters, 65(18):2308–2310, 1994.

[75] Hongmei Zhang, Han You, WeiWang, Jiawei Shi, Shuxu Guo, Mingda Liu, and Dongge Ma. *Organic white-light-emitting devices based on a multimode resonant microcavity.* Semiconductor science and technology, 21:1094–1097, 2006.

[76] Wallace C.H. Choy and C. Y. Ho. *Improving the viewing angle properties of microcavity OLEDs by using dispersive gratings.* Optics Express, 15(20):13288–13294, 2007.

[77] Ali M. Adawi, Liam G. Connolly, David M. Whittaker, David G. Lidzey, Euan Smith, Matthew Roberts, Faisal Qureshi, Clare Foden, and Nicky Athanassopoulou. *Improving the light extraction efficiency*

of red-emitting conjugated polymer light emitting diodes. Journal of Applied Physics, 99:04505, 2006.

[78] S. Moller and S. R. Forrest. *Improved light out-coupling in organic light emitting diodes employing ordered microlens arrays.* Journal of Applied Physics, 91(5):3324–3327, March 2002.

[79] Huajun Peng, Yeuk Lung Ho, Xing-Jie Yu, Man Wong, and Hoi-Sing Kwok. *Coupling Efficiency Enhancement in Organic Light-Emitting Devices Using Microlens Array - Theory and Experiment.* Journal of Display Technology, 1(2):278–282, December 2005.

[80] Jongsun Lim, Seung Seok Oh, Doo Youp Kim, Sang Hee Cho, In Tae Kim, S. H.Han, Hideo Takezoe, Eun Ha Choi, Guang Sup Cho, Yoon Ho Seo, Seung Oun Kang, and Byoungchoo Park. *Enhanced out-couplingfactor of microcavity organic light-emitting devices with irregular microlens array.* Optics Express, 14:6564–6570, 2006. 80

[81] S. Wedge, A. Giannattasio, and W.L. Barnes. *Surface plasmonpolariton mediated emission of light from top-emitting organic light-emitting diode type structures.* Organic Electronics, 8:136147, 2007.

[82] Yong-Jae Lee, Se-Heon Kim, Joon Huh, Guk-Hyun Kim, Yong-Hee Lee, Sang-Hwan Cho, Yoon-Chang Kim, and Young Rag Do. *A high-extraction-efficiency nanopatterned organic light-emitting diode.* Applied Physics Letters, 82(21):3779–3781, May 2003.

[83] Y.R. Do, Y.C. Kim, Y.-W. Song, H. Jeon C.-O Cho, Y.-J. Lee, S.-H. Kim, and Y.-H. Lee. *Enhanced Light Extraction from Organic Light-Emitting Diodes with 2D SiO2/SiNx Photonic Crystals.* Advanced Materials, 15(14):1214–1218, July 2003.

[84] Y.R. Do, Y.C. Kim, Y.W. Song, and Y.H. Lee. *Enhanced light extraction efficiency from organic light emitting diodes by insertion of a two-dimensional photonic crystal structure.* Journal of Applied Physics, 96(12):7629–7636, December 2004.

[85] A.M. Adawi, R. Kullock, J.L. Turner, C. Vasilev, D.G. Lidzey, A. Tahraoui, D. Gibson P.W. Fry, E. Smith, C. Foden, M. Roberts, F. Qureshi, and N. Athanassopoulou. *Improving the light extraction effciency of polymeric light emitting diodes using two-dimensional photonic crystals.* Organic Electronics, 7:222–228, 2006.

[86] Jonathan M. ZieBarth, Ameen K. Saafir, Shanhui Fan, and Michael D. McGehee. *Extracting light from polymer light-emitting diodes using stamped bragg gratings.* advanced functional materials, 14(5):451–456, May 2004.

[87] Kuniaki Ishihara, Masayuki Fujita, Ippei Matsubara, Takashi Asano, Susumu Noda, Hiroshi Ohata, Akira Hirasawa, Hiroshi Nakada, and Noriyuki Shimoji. *Organic light-emitting diodes with photonic crystals on glass substrate fabricated by nanoimprint lithography.* Applied Physics Letters, 90(11):111114, 2007.

[88] Jongsun Lim, Seung Seok Oh, Doo Youp Kim, Sang Hee Cho, In Tae Kim, S. H. Han, Hideo Takezoe, Eun Ha Choi, Guang Sup Cho, Yoon Ho Seo, Seung Oun Kang, and Byoungchoo Park. *Enhanced out-coupling factor of microcavity organic light-emitting devices with irregular microlens array.* Optics Express, 14:6564–6571, 2006.

[89] F. Olyslager. *Electromagnetic Waveguides and Transmission Lines.* Oxford Engineering Science, isbn 0198564503 edition, 1999.

[90] V. Bulovic, V. B. Khalfin, G. Gu, P. E. Burrows, D. Z. Garbuzov, and S. R. Forrest. *Weak microcavity effects in organic light-emitting devices.* Physical Review B, 58(7):3730–3740, August 1998.

[91] John D. Joannopoulos, Robert D. Meade, and Joshua N. Winn. *Photonic Crystals: Molding the flow of light.* Princeton University Press, 1995. chapter 3: symmetries and solid state electromagnetism.

[92] H. Benisty, R. Stanley, and M. Mayer. *Method of source terms for dipole emission modification in modes of arbitrary planar structures.* Journal of Optical Society of America A, 15(5):1192–1201, 1998.

[93] Danae Delbeke, Peter Bienstman, Ronny Bockstaele, and Roel Baets. *Rigorous electromagnetic analysis of dipole emission in periodically corrugated layers: the grating-assisted resonant-cavity light-emitting diode.* Journal of the Optical Society of America A, 19(5):871–880, May 2002.

[94] Jean G. Van Bladel. *Electromagnetic Fields.* IEEEE press, 2007.

[95] P. Bienstman and R. Baets. *Optical modelling of photonic crystals and VCSELs using eigenmode expansion and perfectly matched layers.* Optical and Quantum Electronics, 33:327–341, 2001.

[96] M. G. Moharam and T. K. Gaylord. *Rigorous coupled-wave analysis of planar-grating diffraction.* Journal of Optical Society of America, 71:811–, 1981.

[97] P. Lalanne and G.M. Morris. *Highly improved convergence of the coupled-wave method for TM polarization.* Journal of the Optical Society of America A-Optics Image Science and Vision, 13(4):779–784, April 1996.

[98] Philippe Lalanne and Jean-Paul Hugonin. *Numerical performance of finite-difference modal methods for the electromagnetic analysis of one-dimensional lamellar gratings.* Journal of Optical Society of America A, 17(6):1033–1042, 2000.

[99] Hans De Neve. *Design and realisation of light emitting diodes based on the microcavity effect (PhD).* PhD thesis, Universiteit Gent, 1997.

[100] Bienstman P Baets R Benisty H Delbeke D, Bockstaele R. *High-efficiency semiconductor resonant-cavity light-emitting diodes: A review.* IEEE Journal of Selected Topics in Quantum Electronics, 8(2):189–206, March-April 2002.

[101] Lee Tutt and Joseph F. Revelli. *Distribution of radiation from organic light-emitting diode structures with wavelength-scale gratings as a function of azimuth and polar angles.* Optics Letters, 33(5):503, 2008.

[102] W.G. Quirino, R.D. Adati, S.A.M. Lima, C. Legnani, M. Jafelicci Jr, M.R. Davolos , and M. Cremona. *Electroluminescence of a device based on europium -diketonate with phosphine oxide complex.* Thin Solid Films, 515:927–931, 2006.

[103] Mitsunori Saito, Naoki Adachi, and Hiroyasu Kondo. *Full-color illumination that needs no electric power.* Optics Express, 15(4):1621, 2007.

[104] CIE 177:2007. *Colour Rendering of White LED Light Sources.* ISBN 978 3 901 906 57 2.

[105] Shigeo Shionoya and William M. Yen, editors. *Phosphor Handbook.* CRC Press, 1999.

[106] Daisaku Tanaka, Yuya Agata, Takashi Takeda, Soichi Watanabe, and Junji Kido. *High Luminous Efficiency Blue Organic Light-Emitting Devices Using High Triplet Excited Energy Materials.* Japanese Journal of Applied Physics, 46(5):L117–L119, 2007.

[107] T. H. Maiman. *Stimulated optical radiation in ruby.* Nature, 187:493–494, 1960.

[108] N.G. Basov, O.N. Kroklin, and Y.M. Popov. *Production of negative-temperature states in p-n junctions of degenerate semiconductors.* Soviet Physics JETP, 13:1320, 1961.

[109] F. P. Kapron, D. B. Keck, and R. D. Maurer. *Radiation losses in glass optical waveguides.* Applied Physics Letters, 17:423–425, 1970.

[110] MK. Smit and C. vanDam. *PHASAR-based WDM-devices: Principles, design and applications.* IEEE Journal of Selected Topics in Quantum Electronics, 2(2):236–250, 1996.

[111] W. Bogaerts, R. Baets, P. Dumon, V. Wiaux, S. Beckx, D. Taillaert, B. Luyssaert, J. Van Campenhout, P. Bienstman, and D. Van Thourhout. *Nanophotonic waveguides in silicon-on-insulator fabricated with CMOS technology.* Journal of Lightwave Technology, 23(1):401–412, 2005.

[112] Allen Taflove. *Computational Electrodynamics The Finite-Difference Time-Domain Method.* Artech House, 1995.

[113] EP Kosmidou and TD Tsiboukis. *An FDTD analysis of photonic crystal waveguides comprising third-order nonlinear materials.* Optical And Quantum Electronics, 35(10):931–946, August 2003.

[114] J.M. Burzler, S. Hughes, and B.S. Wherrett. *Split-step Fourier methods applied to model nonlinear refractive effects in optically thick media.* Applied Physics B, 62(4):389–397, April 1996.

[115] Bjorn Maes, Peter Bienstman, and Roel Baets. *Modeling of Kerr nonlinear photonic components with mode expansion.* Optical and Quantum Electronics, 36(1-3):15–24, January-February 2004.

[116] Hadley G. Ronald. *A complex Jacobi iterative method for the indefinite Helmholtz equation.* Journal of Computational Physics, 203(1):358–370, February 10 2005 2005.

[117] Weng Cho Chew and Weedon William H. *A 3D perfectly matched medium from modified Maxwell's equations with stretched coordinates.* Microwave and optical technology letters, 7(13):599–604, September 1994.

[118] G.R.A. Priem, I. Notebaert, B. Maes, P. Bienstman, G. Morthier, and R. Baets. *Design of all-optical nonlinear functionalities based on resonators.* IEEE Journal of selected topics in quantum electronics, 10(5):1070–1078, 2004.

[119] G.R.A. Priem, P. Dumon, W. Bogaerts, D. Van Thourhout, G. Morthier, and R. Baets. *Optical bistability and pulsating behaviour in Silicon-On-Insulator ring resonator structures.* Optics Express, 13(23):9623 – 9628, November 2005.

[120] John Mollon. *Colour: Art & Science*, volume Darwin College Lectures, chapter Chapter 5: Seeing Colour, pages 127–150. Cambridge University Press, 1995.

List of Figures

List of Tables

Index